Vol. 286, No. 1, February 10, 1994

ISSN 0003

Special Issue
PAPERS PRESENTED AT THE INTERNATIONAL SYMPOSIUM ENTITLED ISSUES AND CONTROVERSY: THE MEASUREMENT OF CRYSTALLINE SILICA, CAMBRIDGE, MA, USA, AUGUST 20–21, 1992

ANALYTICA CHIMICA ACTA

An international journal devoted to all branches of analytical chemistry

ELSEVIER

ANALYTICA CHIMICA ACTA

Scope. *Analytica Chimica Acta* publishes original papers, rapid publication letters and reviews dealing with every aspect of modern analytical chemistry. Reviews are normally written by invitation of the editors, who welcome suggestions for subjects. Letters can be published within **four months** of submission. For information on the Letters section, see inside back cover.

Submission of Papers

Americas

Prof. Harry L. Pardue
Department of Chemistry
1393 BRWN Bldg, Purdue University
West Lafayette, IN 47907-1393
USA

Tel:(+1-317) 494 5320
Fax:(+1-317) 496 1200

Computer Techniques

Prof. J.T. Clerc
Universität Bern
Pharmazeutisches Institut
Baltzerstrasse 5, CH-3012 Bern
Switzerland

Tel:(+41-31) 6314191
Fax:(+41-31) 6314198

Prof. Sarah C. Rutan
Department of Chemistry
Virginia Commonwealth University
P.O. Box 2006
Richmond, VA 23284-2006
USA
Tel:(+1-804) 367 1298
Fax:(+1-804) 367 7517

Other Papers

Prof. Alan Townshend
Department of Chemistry
The University
Hull HU6 7RX
Great Britain

Tel:(+44-482) 465027
Fax:(+44-482) 466410

Prof. Willem E. van der Linden
Laboratory for Chemical Analysis
Department of Chemical Technology
Twente University of Technology
P.O. Box 217, 7500 AE Enschede
The Netherlands
Tel:(+31-53) 892629
Fax:(+31-53) 356024

Prof. Paul Worsfold
Dept. of Environmental Sciences
University of Plymouth
Plymouth PL4 8AA
Great Britain

Tel:(+44-752) 233006
Fax:(+44-752) 233009

Submission of an article is understood to imply that the article is original and unpublished and is not being considered for publication elsewhere. *Anal. Chim. Acta* accepts papers in English only. There are no page charges. Manuscripts should conform in layout and style to the papers published in this issue. See inside back cover for "Information for Authors".

Publication. *Analytica Chimica Acta* appears in 16 volumes in 1994 (Vols. 281-296). *Vibrational Spectroscopy* appears in 2 volumes in 1994 (Vols. 6 and 7). Subscriptions are accepted on a prepaid basis only, unless different terms have been previously agreed upon. It is possible to order a combined subscription (*Anal. Chim. Acta* **and** *Vib. Spectrosc.*).
Our p.p.h. (postage, packing and handling) charge includes surface delivery of all issues, except to subscribers in the U.S.A., Canada, Australia, New Zealand, China, India, Israel, South Africa, Malaysia, Thailand, Singapore, South Korea, Taiwan, Pakistan, Hong Kong, Brazil, Argentina and Mexico, who receive all issues by air delivery (S.A.L.-Surface Air Lifted) at no extra cost. For Japan, air delivery requires 25% additional charge of the normal postage and handling charge; for all other countries airmail and S.A.L. charges are available upon request.

Subscription orders. Subscription prices are available upon request from the publisher. Subscription orders can be entered only by calendar year and should be sent to: Elsevier Science B.V., Journals Department, P.O. Box 211, 1000 AE Amsterdam, The Netherlands. Tel: (+31-20) 5803 642, Telex: 18582, Telefax: (+31-20) 5803598, to which requests for sample copies can also be sent. Claims for issues not received should be made within six months of publication of the issues. If not they cannot be honoured free of charge. Readers in the U.S.A. and Canada can contact the following address: Elsevier Science Inc., Journal Information Center, 655 Avenue of the Americas, New York, NY 10010, U.S.A. Tel: (+1-212) 6333750, Telefax: (+1-212) 6333990, for further information, or a free sample copy of this or any other Elsevier Science journal.
Advertisements. Advertisement rates are available from the publisher on request.

US mailing notice - Analytica Chimica Acta (ISSN 0003-2670) is published 3 times a month (total 42 issues) by Elsevier Science B.V. (Molenwerf 1, Postbus 211, 1000 AE Amsterdam). Annual subscription price in the USA US$ 3035.75 (valid in North, Central and South America), including air speed delivery. Second class postage paid at Jamaica, NY 11431. *USA Postmasters*: Send address changes to Anal. Chim. Acta, Publications Expediting, Inc., 200 Meacham Av., Elmont, NY 11003. Airfreight and mailing in the USA by Publication Expediting.

ANALYTICA CHIMICA ACTA

An international journal devoted to all branches of analytical chemistry
Revue internationale consacrée à tous les domaines de la chimie analytique
Internationale Zeitschrift für alle Gebiete der analytischen Chemie

Anal. Chim. Acta, Vol. 286 (1994)

ELSEVIER, Amsterdam–London–New York–Tokyo

ANALYTICA CHIMICA ACTA
VOL. 286 (1994)

ANALYTICA CHIMICA ACTA

An international journal devoted to all branches of analytical chemistry

(Full texts are incorporated in CJELSEVIER, a file in the Chemical Journals Online database available on STN International; Abstracted, indexed in: Aluminum Abstracts; Anal. Abstr.; Biol. Abstr.; BIOSIS; Chem. Abstr.; Curr. Contents Phys. Chem. Earth Sci.; Engineered Materials Abstracts; Excerpta Medica; Index Med.; Life Sci.; Mass Spectrom. Bull.; Material Business Alerts; Metals Abstracts; Sci. Citation Index)

VOL. 286 NO. 1 CONTENTS FEBRUARY 10, 1994

Papers presented at the International Symposium entitled Issues and Controversy: The Measurement of Crystalline Silica, Cambridge, MA, USA, August 20–21, 1992

0003-2670/94/$07.00

SPECIAL ISSUE

PAPERS PRESENTED AT THE INTERNATIONAL SYMPOSIUM ENTITLED ISSUES AND CONTROVERSY: THE MEASUREMENT OF CRYSTALLINE SILICA, CAMBRIDGE, MA, USA, AUGUST 20–21, 1992

Analytica Chimica Acta, 286 (1994) 1
Elsevier Science B.V., Amsterdam

FOREWORD

Crystalline silica is ubiquitous. It is present throughout the environment, not only in nature but also in many raw materials and consumer items. On the one hand, it is an essential component of many essential products and technologies; on the other hand, it can constitute a health hazard.

It has been known for many years that prolonged exposure to crystalline silica dust such as experienced in mining environments can cause silicosis, a noncancerous lung disease. More recent studies have indicated that crystalline silica may also be a carcinogen. Consequently, regulations related to the use of and exposure to crystalline silica have been implemented. For example, in the United States of America crystalline silica has been regulated under the Occupational Safety and Health Administration's (OSHA) Hazard Communication Standard (HCS). Under these regulations, businesses that use materials containing 0.1% or more of crystalline silica must follow guidelines concerning communication and training related to the hazards associated with it. Accordingly, it is very important that there be a clear understanding of what is and is not crystalline silica as well as methods used to identify and quantify it in a wide range of raw materials, products, environments and matrices.

In August, 1992, an international symposium entitled, *Issues and Controversy: the Measurement of Crystalline Silica*, was held in Cambridge, MA, USA under the sponsorship of The Crystalline Silica Panel of The Chemical Manufacturers Association and the cosponsorship of the American Industrial Hygiene Association, US Bureau of Mines, Ceramic Industry Magazine, The Clay Minerals Society, Occupational Safety and Health Administration and the Sorptive Minerals Institute. The technical program focused primarily on analytical methodologies for the determination of crystalline silica in different matrices. The program included review lectures on x-ray diffraction, chemical methods, infrared methods and microscopy. Research papers emphasized a variety of analytical methodologies including those mentioned above as well as nuclear magnetic resonance spectroscopy, thermal methods, Fourier transform infared spectroscopy and electron microscopy. Presentations also emphasized matrix-specific needs when making quantitative determinations in a variety of materials such as minerals, powdered carbonate, clays, dusts, and ceramic fibers. There were also more general lectures by representatives from government laboratories including the National Institute for Standards and Technology and the Mine Safety and Health Administration.

Analytica Chimica Acta is pleased to feature papers from this important symposium in this issue. It is hoped that this issue will be beneficial to those already working in the area and will alert others to challenging problems that remain to be resolved in this important area.

Harry L. Pardue

SSDI 0003-2670(93)E0694-3

Analytica Chimica Acta, 286 (1994) 3–7
Elsevier Science B.V., Amsterdam

Chemical methods of analysis for crystalline silica

A critical literature review

William J. Miles

Bentonite Corporation, 1999 Broadway, Denver, CO 80202 (USA)

Robert D. Hamilton

Schuller International, Inc., Mountain Technical Center, P.O. Box 625005, Littleton, CO 80162-5005 (USA)

(Received 11th November 1992; revised manuscript received 16th February 1993)

Abstract

This literature review addresses the significant chemical and physical methods that have been developed for the analysis of the environmentally or commercially significant polymorphs of crystalline silica: quartz, cristobalite and tridymite. It is a brief summary of a more extensive literature review of the chemical methods of analysis for crystalline silica presented at the Chemical Manufacturers Association Crystalline Silica Panel Workshop on November 18, 1991 and their International Symposium in August 20–21, 1992.

Keywords: Crystalline silica; Review

In 1987, the International Agency for Research on Cancer (IARC) classified crystalline silica as a probable carcinogen. As a result of this classification, crystalline silica became a regulated substance in bulk materials under the Hazard Communication Standard (HCS) [1]. Since this standard requires hazard warning for carcinogens at a threshold of 0.1% concentration in materials found in the workplace, reliable analytical methods are required for measuring crystalline silica at this very low concentration in bulk materials. These methods must also distinguish the polymorphs of crystalline silica from each other for other regulatory requirements. This paper reviews the relevant chemical methods for identification, isolation, concentration and quantification of crystalline silica.

Correspondence to: W.J. Miles, Bentonite Co., 1999 Broadway, Denver, CO 80202 (USA).

The structure of the crystalline forms and morphology of amorphous phases of silica directly influence the reactivity and reaction rates of each form with the various acids and bases that are presented in this literature review. Previous reviews of analytical methods for determination of crystalline silica have been published by McGlinn [2] in 1968, Anderson [3] in 1975 and Babyak and Kaschak [4] in 1978. Drees et al. [5,6] have published informative chapters about the occurrence of polymorphs of silica in the first (1977) and second (1989) editions of "Minerals in Soil Environments". Iler [7] published a thorough treatise in 1979 entitled "The Chemistry of Silica: Solubility, Polymerization, Colloid and Surface Properties, and Biochemistry".

In general, the crystalline forms of silica are less reactive with the majority of these reagents while silicate minerals, amorphous silicas and opal silica hydrates are more reactive.

SSDI 0003-2670(93)E0198-G

The surface area of ground silica directly influences the reaction rates that each polymorph has with the various acids and bases used for chemical determination. As particle size decreases, the surface area of the substance increases and surface area controlled kinetics can become significant in < 5 μm respirable dusts. In addition, biogenic amorphous silicas may exhibit relic structures related to their biological origin which have much larger surface areas than crystalline silicas of igneous origin, creating the potential for accelerated reaction rates.

Many authors, Alexian [8], Sakabe et al. [9] and Stober and Arnold [10], reported amorphous or "disturbed" layers on the surface of quartz. The disturbed layer was found to be as high as 35% by Ganischenko et al. [11] and Koopmans and Rieck [12], when quartz was intensely pulverized in water. Holt and King [13], and O'Connor and Chang [14] reported that this amorphous layer can be a major source of error in chemical methods that are sensitive to differences in reactivities of amorphous and crystalline silicas and silicates.

Separation of the polymorphs of crystalline silica from each other is possible by heavy media sink-float methods that rely on differences in density of minerals. Henderson et al. [15,16], Jones and Beavers [17], Rovner [18], and Francis and Tamura [19] reported that quartz can be separated from cristobalite; cristobalite can be separated from tridymite; however, tridymite cannot be separated from opal and other amorphous silicas. When other silicate minerals are also present, quartz cannot be separated from them except in unusual situations. Density separations are best used as concentration techniques prior to other analytical techniques for crystalline silica.

Chemical methods rely on the solubility of amorphous silica, silicate minerals and non-silicate minerals in a variety of solvents, acids and bases with respect to relatively inert crystalline silica. Chemical methods also include differences in reactivity in high temperature fusions with strong bases. The methods that rely on the reactivity of crystalline and amorphous silica in the presence of silicates and other minerals are destructive so that the polymorph of silica cannot be identified with certainty and quantified thereby failing to satisfy regulatory requirements.

Chemical methods based on the reactivity of crystalline silica

Amorphous and crystalline polymorphs of silica are soluble in hydrofluoric acid and solutions of ammonium fluoride and strong bases such as sodium hydroxide [20]. These methods are based on differences in reaction rates of the various silicas and silicates. Consequently, they do not adequately distinguish between amorphous and crystalline silica or silicates.

Basic catechol (1,2-dihydroxybenzene) solutions also dissolve silica and are the basis of several methods for analyzing silica [21–24]. There is extensive data on the rates of dissolution of different forms of silica in dilute alkali with catechol; however, selectivity between the various forms is poor.

Fusion of silica with potassium bicarbonate and potassium chloride has been extensively evaluated by Polezhaev [25,26] and Dobreva [27]. The silica is converted into a water soluble alkaline silicate while other silicates remain unreacted under experimental conditions. Unfortunately volcanic glasses and feldspars also react in the fusion and can give elevated results for crystalline silica concentrations without distinguishing the polymorph of silica.

Chemical methods based on inertness of crystalline silica

Chemical methods of analysis that concentrate unreacted crystalline silica have the potential for identification and distinction of silica polymorphs by other techniques. Although these methods currently lack the required sensitivity to determine the polymorphs of crystalline silica at the regulatory threshold of 0.1% concentration in bulk materials, they do have the potential to extend the sensitivity of other analytical methods which can quantitatively distinguish the different polymorphs to meet regulatory requirements. For example, the OSHA laboratory in Salt Lake City is currently using a modification of NIOSH Meth-

od 7601 to remove certain interfering silicate minerals prior to x-ray diffraction analysis.

Several chemical methods rely on the greater reactivity of silicate minerals and concentrate the polymorphs of crystalline silica in a residue. These methods warrant further investigation to determine if separation methods can be refined enough to isolate crystalline silica at a 0.1% detection limit. Even if these methods do not distinguish amorphous silica from crystalline silica, they may serve as concentration techniques for subsequent spectroscopic or x-ray diffraction analysis.

The first method is based on digestion of silicate minerals in pyrophosphoric acid at 240°C for a controlled period of time. Many studies have been reported [28–37]. Digestion of silicates in refluxing phosphoric acid was refined and published as NIOSH Analytical Method 7601 [38]. This method suffers from incomplete dissolution of many silicates and amorphous silicas, and significant dissolution of very fine crystalline silica in the phosphoric acid digestion process.

These partially or completely insoluble silica and silicate minerals create positive interferences and errors unless the mineralogy is completely identified and appropriate corrections are made. Amorphous silicas of biogenic and volcanic origin are particularly slow to react with refluxing phosphoric acid and incompletely dissolve in the digestion process under recommended reaction conditions. Jones et al. [39] and Jones and Segnit [40], have studied the opal silicas and have named three distinct phases as opal A, opal CT and opal C. Structural water is present in opal as hydroxyl groups attached to silicon in concentrations typically ranging from 2 to 9%, differing significantly from crystalline silica in chemistry. The opals exhibit almost complete reactivity and solubility in refluxing phosphoric acid under the conditions specified in NIOSH Method 7601, distinguishing them from quartz and cristobalite of high temperature origin. Crystalline silicas exhibit low solubilities in refluxing phosphoric acid of approximately 10% for quartz and 20% for cristobalite respirable sized particles.

The second chemical analytical method is based on fusion of dusts and bulk samples with potassium pyrosulfate. Trotsel and Wynne [41], Chapman et al. [42] and Cummings et al. [43] have studied this system. Although there is very little information in the literature concerning this method, the silicate minerals react to form soluble products, while quartz, cristobalite, tridymite and opal are left as an insoluble residue.

A third chemical method is based on the work of Schekaturina et al. [44] and Schekaturina and Petrasken [45] which studied the reactivity of silicate minerals with refluxing sodium sulfide solution. The forms of crystalline silica are reported to be insoluble in this reagent. The literature does not provide much information about this method.

Goldman [46] and Knopf [47] used hydrofluorosilica acid for the dissolution of silicates in the presence of quartz. Line and Aradine [48] used fluoroboric acid for the removal of silicate minerals from quartz. These acids are not very selective in their reaction with silicate minerals and dissolve significant quantities of crystalline silica. Perhaps the greatest problem with these techniques is that reaction times of up to a week at ambient or lower temperatures are required to prevent formation of HF with subsequent loss of selective reactivity.

Evaluation of NIOSH Method 7601

When applying NIOSH Analytical Method 7601 to the analysis of respirable dust and bulk samples, a detailed understanding of the dust being sampled is critical for interpretation of results. There are a number of silicate minerals that are incompletely dissolved in the phosphoric acid digestion process that contribute positive interferences to crystalline silica analysis unless they are detected and appropriate corrections are applied.

In addition to silicates, amorphous silicas of both volcanic and biogenic origin including hydrous and anhydrous volcanic glasses and biogenic opal from plants and diatoms are incompletely dissolved in the NIOSH Method 7601 phosphoric acid digestion process. When present in significant quantities, total crystalline silica, as determined colorimetrically by NIOSH Method 7601, may be as much as an order of magnitude too high.

The digestion residues of amorphous silicas of biogenic and volcanic origin contain concentrates of the crystalline silica associated with the original phases. When these residues are evaluated by x-ray diffraction techniques such as NIOSH Method 7500 [49], their sensitivity can be extended due to the concentration of the crystalline silica.

Diagenetic opal, with only short range order similar to cristobalite, is completely dissolved by the phosphoric acid digestion process. In this respect, its solubility in phosphoric acid is completely different from cristobalite formed at temperatures above 1000°C. This dramatic difference in solubility is due to the different chemistry of hydrated silica with respect to anhydrous crystalline silica and may provide a direct method for distinguishing these materials from each other, rather than a subjective judgment based on apparent similarities of crystallinity as determined by x-ray diffraction methods.

Excessive grinding of crystalline silica causes amorphous surfaces, amorphous milling debris, more soluble disturbed surfaces of the silica and a significantly greater proportion of soluble fine particles of crystalline silica. Excessive grinding can result in artificially low values for crystalline silica when determined by NIOSH Method 7601.

REFERENCES

1 IARC Monograph on the Evaluation of the Carcinogenic Risk of Chemicals to Humans: Silica and Some Silicates, International Agency for Research on Cancer, Vol. 42, Lyon, 1986.
2 J. McGlinn, A review of Physical and Chemical Methods for the Determination of Quartz, Proceedings of the First Australian Pneumoconiosis Conference, Joint Coal Board, Sydney, 1968, pp. 529–541.
3 P.L. Anderson, Free Silica Analysis of Environmental Samples – A Critical Literature Review, Am. Ind. Hyg. Assoc. J., 36 (1975) 767–776.
4 B.S. Babyak and B.S. Kashak, Free Silica – A Bibliography, Industrial Health Foundation, Pittsburgh, PA, 1978.
5 L.R. Drees, L.P. Wilding, N.E. Smeck and A.L. Senkayi, in J.B. Dixon and S.B. Weed (Eds.), Silica in Soils: Quartz, Cristobalite, Tridymite, and Opal, Minerals in Soil Environments, Soil Science of America, Madison, WI, 1977, Chap. 14, pp. 471–572.
6 L.R. Drees, L.P. Wilding and N.E. Smeck, in J.B. Dixon and S.B. Weed (Eds.), Silica in Soils: Quartz and Disordered Silica Polymorphs, Minerals in Soil Environments, Soil Science of America, Madison, WI, 2nd edn., 1989, Chap. 19, pp. 913–974.
7 R.K. Iler, The Chemistry of Silica: Solubility, Polymerization, Colloid and Surface Properties, and Biochemistry, Wiley, New York, 2nd edn., 1979.
8 C. Alexian, C.R. Acad. Sci., 242 (1956) 2145.
9 H. Sakabe, K. Koshi, K. Matsushima and I. Shima, Bull. Nat. Inst. Ind. Health, 1 (1958) 3.
10 W. Stober and M. Arnold, Beitr. Silikose-Forsch. Sonderb., 4 (1960) 73.
11 L.G. Ganischenko, M.M. Egorov, V.F. Kiselev, K.G. Krasilnikov and G.S. Khodakova, Dokl. Akad. Nauk. S.S.S.R., 131 (1960) 597 (Engl. trans., 1960, p. 275).
12 M. Koopmans and G.D. Rieck, Br. J. Appl. Phys. Res., 16 (1965) 1913.
13 P.F. Holt and D.T. King, Nature, Phys. Sci., 175 (1955) 514; P.F. Holt and D.T. King, J. Chem. Soc., (1955) 773.
14 B.H. O'Connor and W.J. Chang, The Amorphous Character and Particle Size Distributions of Powders Produced with the Micronizing Mill for Quantitative X-ray Powder Diffractometry, X-Ray Spectrosc., 15 (1986) 267–270.
15 J.H. Henderson, M.L. Jackson, J.K. Syers, R.N. Clayton and R.W. Rex, Cristobalite Authigenic Origin in Relation to Montmorillonite and Quartz Origin in Bentonites, Clays Clay Miner., 19 (1971) 229–238.
16 J.H. Henderson, R.N. Clayton, M.L.Jackson, J.K. Syers, R.W. Rex, J.L. Brown and I.B. Sachs, Cristobalite and Quartz Isolation from Soils and Sediments by Hydrofluosilicic Acid Treatment and Heavy Liquid Separation, Soil Sci. Soc. Am. Proc., 36 (1972) 830–835.
17 R.L. Jones and A.H. Beavers, Aspects of Catenary and Depth Distribution of Opal Phytoliths in Illinois Soils, Soil Sci. Soc. Am. Proc., 28 (1964) 413–416.
18 I. Rovner, Potential of Opal Phytoliths for Use in Paleoecological Reconstruction, Quat. Res., 1 (1971) 343–359.
19 C.W. Francis and T. Tamura, An evaluation of Zonal Centrifugation as a Research Tool in Soil Science: II. Characterization of Soil Clays, Soil Sci. Soc. Am. Proc., 36 (1972) 372–376.
20 R.L. Jones, Determination of Opal in Soil by Alkali Dissolution Analysis, Soil Sci. Soc. Am. Proc., 33 (1969) 976–978.
21 R.H. Doremus, F. Alim-Marvasti, E.K. Pavelchek and R.H. Doremus, U.S. N.T.I.S., AD Rep. (1973) 762767, Washington, DC, (available from NTIS).
22 R. Bach and H. Sticher, Experientia, 22 (1966) 515.
23 H. Baumann, Beitr. Silikose-Forsch., 85 (1965) 15–26; Sonderb., 6 (1963) 49 (C.A., 64, 5812, 5813, 5666 (1965)).
24 H. Baumann, W. Klosterkotter and K. Robock, Silicoseber. Nordrhein-Westfalen, 6 (1967) 33.
25 N.G. Polezhaev, Gig. Sanit., 22 (1957) 91.
26 N.G. Polezhaev, New Method of Determination of Free Silica in Presence of Silicates, Opredelenie Svobodnoi Dvuokisi Kremniya v Gorn. Porodakh i Rudn. Pyli, Akad. Nauk. S.S.S.R., Inst. Gorn. Dela. Svornik Statei (1958) 33.

27 M. Dobreva, Chemical Micromethod for Quantitative Determination of Free Crystalline Silica in Finely Dispersed Industrial Dusts, Assoc. Occup. Hyg., 18 (1975) 121–127.
28 H. Hirsch and W. Dawihl, Action of Phosphoric Acid on Ceramic Raw Materials as Well as Calcined Products and a New Method for the Rational Analysis of Clays, Ber. Deutscher. Keram. Ges., 13 (1932) 54.
29 R. Rieke, Ber. Deut. Keram. Ges., 21 (1940) 447.
30 W. Stiger, Determination of Free Silicic Acid, Staub., 28 (1946) 217.
31 T.M. Durkan, Determination of Free Silica in Industrial Dusts, J. Ind. Hyg. Toxicol., 28 (1946) 217–228.
32 N.A. Talvitie, Determination of Quartz in the Presence of Silicates Using Phosphoric Acid, Anal. Chem., 23 (1951) 623–626.
33 G.H. Edwards, Comparison of X-Ray Diffraction, Chemical (Phosphoric Acid), and Dispersion Staining Methods for the Determination of Quartz in Dusts, Am. Ind. Hyg. Assoc. J., 26 (1965) 532–536.
34 C.M. Jephcott, Determination of Quartz of Various Particle Sizes in Quartz-Silicate Mixtures, Arch. Ind. Hyg., 11 (1955) 425.
35 N.A. Talvitie and F. Hyslop, Colorimetric Determination of Siliceous Atmospheric Contaminants, Am. Ind. Hyg. Assoc. J., 19 (1958) 54–58.
36 N.A. Talvitie, Determination of Free Silica. Gravimetric and Spectrophotometric Procedures Applicable to Airborne and Settled Dust, Am. Ind. Hyg. Assoc. J., 25 (1964) 169–178.
37 D.V. Sweet, F.R. Wolowicz and J.V. Crable, Spectrometric Determination of Free Silica, Am. Ind. Hyg. Assoc. J., 34 (1973) 500–506.
38 P.M. Miller (Ed.), NIOSH Method 7601: Silica, Crystalline, Manual of Analytical Methods, DHHS Publication 84–100, 3rd edn., 1984.
39 J.B. Jones, J.V. Sanders and E.R. Segnit, Structure of Opal, Nature, 204 (1964) 990–991.
40 J.B. Jones and E.R. Segnit, The Nature of Opal. I. Nomenclature and Constituent Phases, Geol. Soc. Aust. J., 18 (1971) 57–68.
41 L.J. Trotsel and D.J. Wynne, Determination of Quartz (Free Silica) in Refractory Clays, J. Am. Ceram. Soc., 23 (1940) 18–22.
42 S.L. Chapman, J.K. Syers and M.L. Jackson, Quantitative Determination of Quartz in Soils, Sediments and Rocks by Pyrosulfate Fusion and Hydrofluosilicic Acid Treatment, Soil Sci., 107 (1969) 348–355.
43 W.M. Cummings, P.B. Dempster and P.D. Ritchie, Physico- Chemical Study on Dusts: IV. Accuracy of Chemical Estimation of Free Silica in Rocks and Mineral Dusts, J. Appl. Chem., 2 (1952) 658.
44 L.G. Schekaturina, J.P. Kondratova and V.I. Petrashen, Determination of Free Silicon Dioxide (Quartz) in Ores and Ore Dusts of the Eastern Donets Basin, Trudy Novocherkassk. Politekh. Inst., 31 (1955) 79.
45 L.G. Schekaturina and V.I. Petrashen, Determination of Free Silica in Coal Dust, S. Ordzhonikdze Polytech. Inst. Novocherkassk, Opredenie Svobodnoi Dvuokisi Kremniya v Gorn. Porodakh i Rudn. Pyli, Akad. Nauk. S.S.S.R. (1958) 54.
46 F.H. Goldman, Hydrofluosilicic Acid Method for the Determination of Quartz, Ind. Eng. Chem., Anal. Ed., 13 (1941) 789.
47 A. Knopf, U.S. Public Health Report, No. 48 (1933) 183.
48 W.R. Line and P.W. Aradine, Determination of Quartz in Presence of Silicates, Ind. Eng. Chem., Anal. Ed., 9 (1937) 60.
49 P.M. Miller (Ed.), NIOSH Method 7500: Measurement of Respirable Crystalline Silica Using X-ray Powder Diffraction, Manual of Analytical Methods, DHHS Publication 84–100, 3rd edn., 1984. Revised 1989.

Analytica Chimica Acta, 286 (1994) 9–23
Elsevier Science B.V., Amsterdam

The identity, development and quantification of phases in devitrified, commercial-grade, aluminosilicate, refractory ceramic fibres: an x-ray powder diffractometry study

J.J. Laskowski [1], J. Young *, R. Gray, R. Acheson, S.D. Forder

Applied Physics and Materials, Materials Research Institute, Sheffield Hallam University, Sheffield S1 1WB, UK

(Received 21st August 1992; revised manuscript received 7th December 1993)

Abstract

Aluminosilicate, refractory ceramic fibres devitrify to form cristobalite and mullite in high-temperature applications. The identity of phases and their development with temperature and time has been determined using x-ray powder diffractometry, and the internal standard method with fluorite reference and mullite, β-cristobalite and amorphous standards, has provided phase quantification. The formation of mullite and cristobalite as a function of exposure temperatures and times are mapped, and the presence of β-, α- and disordered cristobalite and of tridymite and α-quartz are confirmed in samples measured at room temperature. The authors are confident that well-developed cristobalite and mullite phases can be quantified and fibres devitrified at 1400°C for greater than 50 h exposure contained (51 ± 2) wt-% mullite and (36 ± 2) wt-% β-cristobalite with the remainder being attributed to other silica phases and remnant glass.

Keywords: X-ray diffraction; Aluminosilicate; Ceramics; Fibres; Refractory ceramic fibres; Silica

1. Introduction

Commercially-available, aluminosilicate, refractory ceramic fibres are manufactured with specific proportions of alumina and silica and also, for certain products, with additional oxide components to improve their high temperature performance. The products are mainly produced by melting the raw materials together in an arc furnace at about 1800°C and fiberizing the melt stream by blowing with high pressure gas or steam, or by spinning. The resulting bulk fibre may be processed to produce a variety of secondary products, including blanket, modular, board and sprayed forms, and used for high-temperature insulation, fire-protection, refractory and engineering applications [1,2].

The fibres are vitreous when first manufactured but subsequent heating to temperatures

* Corresponding author.

[1] Jerry Laskowski, a research assistant and PhD student in the School of Science at Sheffield Hallam University, completed the work for this paper only four weeks before his tragic death in a swimming accident on Saturday 5 September 1992 while on holiday in Malta. He was a researcher of great promise who was well-liked and well-respected by his staff and student colleagues. He remains sadly missed by us all.

SSDI 0003-2670(93)E0680-6

exceeding about 900°C results in their devitrification. For fibres of approximately equal alumina and silica content, the crystallisation products are mullite and cristobalite whereas further oxide components in the original vitreous fibres result in additional crystalline phases, for example zirconia and zircon products in fibres containing zirconia as well as alumina and silica. The resulting crystallisation depends on exposure temperature and time as well as chemical composition and the presence of impurities [3–10].

This study has focused on the phases present when aluminosilicate refractory ceramic fibre of near-equal alumina and silica content has been heat-treated at temperature and time coordinates within the ranges 600 to 1500°C and 2.5 min to 7300 h. This temperature–time domain includes the region of fibre devitrification and the study objectives were to identify the resulting phases, map their development and quantify the phase components. Reported studies [3–10] have not considered a sufficiently wide range of temperature and time coordinates to allow phase development or devitrification threshold conditions to be determined and quantification has not addressed the measurement of the amorphous phase nor the question of the correct forms of the mullite or cristobalite phases [11,12].

In addition to the materials questions posed by the devitrification of fibrous $Al_2O_3 \cdot SiO_2$ glasses, this study is important from the health perspective. Concern has arisen that devitrification of refractory ceramic fibre and the associated formation of cristobalite may pose a health hazard in any subsequent release and inhalation of cristobalite-containing, respirable fibrous dust [9,13]. In this respect, there is interest in the temperature–time threshold for cristobalite formation and in the quantification of cristobalite in the devitrified fibres.

2. Materials and methods

2.1. Fibre samples

Fibre wool samples were prepared for furnace exposure from commercially-available, Standard Grade™ aluminosilicate fibre blankets manufactured by Morganite Thermal Ceramics Ltd. The manufacturer's data for this product gives a classification temperature of 1260°C, an arithmetic mean fibre diameter of 2–3 μm and chemical analysis of Al_2O_3, 43–47 wt-%; SiO_2, 53–57 wt-%; further oxide components each of less than 0.02 wt-%; alkalis, 0.20 wt-%, and leachable chlorides, < 20 ppm. In comparison, our semi-quantitative analysis by x-ray fluorescence gave 53.3 wt-% for SiO_2 and 46.5 wt-% for Al_2O_3.

2.2. Furnace exposures

Fibres were exposed at selected temperature and time coordinates within the ranges 600 to 1500°C and 2.5 min to 7300 h under atmospheric conditions in a laboratory muffle or tube furnace. The samples were introduced into the hot furnace, exposed in alumina or platinum crucibles, removed from the hot furnace and cooled in air. Furnace temperatures were calibrated and measured using Pt/Pt–13% Rh thermocouples.

2.3. Qualitative analysis

Analysis of furnace-exposed fibres to determine the identity and development of phases was mainly undertaken at room temperature using a Philips x-ray powder diffractometer. This system had a type PW 1710 controller, type PW 1830 x-ray generator fitted with long, fine-focus copper tube and type PW 1820 goniometer with graphite monochromator. The system was personal computer controlled using the Philips APD version 3.0 software. Samples were ground to a fine powder by pestle and mortar, well mixed by thorough shaking and compacted into the front-loading diffractometer specimen holder. The holder was rotated during exposure and diffraction data plots were obtained under the following conditions: Cu$K\alpha$ radiation (35 kV, 45 mA); 2θ-range 15 to 40° (5.91 to 2.25 Å), scan speed 0.5° of 2θ per min, 1° divergence slit, 0.2° receiving slit and 1° scatter slit. For qualitative analysis, data plots were analysed and interpreted using APD software to provide d-spacing, relative intensity, and peak profile data. Backgrounds were normally

subtracted using the parabolic background facility and crystalline phases were identified by comparison with the standard data of the JCPDS Powder Diffraction File.

An x-ray powder diffractometer fitted with a variable temperature cell and a differential scanning calorimeter aided in determining the form of cristobalite observed at room temperature in the devitrified fibres. The aim was to determine whether or not the displacive transformation, observed on heating α-cristobalite through 270°C, was seen when the devitrified fibres were heated through this temperature. No transformation would infer β-cristobalite at room temperature, whereas α-cristobalite at room temperature would be indicated by detection of this transformation [14].

The variable temperature, x-ray powder diffractometry was undertaken using a modified Philips powder diffractometer type PW 1050 fitted to a Philips x-ray generator type PW 1130. The diffractometer had a non-ambient, environmental cell manufactured by GTP Engineering and a stepping motor. Control was by a Philips PW 1710 controller and analysis was provided by the VMS version of the Philips APD software. Well-shaken samples were compacted into the sample holder and diffraction data plots were obtained at 20 and 400°C using Cu$K\alpha$ radiation, a scan speed of 1° 2θ per min and a 2θ-range from 20 to 40°.

The differential scanning calorimetry was undertaken using a Mettler type TA3000 system comprising type DSC30 cell and type TC10A processor. Approximately 25 mg of fibre sample was compacted and sealed in the standard aluminium crucible and heating scans were undertaken from 0 to 400°C at a rate of 10 K min^{-1}.

Three samples were analysed in each case: a control sample of α-cristobalite manufactured by devitrifying colloidal silica at 1200°C for 3 h; a control sample of β-cristobalite manufactured by devitrifying stuffed colloidal silica under similar conditions, and a sample of the Standard Grade™ fibres devitrified by heating at 1200°C for 48 days and containing approximately 30 wt-% of cristobalite. It was confirmed practically with the aid of standard samples that for both techniques a concentration of at least 5 wt-% cristobalite would be detected, this level of detection applying to the peaks at d-spacing 0.314 nm, (111) in the x-ray diffractometer case for α-cristobalite.

2.4. Quantitative analysis

Quantitative analysis was undertaken by x-ray powder diffractometry using the internal standard method and room temperature, x-ray powder diffractometer described above. The internal standard method [15,16] requires a reference material to be added in the same proportions to each and every sample and enables each of the separate phases ($i = 1, 2, 3$, etc.) within a sample to be quantified according to the following equation:

$$\frac{I_i}{I_r} = K_i w_i$$

where I_i = integrated peak intensity for analysis peak(s) chosen for phase i, I_r = integrated peak intensity for analysis peak(s) chosen for reference material, K_i = calibration constant for phase i, and w_i = weight fraction of phase i in the sample discounting the reference material.

The reference material used for all measurements was precipitated fluorite (CaF_2) powder of approximately 3.5 μm mean particle size. The material was always taken from the same source bottle following a thorough shaking of the bottle using a turbula shaker and then added to each sample to provide 20% of the final mass. Prior to compaction in the front-loading sample holder, the mixture was thoroughly shaken but it is accepted that the combination of a fine powder of fibres and a fine powder of particles may lead to some subsequent separation of the fibre and particulate forms.

In terms of the size of the diffracting crystallites, it is noted that the critical issue is the sub-micron-sized crystallites within the micron-diametered fibres although the existence of the fibrous form in the ground powder could clearly lead to orientation effects as were observed, and accounted for, in the results for mullite. The internal standard method was chosen to enable

compensation for likely variations in instrumental and specimen factors, notably powder compaction and specimen height.

Calibration graphs showing the relationship between the intensity ratio, I_i/I_r, and weight fraction (expressed in percentage terms), w_i, were obtained for mullite ($3Al_2O_3 \cdot 2SiO_2$), β-cristobalite and amorphous phases using calibration standards. The associated calibration constants, K_i, were obtained from these results.

The mullite calibration standard was prepared from Fibermax Bulk Fibre™, a polycrystalline mullite fibre of 2–3.5 μm arithmetic mean fibre diameter manufactured by Carborundum Resistant Materials. The bulk fibre was lightly ground to a fine powder and, to remove a glassy component, heat treated at 1500°C for 12 h and subsequently cooled in air. The resulting x-ray powder diffractometer data plots (Fig. 1a) show good crystalline peaks, no detectable amorphous component and a good match, in terms of d-spacing and relative intensity, to the JCPDS PDF 15-776 data for mullite. There is confidence from practical analysis that the resulting mullite has a purity greater than 90%.

The β-cristobalite calibration standard was prepared from colloidal silica particles type Nalco™ 1034A supplied by Nalco Colloidal Silicas. This vitreous silica was converted to β-cristobalite [17,18] by (a) mixing the silica particles with nitrates of aluminium and calcium ($Al(NO_3)_3 \cdot 9H_2O$; $Ca(NO_3)_2$) to achieve the molar ratios of SiO_2–Al_2O_3–CaO (38:1:1), (b) heating and mixing this solution in a beaker to drive off water, (c) heating the residue in a platinum crucible for 3 h at 1200°C, and (d) air cooling. Resulting x-ray powder diffractometer data plots (Fig. 1b) showed no amorphous component, good crystalline peaks and a good match, in terms of d-spacing and relative intensity, to the JCPDS PDF 27-605 data for β-cristobalite. The resulting particles had an approximate 2 μm mean particle size and there is confidence from practical analysis that the resulting β-cristobalite has a purity greater than 95%.

Two calibration standards were prepared for the amorphous phase: one from the as-manufactured, vitreous Standard Grade™ aluminosilicate

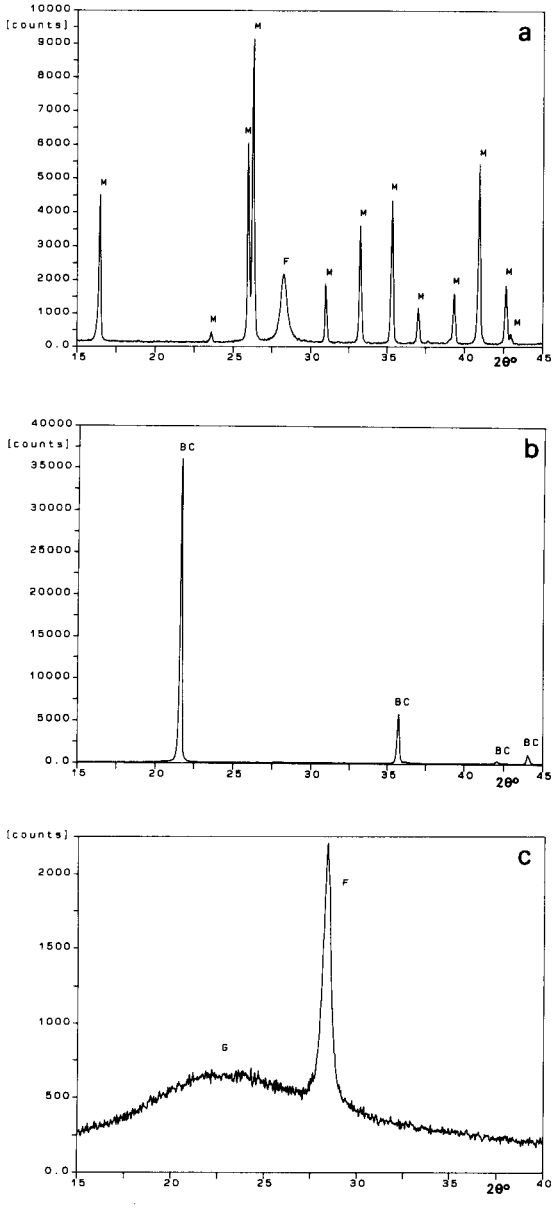

Fig. 1. X-ray powder diffractometer data plots from calibration standards. (a) Mullite calibration standard; (b) β-cristobalite calibration standard; (1) amorphous phase calibration standard. Key: BC = β-cristobalite; F = fluorite; G = glass; M = mullite.

fibres and the other from the Nalco™ type 1034A colloidal silica particles. For the fibrous standard, the Standard Grade™ fibre blanket was lightly ground to a fine powder using pestle and mortar

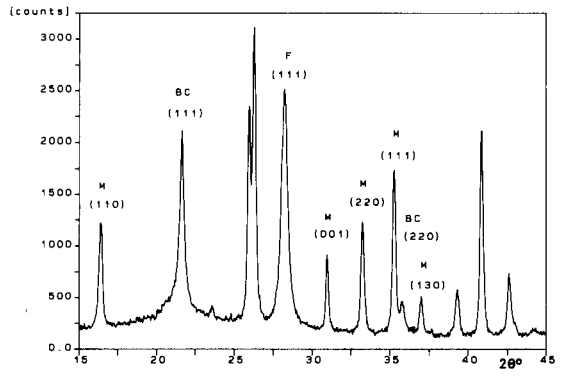

Fig. 2. X-ray powder diffractometry data plot for devitrified Standard Grade™ fibres showing analysis peaks. Key: BC = β-cristobalite; F = fluorite; M = mullite; (hkl).

and the x-ray powder diffractometer data plot for this material is shown by Fig. 1c. A plot of similar form was obtained for the vitreous silica standard.

A set of calibration samples was prepared from these standard materials to enable the calibration graphs and calibration constants to be determined for each of the phases. Each calibration sample contained three standard materials, including one of the amorphous phases, in varying relative proportions together with the reference material.

The powder diffraction peaks chosen for measurement and analysis were the (111), $d = 0.411$ nm and (220), $d = 0.252$ nm peaks for β-cristobalite, the (110) $d = 0.539$ nm, (001) $d = 0.289$ nm, (220) $d = 0.269$ nm, (111) $d = 0.254$ nm and (130) $d = 0.243$ nm peaks for mullite and the (111) $d = 0.315$ nm peak for fluorite. These peaks are identified in Fig. 2 and the choice of 5 peaks for mullite derives from the likelihood of orientation effects with this material [19].

Integrated intensities were determined using the APD software. For the glass phase, the background was first removed with the aid of the constant background facility of the APD software and the integrated intensity measured as the count within a window of 2° of 2θ width centred on the maximum of the amorphous hump. Any overlapping peaks, for example tridymite peaks overlapping cristobalite, demanded profile fitting procedures to separate the analysis peak.

Calibration graphs for β-cristobalite, mullite and the two amorphous phases (Standard Grade™ fibres, SG, and colloidal silica particles, CS) showed good linearity and regression analysis gave the following values for calibration constants and their standard errors:

β-Cristobalite:	$K_{\beta\text{-C}}(111)$	$=(552\pm23)\ 10^{-4}$ wt-%$^{-1}$ (9 Points)
(β-C)	$K_{\beta\text{-C}}(220)$	$=(107\pm4)\ 10^{-4}$ wt-%$^{-1}$ (9 Points)
Mullite:	$K_{M}(110)$	$=(61\pm2)\ 10^{-4}$ wt-%$^{-1}$ (9 Points)
(M)	$K_{M}(001)$	$=(21\pm0)\ 10^{-4}$ wt-%$^{-1}$ (9 Points)
	$K_{M}(220)$	$=(50\pm1)\ 10^{-4}$ wt-%$^{-1}$ (9 Points)
	$K_{M}(111)$	$=(60\pm1)\ 10^{-4}$ wt-%$^{-1}$ (9 Points)
	$K_{M}(130)$	$=(15\pm0)\ 10^{-4}$ wt-%$^{-1}$ (9 Points)
Glass:	K_{SG}	$=(101\pm3)\ 10^{-4}$ wt-%$^{-1}$ (10 Points)
(SG and CS)	K_{CS}	$=(164\pm6)\ 10^{-4}$ wt-%$^{-1}$ (11 Points)

3. Results

3.1. Identity of cristobalite phase

The results obtained by differential scanning calorimetry for Standard Grade™ fibres devitrified at 1200°C for 48 days and the α-cristobalite and β-cristobalite controls are shown by Fig. 3a–c: Fig. 3a for devitrified fibres shows no detectable transition on heating from 0 to 400°C; Fig. 3b for α-cristobalite control indicates an endothermal transition under the same heating conditions, and Fig. 3c for β-cristobalite indicates no detectable transition in this temperature range. These results infer that the cristobalite in the devitrified fibres behaves as the β-form.

Results obtained by x-ray powder diffractometry are shown by Fig. 4a–c. On each figure, the lower plot (A) was obtained at 20°C and the higher (B) at 400°C and, noting necessary corrections for thermal expansion, peaks were identified by comparing measured d-spacing and relative intensity data with standard JCPDS powder diffraction data. The detailed analysis is summarised in Table 1. Fig. 4a for devitrified fibres indicates the presence of β-cristobalite at 20 and 400°C, Fig. 4b for the α-cristobalite control indicates α-cristobalite at 20°C and β-cristobalite at 400°C, and Fig. 4c for the β-cristobalite control

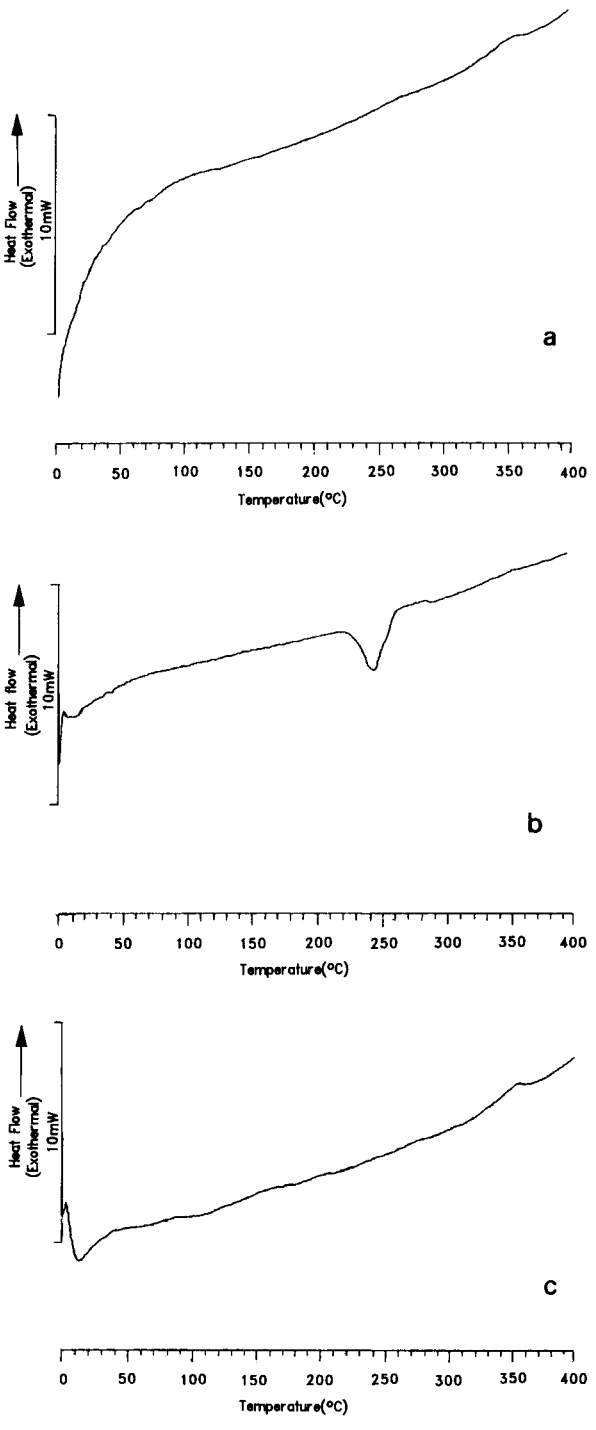

Fig. 3. Results of differential scanning calorimetry for devitrified Standard Grade™ fibres and α- and β-cristobalite controls. (a) Devitrified Standard Grade™ fibres; (b) α-cristobalite control; (c) β-cristobalite control.

indicates β-cristobalite at 20 and 400°C. These results show that the cristobalite in these devitrified fibres has the properties of the β-form.

3.2. Development of amorphous phase

Fig. 5a, which is experimental diffractometer data, illustrates the development with time of the β-cristobalite, mullite and amorphous phases in Standard Grade™ fibres devitrified at 1200°C. Mullite peaks were resolved at the shortest exposure time of 2.5 min, narrowing and increasing in height with time. β-Cristobalite peaks were not observed until 100 h exposure (Fig. 9) and then again they narrowed and increased in intensity with increasing exposure time.

Greater insight into the development of phases was obtained using the Squared-Lorentzian profile fitting facility of the APD software. This facility enabled multiple overlapping peaks to be resolved from experimental data by subtracting trial peaks to obtain a zero remnant. For example, the (110) $d = 0.539$ nm, (120) $d = 0.343$ nm and (210) $d = 0.339$ nm mullite peaks in Fig. 5a could be fitted with associated profiles whereas, as shown by Fig. 5b, the measured (111) $d = 0.411$ nm β-cristobalite peak (1) required three profiles (2, 3 and 4) for a good fit. Profiles 2 and 4 were associated respectively with β-cristobalite and tridymite, and the development of profile 3 as a function of time is presented in more detail by Fig. 5c–e.

Fig. 5c shows the development of profile 3 from the broad amorphous hump observed at shortest exposure times, through a transformation to a sharp, relatively narrow peak after 2256 hour, which then decreased in height with further increase in exposure time. Fig. 5d shows how the decrease in intensity of profile 3 corresponds to an increase in intensity of the β-cristobalite profile (2 in Fig. 5b), and Fig. 5e shows how profile 3 is observed at shorter exposure times and is less prominent at higher fibre devitrification temperatures, here 1500°C. Fig. 6 plots the relationship between the full width at half maximum (FWHM) of profile 3 for fibres devitrified as a function of time at 1200, 1300 and 1400°C. These results indicate a definite transformation in profile 3

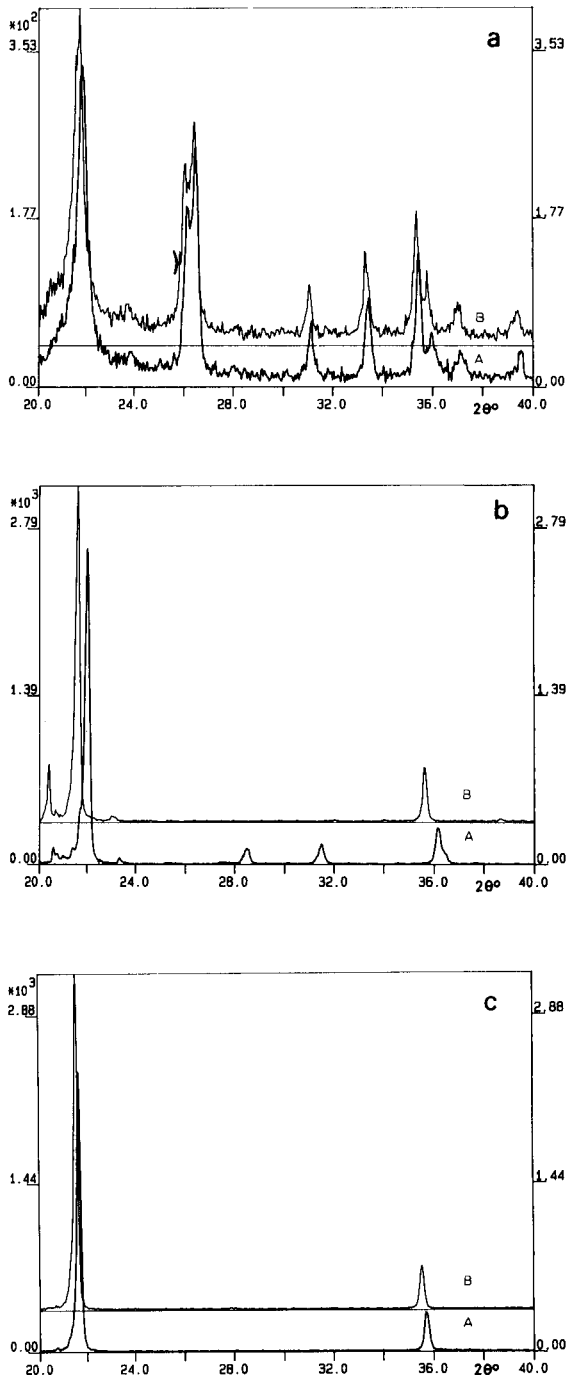

Fig. 4. Results of X-ray powder diffractometry at 20 and 400°C for devitrified Standard Grade™ fibres and α- and β-cristobalite controls. (a) Devitrified Standard Grade™ fibres; (b) α-cristobalite control; (c) β-cristobalite control. Key: A = data plot for 20°C; B = data plot for 400°C.

from a broad amorphous hump at shorter exposure times to the relatively intense narrower peak at longer times. This transformation occurred after exposures of about 100, 50 and 3 h for fibres devitrified respectively at 1200, 1300 and 1400°C. The intense, narrower peak is initially identified as a distinct, pseudo-crystalline phase.

3.3. Development of crystalline phases

Qualitative analysis of x-ray powder diffractometry data indicated, in addition to mullite and β-cristobalite formation, the presence of α-cristobalite and small amounts of tridymite and α-quartz in fibres devitrified under certain exposure conditions. The key analysis peaks employed to determine the existence of these phases were (101) $d = 0.405$ nm and (102) $d = 0.284$ nm for α-cristobalite, (101) $d = 0.343$ nm for α-quartz, and the peak at d-spacing 0.433 nm for S_1 tridymite as identified in Fig. 7a and b. Profile fitting had to be employed to determine the existence of some phases.

Fig. 7a and b shows x-ray powder diffractometry data plots for fibres devitrified, respectively, at 1400°C for 336 h and 1200°C for 336 h. At the higher temperature (Fig. 7a), α-cristobalite and tridymite were detected, whereas trace quartz was indicated by profile fitting. At the lower temperature (Fig. 7b), tridymite and trace quartz were detected but no α-cristobalite was observed. Table 2 shows, for a range of exposure temperatures and times, the result of applying this type of analysis to diffractometry data for a range of exposure temperatures and times, all of which corresponded to the detection of β-cristobalite. In summary, α-cristobalite was only observed at 1500°C and at relatively long exposure times at 1400°C, tridymite was observed at all measurement points except the longer time exposures at 1500°C, and quartz was observed as a trace component at all measured points except longer time exposures at 1500°C.

The development of phases was also typified by the change in width (full-width at half maximum) of analysis peaks as a function of exposure temperature and time. Fig. 8a shows this relation-

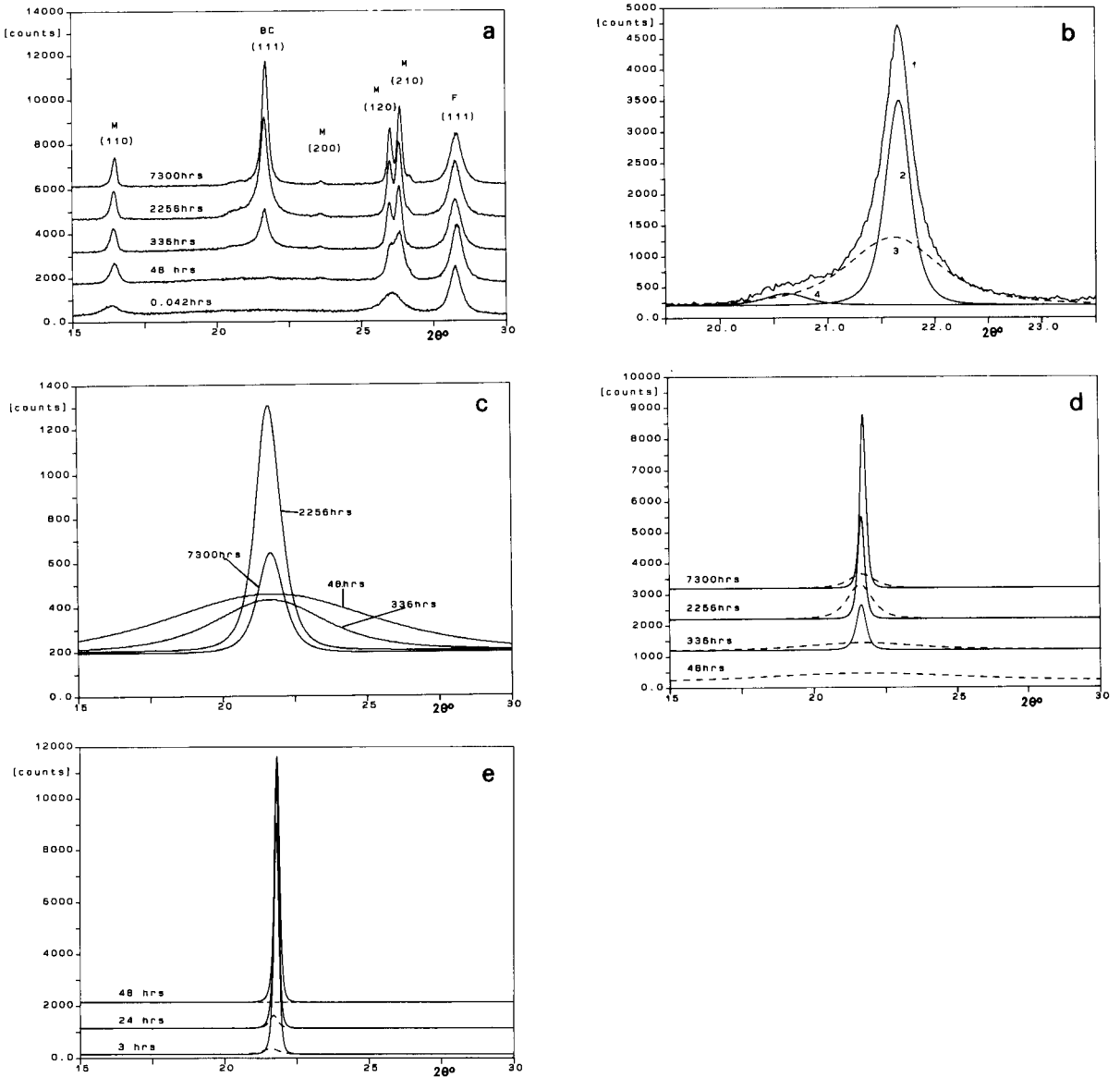

Fig. 5. X-ray powder diffractometry data plots for Standard Grade™ fibres showing development of crystalline and amorphous phases at 1200°C with time. (a) Development of mullite (M), β-cristobalite (BC) and amorphous phases with time; (b) analysis of "2256-h β-cristobalite" peak showing measured peak (1), β-cristobalite hump (2), pseudo-crystalline peak (3) and tridymite peak (4); (c) development of pseudo-crystalline peak from amorphous hump as a function of time; (d) development of β-cristobalite (solid line) from pseudo-crystalline and amorphous phase (dashed line) as a function of time; (e) as (d) but for an exposure temperature of 1500°C. F is fluorite; (hkl).

ship for the (111) $d = 0.411$ nm β-cristobalite peak and indicates, in comparison with the width of the (111) $d = 0.411$ nm peak in the β-cristobalite standard, that a constant and minimum peak width is achieved at a shorter exposure time at 1400°C than at 1200°C. Similar behaviour was

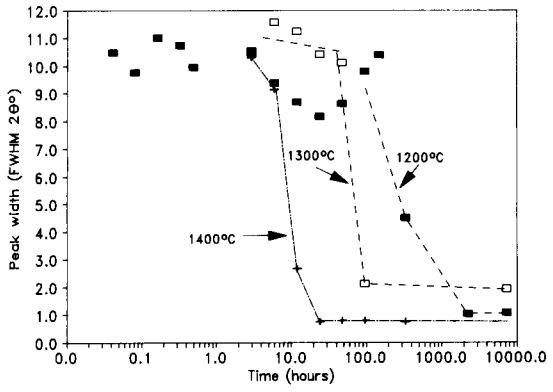

Fig. 6. Development of width of amorphous hump/pseudo-crystalline peak with time in devitrified, Standard Grade™ fibres. Key: ■ = 1200°C; □ = 1300°C; + = 1400°C.

shown by Fig. 8b for the (111) $d = 0.254$ nm mullite peak.

3.4. Exposure thresholds for fibre devitrification

For Standard Grade™ fibres, the relationship between the formation of mullite and cristobalite and furnace exposure conditions is shown by Fig. 9. The results, show that thresholds for the formation of both mullite and cristobalite occur at lower temperatures for longer exposure times.

3.5. Quantitative analysis

Results for the quantification of the β-cristobalite, mullite and amorphous phases in Stan-

Table 1
Comparative diffractometry results for analysis and determination of cristobalite phase in devitrified fibres (data as *d*-spacing (A)/relative intensity (%))

Standard data			Measured data					
α- crist.	β-crist.	Mull	Devitrified fibres		α-crist. control		β-crist. control	
PDF39-1425	PDF27-605	PDF15-776	20°C	400°C	20°C	400°C	20°C	400°C
		5.39, 50%	– [a]	–				
4.04, 100%					4.04, 100%			
	4.11, 100%		4.07, 100%	4.10, 100%		4.11, 100%	4.10, 100%	4.12, 100%
		3.77, 8%	3.73, –	3.74, –				
3.52, < 1%					3.51, 0.6%			
		3.43, 95%	3.41, 64%	3.42, 81%				
		3.39, 100%	3.37, 100%	3.37, 100%				
3.14, 8%					3.13, 6%			
2.84, 9%					2.84, 6%			
		2.89, 20%	2.87, 20%	2.88, 20%				
		2.69, 40%	2.67, 35%	2.68, 33%				
		2.54, 50%	2.54, 53%	2.54, 50%				
	2.52, 12%		2.50, –	2.51, –		2.52, 15%	2.52, 15%	2.53, 15%
2.49, 13%					2.48, 13%			
2.47, 4%								
		2.43, 14%	2.42, 12%	2.43, 13%				
		2.39, < 2%	–	–				
2.34, < 1%								
		2.31, 4%	–	–				
		2.29, 20%	2.28, 10%	2.29, 10%				
Phases present:			Mull. + β-crist.	Mull. + β-crist.	α-crist. + S_1-Trid. [b]	β-crist. + S_4-Trid. [c]	β-crist.-	β-crist.

[a] Not measured or not measurable.
[b] The following peaks which were associated with S_1 tridimite were also identified in the α-cristobalite control at 20°C: 4.29 Å (83 cts), 3.81 Å (27 cts).
[c] The following peaks which were associated with S_4 tridimite were also identified in the α-cristobalite control at 400°C: 4.36 Å (237 cts), 3.85 Å (32 cts).

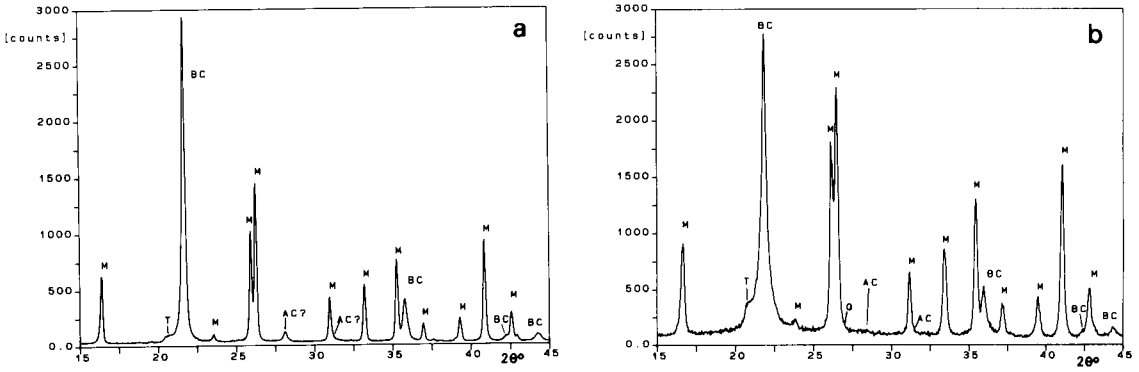

Fig. 7. X-ray powder diffractometry data plots showing possible α-cristobalite peaks in fibres devitrified at temperatures exceeding 1200°C. (a) Standard Grade™ fibres devitrified at 1400°C for 336 h; (b) Standard Grade™ fibres devitrified at 1200°C for 336 h. Key: BC = β-cristobalite; M = mullite; T = tridymite; Q = α-quartz; AC = α-cristobalite.

Table 2
Summary of observation of α-cristobalite, α-quartz and tridymite in devitrified Standard Grade™ fibres showing presence of β-cristobalite and mullite

	1200°C		1300°C		1400°C		1500°C	
	336 h	7300 h	96 h	7300 h	12 h	336 h	3 h	240 h
α-Cristobalite	no	no	no	no	maybe	yes	yes	yes
α-Quartz	yes	yes	yes	yes	yes	yes	no	no
Tridymite	yes	yes	yes	yes	yes	yes	yes	no

dard Grade™ fibres devitrified at 1200 and 1400°C at a range of exposure times are shown by Fig. 10a and b, respectively.

Mullite quantification for each data point was undertaken for the five analysis peaks and the five values averaged to give the value presented. β-Cristobalite quantification was similarly undertaken using the two available analysis peaks. The integrated intensity of the (111) cristobalite peak (2 in Fig. 5b) was separated from the pseudo-crystalline and tridymite components (3 and 4 in Fig. 5b) using the profile fitting procedure of the

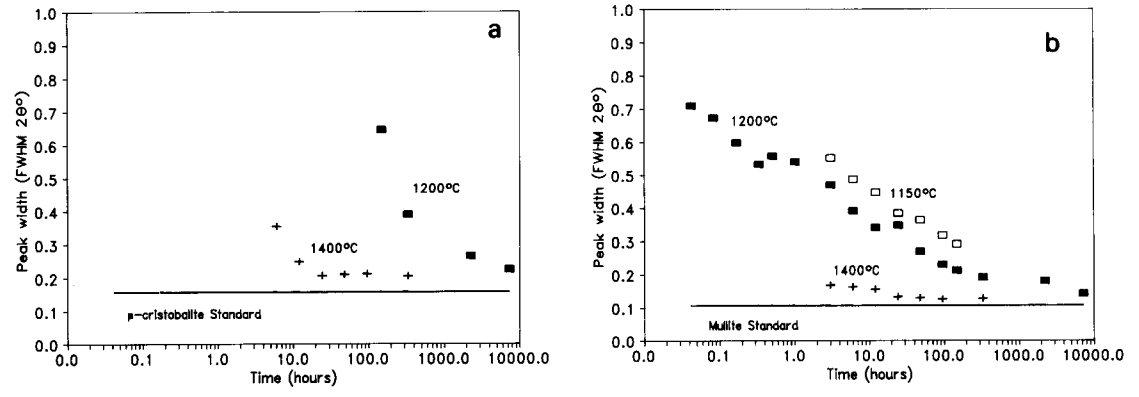

Fig. 8. Development of x-ray peak widths with time for β-cristobalite and mullite phases in devitrified, Standard Grade™ fibres, (a) for (111) β-cristobalite peak at 1200°C (■) and 1400°C (+) compared with the (111) peak of the β-cristobalite standard (solid line); (b) for (111) mullite peak at 1150°C (□), 1200°C (■) and 1400°C (+) compared with the (111) peak of the mullite standard.

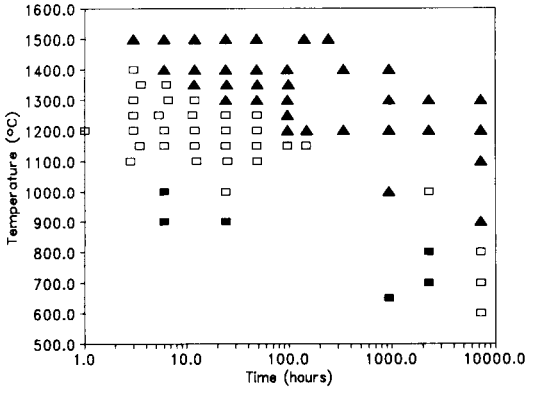

Fig. 9. Exposure dependence of formation of cristobalite and mullite in Standard Grade™ fibres. Key: ▲ = cristobalite plus mullite and further silica phases; □ = mullite plus amorphous phase; ■ = glass.

APD software and it is accepted that this may have introduced some experimental error.

The amorphous phase was quantified using the amorphous standard prepared from as-manufactured, Standard Grade™ fibres. The pseudo-crystalline peaks observed at exposure times exceeding 100 h at 1200°C and 3 h at 1400°C were not quantified.

4. Discussion

4.1. Phase identity and development in devitrified Standard Grade™ fibres

The as-manufactured, Standard Grade™ fibres are amorphous in nature and have a composition of 53.3 wt-% SiO_2 and 46.5 wt-% Al_2O_3. This amorphous nature was confirmed by the broad, amorphous hump shown by x-ray powder diffractometer data (Fig. 1c).

At exposure temperatures and times greater than the threshold for mullite formation but less than the threshold for cristobalite formation (Fig. 9), mullite and amorphous phases were observed in the devitrified fibres.

The data showing the development of mullite at 1200°C (Fig. 5a) indicated how the mullite peaks become narrower and sharper with increasing time and tend towards a minimum width (Fig. 8b) in the region of cristobalite formation. While the good match of x-ray data for relatively high exposure temperatures and long exposure times with standard JCPDS PDF 15-776 data for $3Al_2O_3 \cdot 2SiO_2$ mullite indicated that the mullite in this region was of the $3Al_2O_3 \cdot 2SiO_2$ form, the x-ray data for earlier stages of mullite develop-

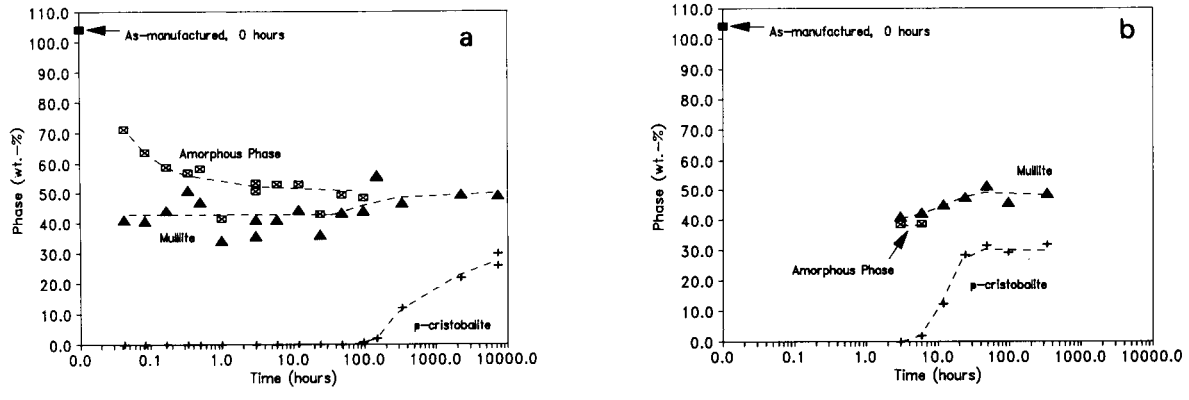

Fig. 10. Quantitative analysis of Standard grade™ fibres devitrified at 1200 and 1400°C for varying exposure times, (a) devitrified at 1200°C; (b) devitrified at 1400°C. Key: ■ for glass phase; ⊠ for amorphous phase, ▲ for mullite phase; + for β-cristobalite phase.

ment did not enable the mullite form to be confidently identified.

Mullite is known to exist in a range of forms from $3Al_2O_3 \cdot 2SiO_2$ to $3Al_2O_3 \cdot SiO_2$ dependent on its structural ordering, and these forms can change with mullite development and exist independently or in some combination in a particular sample [16]. While not confirmed by data, it is possible that developments and changes in the mullite form were taking place before the formation of cristobalite and this would also have affected the composition of the amorphous phase. If, for example, we assume the initial composition of the fibres and a resulting mullite concentration of 40 wt-% after devitrification, calculation of the composition of the amorphous phase gives 70 wt-% SiO_2, 30 wt-% Al_2O_3 and 78 wt-% SiO_2, 22 wt-% Al_2O_3 respectively for the $3Al_2O_3 \cdot 2SiO_2$ and $3Al_2O_3 \cdot SiO_2$ forms of mullite.

At exposure temperatures and times in the region associated with cristobalite formation (Fig. 9), the observed phases are β-cristobalite, pseudo-crystalline phase, mullite and small amounts of tridymite, α-cristobalite and quartz.

The cristobalite observed at room temperature in Standard Grade™ fibres devitrified at 1200°C for 48 days was shown by differential scanning calorimetry and x-ray powder diffractometry (Figs. 3 and 4, Table 1) to have the same properties and behaviour as β-cristobalite. The form of the x-ray diffractometer traces matched β-cristobalite and detailed analysis of d-spacings and relative intensity data at 20 and 400°C gave a good match to standard JCPDS PDF 27-605 data for β-cristobalite. In addition, no α to β transition was observed on heating through 270°C.

The pseudo-crystalline peak was distinguished by profile fitting of the experimental (111) $d =$ 0.411 nm β-cristobalite peak (Fig. 5b) and was shown (a) to transform from the broad amorphous peak on initial formation with time (Fig. 5c), (b) to subsequently decrease in intensity with time and with the associated formation of β-cristobalite (Fig. 5d and e), and (c) to not be observed when fibres were devitrified at 1500°C at exposure times of 48 h or longer. In addition, the data in Table 2 indicate that tridymite was always observed when the pseudo-crystalline peak was obtained and that an α-cristobalite component was only detected when the pseudo-crystalline peak was either not detected or of minimal intensity.

The behaviour of the pseudo-crystalline peak is consistent with transformation of the amorphous phase into a defect form of cristobalite, as identified by Eitel [20]. Eitel proposed that decreasing the devitrification temperature below 1500°C would increase stacking faults and the pseudo-crystalline peak and its behaviour is therefore associated with a defective cristobalite structure containing significant stacking faults.

Returning to the cristobalite phase, previous workers have demonstrated (a) how the high-temperature, β-phase can be stabilised to room temperatures and below by substituting Al^{3+} for Si^{4+} in the silica framework and charge compensating with Ca^{2+} or Na^{+} ions [17,18], and (b) how the displacive transformation temperature for β-cristobalite can be depressed well below 270°C by the presence of stacking disorders [20].

Although, as-manufactured Standard Grade™ fibres contain the aluminium necessary for silicon substitution, they do not have the required charge compensating ions. A chemical stabilisation mechanism acting alone is therefore unlikely. However, an α-cristobalite component was observed at room temperature for exposure temperatures and times corresponding to either minimal or no pseudo-crystalline peak (Table 2), and it is suggested that the stacking-fault peak may have a role in stabilising the β-cristobalite to room temperature. The mechanism of stabilisation of β-cristobalite may therefore be some combination of defect and chemical effects.

The question has been asked as to whether such low-temperature forms of stabilised, β-cristobalite are correctly identified as β-cristobalite [18]. Given that the stabilisation mechanism results in an impure and imperfect structure, the term chemical and/or defect stabilised cristobalite would appear more correct.

As noted, small amounts of α-cristobalite were observed in addition to β-cristobalite at higher exposure temperatures and longer exposure times (Table 2). The observation of α-cristobalite was also reported by Strubel et al. [21] and it would

therefore appear that both forms are possible in devitrified aluminosilicate fibres.

In addition to the β-cristobalite, α-cristobalite, pseudo-crystalline and tridymite phases, mullite is a major phase in this region of cristobalite formation and small amounts of quartz are observed (Table 2). In addition, there may be some remnant of amorphous phase although practical analysis with standard samples indicate that levels of less than 10 wt-% would be difficult to detect and quantify.

4.2. Quantitative analysis of devitrified fibres

The quantification of phases observed in Standard Grade™ fibres devitrified at 1200 and 1400°C respectively is presented by Fig. 10a and b. The amorphous, β-cristobalite and mullite phases were quantified using, respectively, the as-manufactured, Standard Grade™ amorphous fibre standard, the β-cristobalite standard and the Fibermax™ $3Al_2O_3 \cdot 2SiO_2$ standard. The results do not include quantification of the pseudo-crystalline, α-cristobalite, α-quartz or tridymite phases.

The results for cristobalite and mullite peak widths (Fig. 8a and b) and for the pseudo-crystalline phase (Fig. 5d) suggest that β-cristobalite and mullite were fully developed in fibres devitrified at 1400°C after 48 h exposure, whereas the development of these phases was not necessarily complete after 7300 h exposure at 1200°C.

The results obtained for the most fully developed phase situation at each temperature were as follows:

(a) 1200°C and 7300 h	Mullite	49 ± 1 wt-%
	β-Cristobalite	30 ± 1 wt-%
	Total = 79 ± 2 wt-%	
	Relative	62 ± 2 wt-% Mullite
		38 ± 2 wt-% β-Cristobalite
(b) 1400°C and 336 h	Mullite	51 ± 2 wt-%
	β-Cristobalite	36 ± 2 wt-%
	Total = 87 ± 3 wt-%	
	Relative:	59 ± 3 wt-% Mullite
		41 ± 3 wt-% β-Cristobalite

Error estimates are expressed as standard errors. The difference between the totals and 100% could be explained as follows: the fibres devitrified at 1200°C contained small amounts of quartz and tridymite (Table 2), pseudo-crystalline phase (Fig. 5d), and possibly some residual amorphous phase below the detection limit, and fibres devitrified at 1400°C also contained small amounts of tridymite, α-cristobalite and α-quartz (Table 2) and possibly some amorphous phase below our effective minimum level of detection and quantification of 10 wt-%. The lack of development of β-cristobalite, reflected in higher contributions from other phase components, could account for the smaller proportion of β-cristobalite in material devitrified at 1200°C and, in addition, some inaccuracy could also arise from the quality and applicability of standards, profile fitting and possible separation effects in analysed specimens.

Reference to the SiO_2–Al_2O_3 stable equilibrium phase diagram [21] for as-manufactured material of composition 53–57 wt-% SiO_2 and 43–47 wt-% Al_2O_3 (manufacturer's data), indicates relative amounts of mullite and cristobalite of 64 ± 2 wt-% and 38 ± 2 wt-% respectively. The discrepancy with our results, notably for 1400°C, may derive from the stabilisation of β-cristobalite with aluminium or from an incorrect assumption that the stable equilibrium phase diagram applies.

Quantification of the phases present in fibres for the region of amorphous glass and mullite at exposure times before the onset of cristobalite formation (Fig. 10a) requires careful attention to calibration standards. The authors are not confident that the mullite is of fully developed $3Al_2O_3 \cdot 2SiO_2$ form, and the composition of the remaining amorphous phase will certainly have changed from the composition of as-manufactured fibres and will depend on the form of mullite. The significance of the composition of the amorphous phase is demonstrated by calibration constants of $(101 \pm 3)\ 10^{-4}$ wt-%$^{-1}$ and $(164 \pm 6)\ 10^{-4}$ wt-%$^{-1}$ for standards prepared respectively from as-manufactured, Standard Grade™ fibres and vitreous colloidal silica particles.

In the region of initial cristobalite development (Fig. 10a and b), the mullite and β-cristobalite standard will apply but a full quantification would require identification and analysis of the amorphous and pseudo-crystalline peaks as well as tridymite and α-quartz.

The ideal calibration standard for each crystalline phase would be a powder comprising pure, single-crystal particles of approximately 1 μm diameter [15].

The mullite standard was manufactured from polycrystalline, mullite fibres of form $3Al_2O_3 \cdot 2SiO_2$ and 2–3.5 μm arithmetic mean fibre diameter (manufacturer's data). The x-ray powder diffractometer data plot (Fig. 1a) from this material indicated high purity and good crystallinity, and analysis was undertaken using 5 analysis lines to minimise fibre orientation effects [19]. While the grain size of the mullite is unknown, the measured peak width of 0.1° for the (111) $d =$ 0.254 nm peak (Fig. 8b) gives some confidence that this is not a problem. It is proposed that this provides a good standard for quantification of the fully developed mullite phase.

The β-cristobalite standard was manufactured by chemical stabilisation of devitrified colloidal silica particles. Again, the x-ray powder diffractometer data plot (Fig. 1b) indicated high purity and good crystallinity but there is concern that there may be a particle size effect as the measured peak width of 0.16° (Fig. 8a) is significantly greater than that for the mullite standard and the initial grain size of the colloidal silica before processing was 20 nm (manufacturer's data). An alternative standard of initial grain size 1 μm is being prepared.

4.3. Exposure thresholds for fibre devitrification

The regions and thresholds for mullite and cristobalite formation in devitrified, Standard Grade™ fibres are shown as a function of exposure temperature and exposure time by Fig. 9. This data indicates the interplay of temperature and time in cristobalite formation and the reduction of the cristobalite threshold to 900°C after 43 week exposure.

5. Conclusions

(A) The regions of cristobalite and mullite formation have been mapped for Standard Grade™ fibres (of near equal alumina and silica content by mass) as a function of exposure temperature and time. The threshold for cristobalite formation decreases in temperature from 1500°C at 2.5 min exposure to 900°C after 43 weeks.

(B) Development of phases has been followed, notably at 1200°C and 1400°C, as a function of exposure time.

Before the formation of cristobalite, and after the initial formation of mullite, mullite is suggested to be developing in form with associated changes in composition of the amorphous phase. The mullite appears to mature to well-developed $3Al_2O_3 \cdot 2SiO_2$ form in the region of cristobalite formation.

After initial cristobalite formation, the silica content comprises β-cristobalite, tridymite, α-quartz and, it is suggested, a highly disordered form of cristobalite. With increasing temperatures and times, the β-cristobalite matures with reductions in the disordered form and in tridymite, and the observation of α-cristobalite.

(C) The main cristobalite component at room temperature was shown to be β-cristobalite and it is suggested that the β-form is stabilised by a mechanism involving chemical stuffing and defects.

(D) Using "pure" calibration standards, x-ray powder diffractometry and the internal standard method, well-developed mullite and β-cristobalite have been quantified: fibres devitrified at 1400°C for longer than 48 h exposure comprise (51 ± 2) wt-% mullite and (36 ± 2) wt-% cristobalite, the difference from a total of 100% being associated with unquantified phases, and discrepancies between relative amounts and the predictions of the stable equilibrium phase diagram are identified and discussed.

Acknowledgement

The authors wish to acknowledge Mr D.J. Taylor of Pilkington Group Analytical Services for the x-ray powder diffractometer data obtained using the non-ambient, environmental cell fitted to their Philips powder diffractometer. These facilities were made available by kind permission of Dr. A. Ledwith, Director of Research, Pilkington

Technology Centre, Lathom, Ormskirk, Lancashire, UK.

The authors also acknowledge Mr M.S. Rea, Research Assisant, Sheffield City Polytechnic for provision of many of the wide range of furnace-exposed samples.

References

[1] J. Young, in D. Liddell and K. Miller (Eds.), Mineral Fibres and Health, CRC Press, Boca Raton, FL, 1991, pp. 37–53.
[2] J. Griffiths, Ind. Miner., London, September (1986) 20.
[3] A.N. Gaodu, N.V. Pitak, R.E. Volfson and M.E. Drizheruk, Inorg. Mater., 13 (1977) 1802.
[4] H. Hickling, D.H. Thomas and J. Briggs, Sci. Ceram., 11 (1981) 397.
[5] D. Holroyd, M.S. Rea, J. Young and G. Briggs, Ann. Occup. Hyg., 32 (1988) 171.
[6] A. Jager, Z. Stadler and J. Wernig, Ber. Dt. Keram. Ges., 61 (1984) 143.
[7] L.E. Olds, W.C. Millera and J.M. Pallo, Ceram. Bull., 59 (1980) 739.
[8] G. Vine, J. Young and I.W. Nowell, Ann. Occup. Hyg., letter to the editor, 28 (1984) 356.
[9] B.A. Gantner, Am. Ind. Hyg. Ass. J., 47 (1986) 530.
[10] J. Khorami, A. Lemieux, J. Dunnigan and D. Nadeau, Thermochim. Acta, 120 (1987) 1.
[11] I.A. Aksay, D.M. Dabbs and M. Sarikaya, J. Am. Ceram. Soc., 74 (1991) 2343.
[12] J. Young, M.S. Rea and G. Briggs, Br. Ceram. Trans. J., 88 (1989) 58.
[13] R.C. Brown, E.A. Sara, J.A. Hoskins, C.E. Evans, J. Young, J.J. Laskowski, R. Acheson, S.D. Forder and A.P. Rood, Ann. Occup. Hyg., 36 (1992) 115.
[14] O.W. Florke and H. Schneider, cfi/Ber. DKG, 63 (1986) 368.
[15] B.D. Cullity, Elements of X-ray Diffraction, Addison-Wesley,Reading, MA, 2nd edn., 1978.
[16] H.P. Klug and L.E. Alexander, X-ray Diffraction Procedures, Wiley, New York, 2nd edn., 1974.
[17] A.J. Perotta, D.K. Gribbs, E.S. Martin, N.R. Dando, H.A. McKinstry and C.-Y. Huang, J. Am Ceram. Soc., 72 (1989) 441.
[18] M.A. Saltzberg, S.L. Bors, H. Bergna and S.C. Winchester, J. Am. Ceram. Soc., 75 (1992) 89.
[19] T. Nakamura, T. Kodama and M. Ishihara, Analyst, 113 (1988) 1737.
[20] W. Eitel, Ceram. Bull., 36 (1957) 142.
[21] G. Strubel, T. Godicke and T. Schwieger, Ann. Occup. Hyg., in press.
[22] S.H. Risbud, V.F. Draper and J. Pask, J. Am. Ceram. Soc., 61 (1978) 471.

Analytica Chimica Acta, 286 (1994) 25–35
Elsevier Science B.V., Amsterdam

Solid state ^{29}Si NMR determination of crystalline silica in natural iron oxide pigments

Gregory Kowalczyk
Binney and Smith, Easton, PA 18044 (USA)

James E. Roberts
Department of Chemistry, Lehigh University, Bethlehem, PA (USA)

(Received 28th August 1992; revised manuscript received 25th January 1993)

Abstract

Synthetic iron oxide pigments have well characterized compositions. In natural iron oxide pigments, commercial products contain various amounts of talc, kaolin, and crystalline silica in addition to the iron oxide. The analysis for crystalline silica requires removing the iron oxide by an acid concentration step followed by x-ray diffraction (XRD) evaluation. However some materials not removed by the acid wash may interfere with quantitative XRD measurements. Another potential drawback of the x-ray analysis is the requirement for the particle size to be on the order of a few micrometers. In principle, nuclear magnetic resonance (NMR) is sensitive to domain sizes down to the order of a few nanometers. We have utilized solid state NMR techniques to obtain ^{29}Si spectra from a number of materials to assess its viability as a quantitative method for measuring crystalline silica in iron oxide pigments. The method employs single pulse excitation with magic angle sample spinning (MASS). A protocol was established for quantitative silica analysis utilizing a reduced pulse angle of 10° with a 20-min relaxation delay between acquisitions. The reduced pulse angle was used to circumvent the long silicon relaxation times (T_1) for the crystalline silica species. The spectra were recorded at a measurement frequency of 59.6 MHz with high power proton decoupling (300.1 MHz). A blind test of silica standards was used for comparison with x-ray diffraction analyses as a test of the protocol. Quantitative determination of crystalline silica employed tetrakis(trimethylsilyl)silane as a spin-counting standard.

Keywords: Nuclear magnetic resonance; X-ray diffraction; Crystalline silica; Iron oxide pigments; Pigments

Quantitative determination of crystalline silica in iron oxide pigments has been accomplished utilizing solid state ^{29}Si nuclear magnetic resonance spectroscopy (NMR). The objective of this project was to develop a method for the analysis of trace quantities (0.1 wt.-%) of crystalline silica found as a contaminant in some matrices used in the art products industry. This was in response to the increased regulatory activity since the publication by the International Agency for Research on Cancer (IARC) of Monograph 42, Supplement 7 in 1987 which listed crystalline silica as a possible human carcinogen [1]. The crystalline silica polymorphs of interest include α-quartz, cristobalite and tridymite. Materials used in the production of art products that may contain crystalline silica include calcium carbonates, clays, talc and various inorganic fillers and pigments. X-Ray powder diffraction (XRD) is widely used as a technique for the analysis of trace quantities of crystalline silica. Standardized methods are approved by the National Institute of Occupa-

Correspondence to: G. Kowalczyk, Binney and Smith, 1100 Church Lane, P.O. Box 431, Easton, PA 18044-0431 (USA).

SSDI 0003-2670(93)E0179-B

tional Safety and Health (NIOSH) [2]. Although XRD is sensitive to trace quantities of crystalline materials there are a few limitations of x-ray analysis. X-Ray diffraction is inappropriate for the analysis of non-crystalline species. A second limitation is the requirement for particle sizes to be on the order of a few micrometers which could be a hindrance in the analysis of respirable samples. A third factor is possible interferences with the diffraction pattern from other minerals within the analyzed matrix. Solid state NMR was chosen as a technique to address these issues and to serve as a possible adjunct to XRD analysis.

The initial use of solid state ^{29}Si NMR for structure elucidation was by Lippmaa et al. [3]. Their investigation provided qualitative identification of silica containing minerals based on chemical shift differences. Minerals included α-quartz, cristobalite, talc and other silicates. Another area investigated by Lippmaa et al. [4] was aluminum oxide silica linkages in zeolites. Klinowski et al. [5] utilized solid state ^{29}Si NMR to derive the ratio of Si to Al in aluminum silicate matrices from peak areas. Smith and Blackwell [6] followed with their investigation of Si–O bond lengths and Si–O–Si bond angles of silica polymorphs using solid state ^{29}Si NMR. Graetsch et al. [7] used NMR in conjunction with XRD, near infrared and thermal analysis for analyzing non-crystalline species including opals. Kanzaki et al. [8] characterized calcium silicates with NMR and XRD.

There are several advantages in the selection of solid state ^{29}Si NMR as an approach for the analysis of crystalline silica. Solid state ^{29}Si NMR provides qualitative identification of silica polymorphs including amorphous species. Solid state NMR as a technique is sensitive to crystallite particle sizes on the order of a few nanometers compared to micrometers for XRD analysis. Matrix interferences are not a problem for solid state ^{29}Si NMR providing there is sufficient separation between chemical shifts of the signals.

There are also disadvantages associated with NMR as an analytical technique. The primary disadvantage is sensitivity. X-Ray diffraction methods have been established for trace determination of crystalline silica below 0.05 wt.-% [9,10]. Silicon-29 has a natural abundance of only 4.7% [11]. This requires on the order of 10^{18} spins to obtain reasonable signal intensity. A second disadvantage of solid state ^{29}Si NMR is the long silicon relaxation time (T_1) in crystalline samples. Silicon T_1 values have been measured for silicates at greater than 5000 s [12]. For quantitative NMR it is beneficial to wait 5 T_1 values between acquisitions. This provides greater than 99% confidence that all spins have relaxed and quantitative information is obtained [13]. A third disadvantage of NMR analysis involves the effects of paramagnetic centers which can decrease the signal of the observed species [14]. Sensitivity and paramagnetic effects can be addressed through sample preparation. The problem with long T_1 values has been circumvented by developing a protocol that utilizes reduced pulse angles and significantly decreases the time required between acquisitions. These provisions enable solid state ^{29}Si NMR to be used for the analysis of crystalline silica at low levels.

The NMR analysis protocol is based on a reduced pulse angle. In standard single pulse excitation NMR analysis a 90° pulse ($\pi/2$) is applied to the sample at the appropriate frequency. The resulting signal is recorded as the spins return to equilibrium. For single pulse experiments a 90° tip angle provides the highest intensity for the signal. The purpose in developing the protocol was to determine what fraction of a 90° pulse would not show a decrease in signal intensity for a given relaxation time. Solid state ^{13}C NMR analyses were performed at various pulse angles (θ) from 5° to 90° on aminoacetic acid (glycine, NH_2CH_2COOH). Glycine has two ^{13}C resonances of known T_1. The objective of the experiment was to determine the limiting tip angle for the applied pulse where no decrease in signal intensity for a particular pulse angle was observed. A second aspect was to decrease the time required between pulse acquisitions. Well established theory predicts a smaller tip angle and requires a shorter time between acquisitions for maintaining quantitative conditions [15]. The protocol provided a reduction in the time between acquisitions while obtaining maximum signal intensity through signal averaging.

EXPERIMENTAL

Materials

Reagent grade materials used in sample preparation were obtained from Fisher Scientific and used as received. Hexamethylcyclotrisiloxane was obtained from Huls and used as received. Tetrakis(trimethylsilyl)silane, adamantane and glycine were obtained from Aldrich and used as received. The samples of α-quartz, cristobalite and amorphous (fumed) silica used as standards were obtained from Pfizer (Easton, PA), along with six unknown blends of the standards and all x-ray analyses. Samples of commercial grade natural iron oxide pigments were provided by Hoover. Other commercial grade materials used include talc (magnesium silicate, Pfizer) and kaolin (aluminum silicate, Evans Clay).

Iron oxide pigment preparation

Prior to ^{29}Si NMR analysis of the pigment samples the iron oxide was removed with an acid digestion step. This procedure provided two benefits: it increased the relative silica concentration present in the sample and removed the paramagnetic centers (Fe_2O_3 and manganite). Concentrated hydrochloric acid was used to dissolve the iron oxide. Between 1 and 3 g of pigment sample were digested in 30 ml of 12 M HCl for one hour at 100°C with agitation. The samples were diluted to twice the original volume with deionized water followed by gravity filtration through a Whatman 12 ashless filter paper. Approximately 300 to 400 ml of deionized water was used to rinse the sample. When the effluent was free of chlorides (precipitation test with 0.1% silver nitrate and nitric acid) the filter paper was transferred to a 40 ml porcelain crucible and placed in a muffle furnace at 750°C for two hours. The samples were cooled to room temperature in a desiccator, then reheated and cooled until a constant weight had been obtained. Blanks containing all reagents were run for each series of samples. For the first few series a second acid digestion was employed to insure complete removal of the iron oxide. Repetitive sample preparations of the pigments yielded total acid insolubles within 1% for the replicates.

Instrumentation

Solid state ^{29}Si and ^{13}C NMR analyses were performed on a modified General Electric Model GN-300 FT-NMR Spectrometer equipped with a Doty Scientific 7 mm magic angle sample spinning (MASS) probe. The spectra were obtained at 59.62 MHz for silicon and 75.47 MHz for carbon. High power proton decoupling at 300.1 MHz was performed during all acquisition times. All samples were packed in 7 mm single crystal sapphire rotors (0.35 cm^3) with Kel-F® end caps. Hexamethylcyclotrisiloxane was used as an external chemical shift reference [$\delta = -9.00$ ppm relative to tetramethylsilane(TMS)], and tetrakis(trimethylsilyl)silane (TKS) was used as an internal standard for spin counting experiments. Tetrakis (trimethylsilyl)silane has two resonances: $\delta = -9.4$ ppm and $\delta = -134$ ppm relative to TMS. Adamantane was used as an external chemical shift reference for ^{13}C NMR of glycine. X-Ray powder diffraction data for the standards and unknown blends were recorded on a Siemens D-500 x-ray powder diffractometer.

NMR parameters

All NMR analyses were recorded with high power proton decoupling and MASS at speeds from 3 to 5 KHz. Proton decoupling radio frequency field strength during acquisition was 50 KHz. The spectrometer sweep width was 25 000 Hz, corresponding to a dwell time of 20 μs. Typical experimental block sizes were 4 K or 8 K data points (real plus imaginary) with corresponding acquisition times of 41 and 82 μs, respectively. The silicon 90° pulse length and offset were determined with hexamethylcyclotrisiloxane prior to analysis. The primary experimental technique used for the ^{29}Si NMR analyses was single pulse excitation. It was also used for the ^{13}C NMR analyses of the glycine sample for the reduced pulse angle experiments, and the analysis of a 50:50 wt.-% blend of α-quartz/amorphous silica. This method was used as a check of the NMR protocol for analyzing the six unknown (blind) standard blends and for silica determination in the iron oxide pigment samples There were two other NMR techniques employed during the project. The pulse saturation method was

used to determine the ^{29}Si T_1 values for the α-quartz, cristobalite and amorphous silica standards [16]. The other technique employed was cross-polarization for the determination of the silicon T_1 values for TKS. The latter experimental pulse sequence used was described by Torchia [17]. The relaxation delay varied from 8 ms to 256 s with the number of excitations equivalent to 48 for this determination.

Spin counting was employed in conjunction with the single pulse excitation technique for the determination of crystalline silica in the acid insoluble fraction of the iron oxide pigment samples. There were two series of spin counting experiments. The first set examined the percent recovery of α-quartz with TKS as an internal standard and the second set determined the weight percent of crystalline silica in the pigment samples. For the spin counting experiment of the α-quartz standard the sample was prepared by weighing known quantities and physically blending the materials under a nitrogen atmosphere. The sample contained 179 mg ($\pm$1.0 mg) of α-quartz and 57 mg ($\pm$1.0 mg) of TKS. The silyl peak integral of TKS ($\delta = -9.4$ ppm) was set at 1000. The spectra were obtained with the single pulse excitation technique utilizing the reduced tip angle protocol. Each spectrum was integrated and the TKS resonance at $\delta = -9.4$ ppm was standardized at a value of 1000. The number of silicon atoms contributing to that peak was determined which was then used to calculate the number of atoms contributing to the resonance for the crystalline species. The concept was based on the technique used by Hagaman et al. [18]. Weighed quantities of TKS and the samples were physically blended during loading of the sample rotor to provide an even distribution of the standard and sample. The samples typically contained approximately 25 wt.-% of TKS.

For all experiments the samples ranged in weight from 200 to 300 mg; each sample weight was determined to within 1.0 mg. The number of acquisitions varied between 24 and 200 with experiments typically requiring 24 h of instrument time. All spectra were processed with exponential line broadening equivalent to 10 Hz. The time domain data were zero filled once before Fourier transform. Curve fitting analyses were performed with the software of the GN-300 spectrometer. Parameters that are specific for a given series of experiments are provided in the results section.

RESULTS

The initial set of experiments investigated the relaxation times for the standard samples of α-quartz, cristobalite and amorphous silica. Devreux et al. [19] have investigated silicon T_1 values for amorphous and crystalline species. Their findings indicate complete relaxation of the crystalline species required 10 000 s while the amorphous T_1 was on the order of 1000 seconds. The pulse saturation technique was employed for ^{29}Si T_1 determination of the standards [20]. The time between pulse acquisitions was varied from 4 to 5121 s with the number of excitations equal to 16. Figure 1 is a plot of the magnetization recovery for the α-quartz and amorphous silica standards at various recycle delays. The T_1 is determined by fitting the data to the equation $M_z = M_0(1 - e^{-t/T_1})$ where M_z is the magnetization recovery,

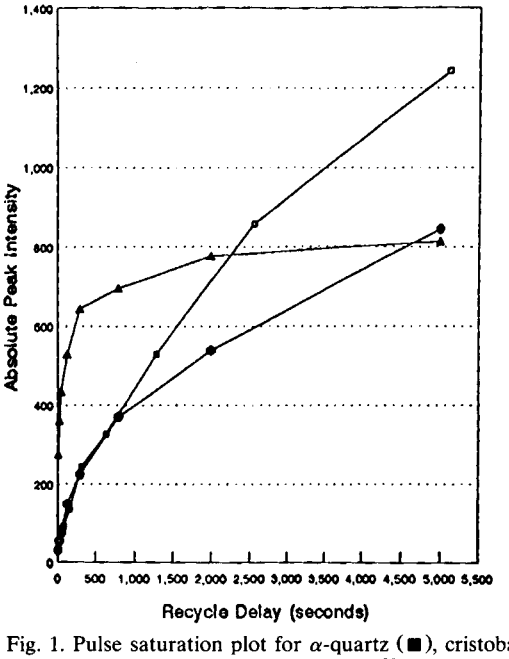

Fig. 1. Pulse saturation plot for α-quartz (■), cristobalite (●) and amorphous silica (▲) to determine ^{29}Si T_1.

M_0 is the value of the magnetization at infinite relaxation time and t is the time between pulse acquisitions [15]. Two pieces of information were obtained from these experiments. The first is that α-quartz and cristobalite have T_1 values greater than 5000 s. The second point demonstrated was the ability to differentiate the polymorphs of silica base on chemical shift values: α-quartz is at $\delta = -107$ ppm, cristobalite appears at $\delta = -109$ ppm and amorphous silica yields a broad peak at $\delta = -111$ ppm (Fig. 2).

The second series of experiments involved developing a protocol of a reduced pulse angle to decrease the time required for the spins to return to equilibrium. The objective was to increase the number of excitations during a given time period. The number of acquisitions (NA) improves the signal-to-noise ratio (S/N) for the spectrum by the relation $S/N \propto \sqrt{NA}$. Solid state ^{13}C NMR analyses of glycine were recorded with variable excitation pulse angles. The tip angles evaluated

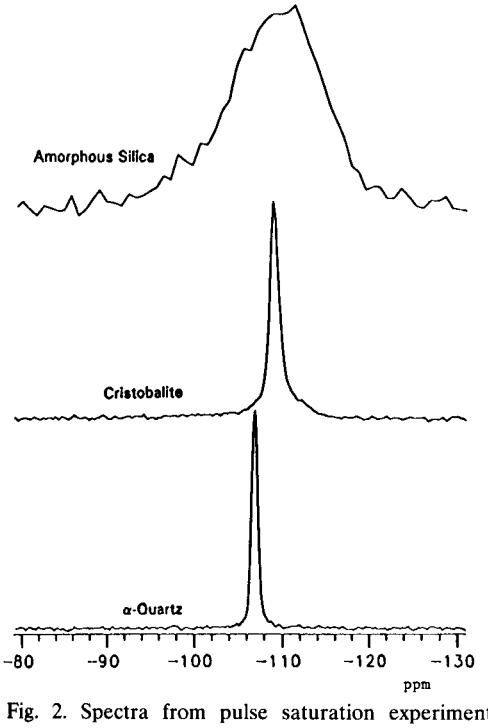

Fig. 2. Spectra from pulse saturation experiment provide chemical shift (δ) values of silica standards for α-quartz ($\delta = -107$ ppm), cristobalite ($\delta = -109$ ppm) and amorphous silica ($\delta = -111$ ppm).

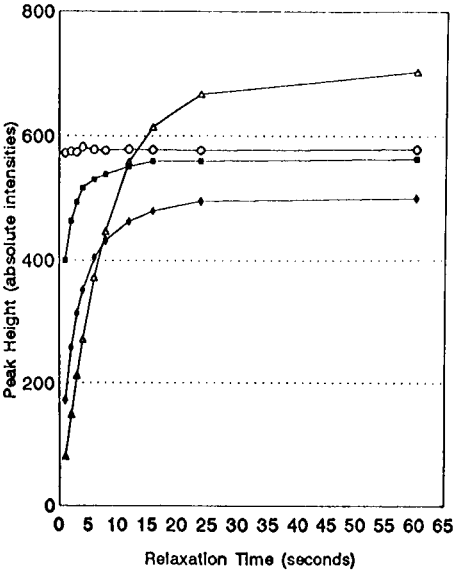

Fig. 3. Absolute peak height vs. relaxation time for carbonyl resonance of glycine at selected tip angles: 10° (○), 20° (■), 45° (♦), and 90° (△). The experimental technique was ^{13}C NMR single pulse excitation.

were $\theta = 5°$, 10°, 15°, 20°, 30°, 45°, 60° and 90°. The time between acquisitions was varied from 1 to 60 s with the number of transients equal to 96. Four dummy scans were taken prior to acquiring each data set. Glycine has two resonances, a methylene line at 44 ppm and the carbonyl peak at 176 ppm. Fig. 3 is a plot of absolute peak intensities at selected pulse angles as a function of the relaxation time for the carbonyl resonance. There was no decrease in peak intensity for either signal at pulse angles $\theta \leq 10°$ at reduced recycle delays.

The next series of experiments determined the appropriate recycle delay between acquisitions for silica containing samples to insure complete relaxation of the spins. A 50:50 wt.-% blend of α-quartz and amorphous silica was mixed by hand and loaded into a rotor. Single pulse excitation NMR spectra were recorded at various recycle delays from 1 to 60 min. The relative areas for the spectra were determined with the curve resolving software of the GN-300 spectrometer. The results of the two component blend are shown in Table 1. Recycle delays at or greater than 20 min provide total recovery of the quartz signal. Repli-

TABLE 1

Quantitative analysis for 50:50 wt.-% blend of α-quartz and amorphous silica utilizing a 10° pulse angle (The weight percent for each fraction was determined with the curve resolving software of the instrument)

Recycle delay (min)	Number of acquisitions	α-Quartz (%)	Amorphous (%)
1	40	28	72
5	40	37	63
10	64	33	67
15	40	33	67
20	24	48	52
20	24	49	51
40	24	50	50
60	24	49	51

TABLE 2

Comparison of NMR and XRD analysis for six blended samples analyzed as blinds by the NMR protocol utilizing a 10° pulse angle with a 20 min recycle delay

Sample	α-Quartz (%)			Cristobalite (%)		Amorphous (%)	
	NA [a]	NMR	XRD	NMR	XRD	NMR	XRD
1	200	37	35	37	35	26	30
2	104	90	80	10	10	–	10
3	187	10	10	11	10	79	80
4	136	100	100	–	–	–	–
5	136	–	–	–	–	100	100
6	200	2	–	98	95	–	–

[a] *NA* equals the number of acquisitions.

cate analysis with a 20 min relaxation time between acquisitions yielded the same results. The signal-to-noise ratios, corrected for the number of acquisitions, were comparable for spectra with recycle delays ≥ 20 min.

The protocol for quantitative ^{29}Si NMR determination of crystalline silica was established with a pulse angle of 10° and a recycle delay of 20 min between acquisitions. Six blends of the α-quartz, cristobalite and amorphous silica standards were submitted as blind unknowns to test the protocol. The samples were analyzed by single pulse excitation NMR. The number of acquisitions varied from 104 to 200 with individual experiments running from 35 to 67 h. Components were identified by chemical shift values; the relative percent compositions of the samples were determined from peak areas as before. The ^{29}Si NMR data are shown in Table 2 along with XRD results. Figure 4 is a plot of the spectrum for sample 1 and the curve fitting profile.

The single pulse excitation protocol was used for the determination of crystalline silica in natural iron oxide pigments. The analyses employed spin counting with TKS as an internal standard. Prior to analysis of the pigment samples it was necessary to run spin counting experiments on the α-quartz standard to determine the percent recovery for the α-quartz signal with TKS as an internal standard. This was done as a check on the technique and to determine if TKS is an appropriate reference for the solid state ^{29}Si NMR analysis. This experiment utilized the protocol of a 10° pulse angle with recycle delays of 20 and 100 min. The number of acquisitions was 120 for the 20 min relaxation series and 32 for the 100

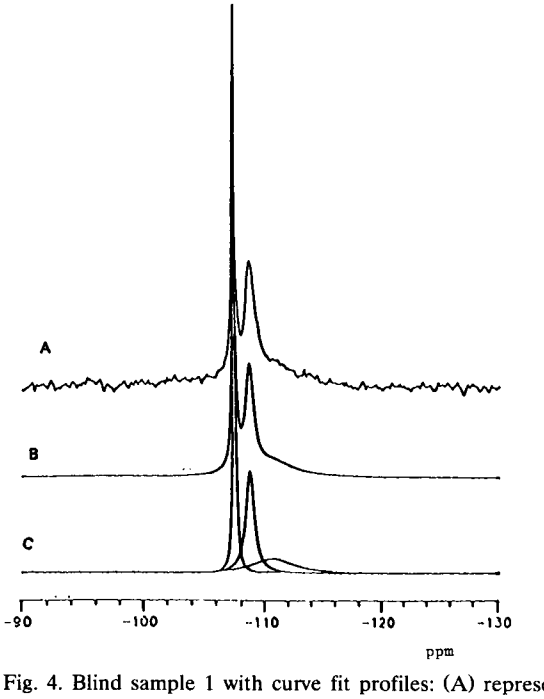

Fig. 4. Blind sample 1 with curve fit profiles: (A) represents the experimental spectrum, (B) is the combined fitted peaks, and (C) represents the individual peaks. The NMR analysis for sample 1 yielded 37% α-quartz, 37% cristobalite and 26% amorphous silica compared to XRD analysis of 35%, 35% and 30% respectively.

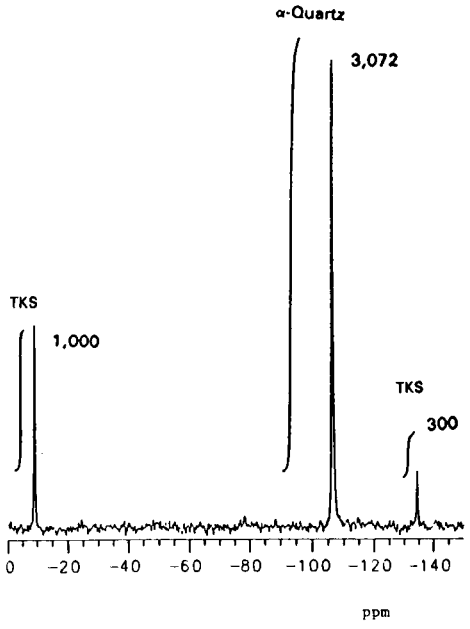

Fig. 5. Integrated spectrum of the spin counting experiment for α-quartz with TKS utilizing 10° pulse angle. The recycle delay was 20 min and the number of acquisitions was 120. Peaks and integrals are labeled.

min data set. The spectrum for the 20 min recycle delay is shown with the peak integration in Fig. 5.

Based on the sample weight of TKS the number of silicon atoms contributing to the signal observed at $\delta = -9.4$ ppm was determined. The weight of α-quartz observed was determined from the ratio of the integrals for the α-quartz peak ($\delta = -107$ ppm) to the silyl peak for TKS ($\delta = -9.4$ ppm). The calculation included the molecular weight for both materials and the molar ratio of silicon atoms for TKS and α-quartz. The percent silica recovered was given by the ratio of the weight observed divided by the initial weight times 100. For the relaxation delay of 20 min the integral of the α-quartz peak was 3072 corresponding to a recovery of 73.3%. The series for the 100 min recycle delay had 3007 for the integral of the α-quartz peak corresponding to a recovery of 71.7%. The integral values for the α-quartz peak were within two percent for the both relaxation series. A correction coefficient of 1.36 was applied to calculate the percent crystalline silica for the analyses of the pigment samples based on the percent recovery of the α-quartz standard for the 20 min recycle delay. The 20 min series was chosen because of the better signal-to-noise ratio obtained from 120 acquisitions.

Seven NMR runs of iron oxide pigment samples were performed with TKS as a spin count reference. The percent crystalline silica for each sample was determined as described previously with two additions: the correction coefficient of 1.36 was applied to the weight SiO_2 recovered and the percent acid insoluble fraction was used to determine the percent silica for the bulk sample. There were two lots of a Sienna iron oxide pigment and one lot of a Brown Shade iron oxide pigment. The acid digestion procedure to remove the iron oxide was done twice per lot to yield six samples; four sienna pigments (Sienna 1, 2, 3 and 4) and two brown pigments (1 and 2). Known quantities (±1.0 mg) of TKS and the pigment acid insoluble fraction were blended for each sample by hand providing uniform distribution in the rotor. The spectra were recorded utilizing the protocol of a 10° pulse angle with 20 min recycle delays. The number of acquisitions varied from 48 to 176. A third sample of the brown pigment (Brown 3) was prepared by spiking weighed quantities of TKS and brown pigment acid insoluble fraction with 2% by weight of the α-quartz standard. The amount of crystalline silica present in

TABLE 3

Spin counting results of crystalline silica determination for acid insoluble fraction of iron oxide pigment samples (Weight recovered includes the integral correction coefficient of 1.36 as described in the text)

Sample	Sample weight (g)		Integral at −107 ppm	Crystalline silica total wt.%
	TKS	Pigment		
Sienna 1	0.033	0.174	3128	20.7%
Sienna 2	0.033	0.174	2797	18.5%
Sienna 3	0.054	0.163	408	18.2%
Sienna 4	0.082	0.125	753	19.4%
Brown 1	0.076	0.244	188	0.018%
Brown 2	0.025	0.245	720	0.024%
Brown 3 [a]	0.047	0.214	438	0.023%

[a] The weight recovered represents the weight of crystalline silica in the sample after the quantity of α-quartz used to spike the sample was subtracted from the total SiO_2 found by NMR analysis.

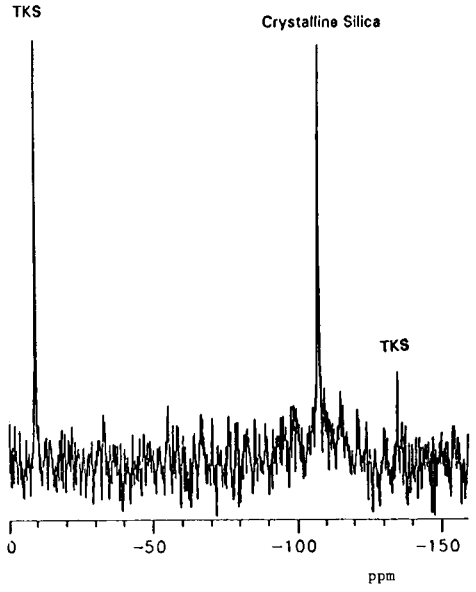

Fig. 6. Sienna 1 with TKS. The integral at $\delta = -9.4$ ppm is 1000 and the integral for the crystalline silica region $\delta = -106$ to -109.5 ppm is 3128.

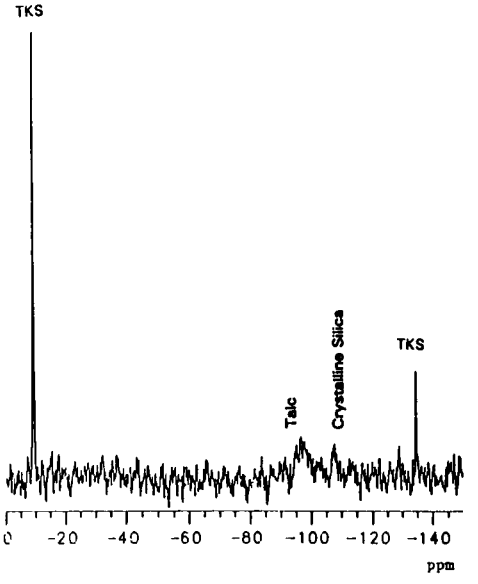

Fig. 8. Brown 1 with TKS. The integral at $\delta = -9.4$ ppm is 1000 and the integral for the crystalline silica region $\delta = -106$ to -109.5 ppm is 188.

each sample was determined as before. The weight of crystalline silica observed in the sample was determined with the integral value from $\delta =$ -106 to -109.5 ppm (incorporating both α-quartz and cristobalite). For Brown 3 the weight of the added α-quartz was subtracted from the corrected weight observed prior to determining the percent silica in the bulk material. The results of the pigment analyses are presented in Table 3. Spectra for Sienna 1, Sienna 3 and Brown 1 are shown in Figs. 6–8.

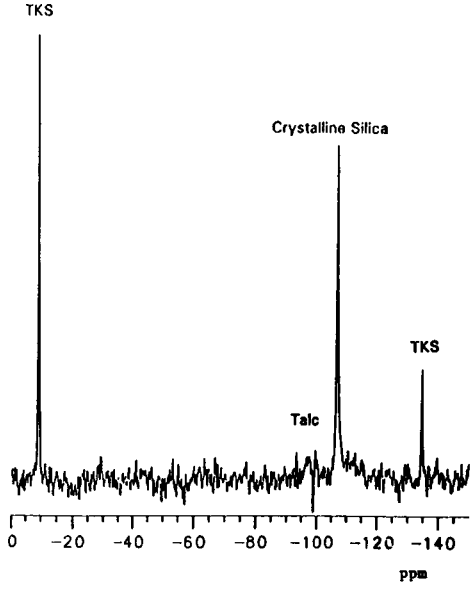

Fig. 7. Sienna 3 with TKS. The integral at $\delta = -9.4$ ppm is 1000 and the integral for the crystalline silica region $\delta = -106$ to -109.5 ppm is 1408.

DISCUSSION

The original objective for this project was to develop an alternative test method for the analysis of crystalline silica. In developing the solid state ^{29}Si NMR technique there were several factors to address. The primary limitation at the start of the project was the sensitivity required to achieve reproducible analyses of silica at the 0.1 wt.-% level. The definition of the spectrum is improved with signal averaging (i.e. increase the number of acquisitions). The silicon T_1 values are the limiting factor in how many acquisitions can be recorded in a reasonable time. Quantitative NMR is best accomplished by waiting a minimum

of 5 T_1 values between acquisitions for a 90° pulse. The first series of experiments determined the T_1 values for α-quartz and cristobalite samples were greater than 5000 s. With T_1 values of that magnitude the experiment would require greater than 8 h between acquisitions. The protocol was developed to provide a reduced acquisition time between pulses and maximize the number of pulses for the best signal to noise ratio while maintaining accuracy of the quantitative analysis.

In the development of the protocol a maximum tip angle of 10° was established. For our analyses it was necessary to increase the silicon pulse length to 9 μs to give a silicon 10° tip angle of a minimum of 1.0 μs. Pulses shorter than 1.0 μs suffer from increasing amounts of distortion due to limitations of the NMR spectrometer. A second situation involved determining the appropriate recycle delay for the silica analysis. Initial experiments with the α-quartz/amorphous blend utilizing a 10° pulse angle and relaxation times from 1 to 60 min yielded an effective pulse delay of 20 min. Replicate analyses with a recycle delay of 20 min showed no decrease in the α-quartz signal and had similar signal to noise ratios to the 40 and 60 min series. Based on this data the protocol was established at a pulse angle of 10° with 20 min between acquisitions.

The six blended samples provided a blind test of the protocol. Based on the data the agreement between XRD and NMR analyses for the samples is with in a few percent. The only exception is sample 2 where NMR did not detect the amorphous component. There are three factors that provide possible explanations. The amorphous silica peak is broad in comparison to the α-quartz and cristobalite signals. The width and short peak height make it difficult to distinguish this weak resonance at low concentrations of amorphous silica in the presence of high concentrations of α-quartz or cristobalite. The 10 Hz exponential line broadening used to process the spectra is appropriate for α-quartz and cristobalite but not for amorphous silica. Because of the broad peak a suitable exponential line broadening for amorphous silica would be 50 Hz or greater, but this could distort the quantification of the α-quartz and cristobalite. The subjectivity of the operator in processing the spectrum with the curve-fitting software is also important. The overall agreement between the NMR and XRD analysis for the blend samples provides proof of the effectiveness of the protocol utilizing a reduced pulse angle for analyses of silica polymorphs.

Based on the success of the blended samples the next phase of the project was the analysis of bulk samples. Natural iron oxide pigments were chosen as a matrix for NMR analysis. The natural pigments differ from the synthetic pigments in the complexity of composition. The synthetic pigments typically contain 99% Fe_2O_3 while the natural pigments may contain as much as 40% of other species. Other minerals present may include talc, kaolin, and amorphous silica in addition to crystalline silica. These materials may interfere with XRD patterns. For brown shades the opacity of the pigments prohibit analysis by optical microscopy. Two negative aspects of this choice for bulk analysis are apparent: the complete composition of the matrix is not known (i.e. it may contain paramagnetic centers), and a poor concentration ratio is achieved during the acid wash preparation. Typically the acid digestion step only improves the proportion of crystalline silica moieties by a factor of three for these natural brown materials.

Several preliminary experiments were required prior to NMR analysis of the pigments. The first step is the sample concentration procedure described in the experimental section. The acid insoluble fractions for the natural iron oxide pigment samples were on the order of 30 to 39%. Single pulse excitation spectra were recorded for talc and kaolin to insure no chemical shift interferences with crystalline silica and that the T_1 values were less than that of α-quartz. Once the pigments were prepared a technique was required for quantitative analysis. Spin counting was employed to quantify the amount of crystalline silica present in the acid insolubles of the pigment. Spin counting relies on an internal standard of a known number of spins to standardize the spectrum.

Effective spin counting requires a standard that is nonvolatile, possesses a narrow band width,

with T_1 less than the analyzed species. The hexamethylcyclotrisiloxane used as an external reference is too volatile to be used as a spin count reference for overnight runs. Tetrakis(trimethylsilyl)silane (TKS, $[(CH_3)_3Si]_4Si$) has been used as a chemical shift reference for solid state ^1H and ^{13}C NMR and has been used for quantitative spin counting [21,22]. In order to use TKS as a spin count reference the silicon T_1 had to be less than α-quartz and cristobalite. The silicon T_1 for TKS was measured at approximately 250 s, substantially less than the T_1 values for the silica polymorphs. A second requirement was that none of the TKS silicon resonances interfered with any of the crystalline silica signals. The two resonances for TKS ($\delta = -9.4$ and $\delta = -134$ ppm) are well separated from the region of interest.

The spin counting experiment for the α-quartz standard had a percent recovery of approximately 73%. The explanation for the incomplete recovery is not known at this time. One possible factor is that TKS is inappropriate as a silicon spin count reference for the silica species we are analyzing. The fact that the weight recovery for both relaxation cycles was the same provides proof of the protocol. The correction coefficient of 1.36 was employed based on a recovery of 73% for the α-quartz standard. Alternative spin count standards will be evaluated against TKS in future experiments.

The weight percent obtained for the spin counting experiments of the iron oxide pigment samples are in agreement within $\pm 2\%$ for the replicates of the Sienna samples. For the brown samples, where the concentration of crystalline silica is low, the error bars range from 10 to 18%. The weight recovered in each instance was calculated with the correction coefficient of 1.36. The brown shade pigment samples represent a blend of iron oxide and other minerals. These other minerals and the opacity hinder crystalline silica analysis at trace levels. Solid state ^{29}Si NMR provided crystalline silica determination at levels below 0.1% for this material. A problem exists in that an alternative analytical technique is needed as a check on the NMR results. More replicates and comparison techniques are planned.

A second problem associated with the NMR technique as developed is lengthy analysis time. An experiment utilizing 48 acquisitions requires 16 h. This can be addressed by increasing the sample size. The sample volume of the 7 mm rotor is 0.35 cm^3. Maciel and Zhang [23] have demonstrated the effectiveness of solid state MASS NMR utilizing large volume sample rotors, 2.5 cm^3 and 6 cm^3, for ^{13}C and ^{29}Si NMR analysis, respectively. With the 2.5 cm^3 rotor the sensitivity would be improved by a factor of approximately seven over the current probe and rotor system used in this project, reducing the total number of acquisitions to one for the same sensitivity. Such probe systems are commercially available (Doty Scientific, Columbia, SC). Increasing the sample size increases the number of observed nuclei improving the signal strength. A second approach to improve the sensitivity is through sample preparation. Vassallo et al. [24] have demonstrated the effectiveness of reducing paramagnetic contributions of iron and manganese through treatment with sodium dithionite and improving their spin count efficiency.

Conclusion

A solid state ^{29}Si NMR method utilizing a 10° pulse angle coupled with a 20 min recycle delay has been developed for the analysis of crystalline silica. The benefits associated with the NMR approach are: there are no restrictions based on particle size, it is appropriate for all silica polymorphs, and is free of interferences based on work completed. The NMR protocol was successfully demonstrated in blind analyses of blended standards. The technique was utilized in the analysis of the acid insoluble fraction of brown shades of natural iron oxide pigments. The total weight percent crystalline silica was determined with spin counting using TKS as an internal standard. The NMR analyses for pigment samples were in agreement to within two percent per lot. A correction coefficient was utilized based on spin count analysis of the α-quartz standard.

The experiments to date indicate that solid state ^{29}Si NMR can be used as an alternative technique for the analysis of crystalline silica. Solid state NMR could be used for analysis of other silica containing matrices (i.e. calcium car-

bonate or talc). It is also possible that the solid state ^{29}Si NMR could be used to determine respirable crystalline silica. There are currently some limitations associated with the technique. The utility of ^{29}Si NMR as a technique for the quantification of crystalline silica is dependent upon increasing the sensitivity, decreasing analysis time, and providing complete recovery for spin count experiments. The protocol of a 10° pulse angle with a 20 min relaxation delay enabled us to perform quantitative analysis for crystalline silica. Analyses of the blind samples provided a positive test of the protocol and the ability of NMR to differentiate silica polymorphs. More work is needed regarding spin counting and bulk analysis.

The authors gratefully acknowledge Gary Tomaino of Pfizer Inc., Easton, PA for providing standards, the blind test samples, XRD analyses of the materials and valuable discussion during the course of the project. The authors also extend special thanks to William Mellick and Dr. Armand Brachman of Binney and Smith for valuable suggestions during the project. We also thank Deanna Quay and Michael Alaimo of Lehigh University for their assistance with the spectrometer. Thanks are offered to Charles Hoover Jr. of Hoover Color Co. for providing pigment samples.

REFERENCES

1 World Health Organization, IARC Monographs on the Evaluation of the Carcinogenic Risk of Chemicals to Humans: Silica and Some Silicates, Vol. 42, IARC Working Group, Lyon, 1986.
2 National Institute of Occupational Safety and Health, NIOSH Manual of Analytical Medthods, Silica: Crystalline-Respirable, Method 7500, revised May 1989.
3 E. Lippmaa, M. Magi, A. Samoson, G. Engelhardt and A.R. Grimmer, J. Am. Chem. Soc., 102 (1980) 4889.
4 E. Lippmaa, M. Tarmak and G. Engelhardt, J. Am. Chem. Soc., 103 (1981) 4992.
5 J. Klinowski, S. Ramadas, J.M. Thomas, C.A. Fyfe and J.S. Hartman, J. Chem. Soc., Faraday Trans., 2, 8 (1982) 1025.
6 J.V. Smith and C.S. Blackwell, Nature, 303 (1983) 233.
7 H. Graetsch, A. Mosset and H. Gies, J. Non-Crystalline Solids, 119 (1990) 173.
8 M. Kanzaki, J.F. Stebbins and X. Xue, Geophys. Res. Lett., 18 (1991) 463.
9 J.E. Emig and D.K. Smith, Powder Diffraction, 4 (1989) 209.
10 R. Carter, M.T. Hatcher and L. DiCarlo, Anal. Chem., 59 (1987) 513.
11 R.K. Harris and B.E. Mann, NMR and the Periodic Table, Academic Press, London, 1978.
12 P.F. Barron, R.L. Frost and J.O. Skjemstad, J. Chem. Soc., Chem. Commun., (1983) 581.
13 A.E. Derome, Modern NMR Techniques for Chemistry Research, Organic Chemistry Series, Pergamon, Oxford, New York, 1987.
14 R. Wolf, R. Radeglia and C. Vogel, J. Phys. Chem. Solids, 51 (1990) 123.
15 R.J. Abraham, J. Fisher and P. Loftus, Introduction to NMR Spectroscopy, Wiley, New York, 1988.
16 M.L. Martin, G.J. Martin and J.J. Delpuech, Practical NMR Spectroscopy, Ann Arbor Science Publ., Ann Arbor, MI, 1980.
17 D.A. Torchia, J. Magn. Reson., 30 (1978) 613.
18 E.W. Hagaman, R.R. Chambers and M.C. Woody, Anal. Chem., 58 (1986) 387.
19 F. Devreux, J.P. Boilot, F. Chaput and B. Sapoval, Phys. Rev. Lett., 65 (1990) 614.
20 C. Dybowski and R.L. Lichter, NMR Spectroscopy Techniques, Practical Spectroscopy Series, Marcel Dekker, New York, 1987.
21 L.M. Stock, J.V. Muntean and R.E. Botto, J. Magn. Res., 76 (1988) 540.
22 L.M. Stock, J.V. Muntean and R.E. Botto, Nato Advanced Study Institute on New Trends in Coal, Kluwer, Dordrecht, 1988.
23 G.E. Maciel and M. Zhang, Anal. Chem., 62 (1990) 633.
24 A.M. Vassallo, M.A. Wilson, P.J. Collin, J.M. Oades, A.G. Waters and R.L. Malcom, Anal. Chem., 59 (1987) 558.

Analytica Chimica Acta, 286 (1994) 37–47
Elsevier Science B.V., Amsterdam

Determination of quartz in kaolins by x-ray powder diffractometry

N.J. Elton, P.D. Salt and J.M. Adams

ECC International, Research and Development Department, John Keay House, St. Austell, Cornwall PL25 4DJ (UK)

(Received 13th August 1992; revised manuscript received 10th November 1992)

Abstract

Depending upon their origin, naturally occurring kaolins contain various accessory minerals including micas, feldspars and quartz. These minerals may be partially removed, but rarely eliminated, by refining. When determining quartz by x-ray diffractometry, serious problems are encountered even with refined kaolins due to overlapping peaks from micas, feldspars and kaolinite itself. This paper discusses the peak overlap and other problems and describes how optimisation of sample preparation and diffractometer parameters, together with the use of profile fitting techniques permits the determination of crystalline quartz in bulk samples to $\pm$ 0.015 wt.% (1σ absolute) at the 0.1 wt.% level. A detailed examination of the errors involved in the analysis shows that counting and particle statistics are the most important error sources. For the samples examined in this study, counting statistics is the major contributor to the observed 15% relative error. Preliminary results on the use of a laboratory air classifier to generate "large" respirable dust samples from bulk powders for quartz analysis are given.

Keywords: X-Ray diffraction; Crystalline quartz; Kaolins; Quartz

Legislation controlling health and safety in the workplace and for both commercial and domestic products presents the analyst with many challenges. In particular, the concentration level at which a hazardous component necessitates either a warning label or a specific statement on a safety data sheet may be set at a value which is near or even beyond that attainable by current analytical techniques. An example is crystalline silica, for which the limits are as low as 0.1 wt.% in bulk samples and 0.05 mg/m^3 in respirable dust samples when collected over an 8 h time period [1,2].

Whilst crystalline silica occurs in various distinct forms, only quartz has been found in commercial kaolins. This paper discusses in detail some of the sources of error involved in the determination of low levels of quartz in kaolins by x-ray powder diffractometry. The quantitative method has been described in detail elsewhere [3], but is briefly reviewed here.

The method described here is applicable to "bulk" specimens, but respirable dusts can also be analysed if sufficient sample is available. Some preliminary results are given which compare the analysis of specimens from personal samplers (i.e. respirable dusts) with analysis of bulk specimens of respirable size obtained by air classification of the materials being processed when the personal samples were collected.

Correspondence to: P.D. Salt, ECC International, Research and Development Department, John Keay House, St. Austell, Cornwall PL25 4DJ (UK).

EXPERIMENTAL

Instrumentation

All the x-ray data presented were obtained using a Philips PW 1825 programmable generator

SSDI 0003-2670(93)00465-P

fitted with a long fine-focus copper anode x-ray tube run at 40 kV and 45 mA. Philips APD 1700 software controlled the PW 1050 vertical goniometer which was equipped with a proportional detector, graphite monochromator and automatic sample changer. For the quartz determinations, step scans were made at 0.02° 2θ intervals over the range $49.7° \leq 2\theta \leq 50.5°$ using a 0.3 mm receiving slit and a 2° divergence slit. A counting interval of 500 s per step was used for quartz contents ≤ 0.5 wt.% (giving a single sample time of 5.7 h) and 100 s per step (i.e. 1.5 h per sample) when the quartz content was greater than 0.5 wt.%. For the investigation of errors, a 1° divergence slit was used and scans made in range $25.8° \leq 2\theta \leq 27.3°$ using 0.02° 2θ steps. The counting time per step depended upon the concentration of quartz examined and varied from 10 s to 1000 s to reduce the counting statistics error to a negligible level which was approximately the same irrespective of quartz content.

Selection of quartz peak for commercial kaolin analysis

Kaolins contain a range of accessory minerals including quartz, mica, feldspars, tourmaline, anatase, rutile, graphite and montmorillonite in addition to the major component, kaolinite itself. Processing of the naturally occurring material often significantly reduces the concentrations of many of these contaminants, but detectable levels usually remain. In particular, the presence of mica in nearly all kaolins examined was a major influence on the choice of the quartz peak used for analysis. The three principal quartz peaks are listed in Table 1 together with potentially overlapping ones arising from other minerals present.

Heating to 800°C removes interference from kaolinite (dehydroxylation causes formation of amorphous metakaolin) and graphite (carbon removed as dioxide). This procedure does not affect mica or feldspars, and their interferences remain. As indicated in Table 1, both the (100) and (101) quartz peaks can suffer significant mica and feldspar interference.

Early in this study, an attempt was made to use profile fitting techniques to separate the overlapping peaks. Although the software was written specifically for this particular problem, profile fitting was found to be unreliable for the accuracy required, even with appropriate constraints, owing to the chemical and crystallographical variability of mica [3,5].

TABLE 1

Potential peak overlaps (Data for Cu $K\alpha$ radiation) [a]

Quartz °2θ	Kaolin °2θ	Muscovite mica °2θ	K-Feld-spar °2θ	Graphite °2θ
20.86 (19)	19.88 (19)	20.22 (10)	19.28 (3)	
100	20.36 (47)	20.63 (22)	21.08 (53)	
	21.36 (44)	21.64 (16)		
26.64 (100)	26.02 (2)	25.60 (62)	25.70 (51)	26.51 (100)
101	26.44 (17)	26.70 (83)	26.92 (100)	
			27.58 (82)	
50.14 (11)	49.84 (3)		49.92 (2)	50.67 (5)
112	50.68 (1)		50.50 (2)	
			50.56 (20)	
			50.68 (13)	

[a] The numbers given in parentheses are the intensity of the peak relative to the maximum in the given individual patterns (= 100) for a 1° divergence slit. Miller indices for the quartz peaks are given in italics. The peak positions given for mica and feldspar are illustrative only and will vary depending upon the mineralogy and chemical composition of the particular species present in the kaolin. Data for Quartz, Kaolin, Muscovite ($2M_1$) and K-Feldspar (orthoclase) from Borg and Smith [4]. Data for Graphite from JCPDS card 23–64.

The (112) quartz peak at 50.14°2θ(Cu $K\alpha$) (1.818 Å) was selected for quantification because the feldspar overlap could be readily resolved by the 'in house' profile fitting program, avoiding the potential ambiguities involved in fitting close overlaps [3,5].

Sample preparation

For reproducible results, it is essential that a standard procedure is adopted for sample preparation. Klug and Alexander [6] demonstrated that the precision of replicate analyses of quartz specimens was dependent upon particle size (see below). Samples were wet ground in a McCrone micronising mill to less than 5 μm size using corundum elements. The resultant slurries were filtered and dried. All samples and standards were further milled in a Janke and Kunkel labo-

ratory mill for a further 30 s and then calcined at 800°C for one hour to destroy any graphite and dehydroxylate the kaolinite.

Variability in sample holder packing can introduce variations in measured peak intensity. These effects were minimised by gently backfilling 0.500 ± 0.005 g sample into a standard Philips circular sample holder (27 mm internal diameter by 2.4 mm deep) and then applying a fixed pressure using a tool specially developed for the purpose (Fig. 1).

Calibration

Calibration was by external standard. A set of standards was analysed with each run of unknowns to minimise variations from batch to batch. In addition, an external reference sample (Arkansas stone) was analysed for the (101) quartz peak area at the beginning and end of each run to check on instrument stability. A reference kaolin was selected in which quartz, mica and feldspar were below the detection limits at their strongest reflection (measured using 0.2° 2θ steps with a counting time of 500 s per step and instrument parameters optimised for counts). Standard quartz, NIST SRM 1878 (95.5% crystalline α-quartz), was added to this reference kaolin in amounts to cover the range from 0 to 2 wt.%. The area of the (112) quartz peak was derived by profile fitting and the calibration line of peak area vs. wt.% quartz added obtained using unweighted least squares.

ANALYSIS OF COMMERCIAL KAOLINS

A series of commercial kaolins from various sources were first analysed using the 100 s per step counting time. Those samples found to contain less than 0.5 wt.% quartz were re-analysed using the 500 s per step counting time. The calculated quartz contents were corrected for both matrix absorption and loss on calcination (LOC) differences relative to the standard kaolin.

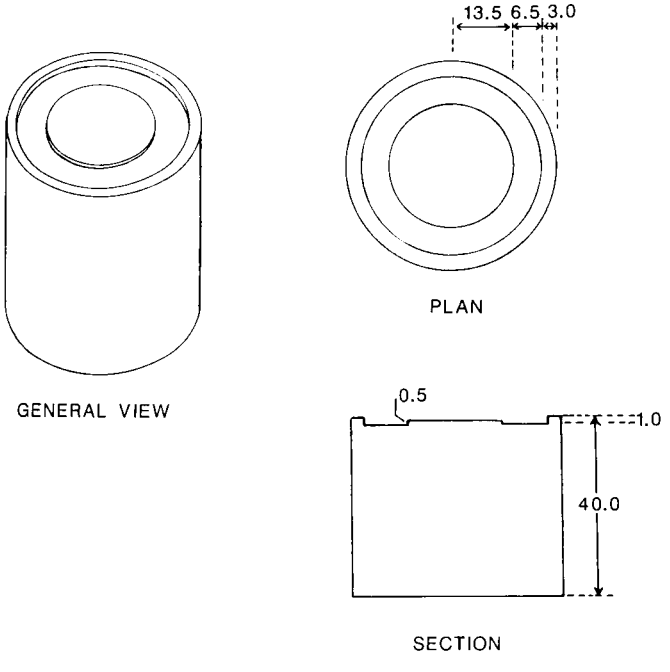

Fig. 1. Tool for the uniform pressing of samples. Tool is manufactured from aluminium. All dimensions shown are in mm, and are approximate.

TABLE 2

Analytical data for commercial kaolins from a range of producers [a]

Sample	μ^* ($cm^2\ g^{-1}$)	LOC wt.%	Wt.% total quartz	
			Uncorrected	Corrected
S	36.13	14.0	0.00 (0.005)	0.00 (0.005)
A	36.62	14.2	0.00 (0.015)	0.00 (0.015)
B	39.26	14.1	0.05 (0.011)	0.06 (0.011)
C	37.16	14.0	0.12 (0.012)	0.12 (0.012)
D	37.08	12.6	0.28 (0.035)	0.27 (0.035)
E	37.96	13.4	0.32 (0.015)	0.32 (0.015)
F	37.65	12.3	0.54 (0.04)	0.53 (0.04)
I	36.42	13.2	0.80 (0.045)	0.76 (0.045)
J	38.89	11.1	1.10 (0.055)	1.10 (0.055)
L	38.99	11.6	1.23 (0.06)	1.23 (0.06)
M	40.91	9.3	2.10 (0.06)	2.15 (0.06)

[a] Numbers in parentheses are 1σ absolute estimated from the profile fit error on a single sample (mainly counting statistics). LOC = Loss on calcination. Sample 'S' is the standard matrix, quartz content determined by standard addition. 'Corrected' refers to correction for mass absorption, LOC variations and also the amorphous content of the standards.

The total correction is given by $x' = c_{\mu^*} c_L x$ where x is the uncorrected wt.% quartz in the unknown, x' the corrected value, and

$c_{\mu^*} = \mu^*/\mu_1^*$ is the mass absorption correction

and

$c_L = (100 - L_1)/(100 - L)$ is the LOC correction.

μ^* is the mass absorption coefficient of the unknown, μ_1^* is the mass absorption coefficient of the 1 wt.% standard. L is the loss on calcination of the unknown, and L_1 that of the 1 wt.% standard. A correction was also applied to take account of the non-crystalline content of the standard calibration quartz (see below).

Some results are given in Table 2. The reproducibility of the whole procedure was estimated by measuring 10 preparations of a given sample and comparing the average standard deviation calculated from the profile fitting (based on fit and counting statistics) with the observed standard deviation. From the results given in Table 3 it was concluded that the total quartz content of bulk commercial kaolins could be determined to $\pm$ 0.015 wt.% (1σ absolute) at the 0.1 wt.% level, (i.e. 15% relative error), with the given analytical procedure and that the error was probably dominated by counting statistics.

TABLE 3

Reproducibility analysis data (Based on measurements on 10 replicates preparations of each sample) [a]

Sample	Counting time (s)	R(%) wt.%	$\langle\sigma_{PF}\rangle$ wt.%	σ_{obs} wt.%
0.10 wt.% standard	500	0.06	0.014	0.018
Sample C (0.12 wt.%)	500	0.03	0.012	0.014
Sample B (0.06 wt.%)	500	0.02	0.011	0.010

[a] R = Observed range of calculated quartz content. $\langle\sigma_{PF}\rangle$ = Average standard deviation calculated from the profile fit. σ_{obs} = Observed standard deviation, calculated from the reproducibility data.

ORIGIN OF ERRORS IN QUANTITATIVE ANALYSIS OF QUARTZ

Introduction

Whilst the observed standard deviation given above is adequate for many routine analyses, a 15% (relative) uncertainty is undeniably large and a reduction of this figure would be very desirable. Furthermore, it is not clear to what extent this estimated error provides limits on the accuracy of the procedure as opposed to simply its precision. In the present section, the various errors contributing to the overall measurement uncertainties are examined and quantified (as far as possible), thus enabling the accuracy of the method to be judged and reasoned suggestions to be made for reducing the overall error.

TABLE 4

Sources of error in quantitative XRD

Instrument related	Sample related	Data processing effects
Instrument instability	Particle statistics	Peak area measurement
Counting statistics	Sample preparation	Peak overlap treatment
Detector dead time	Particle size effects	μ^* + LOC corrections
Mis-alignment	Orientation	
	Weighing errors	

In quantitative XRD, numerous factors have an influence on the measured line intensity [7,8], random or systematic variations in which lead to uncertainties in quantification. The sources of error can be broadly categorised according to whether they are predominantly instrument related, sample related or data processing related (Table 4), however, such categorisation is far from absolute as many effects are interrelated.

A second way of categorising the various sources of error is according to whether they are 'determinable' or 'non-determinable' on the basis of the measurements made. This categorisation depends on whether a single sample is measured, replicate measurements are made on a single sample, or measurements are made on replicate preparations of a given sample (Table 5). A single measurement of a single sample has a large number of non-determinable errors. For a routine analysis method, measurement of single samples is most desirable, but a reliable assessment of the measurement precision and accuracy is crucial. The purpose of this section is to examine and quantify (as far as possible) the relative contributions of the various error sources, both theoretically and experimentally. Much of this discussion will be familiar to practitioners of x-ray diffraction, but it is useful to repeat it in the specific context of the analysis of quartz, and with the benefit of relevant experimental data.

Instrument related effects

Included in this category is the counting statistics error. Although this error may be regarded as a property of the measurement, it has its origins in the random emission of x-rays from the tube anode. The distribution of errors on a measurement of N quanta is governed by Poisson statistics and will therefore have the standard deviation $\sigma(N) = \sqrt{N}$. Counting statistics is the only error that can be reliably estimated for a single measurement. The fractional error $\sigma(n)/N$ is obviously reduced by increasing the number of counts N. For a given specimen, increasing x-ray power, counting for longer times, and using wider collimating slits will contribute to a reduction in the counting statistics error. The practical power limit for a typical x-ray tube is about 2.7 kW for a broad focus tube and 2.2 kW for a long fine-focus tube. A rotating anode generator could be used to give an eight-fold increase in power (i.e. the counting statistics error would be reduced by a factor of $1/\sqrt{8}$).

The maximum width of the divergence slit is governed by the diffractometer geometry and the size of the sample, with wider slits possible at higher angles. The maximum size of the receiving slit is not only limited by geometry, but also by the requirements of adequate peak resolution. The latter may be important if profile fitting techniques are being used to deal with peak over-

TABLE 5

Determinable and non-determinable errors in quantitative XRD

Error source	Estimated by measurement of	
	Single sample	Replicate preparations
Counting statistics	yes	yes
Particle statistics	no	yes
Sample packing effects	no	yes
Profile fit errors	no	yes
Short-term instrument flucuations	no	yes
Particle size effects (amorphous layer problem)	no	no [a]
Long-term instrument fluctuations	no	no [a]
Errors in decomposition of close peak overlaps	no	no [a]
Mass absorption variations between sample and standard	no	no [a]
Loss on calcination variations	no	no [a]

[a] These systematic effects may be eliminated or corrected for.

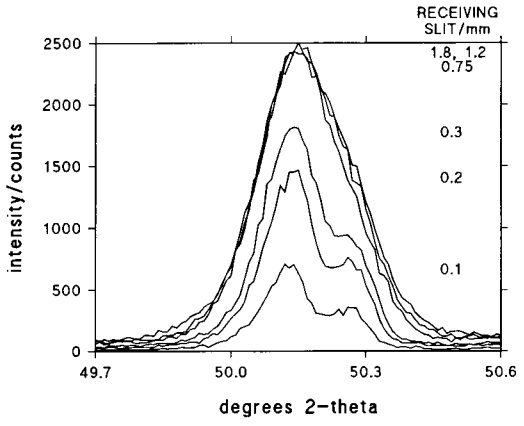

Fig. 2. Effect of receiving slit width on peak intensity and resolution. Wider receiving slits give increased intensity until they exceed the width of the x-ray beam. Resolution decreases with increasing slit width.

laps. The width of the divergence slit also affects resolution. In both cases wider slits give poorer resolution. Figure 2 illustrates the effect of varying the receiving slit width on the (112) quartz peak using a fixed divergence slit (2°) system and with a long fine-focus tube. The loss in resolution with increasing receiving slit width is obvious. Moreover, when the width of the receiving slit exceeds that of the x-ray beam, no further increase in intensity is observed. If increased intensity were the sole consideration, then a broad focus tube and wider receiving slit could be used, but resolution would be severely limited. In any experiment there must be a trade-off between narrow slits for resolution and wide slits for counts. The balance will be determined by the nature of the measurements being made. In the present work, whilst high counts are vital, adequate resolution was also considered to be an important requirement.

A second instrument-related error source is thermal and electrical instabilities in the diffractometer itself. For the generator used in the present work, the stability specification is about 0.01% power variation per 1% mains fluctuation; in practice this leads to negligible intensity variation. However, Brown et al. [9] observed a variation in peak intensity of around 1.5% with 5°C change in ambient temperature. The instrumentation used in the present work is not operated in a closely controlled environment and significant variation in temperature may be expected during a run of samples. To examine the significance of such effects a single (stationary) sample of 5 wt.% quartz in pure calcined kaolin was scanned 10 times over the range 25.8° to 27.3° 2θ during a $10\frac{1}{2}$ hour period. The total area was measured for each scan (peak + background) and the uncertainty due to counting statistics calculated. The observed spread of results $\sigma_{obs} \approx 0.4\%$ (relative) whereas the expected counting statistics error was only $\sigma_{cs} \approx 0.04\%$ (relative). The most obvious explanation of the unexpectedly large σ_{obs} is in terms of thermal and other instrumental fluctuations. In this instance, such fluctuations limit the overall precision to about 0.5% (relative). Environmental control may significantly reduce variations due to thermal instabilities, but in *practical* terms, this error source is of little importance (see below).

Sample related effects

Sample preparation. Careful and reproducible preparation of the sample received for analysis is essential for any accurate quantitative method. Unfortunately, uncertainties arising from variations in sample preparation are difficult to quantify.

Representative sampling is a basic requirement and assumes homogeneous mixing of the various components of a multiphase mixture. Methods for achieving representative sampling are well documented [10]. Homogeneous mixing is critical in the preparation of standards, particularly at low concentrations. In the present work, after weighing, standards are mixed in a SPEX mill for 15 min in polyacrylate vials using polymethacrylate balls. Random uncertainties introduced by inhomogeneous mixing or weighing errors in preparation of the standards are accounted for in the estimated error in the calibration line fit (the error on the calibration line slope is typically about 1% relative. See for example [3]). It is generally necessary to micronise all test samples. However, agate elements can introduce significant quartz contamination (ca. 0.1 wt.% in 15 min grinding for a kaolin sample) and their use should be avoided.

Non-reproducible packing of the sample in the specimen holder is another potential source of error. Variations in packing density lead to variations in transparency effects and possible orientational effects. Ideally, the sample surface should be uniformly flat and smooth [11]. To achieve reproducible packing for a given type of specimen, a carefully measured mass is backfilled into the sample holder using a special tool as described in *Sample preparation* in the Experimental section.

Particle statistics. The influence of particle statistics on the reproducibility of intensity measurement is well documented [6,11–13]. Particle statistics simply refers to statistical variations in the number of particles contributing to diffraction. The effect is often called crystallite statistics, but because the present discussion will refer to actual particles, the former term seems most appropriate. Calculation of the effect requires knowledge of the average number of particles in a position to contribute to the measured diffracted intensity, which is typically a small fraction of the total number of particles present. The uncertainty in the average number contributing to diffraction, N_{diff}, is appropriately described by Poisson statistics, and is simply given by $\sigma_{\text{PS}} = \sqrt{N}_{\text{diff}}$.

Accurate theoretical estimates of the magnitude of the effect are difficult, and in this section an empirical approach is taken.

A sample of Sikron F600 quartz standard (obtained from the U.K. Health and Safety Executive) was taken and two particle size cuts made by sedimentation, yielding samples with $\langle d \rangle = 3.3$ μm and $\langle d \rangle = 6.9$ μm. In each case the distributions were fairly sharp with 80% by mass between 2 and 5 μm for the finer fraction and 80% between 4 and 10 μm for the coarser fraction (measured by laser diffraction using a Malvern Mastersizer).

Ten replicates of both the fine and the coarse quartz were prepared in a pure calcined kaolin at concentrations in the range 0.05 wt.%–50 wt.%. Samples were packed to a uniform density of 0.44 g cm^{-3} using the technique described earlier. The samples were measured using an appropriate scan time to reduce counting statistics errors to a negligible level whilst allowing a practical run time (20 min to 10.5 h per sample, depending on concentration). Scans were made over the range 25.8°–27.3° 2Θ and the area of the (101) quartz peak determined by profile fitting. For each set of replicates, the standard deviation in fitted peak area, σ_{obs}, was calculated and the contribution due to counting statistics removed. The results are shown in Fig. 3.

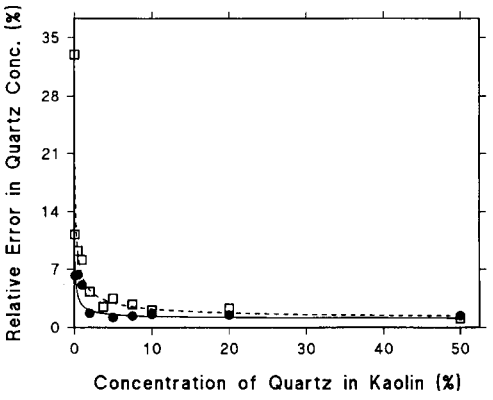

Fig. 3. Observed reproducibility data with corresponding least squares fit to Eqn. 1. Data were collected for 10 replicate preparations of samples containing a close-cut size fraction of quartz at various concentrations. Counting statistics errors were negligible. □ = Coarse (7 μm); ● = fine (3 μm).

At high concentrations, where the effects of particle statistics are minimal, the observed data levels out at around $\sigma_{\text{obs}} \approx 1.5\%$ (relative). If the errors were purely due to particle statistics, the observed error would be expected to continue falling. The levelling is due to a 'residual' error (σ_{residual}) which represents the combined effects of sample preparation (packing etc.), instrument instabilities and random data processing errors. The observed relative error in measured peak intensity, after removing the calculable effects of counting statistics, can be expressed by

$$\sigma_{\text{obs}} = \left(\sigma^2_{\text{residual}} + \sigma^2_{\text{PS}}\right)^{1/2} = \left(\sigma^2_{\text{residual}} + f/c\right)^{1/2} \quad (1)$$

Where c is the concentration of quartz in the sample (wt. fraction). The parameter f is a function of diffractometer geometry, crystal structure,

particle size and lattice plane. For a given geometry (see for example [12])

$$f = \frac{k\mu\langle v\rangle}{m \tan \gamma} \quad (2)$$

where k = constant (mainly geometrical factors), μ = linear absorption coefficient of the powder, $\langle v\rangle$ = mean particle volume, m = multiplicity factor for the given reflection and γ = divergence slit width (degrees). The curves on Fig. 3 represent a least squares fit of the data to Eqn. 1. On the basis of this fit, the residual error, $\sigma_{\text{residual}} \approx$ 1% (relative).

Figure 3 shows clearly that particle statistics can be a very significant source of error at low concentrations. At 50° 2θ, a 2° divergence slit may be used, and this increases the effective volume of sample. For quartz with $\langle d\rangle = 3.3$ μm, at 50° 2θ, the expected particle statistics error is about 4% (relative) at 0.1 wt.% concentration; for 7 μm quartz, the error is approximately 13% (relative).

Sample spinning is one way of improving particle statistics [12,13]. As a brief check on this, one set of 10 replicates (5 wt.% quartz) was measured stationary and spinning. The observed error for spinning samples was approximately 0.7 times that for stationary samples. Sample spinning can, therefore, offer a small, but useful, improvement in reproducibility where the total error is dominated by particle statistics. The most effective way of improving particle statistics is to ensure a small particle size. For clays and similar materials, 5 μm is probably adequate. However, particle statistics effects will obviously be more acute in a highly absorbing matrix and a smaller particle size or perhaps some form of quartz pre-concentration would be useful in such samples [5].

Other particle size and shape effects. Besides its major influence on particle statistics, particle size can also have an influence on measured intensity through the effects of extinction and microabsorption [11,14]. These effects are minimised by using fine powders and by ensuring the external standards are similar in particle size and matrix to the 'unknowns'. In practice, providing all samples are micronised as described earlier, the relative error introduced by differences in extinction and microabsorption between standards and unknowns is likely to be negligible in comparison with other error sources at the 0.1 wt.% level.

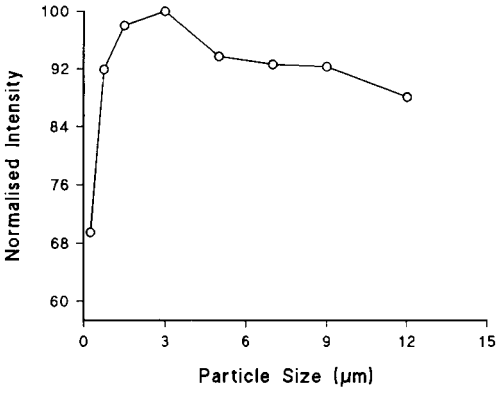

Fig. 4. The effect of particle size on the intensity of quartz (amorphous layer problem). Finer size particles show a decrease in intensity response as the amorphous layer becomes a relatively larger fraction of the total volume. The drop in intensity for large particles is due to extinction and microabsorption.

In the case of quartz, many workers have shown an additional systematic intensity dependence on particle size [15–17]. This effect is usually attributed to the formation of an amorphous layer approximately 0.03 μm thick around the particles. Finer particles show a relative decrease in intensity as the amorphous layer becomes a larger fraction of the particle volume. Fig. 4 shows a plot of normalised quartz (101) peak area as a function of mean particle size. The relative decrease in intensity below 3 μm is attributed to the amorphous layer. The smaller relative decrease for quartz coarser than about 3 μm is due to extinction and microabsorption effects.

The presence of an amorphous component can lead to a systematic error in the crystalline quartz determination. If the calibration standards are prepared by weighing the 'total' quartz as supplied, it will be necessary to later correct the calibration for the non-crystalline content of the standards. Fortunately, the NIST SRM 1878 standard quartz does have a certified crystalline content which enables a correction to be made. At the 0.1 wt.% level this correction is very small. Note that it is not necessary to know the particle

size distribution of quartz in the unknowns unless the analysis is aimed at estimating the 'total' quartz content, rather than just the crystalline.

Data processing errors

Errors involved in the measurement of peak areas can also be difficult to quantify. Profile fitting can be a very accurate method of determining peak areas, provided that the peak shape function used is valid and constrained appropriately, and that an appropriate background function is used. Serious systematic errors may occur in the fitting of closely overlapping peaks, particularly where variable minerals such as mica are involved. A fuller discussion of the problems is given by Elton and Salt [5]. In the case of simple count summation methods for isolated peaks, the treatment of the background is likely to be a source of error, more significant as peak intensity decreases. A straight line background is generally adequate over the range of a single peak, but should be fitted to a number of background points on either side of the peak.

Additional possible sources of error are mass absorption and loss on calcination corrections. If the corrections themselves are not made, significant systematic errors may be introduced. However, errors in actually calculating μ^* are typically fairly small and have a negligible effect on the accuracy of the quartz determination when compared with other error sources. The same applies to weighing errors in the loss on calcination calculation.

Overview of the measurement errors in the determination of quartz

It is now possible to estimate the various contributions to the observed 15% relative error quoted in the *Analysis of commercial kaolins* section. The 'residual error' of instrument effects, sample preparation effects and measurement errors is not expected to vary significantly with 2θ or concentration. For measurements on the (112) quartz peak, $\sigma_{\text{residual}} \approx 1\%$ (relative). At the 0.1 wt.% level, the expected effect of particle statistics for this peak is $\sigma_{\text{ps}} \approx 4\%$ (relative) for 3.3 μm quartz. It is difficult to determine the size of the quartz fraction within a kaolin sample. Although the kaolin may itself be fine (e.g. 80 wt.% less than 2 μm for a typical paper coating grade), a small but significant fraction remains greater than 5 μm, or even 10 μm. This coarse fraction frequently contains a significant portion of the quartz. Micronising of all samples is therefore vital, and should reduce the quartz to less than 5 μm. For quartz of this size, the combined particle statistics and residual error amounts to about 8% (relative). This value is consistent with the results of Table 3. It is clear therefore, that the measurements at 50.1° 2θ on the samples examined in this study are presently limited by counting statistics. Data are already collected using the highest practicable generator power, widest slits and longest practicable counting times. Further improvement in precision would call for the use of a rotating anode generator in the first instance.

However, it should be noted that the particle statistics error is strongly dependent on particle size and therefore, measurements on samples containing coarser quartz may well be dominated by particle statistics. Similary, the use of a rotating anode generator with the same counting times as at present would reduce the counting statistics error to a level where the effects of particle statistics would become significant. The analysis of replicate preparations is crucial to establish the overall measurement precision.

Ultimately, accuracy achievable depends upon correcting for, or eliminating certain systematic error sources. The dependence of diffracted x-ray intensity on particle size may be corrected for providing the non-crystalline content of the standard quartz is known (as it is for NIST SRM 1878). In practice, with micronising of all samples, the effects of extinction and microabsorption are likely to be negligible compared with other error sources at the 0.1 wt.% level.

Other effects which might be difficult to quantify, and which would not be revealed by reproducibility studies include erroneous fitting of overlapping peaks [5], diffractometer misalignment, and failure to apply mass absorption or loss on calcination corrections (if appropriate). However, if the measurement and analysis are carried out properly, these systematic errors should not be a problem.

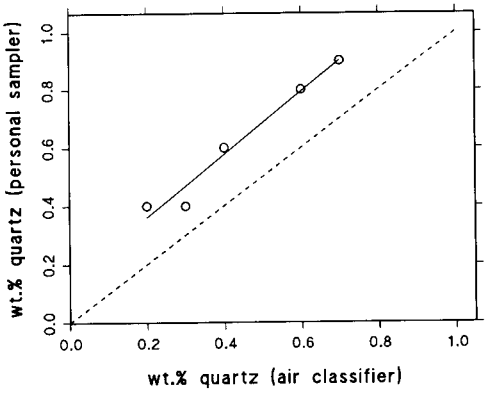

Fig. 5. Correlation between the quartz content of respirable samples from personal samplers and air classified material.

EXTENSION OF THE METHOD TO RESPIRABLE SAMPLES

The procedure described in this paper for the analysis of bulk samples would be applicable to respirable sized dusts if sufficient specimen were available.

A method presently under development in these laboratories uses an air classifier to collect large respirable-sized fractions from bulk powders. These samples are then analysed using the methods described above. The results of an initial study to compare quartz contents derived in this manner with those collected by personal sampling during processing of the same bulk samples are illustrated in Fig. 5. It should be noted that these particular samples were not *commercial* kaolins. Analysis of the personal sampler specimens was by the U.K. Health and Safety Executive Method for the Determination of Hazardous Substances, M.D.H.S. 51/2 [18]. Whilst the results of the two methods show good correlation, the quartz contents derived from the personal sampler method are consistently higher than those from the air classification method. Reasons for this discrepency are being investigated. One factor may be differences between the particle size distributions sampled by the two methods. A second is the effect of multiple phases on the quartz calibration procedure of the HSE method [18]. Air classification offers the advantage of being able to determine the respirable quartz content of the bulk material. This is not possible by personal sampling methods alone.

Conclusions

An x-ray diffraction method has been described which will determine crystalline quartz at the 0.1 wt.% level with an observed precision of ± 0.015 wt.% (1σ absolute) using standard XRD equipment and with acceptable counting times.

An evaluation of the various sources of error contributing to the measurement uncertainty at the 0.1 wt.% quartz level has been carried out. Assuming that micronising of samples reduces the quartz particle size to about 5 μm or less, with the present procedures, counting statistics is the dominant error source; particle statistics contributes about 8% relative error. Use of a rotating anode generator with existing counting times could reduce the total observed standard deviation to about 9% (relative) (i.e. ± 0.009 wt.% absolute), at which point particle statistics would become the dominant error source.

Errors due to specimen preparation and sample holder packing are negligible. The systematic error due to the amorphous layer problem may be corrected for if the crystalline quartz content of the standard is known. The use of NIST SRM 1878 is recommended. Other potential systematic errors may also be accounted for, or are likely to be negligible.

Air classification may be used to isolate large respirable sized samples from bulk powders. These samples may then be analysed using the procedures described above. This combination offers the ability to determine the respirable quartz content of the bulk powder.

REFERENCES

1 W.J. Miles and P.W. Harben, Industrial Minerals, December (1991) 21.
2 S.G. Ampian and R.L. Virta, Crystalline Silica Overview: Occurrence and Analysis, Bureau of Mines Information Circular/9317, United States Dept. of the Interior, Washington, DC, 1992.
3 N.J. Elton, P.D. Salt and J.M. Adams, Pow. Diff., 7 (1992) 71.

4 I.Y. Borg and D.K. Smith, Calculated X-ray Powder Patterns for Silicate Minerals, Geological Society of America, Boulder, CO, Memoir 122, 1969.
5 N.J. Elton and P.D. Salt, Anal. Chim. Acta, 286 (1994) 57.
6 H.P. Klug and L.E. Alexander, X-Ray Diffraction Procedures, Wiley, New York, 1974.
7 R. Jenkins, in D.L. Bish and J.E. Post (Eds.), Modern Powder Diffraction, Reviews in Mineralogy, 20 (1989) (Mineralogical Society of America) pp. 19–45.
8 R. Jenkins, in D.L. Bish and J.E. Post (Eds.), Modern Powder Diffraction, Reviews in Mineralogy, 20 (1989) (Mineralogical Society of America) pp. 47–71.
9 G. Brown, I.G. Wood and L. Nicholls, Pow. Diff., 2 (1987) 7.
10 T. Allen, Particle Size Measurement, Chapman and Hall, London, 1981.
11 D.L. Bish and R.C. Reynolds, Jr., in D.L. Bish and J.E. Post (Eds.), Modern Powder Diffraction, Reviews in Mineralogy, 20 (1989) (Mineralogical Society of America) pp. 73–99.
12 P.M. De Wolff, Appl. Sci. Res., 7 (1958) 102.
13 P.M. De Wolff, J.M. Taylor and W. Parrish, J. Appl. Phys., 30 (1959) 63.
14 M.M. Woolfson, An Introduction to X-Ray Crystallography, Cambridge University Press, London, 1970.
15 G. Nagelschmidt, Analyst (London), 81 (1956) 210.
16 J.W. Edmonds, W.W. Henslee and R.E. Guerra, Anal. Chem., 49 (1977) 2196.
17 B.H. O'Connor and W.J. Chang, X-ray Spectrosc., 15 (1986) 267.
18 HSE, Quartz in Respirable Airborne Dusts, Laboratory Method using X-Ray Diffraction (Direct Method), Methods for the Determination of Hazardous Substances: MDHS 51/2. U.K. Health and Safety Executive, 1988.

Analytica Chimica Acta, 286 (1994) 49–55
Elsevier Science B.V., Amsterdam

Quartz determination in kaolin at the 0.1% level

Timothy L. Salter and William E. Riley

Thiele Kaolin Co., P.O. Box 1056, Sandersville, GA 31082 (USA)

(Received 20th August 1992; revised manuscript received 5th February 1993)

Abstract

An analytical method was developed to detect quartz in kaolin at the 0.1% level to meet OSHA regulations. The x-ray diffraction quantitation method for the three kaolins investigated was adapted from the method of known additions. Careful sample preparation was necessary to minimize sample variations and to eliminate peak overlaps with the quartz (101) diffraction maximum. Several characteristics of the kaolins studied, including fine grain-size and low abundance of mica, simplified analysis of the kaolins. The linear relationship between amount of quartz added to the sample and the integrated peak area for the quartz (101) diffraction peak can be used both to estimate the quartz content of the original kaolin and as calibration line for analysis of unknown kaolins. The statistics of regression provide estimates of the precision and lower detection limit of the method. Data collection for the calibration lines is time-consuming owing to the low abundance of quartz. The quartz content of kaolin can be determined at the 0.1% level if the mica content of the kaolin is low. Mica shows a severe peak overlap with quartz that cannot be removed without creating other peak overlaps. The maximum quartz contents (quartz + mica) of the kaolins studied were: Cretaceous paper-coating kaolin, 0.04%; Arkansas lateritic kaolin, 0.05%; Eocene filler kaolin, 0.12%. The Eocene kaolin likely contains less than 0.1% quartz when the substantial mica content is considered.

Keywords: X-ray diffraction; Quartz; Kaolin

The Occupational Safety and Health Administration (OSHA) has classified respirable crystalline silica (including quartz) as a potential carcinogen under Hazard Communication Rules. Any product containing more than 0.1% respirable crystalline silica, or crystalline silica that can be made respirable, must be labeled as a potential carcinogen. This labeling requirement created several analytical difficulties that fall into two general categories: (1) quantitative analysis of quartz and other crystalline silica minerals; (2) definition of the term "respirable," which depends on the size distribution of the constituent particles.

Correspondence to: T.L. Salter, Chemical Lime Group, P.O. Box 121874, Fort Worth, TX 76121-1874 (USA) (present address).

OSHA Hazard Communication regulations for crystalline silica will affect almost all industrial mineral mining companies, and are of particular interest to clay mineral mining companies owing to the common association between silica polymorphs and clay deposits. No widely accepted method for crystalline silica determination at the 0.1% level is currently available. This study was initiated at Thiele Kaolin Co. to develop a method of quantitative analysis for quartz in kaolin that is accurate at 0.1 wt.-%.

Methods that are presently under consideration for quantitative quartz determination including x-ray diffraction (XRD), infrared spectroscopy, and automated scanning electron microscopy. Each method has distinct advantages and disadvantages. XRD can distinguish the silica polymorphs and excludes the noncrystalline ma-

SSDI 0003-2670(93)E0191-9

terials that are rich in SiO_2, but XRD cannot distinguish the particle size distributions of constituent particles. Scanning electron microscopy can estimate the size distributions of high-silica particles, but cannot distinguish crystalline silica from amorphous silica, and suffers from particle shape artifacts. XRD was chosen for quartz determination in kaolin owing to its extreme sensitivity to quartz, and for its ability to discriminate between silica polymorphs.

This study presents a method of quantitative analysis for quartz in kaolin which is accurate at 0.1 wt.-%. The objective of the investigation was to develop a method that could determine whether several commercial kaolin products contained more or less than 0.1% quartz. No attempt was made to develop a generalized quartz determination method useful over a wide range of quartz contents or in matrices other than kaolin. The restricted goals of the investigation led to several simplifications of our analytical methods which might not apply to greater ranges of quartz content or other matrix materials.

Kaolinite is a naturally occurring clay mineral that is common in fine-grained sedimentary rocks [1]. Kaolin is the term applied to mineral deposits composed substantially of the mineral kaolinite. The ideal composition of kaolinite is $Al_2Si_2O_5(OH)_4$, although few natural kaolins rocks approach the theoretical ratios of 38.5% Al_2O_3, 44.5% SiO_2, and 14.0% H_2O. Kaolins are typically contaminated with other clay minerals, micas, Ti-bearing minerals, quartz and other silica polymorphs, and many other fine-grained minerals. As will be illustrated below, these contaminants commonly complicate analysis of quartz in kaolin by XRD.

Kaolins are mined worldwide and provide functional fillers and coating materials for a myriad of diverse products. The characteristics of extreme resistance to attack by many chemicals and natural brightness and whiteness make kaolin one of the most ubiquitous materials used in manufacturing. This investigation was initiated at Thiele Kaolin Co. to determine the quartz contents of two typical kaolins from Georgia, USA. The quartz content of kaolin and the new OSHA quartz classification is understandably of considerable importance to an industry that supplies natural materials to a great diversity of end users.

Quantitation was attempted for three kaolins chosen for their unique physical and mineralogic characteristics and their diversity in particle size and mode of origin. These three kaolins, a Cretaceous paper coating kaolin from Georgia, an Eocene filler kaolin from Georgia, and a kaolin from the bauxite district of Arkansas, represent both commercial products of sedimentary origin and a residual kaolin formed by lateritic weathering. This preliminary study was initiated to both to develop the techniques necessary to quantitate quartz content at the 0.1% level, and to provide initial estimates of the quartz contents in three kaolins of diverse origin and composition.

EXPERIMENTAL

Materials

Cretaceous Kaolin, Georgia (KG). The Cretaceous kaolin studied is a paper coating kaolin marketed by Thiele Kaolin Co. under the commercial name "Kaogloss." Kaogloss is derived from a coarse-grained sedimentary kaolin comprised almost entirely of the mineral kaolinite. Quartz, anatase, and mica are the only common impurities. Kaogloss has been subjected to several methods of particle size separation that re-

TABLE 1

Compositions of kaolins considered in this investigation (Cretaceous kaolin, KG; Eocene kaolin, EG; Lateritic kaolin, LRA)

Kaolin Type	Al_2O_3	SiO_2	TiO_2	Fe_2O_3	K_2O	CaO	MgO	Na_2O	P_2O_5
Kaogloss	39.18	45.85	2.04	0.48	0.07	0.017	0.023	0.21	0.13
EG 44	38.28	45.66	2.59	0.96	0.17	0.023	0.033	0.09	0.057
LRA	38.86	46.01	0.38	0.72	0.16	0.096	0.027	0.21	0.164

move the coarse (> 5 μm) quartz and mica, and has been beneficiated by standard industry techniques. The chemical composition of the material studied is presented in Table 1.

Eocene Kaolin, Georgia (EG). The Eocene kaolin considered in this study is a commercial filler clay, "EG 44," marketed by Thiele Kaolin Co. The Eocene kaolins are also sedimentary deposits composed almost entirely of the mineral kaolinite. However, the Eocene kaolin is composed of individual kaolinite particles that are much smaller than are present in the Cretaceous kaolins. EG 44 is produced as a dry powder by air classification, in which pulverized kaolin is introduced into a rising air current, entraining the fine particles, and allowing the coarser material to settle out of the air column. This type of kaolin typically contains more quartz and mica than kaolins processed by "wet" methods. The composition of EG 44 is listed in Table 1.

Lateritic Kaolin, Arkansas (LRA). The lateritic kaolin was collected from a thick kaolin located in the wall of a bauxite mine near Little Rock, Arkansas. The laterite was formed on a sodalite-rich syenite, and contains very little, if any, quartz. Sodalite is a feldspathoid mineral that can only form in magmas that are undersaturated in SiO_2 and therefore (presumably) should not precipitate quartz. The Arkansas kaolin is composed of a mixture of well-crystallized kaolinite with a coarse particle size and fine-grained dehydrated halloysite. Halloysite has the same composition as kaolinite with the exception of two extra water molecules contained in the latter. The oxide composition of the Arkansas kaolin is presented in Table 1.

Respirable quartz. The quartz standard used for quantitation is National Bureau of Standards Standard Reference Material 1878, "Respirable Alpha Quartz". This material is used for preparing calibration standards for NIOSH Analytical XRD methods.

Methods

The method of quartz quantitation employed in this investigation is standard addition (quartz) to a two component mixture (quartz and kaolin), and is essentially similar to the method of known additions described in Brindley and Brown [2] and Snyder and Bish [3]. In this method, known amounts of quartz are added to the kaolin of interest and the resulting intensity of the quartz (101) diffraction peak (dependent variable) is regressed on the amount of quartz added (independent variable). The quartz versus peak intensity relationship is useful in three ways. First, the intercept of the resulting line with the 0% added quartz axis provides an estimate of the initial quartz content of the kaolin. Second, the statistics of linear regression provide estimates of the precision and lower detection limits of the method. Finally, the quartz content of an unknown kaolin *of similar composition* can be determined by comparing the intensity of the quartz (101) diffraction peak in the unknown with the reference line. The relationship between peak intensity and quartz content can be assumed to be linear over the interval studied because the mass attenuation coefficient of calcined kaolin is approximately equal to that of quartz, and because only a very small range of quartz from 0% to 0.4% was considered.

Although the method here described is straightforward in principle, quartz analysis in kaolin requires careful attention to sample preparation, data collection, and data analysis. The most common difficulties encountered in quartz analysis include: (1) peak overlaps between quartz and other minerals (including kaolinite), and (2) the low intensity of the quartz (101) diffraction peak at 0.1% compared to background radiation. Peak overlaps can be reduced or eliminated by heating the kaolin to 680°C for 30 min, which destroys the kaolinite crystal structure while keeping mullite formation to a minimum. Mica (muscovite) peak overlaps cannot be removed by heat treatment because the temperatures necessary to destroy muscovite also create substantial mullite and produce another peak overlap with quartz. The x-ray diffraction instrument configuration must be optimized and the instrument maintained in near-perfect alignment to maximize the quartz (101) diffracted peak intensity [4].

In addition to the concentration of individual quartz grains present, the intensity of the quartz (101) diffraction peak depends on a variety of

factors including particle size, degree of crystal perfection, and preferred orientation of the grains, and other factors involving the matrix material. The kaolins considered are extremely fine-grained and have been size fractionated to exclude coarser particles. The remaining kaolinite, quartz, and mica grains are approximately 1 μm or less in diameter, which is also the approximate particle size of the NBS 1878 Respirable Quartz material. In addition, it was assumed that the quartz in the kaolin and the NBS 1878 standard had approximately the degree of crystal perfection and would therefore produce similar intensities for the (101) diffraction peak as similar concentrations. However, to obtain a precise quartz particle size distribution from the kaolins of interest, and to match the distribution with an artificially prepared quartz standard of identical distribution and degree of crystal perfection, is beyond the scope of this investigation. The NBS 1878 Respirable Quartz was considered the best available standard at the time the investigation was initiated.

Sample preparation and analytical techniques

The quartz content of kaolin can only be attempted by measuring the intensity of the (101) diffraction peak (0.3343 nm): other diffraction peaks provide too little intensity for detection at the desired 0.1% level. Unfortunately, peak overlaps between quartz and other minerals in this region are common [2] (Fig. 1) and include micas from 0.336 to 0.319 nm, mullite at 0.339 nm, kaolinite at 0.337 nm, and brookite at 0.351 nm. Each kaolin sample was identically prepared by the following methods to minimize between-sample variation: (1) the kaolin was dried overnight in an enclosed oven at 105°C; (2) the respirable quartz standard and the kaolin were weighed and mixed for three minutes in a coffee-grinder type pulverizer; (3) the mixture was heated to 680°C for 30 min in a muffle furnace; (4) the mixture was pulverized for an additional three minutes; (5) the mixture was carefully packed in a sample holder and placed on the diffraction unit.

Peak intensity data was collected with a Scintag PAD V x-ray diffraction unit using Cu K_α radiation. Diffractograms were collected from

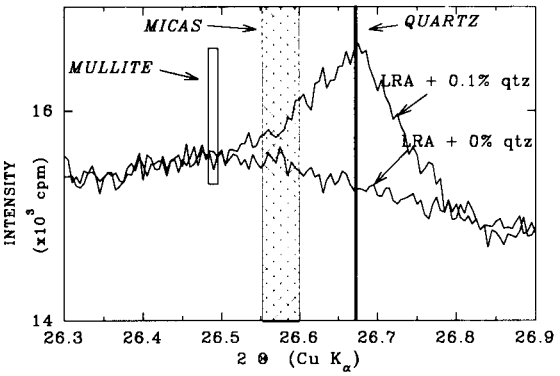

Fig. 1. Peak overlaps between quartz and other common minerals. Illustrated are the diffractograms for LRA kaolin and LRA kaolin + 0.1% quartz.

26.3° to 26.9° 2Θ (0.339 nm to 0.331 nm). In addition, diffractograms were collected near the 1.0 nm region to estimate the amount of mica in each kaolin. The diffraction unit was optimized for quartz analysis by the following procedures adapted from Klug and Alexander [4]: (1) the focusing circle was decreased to a minimum distance; (2) the primary beam and detector slits were as large as practical; (3) the step size of 0.005° 2Θ was chosen for the preliminary determinations. A larger step size could likely be used without altering the accuracy of the method; (4) counting times as long as 200 s were used to increase the peak to background ratio. These conditions led to diffraction runs which lasted 6 h; (5) the x-ray tube was run at near maximum output (45 kV, 40 mA).

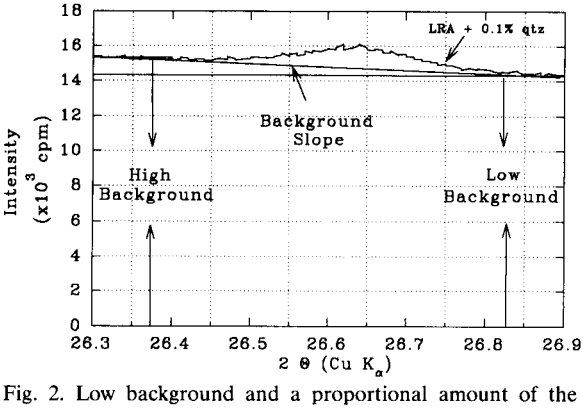

Fig. 2. Low background and a proportional amount of the background slope are subtracted for each diffractogram.

TABLE 2

Integrated peak intensities of kaolin–quartz mixtures

	Quartz (%)				
	0.0	0.1	0.2	0.3	0.4
Cretaceous kaolin, KG					
Run 1	68.2	262.6	411.1	572.1	660.3
Run 2	33.9	203.3	424.3	554.4	665.7
Run 3	24.0	207.1	384.6	598.4	685.7
Lateritic kaolin, LRA					
Run 1	105.0	285.2	390.5	598.0	720.1
Run 2	75.8	246.2	394.6	532.4	727.1
Run 3	65.2	203.6	392.9	570.0	728.0
Eocene kaolin, EG					
Run 1	243.4	508.5	734.1	768.1	1084
Run 2	260.7	500.1	563.2	807.6	1040
Run 3	258.8	465.3	546.0	–	1243

Background correction and data analysis were performed on a PC-type microcomputer using standard spreadsheet, statistics, and graphical programs. Background correction was accomplished by first averaging the first 10 data points (spanning 0.05°) and the last 10 data points of each diffractogram, then calculating the slope of the line between the initial and final data points. A proportional amount of the background was subtracted at each intermediate data point (Fig. 2). After correcting the raw data for background, the peak area of the quartz (101) peak calculated, and the area versus quartz content line determined. The peak area was obtained by simply summing the product of the background-corrected intensity and the step size over the interval of interest.

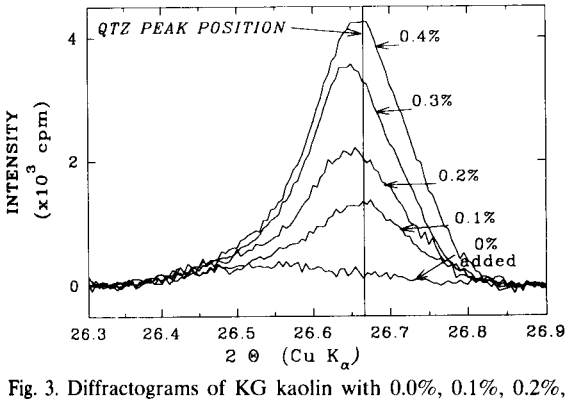

Fig. 3. Diffractograms of KG kaolin with 0.0%, 0.1%, 0.2%, 0.3%, and 0.4% added quartz.

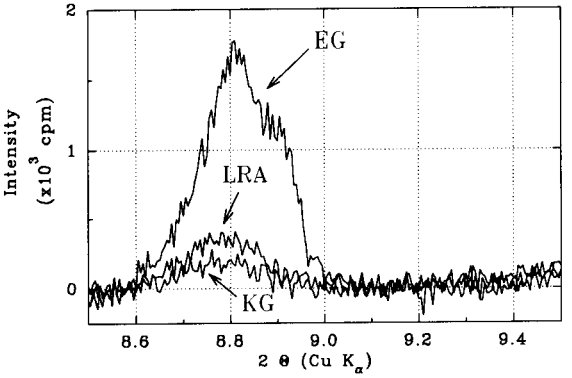

Fig. 4. Diffractograms illustrating the relatively high mica content of EG kaolin compared to KG and LRA kaolins.

RESULTS

Results of the peak area determinations for the various experimental runs are listed in Table 2 for Cretaceous kaolin Kaogloss, Eocene kaolin EG 44, and the Arkansas lateritic kaolin. As indicated in Fig. 3, added quartz contents of 0.1% were readily detectable in the KG sample using the procedures described above. The peak area for each quartz level was determined three times.

The integrated peak intensity of the mica peak at 1.0 nm also provides an indication of the relative mica content of each sample (Fig. 4). The Cretaceous kaolin displayed integrated peak intensities of 33.5 and 41.9 for two determinations, and the Lateritic kaolin had integrated intensities of 65.1 and 76.1. The airfloated Eocene kaolin, which typically contains more mica than the other

TABLE 3

Regression analysis peak area (dependant variable) versus added quartz (independant variable)

Statistic	Cretaceous, KG	Lateritic, LRA	Eocene, EG
Slope	1607.7	1607.9	2058.8
Intercept	62.2	80.1	247.5
F-Statistic	688.7	1432.1	191

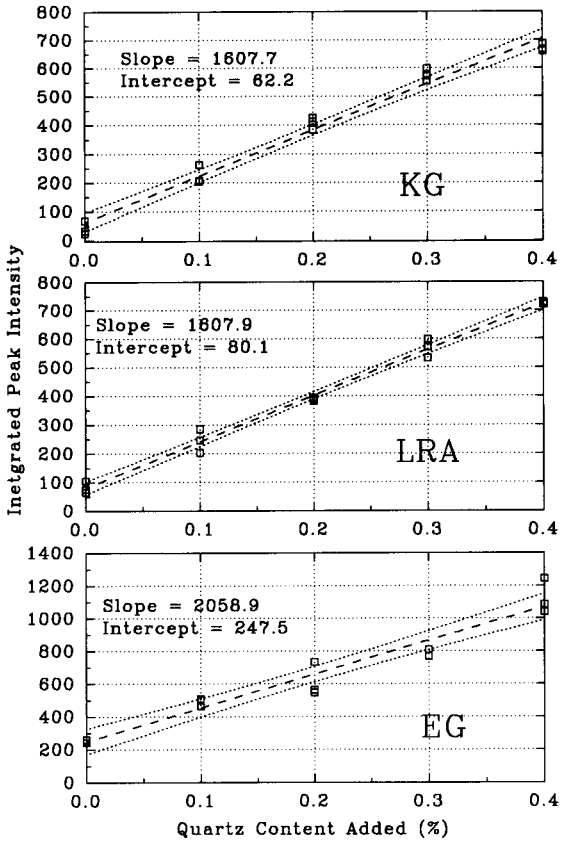

Fig. 5. Regression lines relating peak area to quartz content for the three kaolins studied.

two types, exhibited relatively large integrated peak intensities of 434.4 and 342.7 for two determinations. A greater amount of peak area variability would be expected in the mica-rich samples owing to variations in the degree of preferred orientation of platy mica particles induced by sample preparation. Results of regression analysis relating peak area to quartz content are listed in Table 3 and illustrated in Fig. 5. A linear model was employed in each case; the F-ratio is the ratio of the explained variation to the unexplained variation for the linear model. The regression was highly significant for each kaolin tested.

TABLE 4

Lower detection limits (%) for quartz using either three replicates of one level of added quartz, or three replicates each of five levels of added quartz

Kaolin	Cretaceous, KG	Lateritic, LRA	Combined KG+LRA	Eocene EG
Det. limit: 5 levels, 3 replicates	0.009	0.013	0.006	0.025
Det. limit: 1 level, 3 replicates	0.036	0.034	0.034	0.063

DISCUSSION

Regression analysis for Arkansas lateritic kaolin and Cretaceous kaolin yielded virtually identical regression slope coefficients. This result suggests that a single quantitation line can be employed for quartz determination in kaolins that are similar to the lateritic and Cretaceous kaolins in chemical composition and mica content, providing the instrumental parameters are not changed and the unknown kaolins are analyzed soon after the quantitation line is developed. The peak area data from lateritic and Cretaceous kaolins were combined and the regression line was recalculated yielding a slope of 1607.8 and an intercept of 71.1. This regression was highly significant with an F-statistic of 1803. The quartz content for any similar unknown kaolin can be easily determined by measuring the quartz (101) peak area for the unknown and comparing the peak area to the regression (calibration) line. Accuracy of the method can be improved by determining the quartz peak area of an unknown kaolin to which 0%, 0.1%, 0.2%, 0.3%, and 0.4% respirable quartz has been added. The intercept of the resulting peak area versus quartz content line with the 0% quartz added axis is an estimate of the quartz peak area of the unknown kaolin. The quartz content of the unknown is then calculated from the slope of the calibration line.

The regression line for Eocene kaolin, which contains appreciable mica, is divergent from the regression lines for Cretaceous and lateritic kaolins. The presence of mica appears to cause considerable variability in the integrated peak area for quartz, likely owing to preferred orientation of the mica grains (which are not decrystal-

lized by the heat treatment). If the two experimental runs that have uncharacteristically large peak intensities are eliminated, the slope of the Eocene kaolin line becomes much nearer to the slopes displayed Cretaceous and lateritic kaolins.

The quartz contents of the three kaolins estimated from the 0% added quartz intercept were 0.04% for the Cretaceous kaolin, 0.05% for the Lateritic kaolin, and 0.12% for the Eocene kaolin. These represent maximum quartz contents because they also contain the entire contribution (if any) of the mica and mullite peaks. Both the Cretaceous and the lateritic kaolin contain less than 0.1% *maximum total* quartz, and therefore must contain less than 0.1% respirable quartz. The slightly shifted position of the most intense peak in the Eocene kaolin (26.58° 2Θ), and the considerable mica peak detected at 1.0 nm, both strongly suggest that much of the quartz peak intensity observed in the Eocene kaolin can be attributed to the mica (003) diffraction peak. Therefore, the Eocene kaolin, which contains only 0.120% combined quartz and mica, likely contains less than 0.1% total quartz.

The regression lines can also be used to estimate the lower detection limit for quartz (Table 4). The detection limit (95% probability) has been calculated both for the method here described (5 quartz levels, 3 replicates each), and for a single sample composed of 3 replicates, each containing 0% added quartz. The estimate of the errors associated with this method combines all sources of sample variation and no attempt was made to quantify the magnitudes of the individual sources of error in the method. Only estimation of the total error was necessary because the total variance was low enough to permit accurate determination of the quartz contents of the kaolins at the 0.1% OSHA limit. These detection limits represent the level of quartz that will produce an intercept on the added quartz axis that is significantly greater than 0%: if an intercept calculated for a quartz calibration line is above the corresponding level listed in Table 4, then quartz has been detected with 95% certainty.

Conclusions

(1) The quartz content of kaolin can be estimated accurately below 0.1%.

(2) The presence of detectable mica increases the apparent quartz content and makes peak area determinations more variable at each increment of added quartz.

(3) Careful sample preparation and instrument optimization are necessary to determine quartz in kaolin at the 0.1% level.

(4) A Cretaceous paper coating kaolin from Georgia and lateritic kaolin from Arkansas contain less than 0.1% *total* quartz and therefore must contain less than 0.1% respirable quartz.

(5) An Eocene filler kaolin from Georgia likely contains less than 0.1% *total* quartz when the overlap between mica and quartz is taken into consideration.

(6) The method here described, although quite accurate and sensitive, is time consuming in preparation of calibration standards. Individual samples typically require 2 to 6 h for each determination.

REFERENCES

1 R.E. Grim, Clay Mineralogy, McGraw-Hill, New York, 2nd edn., 1968.
2 G.W. Brindley and G. Brown (Eds.), Crystal Structures of Clay Minerals and Their X-ray Identification, Mineralogical Society Monograph No. 5, Mineralogical Society, London, 1980.
3 R.L. Snyder and D.L. Bish, in D.L. Bish and J.E. Post, (Eds.), Modern Powder Diffraction, Reviews in Mineralogy Vol. 20, Mineralogical Society of America, Washington, DC, 1989, pp. 101–144.
4 H.P. Klug and L.E. Alexander, X-Ray Diffraction Procedures, Wiley, New York, 2nd edn., 1974.

Analytica Chimica Acta, 286 (1994) 57–66
Elsevier Science B.V., Amsterdam

Determination of low levels of quartz in calcium carbonates by x-ray diffractometry

N.J. Elton and P.D. Salt

ECC International, Research and Development Department, John Keay House, St. Austell, Cornwall PL25 4DJ (UK)

(Received 13th August 1992; revised manuscript received 21st December 1992)

Abstract

Naturally occurring calcium carbonates often have a complex accessory mineralogy. Quartz is a common associate, typically present at concentrations < 1 wt.%. A method is described whereby x-ray powder diffractometry may be used to quantify quartz in such samples to better than ±0.01 wt.% (1σ error) at the 0.1 wt.% level. The quartz in the samples is pre-concentrated by partial acid dissolution of the calcium carbonate, and careful attention is given to reproducible sample preparation of the resultant partial residues. Calibration is by an external standard with mass absorption corrections being applied to compensate for variations in sample chemistry. The presence of additional accessory minerals such as mica and feldspar can lead to problems due to overlapping diffraction peaks. These problems are discussed and the use and limitations of the short range profile fitting techniques employed in this method are described. The significance of particle statistics, counting statistics, and the variability associated with sample preparation in limiting the accuracy of quantification at low levels is also examined.

Keywords: Calcium carbonate; Quartz; X-ray diffraction

X-Ray powder diffraction has previously been applied to the determination of low levels of quartz in kaolins [1,2], quartz in dolostones [3] and quartz and cristobalite in bentonites [4].

The present paper describes an x-ray diffraction (XRD) procedure for the accurate determination of low levels of quartz in calcium carbonates.

A particular problem in the analysis of quartz in calcium carbonates is the presence of accessory minerals with diffraction peaks which overlap those of quartz. A method of 'short-range' profile fitting is described in some detail and the benefits and pitfalls of such an approach are discussed. Additional difficulties arise from the high mass absorption coefficient of calcium carbonate. To obtain adequate quartz intensity and to reduce the effects of particle statistics, quartz pre-concentration is employed.

Correspondence to: N.J. Elton, ECC International, Research and Development Department, John Keay House, St. Austell, Cornwall PL25 4DJ (UK).

ACCESSORY MINERALOGY OF CALCIUM CARBONATES AND THE QUARTZ TRACE

Accessory minerals

Analysis of calcium carbonate acid insoluble residues (AIRs) by energy dispersive x-ray analysis on a scanning electron microscope (SEM) has shown that they may contain a very wide range of accessory minerals. Furthermore, the composition can be quite variable even between adjacent

0003-2670/94/$07.00
SSDI 0003-2670(93)E0083-J

deposits. The mineralogy may be particularly complex in deposits where regional or contact metamorphism has taken place.

Minerals which may be present include graphite, pyrite, quartz, iron oxides, monazite, sphalerite, millerite and other Ni sulphides, chalcopyrite, titanite, chlorite, margarite, biotite, rutile, plagioclase feldspars, K-feldspar, muscovite and kaolin. The AIR typically accounts for 0.2–0.5 wt.% of the total, but may be substantially more. Evidence from SEM work suggests that, of the minerals noted above, quartz, muscovite, chlorite, graphite and pyrite can form a significant portion of the AIR. Qualitative XRD analyses of AIRs has shown the presence of mica and feldspar (not specifically identified), also quartz, pyrite, haematite, clinoptilolite, diopside, and kaolin.

Quartz trace and potential peak overlaps

It would be desirable to measure the (101) quartz peak ($d = 3.343$ Å), i.e. that near 26.6° 2θ (using Cu K_α radiation) to maximise the signal-to-noise ratio. However, muscovite-type micas are very commonly observed in calcium carbonates. These species are problematical since they have XRD peaks nearly coincident with the (101) quartz peak. There is no reliable treatment for removing mica. Graphite, K-feldspar, and certain iron oxides also have XRD peaks close to 26.6° 2θ. The graphite monochromator used in the present work transmits a certain amount of Cu K_β radiation. The (104) calcite reflection produces a peak at 26.52° 2θ with Cu K_β radiation giving yet another overlap with the (101) quartz reflection.

Use of the (101) quartz peak would, therefore, require procedures capable of dealing with overlap by mica and possibly other species. The second most intense quartz peak, i.e., the (100) reflection ($d = 4.255$ Å) near 20.8° 2θ (using Cu K_α radiation), also suffers from close mica and feldspar overlap. The presence of vaterite (a form of $CaCO_3$) may also cause overlap problems with this peak. The (112) peak ($d = 1.8178$ Å) near 50.1° 2θ (with Cu K_α radiation) suffers only mild K-feldspar interference, but has just 1/7th of the intensity of the (101) peak (as measured using a 1° divergence slit). Phlogopite, albite and millerite have XRD peaks close to 50.1° 2θ, but are rarely observed and only in very low concentrations.

PROFILE FITTING FOR DECOMPOSITION OF OVERLAPPING PEAKS

Profile fitting, based on a least-squares refinement of a suitable model of the diffraction pattern, is potentially the most accurate method of determining peak areas [5] and also enables the decomposition of overlapping peaks. A comprehensive review of profile fitting of powder diffraction patterns is given by Howard and Preston [5] who point out some of the advantages and some of the pitfalls of the technique. The approach used in the present work is to fit only a small range of 2θ, centred on the quartz peak of interest. The use of profile fitting in the quantitative determination of quartz is described in [1], and outlined in the Appendix.

The application of profile fitting to close overlap situations involving crystallographically variable minerals such as mica or feldspar is fraught with danger. In such situations, profile fitting does allow decomposition of the overlapping peaks, but the result may be unreliable and subject to large errors. With variable minerals it is difficult to apply constraints to the fitting procedure which are accurate enough for quantification at the 0.1 wt.% level.

Both the (100) and (101) quartz peaks suffer close mica and feldspar overlap, and as such, are not suitable for unambiguous quartz analysis. Only the (112) quartz peak is free from close feldspar and mica interferences and yet is of sufficient intensity to make analysis at low quartz levels feasible. Since mica is a common contaminant in calcium carbonates, use of the (112) quartz peak is strongly recommended. This peak is also free from close interference by other likely accessory minerals and offers the best option for reliable analysis.

Software for profile fitting, based on the split Pearson VII function and the non-linear least squares fitting algorithm of Levenberg and Marquardt [6], has been developed 'in-house' specifically for the analysis of quartz.

EXPERIMENTAL

Sample preparation

All samples were partially dissolved in hydrochloric acid prior to analysis. This process removes about 80–95% of the calcium carbonate whilst leaving the quartz (and most other accessory minerals) unaffected. The effect is to concentrate the quartz giving a 5–50 fold increase in measured intensity whilst still retaining a predominantly calcium carbonate matrix (to maintain similar mass absorption and packing properties between samples). The amount of dissolution was measured and a correction factor derived. The weighing errors introduced in this procedure are negligible when compared with other error sources. Experiments indicate that the quartz recovery by this procedure is at least 99.5 wt.%

All samples were wet ground to less than 10 μm particle size using a McCrone micronising mill [7] with corundum cylinders and 15 min grinding time. Milling with agate elements is inadvisable as quartz contamination may result.

Experience with the analysis of quartz in kaolins has shown that variations in sample holder packing can introduce variability in measured peak intensity. To minimise such effects, 1.200 ± 0.005 g samples were gently back-filled into a standard Philips circular sample holder and pressed into the holder at a fixed pressure using a tool specifically developed for the purpose [1,2]. Hydraulic pressing has been investigated, but does not appear to offer any advantages.

Data collection

Data were collected using a Philips PW 1825 x-ray generator with Cu anode long fine focus x-ray tube and a PW 1050 vertical goniometer with fixed slits, diffracted beam graphite monochromator and proportional counter. The relevant quartz XRD peak areas were determined by profile fitting.

The x-ray tube power was set to the maximum practical value of 40 kV, 45 mA. A 2° divergence slit was used, together with an 0.3 mm receiving slit and scans made over the range $49.7° \leq 2\theta \leq 50.5°$ in 0.02° steps.

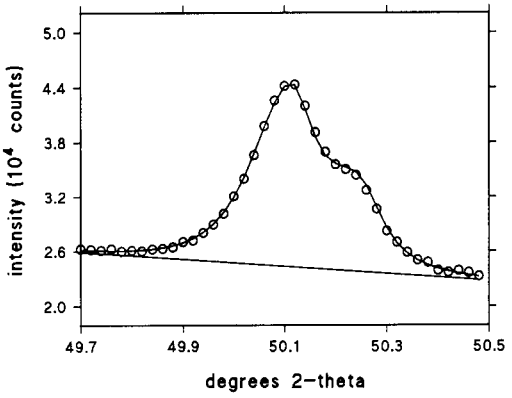

Fig. 1. Illustrating the fit to a 2 wt.% standard at 50.1° 2θ.

All samples were measured with a counting time of 200 s/step. At this counting level, data collection took 2.25 h for each sample. In general, samples were spun during measurement.

Calibration

Calibration was carried out by using an external standard. This method is both the simplest and the most economic in terms of diffractometer time. Experience suggests that fluctuations in x-ray power are not a problem providing that a series of standards is run with each batch of samples. Standards covering the range 0.0–5.0 wt.% were prepared by doping known amounts of NIST standard quartz (SRM 1878, 95.5% crystalline α-quartz) into a matrix of micronised analytical reagent grade calcium carbonate and dry mixing prior to use. The areas of the relevant quartz peaks were determined by profile fitting. Fig. 1 illustrates the profile fit to data for a 2.0 wt.% quartz standard. Calculated mass absorption corrections were applied to the measured areas (A) to correct for the change in absorption produced by the added quartz and the calibration line ($A = mx + c$) of peak area (A) versus wt.% added quartz (x) was then fitted using unweighted least squares.

Weighing errors in the preparation of the standards are minimal and the largest error on the individual measured peak area for each standard is due to the XRD measurement. This error is dominated by particle and counting statistics. Counting statistics is not necessarily the largest

error source, and unweighted least squares fitting of the calibration line is recommended. The error on the calibration line parameters is taken into account when estimating the errors on the quartz contents of 'unknowns'. The calibration for the data presented in Table 1 was $A = (2222 \pm 50)x + (98 \pm 124)$, giving an calibration error of about 2.3% relative.

Mass absorption corrections

The partial acid dissolution of the calcium carbonate increases the relative concentrations of all the accessory minerals. The composition of the acid insoluble residue can be quite variable, depending largely on the origin of the carbonate, and this introduces significant variability in the x-ray absorption of the samples. The resultant variations in the apparent quartz intensity relative to the external standard (by up to 20% in the samples studied here) must be corrected for.

The chemical composition of the samples was determined by x-ray fluorescence (XRF) and expressed as wt.% oxides. These data were then used to calculate the mass absorption coefficient for each sample [9]. The correction is given by $x' = (\mu^*/\mu_1^*)x$, where x' is the corrected quartz content, x, the uncorrected quartz content, μ^* the mass absorption coefficient of the unknown, and μ_1^* the mass absorption coefficient of the 1 wt.% standard. Values of μ^*/μ_1^* for individual samples are given in Table 1.

Amorphous content correction

It is well known that quartz particles are surrounded by an amorphous layer about 0.03 μm thick [8]. As the particle size of the quartz decreases, the amorphous layer becomes a greater fraction of the total volume. This is a potential systematic error source, because, in preparing standards, the total (quartz + amorphous layer) is weighed, but only the crystalline fraction contributes to the XRD response. If the amorphous content of the standards is not known, the quartz contents of 'unknowns' will be overestimated. Fortunately, the NIST SRM 1878 standard quartz has a certified crystalline content (95.5%). Quartz contents of 'unknowns' are multiplied by 0.955 to correct for the non-crystalline content of the standards.

ANALYSIS OF COMMERCIAL CALCIUM CARBONATES

A variety of commercial calcium carbonates originating from several deposits around the world

TABLE 1

Analysis of commercial calcium carbonates

Sample	Peak area [a] (counts)	Quartz in partial AIR, wt.% (x)	Dilution fac.	μ^* Corr^n.	Quartz in original sample wt.% [b] (x')
Marble a	15252 (87)	6.864	41.22	0.912	0.14
b	21239 (84)	9.559	31.56	0.889	0.26
c	13613 (74)	6.127	19.14	0.943	0.29
d	4473 (66)	2.013	5.49	0.985	0.34
e	1810 (51)	0.815	11.01	0.977	0.07
f	2904 (63)	1.307	9.13	0.986	0.13
Chalk a	26609 (131)	11.973	51.50	0.791	0.17
b	10571 (97)	4.757	9.40	0.925	0.45
c	35708 (107)	16.070	8.35	0.864	1.59
d	38198 (98)	17.191	9.12	0.871	1.57
Limestone a	29402 (86)	13.232	57.70	0.914	0.20

[a] Figures in brackets are the standard deviations calculated by profile fitting. [b] The 1σ error on these final values $\leq 10\%$. See the Accuracy and precision of the measurement procedure section. The relationship between quartz in the partial AIR (x) and quartz in the original samples (x') is given by: $x' = x(\mu^*$ corr^n.)(amorphous layer corr^n.)/(dilution fac.).

were analysed. Some results are summarised in Table 1.

ACCURACY AND PRECISION OF THE MEASUREMENT PROCEDURE

Elton et al. [2] give a detailed discussion of the various sources of error associated with the determination of low levels of quartz by quantitative XRD.

Counting statistics and particle statistics are likely to be the main sources of error, provided that truly systematic effects such as variations in mass absorption and particle size (amorphous layer effects) relative to the standard are adequately dealt with.

The error due to counting statistics is the only one that can be estimated for measurements on a single sample. Measurements on a number of replicate preparations can reveal the effects of other important error sources, notably, particle statistics, short term instrumental fluctuations, random errors in peak area measurements and variations due to sample preparation. Of these error sources, counting and particle statistics are likely to be dominant [2].

TABLE 2

Measurement reproducibility

[Measurements made on (112) reflection with 2° divergence slit and 0.3 mm receiving slit. Ten preparations of each sample were analysed. All samples were measured stationary except for C which was measured both spinning and stationary. See the Accuracy and precision of the measurement procedure section for detailed discussion. σ_{obs} is the standard deviation derived from the observed variability between preparations. σ_{calc} is the average standard deviation calculated by the profile fitting routine (essentially the counting statistics error)].

Sample	Quartz content (wt.%)	σ_{obs} (%)	σ_{calc} (%)	Comments
A1	2.2	8.9	1.3	Marble
A2	2.2	3.3	1.5	As A1, but milled
B	0.8	4.0	2.5	Marble (milled)
C	2.0	4.8	0.8	Not spun
C	2.0	2.2	0.8	Spun

(7 μm quartz in AnalaR $CaCO_3$)

Reproducibility studies were carried out on selected samples (Table 2). Sample A1 was a natural marble product containing 90 wt.% less that 2 μm particle size. Sample A2 was formed by micronising a portion of A1 according to the prescription given in the *Sample Preparation* section. Sample B is a micronised marble. Sample C was micronised analytical grade calcium carbonate doped with 2.0 wt.% quartz with a mean particle size of about 7 μm (generated by sedimentation from a sample of Sikron F600 quartz standard obtained from the UK Health and Safety Executive). This sample was measured both stationary and spinning.

Ten preparations of each of the above samples were made and the area of the (112) quartz peak determined. Results are summarised in Table 2.

The observed uncertainty in the quartz determinations is rather higher than that indicated by the profile fit error (which is largely determined by counting statistics). Of the error sources contributing to the observed error, instrument instabilities, sample preparation effects and measurement errors constitute a 'residual' error amounting to approximately 1% relative [2]. Estimates of the magnitude of the particle statistics error demands a knowledge of the particle size distribution of the quartz in the sample under investigation [10,11]. This is illustrated in Fig. 2, which shows theoretical estimates of the combined particle statistics and 'residual' error for three particle sizes as a function of concentration (see [2] and references therein). The magnitude of the particle statistics error is very sensitive to particle size at low concentrations.

Although certain commercial ground carbonates may be very fine (often about 90 wt.% less than 2 μm), they still usually contain a small, but significant amount of material in excess of 5 or 10 μm. Moreover, this coarse material is often composed largely of quartz and other accessories. The reproducibility of measurements on non-micronised material is substantially poorer than that observed for measurements on micronised material, as indicated by samples A1 and A2 in Table 2.

It is clear from the data of Table 2 that particle statistics is a significant error source in the

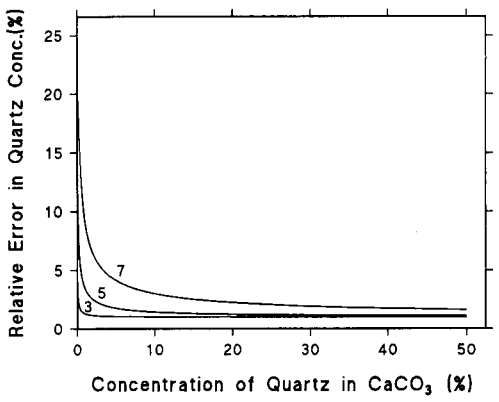

Fig. 2. Theoretical estimates of the combined particle statistics and 'residual' error for various sized quartz particles (7, 5, and 3 μm) as a function of concentration in calcium carbonate (based on measurements on the (112) quartz peak as described in the text).

present measurements on the (112) quartz peak. The 1σ error is about 4% relative for micronised material, but may be substantially greater for samples 'as received'. Where particle statistics is a significant error source, the measurement error can only be reliably determined by reproducibility studies. The effects of particle statistics may be reduced by micronising samples for longer, but with the risk of increasing the amorphous content [12]. Spinning the sample during measurement gives a useful improvement in precision (sample C, Table 2), by bringing more particles into a position to diffract.

Systematic errors that may affect a given result include long term instrumental drift, unquantified amorphous content of standards, incorrect decomposition of overlapping peaks, failure to apply mass absorption corrections, errors in the determination of the dilution factor and dissolution of quartz during the preconcentration.

Long term instrumental drift is not a problem provided standards are run with each batch of 'unknowns'. In addition, it may be advisable to measure an intensity standard at the start and end of each measurement run. Providing measurements are made on the (112) quartz peak, overlap problems should be minimal. Variation in mass absorption coefficient relative to the standards and the systematic effect of amorphous content may both be accurately corrected for. The error on the dilution factor is directly related to the precision with which initial and preconcentrated samples may be weighed. The relative error in this, and other potential systematic error sources, is negligible compared with the random errors, provided that the experimental work is carried out with due care. As mentioned in the *Sample Preparation* section, quartz loss in the preconcentration is less than 0.5 wt.% relative, which also leads to a negligible error on the final quartz determination.

CONCLUSIONS

There are good reasons for avoiding use of the most intense (101) quartz peak for quantitative analysis. Overlap from mica may not be readily apparent, and if ignored could lead to serious errors in the quartz determination. Furthermore, simple profile fitting cannot deal with very close overlap from variable minerals such as mica without careful and detailed constraint, sufficient knowledge for which is rarely available. Other procedures, such as area corrections based on the measurement of other peaks from the overlapping phases elsewhere in the XRD trace offer no advantages and will introduce additional errors. The (112) quartz peak near 50.1° 2θ is free from close overlaps and measurements on this peak are therefore unambiguous.

The use of profile fitting and standardised experimental procedures involving partial acid dissolution of the samples allows reliable and accurate XRD measurement of quartz in calcium carbonates. Error analysis indicates that particle statistics is a significant contributor to the overall error. This being the case, quantification of the error on individual measurements can only be done reliably by replicate measurements. For the method described in this paper, reproducibility studies indicate that the 1σ error is about 4% relative (i.e., ± 0.004 wt.% at the 0.1 wt.% level) for micronised material, but may be substantially greater for samples which have not been milled (up to about 10% relative).

APPENDIX. PROFILE FITTING FOR ACCURATE QUARTZ PEAK AREA DETERMINATION

The basic mathematical functions which describe the shape of x-ray diffraction peaks are well known. The aim of profile fitting is to adjust the parameters of such a function or sum of functions to achieve the best agreement between calculated and observed peak shapes, whether the peak is single or consists of overlapping contributions.

(A1) Profile function

A variety of functions have been used to describe a single XRD peak [5,13,14]. In the present work, the most favourable results were obtained with a split Pearson VII function which consists of two Pearson VII profiles sharing a common Bragg angle a_2 and intensity a_1, but having different half-widths and exponents to model peak asymmetry. It is possible to use a single function plus an asymmetry correction function [15], but experience with our data and algorithms has shown the split Pearson VII to be more reliable and easier to constrain.

In terms of angular position, $x(°2\theta)$, a series of M overlapping peaks may be described by a sum of M split Pearson VII functions plus some background function $B(x)$:

$$I(x) = B(x) + a_{11}\left\{\zeta_1\left[1+\frac{(x-a_{21})^2}{a_{31}^2}\right]^{-a_{41}} + (1-\zeta_1)\left[1+\frac{(x-a_{21})^2}{(a_{31}a_{51})^2}\right]^{-a_{61}}\right\} + \sum_{J=2}^{M} a_{1J}\left\{\zeta_J\left[1+\frac{(x-a_{21}-a_{2J})^2}{a_{3J}^2}\right]^{-a_{4J}} + (1-\zeta_J)\left[1+\frac{(x-a_{21}-a_{2J})^2}{(a_{3J}a_{5J})^2}\right]^{-a_{6J}}\right\}$$

where

$$\zeta_1 = \begin{cases} 1 & x < a_{21} \\ 0 & x \geq a_{21} \end{cases}$$

and

$$\zeta_J = \begin{cases} 1 & x < a_{2J} \quad J \geq 2 \\ 0 & x \geq a_{2J} \end{cases}$$

The quartz peak is assigned $J = 1$ and the positions of other peaks in the group ($J > 1$) defined relative to it.

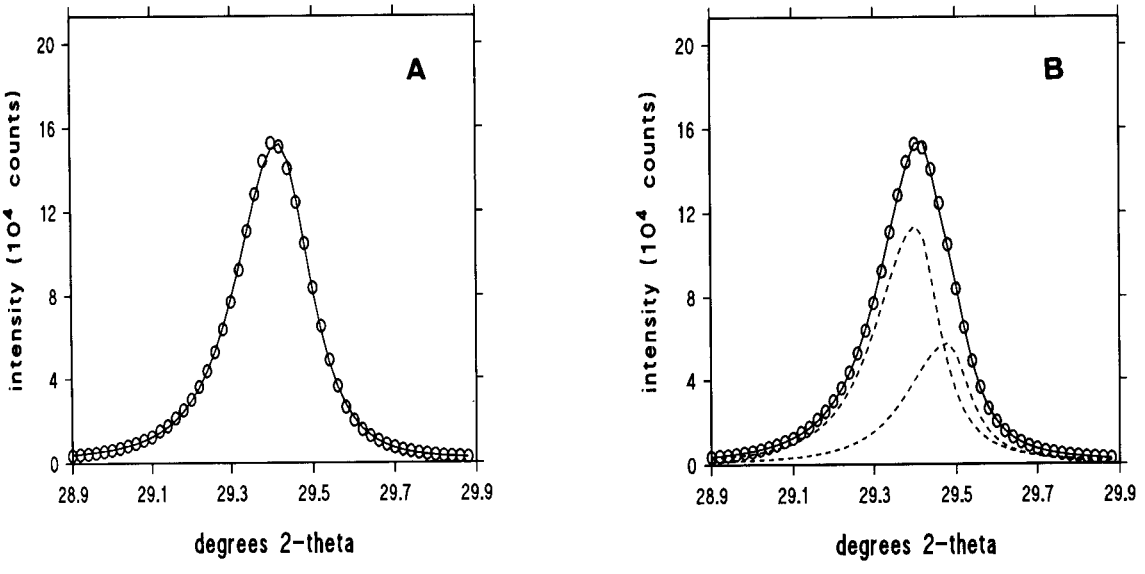

Fig. 3. Good fits to the data may often be obtained with an incorrect number of peaks: (A) a single peak, (B) two peaks.

The XRD equipment used for the work described here utilises a graphite monochromator which has high reflectivity (essential for obtaining reasonable counting statistics), but is insufficiently wavelength specific to select Cu K_{α_1} radiation alone from the α_1, α_2 doublet. Thus all observed peaks are actually doublets with a separation given by $\delta = 0.2838 \tan \theta$ and intensity ratio $I\alpha_2/I\alpha_1 = 0.5$. At high angles the doublet is clearly resolved and both contributions must be explicitly included in the profile function.

Over the small range of 2θ considered in this work, the background was well approximated by a straight line, $B(x) = B_1 + B_2 x$.

(A2) Application of profile fitting

Profile fitting, particularly of the short-range type outlined above, involves a number of subtleties which can lead to totally erroneous results if not fully appreciated. The problems are most manifest in fitting close peak overlaps and with noisy data.

Given a set of data and a model, the final result is a set of parameters corresponding to the 'best' overall fit. However, with non-linear models there may be several combinations of parameters giving good fits and the 'best' fit does not guarantee that the model is realistic. Although this problem of false minima is well known, its importance cannot be over-emphasised, especially with the increasing availability and usage of commercial curve fitting packages and where profile fitting is being used for highly accurate quantitative analysis. Some examples will illustrate the main points most clearly.

Figure 3 shows a profile corresponding to a single peak. A model with a single split Pearson VII fits the data very well. However, a model with *two* split Pearson VIIs also fits very well. Indeed, it is often found that the best overall fit can be obtained by using more or less lines than are expected to be present. It is essential to know how many lines are expected in the peak group under consideration, and this usually calls for some qualitative mineralogical analysis prior to quantitative analysis. A practical example of this is mica or graphite overlap of the (101) quartz peak. If the overlap is very close, it may not be readily apparent from examination of the 26.6° 2θ peak that two (or more) phases are present. Both mica and graphite may be overlooked in this way, and a simple measurement of the 'apparent' 26.6°

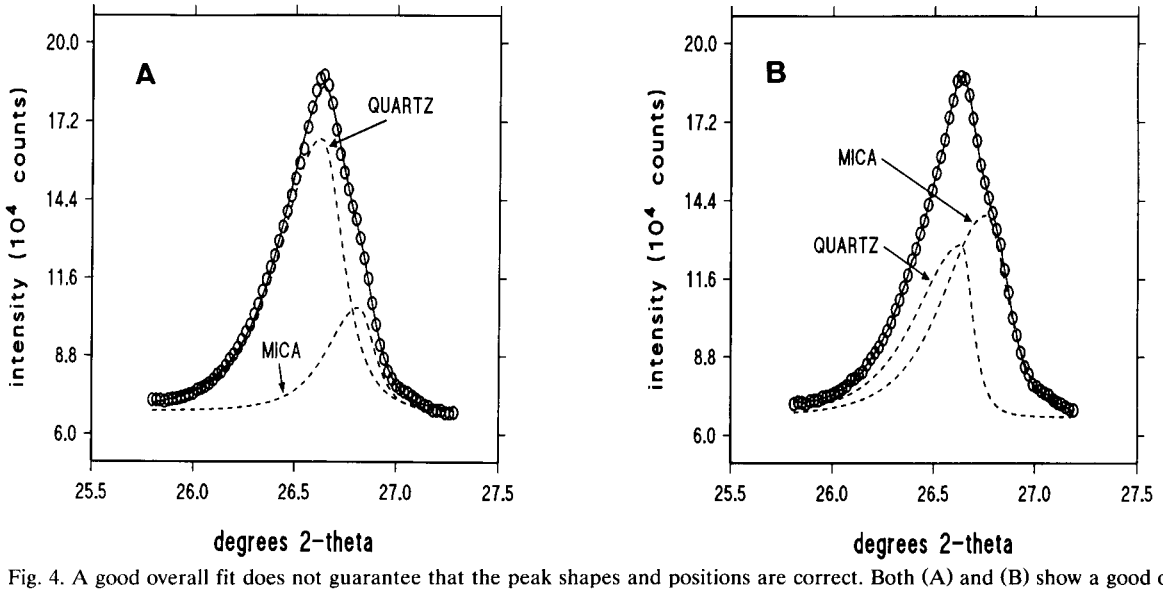

Fig. 4. A good overall fit does not guarantee that the peak shapes and positions are correct. Both (A) and (B) show a good overall fit, but because component peaks in (A) differ slightly in shape and relative position from those in (B), the quartz peak areas in each case are radically different. It is not possible to tell from the data which is correct.

2θ quartz peak would lead to highly erroneous results.

A second problem is that of unconstrained peak shape and position. In this case, one or more peaks may be unphysical in shape, or be at an unrealistic Bragg angle, yet provide the best overall fit. Without restricting the shape of the peaks within a closely overlapping group, such problems are unavoidable and can lead to very poor estimates of peak area.

To illustrate this problem, Fig. 4 shows two profile fits to a set of data collected over the range $25.8° \leq 2\theta \leq 27.2°$ for a sample containing both quartz and muscovite. In both cases the overall profile fit is good, but because the shapes and relative positions of the quartz and mica peaks are slightly different between Figs. 4A and 4B, the fitted area for quartz is radically different. Furthermore, there is no way of identifying from the data which is correct.

(A3) Constraining the fit

In principle, the shape of diffraction peaks is largely determined by instrumental effects, and if values for the parameters defining the peak asymmetry (the half width ratio and exponents) are known, these values can then be held as constants in subsequent analysis.

The determination of constraining values for the exponents (a_{4i}, a_{6i}) and half-width ratio (a_{5i}) in the split Pearson VII is determined for a given mineral at given Bragg angle by obtaining an XRD trace of the pure substance and performing a fitting on the single un-overlapped peak.

In principle, the relative positions of peaks within an XRD trace may also be fixed for a given set of phases. The absolute 2θ position of the peak group is refined to allow for variations in sample placement in the diffractometer from run to run.

The parameters that *are* refined are absolute peak position (in terms of a_{21}), amplitude (a_{1i}) and width factor (a_{3i}).

(A4) Problems with constraints

Constraining the peak shape and relative positions of component peaks is fairly reliable if the minerals involved are chemically and crystallographically stable and show constant diffraction patterns.

However, many minerals found as accessories in natural materials occur in various polytypic forms or within solid solution series. Variability in chemical composition, lattice dimensions, layer stacking and structure in minerals such as mica and feldspar leads to variability in their XRD patterns, particularly in their precise peak positions and intensities. The magnitude of these variations can be quite significant.

Without precise knowledge of the mineralogy of each sample, it is impossible to impose reliable constraints on the relative positions and shapes of the component peaks. Since the mineralogy can vary even within a deposit, such knowledge is very rarely available to the degree needed for highly accurate quantification. Without this constraint, the results of decomposition are questionable for the reasons indicated above.

Whole pattern methods such as Rietveld-type refinements are capable of giving reliable results [16] provided that the crystal structures of the relevant phases are known to high accuracy. However, minerals such as mica and feldspar are again likely to cause problems due to their intrinsic variability. Additionally, data covering a wide range in 2θ are essential (with consequent long data collection times).

For the accurate quantification of low levels of quartz in natural materials, the problems of peak overlap from accessory minerals are severe. Mica and feldspar are the most problematical, interfering with the two most intense quartz reflections, (101) and (100). Measurement of the (112) quartz reflection, which is free from close mica and feldspar overlap, is strongly recommended if analyses are to be reliable.

REFERENCES

1 N.J. Elton, P.D. Salt and J.M. Adams, Powder Diffraction, 7 (1992) 71.
2 N.J. Elton, P.D. Salt and J.M. Adams, Anal. Chim. Acta, 286 (1994) 37.
3 J.A. Emig and D.K. Smith, Powder Diffraction, 4 (1989) 209.

4 J.R. Carter, M.T. Hatcher and L. Di Carlo, Anal. Chem., 59 (1987) 513.
5 S.A. Howard and K.D. Preston, in D.L. Bish and J.E. Post (Eds.), Modern Powder Diffraction, Reviews in Mineralogy, Vol. 20, Mineralogical Society of America, Washington, DC, 1989.
6 W.H. Press, B.P. Flannery, S.A. Teukolsky and W.T. Vetterling, Numerical Recipes, Cambridge University Press, Cambridge, 1986.
7 D.L. Bish and R.C. Reynolds Jr., in D.L. Bish and J.E. Post (Eds.), Modern Powder Diffraction, Reviews in Mineralogy, Vol. 20, Mineralogical Society of America, Washington, DC, 1989.
8 G. Nagelschmidt, R.L. Gordon and O.G. Griffin, Nature, 169 (1952) 539.
9 G.W. Brindley, in G.W. Brindley and G. Brown (Eds.), Crystal Structures of Clay Minerals and their X-ray Identification, Mineralogical Society, London, 1980.
10 P.M. De Wolff, Appl. Sci. Res., 7 (1958) 102.
11 H.P. Klug and L.E. Alexander, X-ray Diffraction Procedures, Wiley, New York, 1974.
12 B.H. O'Connor and W.J. Chang, X-ray Spectrosc., 15 (1986) 267.
13 G.J. Stanisz, J.M. Holender and J. Soltys, Powder Diffraction, 4 (1989) 70.
14 S.A. Howard and R.L. Snyder, Adv. X-ray Anal., 26 (1983) 73.
15 D.B. Wiles and R.A. Young, J. Appl. Cryst., 14 (1981) 149.
16 D.L. Bish and S.A. Howard, J. Appl. Crystallogr., 21 (1983) 86.

Analytica Chimica Acta, 286 (1994) 67–73
Elsevier Science B.V., Amsterdam

Carbonate fusion to determine quartz in respirable and bulk earth samples

Woodhall Stopford

3300 New Sharon Rd., Hillsborough, NC 27278 (USA)

(Received 16th November 1992; revised manuscript received 13th December 1992)

Abstract

The carbonate-fusion technique of Dobreva [*Ann. Occup. Hyg.*, 18 (1975) 121] has been modified to allow the colorimetric assay of solubilized quartz to be done entirely within a 4-ml disposable spectrophotometer cell. An Andreasen Pipette is used to measure respirable size of a sample (that with an aerodynamic diameter less than 3.5 μm) and to obtain samples at the 3.5 μm cut for quartz determinations. Amorphous silica and silicates are removed from the sample by heating an aliquot with 1–2 ml of 48% fluoroboric acid at 70°C. for 1 h. Quartz is then preferentially solubilized by fusing the filtered and ashed residue with a 1:1 mixture of potassium bicarbonate and potassium chloride. After dissolving the carbonate residue with boiling water, a sample is placed in a polymethacrylate spectrophotometer cell with 0.1 ml of 10% ammonium molybdate. This mixture is then adjusted to pH 2.1 and kept at room temperature for 30 min. Color is then developed for 45 min with a solution of citric acid and tartaric acid after which absorbance is measured at 785 nm. This technique recovers 99.8% of 5 μm quartz but retains only 1.1% of amorphous silica. The absolute detection limit of the colorimetric method is 150 ng for silicon, sufficient to detect 8 μg of quartz in a 1–50 mg sample. Analyses of respirable-sized samples disclose that the major mass of quartz in complex earths can fall in the non-respirable range.

Keywords: X-Ray diffraction; Carbonate-fusion technique; Earth samples; Quartz; Silicates

The international Agency for Research on Cancer declared quartz an experimental carcinogen in 1987 [1]. More recently the National Toxicology Program has refined the concern to that of respirable quartz [2]. For a hazard to exist, not only must there be quartz but it must be of small enough size to reach the lungs if inhaled. Materials containing such *respirable* quartz may require warning labels. The key characteristic for determining whether or not a particle can reach the lungs when inhaled is its aerodynamic equivalent diameter (AED), defined as the diameter of a hypothetical sphere of unit density having the same terminal settling velocity as the particle in question regardless of its geometric size, shape, and true density [3]. AED is thus a function of settling velocity, whether measured in water or in air. The American Conference of Governmental Industrial Hygienists has defined respirable fraction (that portion of an aerosol available for lung deposition) as that portion that penetrates a separator with a size collection efficiency described by a cumulative log normal function with a median aerodynamic diameter of 3.5 μm and a geometric standard deviation of 1.5 μm [4]. In air, such a separator can be a cyclone or Anderson impactor. Median aerodynamic diameter with a cumulative log normal distribution can be measured in water with an Andreasen sedimentation pipette [5]. Side-by-side comparisons of respirable fraction of bulk dust samples measured either in

Correspondence to: W. Stopford, 3300 New Sharon Road, Hillsborough, NC 27278 (USA).

SSDI 0003-2670(93)E0045-9

air with a cyclone or in water with an Andreasen pipette show close agreement with a maximum deviation of ±6% [6].

The other element of risk is that the respirable aerosol must contain quartz. For most dusts, x-ray diffraction gives a satisfactory measurement of quartz content. However, for unrefined clays and iron oxide earth pigments, multiple interferences may lead to an underestimation of the amount of quartz present [7]. The phosphoric acid colorimetric method can overcome these interferences but is operator-dependent and colorimetrically unstable, requires variations in technique to maximize solution of silicates depending on the sample under investigation, and cannot be used to accurately quantify quartz in respirable-sized dusts [8]. Dobreva [9] has described another differential solubilization technique that overcomes the limitations of the phosphoric acid method. In this technique, quartz is preferentially solubilized with a carbonate flux. Respirable-sized dusts can be accurately analyzed if interferences (amorphous silica and silicates) are first removed by treating samples with fluoroboric acid. The silicon in the resultant aqueous solution can be quantified either by atomic absorption spectrophotometry [8] or by colorimetry [9]. Although this method was found to be free from interferences by such clay minerals as feldspar [8], it has not been used to determine quartz in complex, unrefined earths.

It has been demonstrated that the Dobreva method can accurately measure quartz in earths. A colorimetric assay was chosen and by reducing reagent volume, it has been possible to carry out the entire colorimetric reaction and analysis in a 4 ml spectrophotometer cell.

EXPERIMENTAL

Equipment and reagents

All chemicals used in this assay are reagent grade and include powdered potassium chloride (Fisher Scientific, Pittsburgh, PA), powdered potassium bicarbonate (Fisher Scientific), 48% fluoroboric acid (Mallinckrodt, Paris, KY), 10% ammonium molybdate (Ricca, Arlington, TX), 1 M sulfuric acid (Ricca), 50% tartaric acid (Ricca), L-ascorbic acid (Fisher Scientific), deionized ultra filtered water (Ricca), silica gel (Sigma, St. Louis, MO), Min-U-Sil 5 (US Silica, Berkeley Springs, WV), Arizona road dirt (Air Cleaner Test Dust, GM Part 1543094, General Motors, Flint, MI), sodium phosphate (Fisher Scientific), 0.5 M potassium hydroxide (Mallinckrodt), and 0.01–1.0 mg/ml silica standards (Ricca). Silica gel is further prepared for use as a standard by grinding it and collecting the fraction passing through a 325-mesh brass screen. Potassium bicarbonate is dehydrated at 120°C for 30 min and then kept in a desiccator until needed. The carbonate flux mixture is prepared by mixing 0.25 g of potassium bicarbonate with 0.25 g of potassium chloride. Reagent-grade deionized, ultra filtered water is used to prepare all reagents and standards and for all assays.

No glassware is used. Pipette tips, flasks, vials and reagent bottles are polypropylene or PTFE. The colorimetric reaction vessel is a polymethacrylate disposable spectrophotometer cell (Fisher Scientific). All assay vessels are rinsed with 0.5 M potassium hydroxide followed by 1% sodium phosphate and then 6 rinses with laboratory-grade deionized, ultra filtered water. All samples are weighted to the nearest μg (S.D. = 1.2 μg). Pipettes are calibrated to the nearest μl and have transfer repeatability of ±0.5% or better. Andreasen pipettes are available from Fisher Scientific. Samples for respirable size fractionation and carbonate fusion are collected on polycarbonate membrane filters (Gelman Supor, available from Fisher Scientific) with a 0.1 μm pore size.

Method

Aerodynamic size analyses are done on samples of bulk dust with an Andreasen pipette using Andreasen's methodology [5] as modified by Creed [6]. Water used in the pipette is equilibrated at room temperature for > 12 h to prevent temperature gradients and turbulence. A 5 ml dust sample is mixed in the pipette for 2 min. 10.00 ml samples are then taken at a 5 cm depth every 10 min for the next 50 min. Each aliquot is deposited either in an aluminum weighing dish or

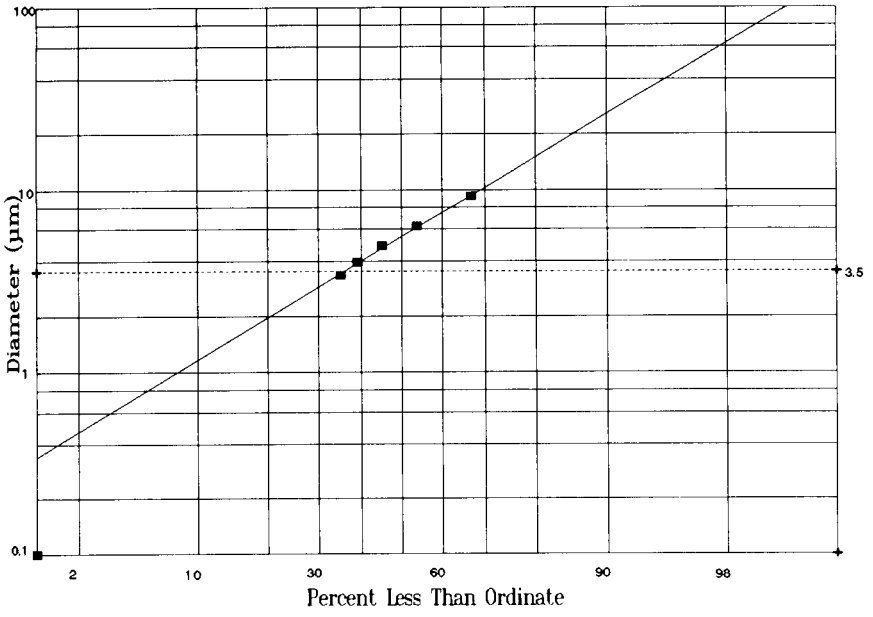

Fig. 1. Respirable fraction analysis of raw sienna old (respirable fraction = 35%)

on a pre-weighted 0.1 μm pore size polycarbonate filter, desiccated and weighted. Aerodynamic equivalent diameter is determined using Stokes Law as follows:

$$\mathrm{AED} = \frac{(18uH)^{1/2}}{(p_p - p_m)gt}$$

where u is the viscosity of the medium in g cm^{-1} s^{-1}, H is the distance a particle has fallen in time t (s), p_p is particle density (assumed to by that of quartz, 2.65 g cm^{-3}), p_m is the medium density (1 g cm^{-3} for water), and g is acceleration due to gravity.

Aerodynamic equivalent diameter is plotted as a cumulative size distribution on log normal paper with a regression analysis (Quattro Pro, Borland) used to determine geometric mean and geometric standard deviation of the dust particle sizes (e.g., see Fig. 1). The respirable fraction is taken to be the percentage of particles having an AED of 3.5 μm or less.

Samples collected on polycarbonate membrane filters are first ashed at 750°C for 10 min. Ashed or bulk samples are mixed with 1–2 ml of fluoroboric acid and heated in a water bath at 70 ± 1°C for 1 h. The treated samples are then collected on 0.1-μm pore size polycarbonate membrane filters under suction, washed six times with deionized, ultra filtered water and ashed. Ashed samples are then covered with the carbonate flux mixture in a platinum crucible. The flux is melted using a propane torch and then heated with a medium flame (sufficient to maintain the liquid flux at a dull red color) for 1–2 min. After cooling, the flux is dissolved by heating it with 4–5 ml deionized, ultra filtered water kept at a rolling boil for 30 s. The crucible is rinsed six times with deionized, ultra filtered water, heated to a dull red color a second time and rinsed again six times with deionized, ultra filtered water. The dissolved flux and combined rinses are then filtered and brought up to a 50.0 ml.

Absorbance is measured with a spectrophotometer with dispersion optics an a slit to isolate the desired wavelength (Gilford Model 240) with a 410 nm filter in place. A 2.00-ml sample of the dissolved flux is placed in a spectrophotometric cell. A blank reading is then taken at 785 nm. After adding 0.10 ml of 10% ammonium molybdate, the sample is acidified to a pH of 2.1 with 1 M sulfuric acid. After incubating at room temper-

ature (20 ± 2°C) for 30 min, absorbance of the yellow silicomolybdic complex is measured at 420 nm. If the absorbance is less than 0.200, the yellow complex is reduced to a blue silicomolybdic complex by adding 0.30 ml of a 1 : 1 mixture of 5% tartaric acid and 1% L-ascorbic acid. After incubating at room temperature for at least 45 min, absorbance is measured at 785 nm.

Quartz was determined in selected split samples by the Industrial Health Foundation (Pittsburgh, PA) using NIOSH Method No. 7500.

RESULTS

Respirable size analysis

Repeat testing of Arizona road dirt shows a relative standard deviation (R.S.D.) of 6%. The geometric mean diameter for this standard dirt is 13.5 μm with a geometric standard deviation of 8.3 μm. A cumulative size analysis, finds 35% to be 5 μm in size or less. This compares with a roller analysis (provided by GM) showing 39 ± 2% to be 5 μm or less. The sensitivity of this method is sufficient to detect a respirable fraction of 1.0%. When combined with a graded sieve separation of fines to a 45 μm cut, this method can detect a respirable fraction of less than 0.01%.

Colorimetric analysis

Colorimetric analyses of serially diluted silicon standards demonstrate a linear relationship between concentration and absorbance to 100 μg of silicon at 420 nm. Results obtained at 785 nm are linear to 30 μg of silicon with a curvilinear relationship at higher concentrations. The relationship between absorbance and silica concentration is described by the equations: Si (μg) = 165(A − 0.045) at 420 nm and Si (μg) = 25(A − 0.110) at 785 nm.

The relative standard deviations for this method are described in Table 1. Detection limits for silicon (μg), corresponding to two times the standard deviation of the reagent blank, range (for various runs) from 0.9 to 2.6 at 420 nm (equivalent to 48–140 μg of quartz in a sample) and from 0.05 to 0.15 at 785 nm (equivalent to 2.7–8.0 μg of quartz in a sample).

TABLE 1

Relative standard deviations of the colorimetric method for silicon analyses

Si (μg)	0.2	5	20	100
420 nm	–	8.0%	1.6%	0.9%
785 nm	2.9%	2.6%	0.7%	0.4%

Sensitivity is decreased by 19% by measuring absorbance at 820 nm vs. 785 nm. Although sensitivity is increased by increasing the pH of the reaction mixture, at a pH above 2.1 the color reaction is unstable. At pH 2.1 the absorbance remains stable for at least 24 h. Sensitivity is not affected by reaction temperatures ranging from 20 to 40°C.

The major contributor to the reagent blank is the diluent, water. Silicon levels (μg/ml) in various available water sources are 0.4 and 0.7 for technical-grade and laboratory-grade deionized, ultra filtered water, respectively, and 55 for well water. Detection limits are improved as the silicon in the reagent blank decreases. However, there is essentially no difference in detection limits when comparing laboratory-grade and reagent-grade deionized, ultra filtered water.

Carbonate fusion

Screening of 20 earth samples for quartz content using x-ray diffraction analysis disclosed 7 samples with less than 1% quartz. One, a refined clay designated WS6, is used as the standard for validating this method. 100% of particles of this clay have aerodynamic equivalent diameters of less than 3.5 μm. Repeat analyses of WS6 using the carbonate fusion method disclose a quartz content of 0.62% and over all R.S.D.s of 5.8%. The R.S.D. attributable to the carbonate fusion portion of the analysis is 3.0%. In order to determine the efficiency of the carbonate fusion, recovery of silica gel (precipitated amorphous silica) is compared with a quartz standard (Min-U-Sil 5) using WS6 as the matrix. At a loading of 8.1–9.8% Min-U-Sil 5 there is a 99.8 ± 3.4% recovery of the amount of added quartz. At a 16.3% loading of the silica gel there is a 1.1% retention.

A standard dust sample, Arizona road dirt, is also analyzed by this method and compared to analyses by x-ray diffraction. Analyses of bulk samples by the two methods determines quartz values of 52.1 ± 1.5% by the carbonate fusion method and 17.9 ± 2.9% when analyzed by x-ray diffraction. The R.S.D (%) is 2.9% for the carbonate fusion method and 16 for the x-ray diffraction method.

Most of the quartz particles in this standard dirt appear to be non-respirable: the quartz content (analyzed by the carbonate fusion method) of a 3.5 μm cut sample is 4.5 ± 0.1%. The respirable quartz (respirable fraction × quartz content of a 3.5 μm cut sample) is even lower at 1.1%.

Analysis of earth pigments:

In order to further study the dichotomy between quartz content of bulk earths and that of the respirable fraction, analyses are made of two earth pigments, Burnt Sienna Old (BSO) and Burnt Sienna New (BSN). Both samples originate from the same quarry. BSN, however, is treated by a proprietary process to remove the bulk of the respirable particles. BSO has a respirable fraction of 35% (Fig. 1) while BSN has a respirable fraction of 4.0% (Fig. 2). Quartz analysis of BSO by x-ray diffraction demonstrates a quartz content of 11.0%. As with Arizona road dirt, analysis by carbonate fusion demonstrates a greater content of quartz: 30.3 ± 0.7%. The removal of the smaller particles does not appreciably affect total quartz content of this earth pigment. A bulk sample of BSN has a quartz content of 24.5 ± 2.7%. Although the quartz content of a 3.5 μm cut samples of BSO and BSN are similar (5.5 and 5.8%), the removal of small particles has a dramatic effect on the respirable quartz content. For BSO, the respirable quartz content is 1.8% while for BSN it is 0.2%.

Sienna earth colors have a high iron oxide content. It is plausible that a very fine iron oxide pigment may break through the filter resulting in a falsely high colorimetric reading. However, a sienna earth pigment, with a similar respirable fraction (35%) to that of BSO but with a quartz content of < 1% by x-ray diffraction, shows a quartz content of 0.85% when analyzed by the carbonate fusion method. Iron oxide does not appear to give a noticeable interference.

DISCUSSION

Measurement of aerodynamic equivalent diameter using the Andreasen sedimentation

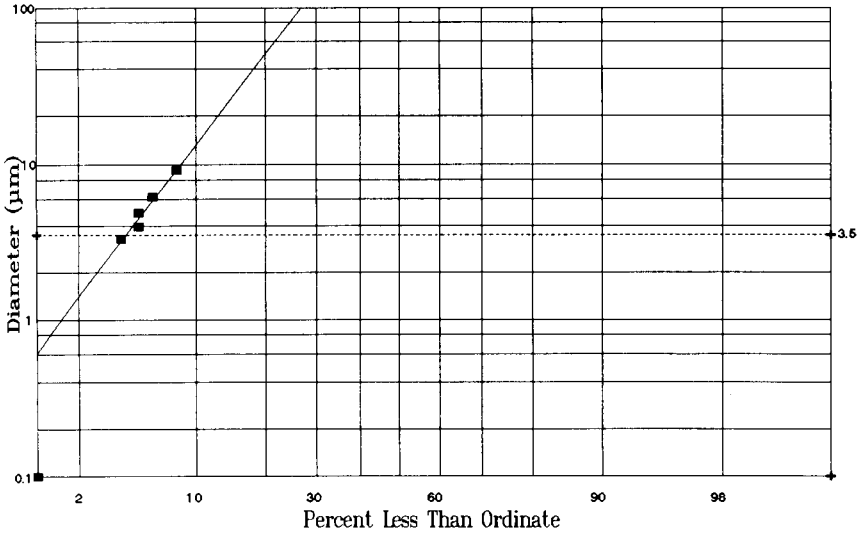

Fig. 2. Respirable fraction analysis of raw sienna new (respirable fraction = 4.0%)

pipette gives results equivalent to that used to characterize a standard dust sample, Arizona road dirt. The colorimetric assay used in this study allows quartz levels to be determined at levels $< 0.05\%$ in a 20 mg sample. Although, for absorbance measured at 420 nm, this assay is linear to 2500 μg of silicon [10], because of the small size of the samples used in the microcolorimetric technique, it was only needed to take the calibration curve to 100 μg of silicon. Although the sensitivity of this assay is said to be only 100 μg of silicon at an absorbance of 420 nm [10], the sensitivity could be extended to 2.6 μg. This allows a measurement of absorbance at 420 nm to suffice for most samples.

The colorimetric assay used in this study is similar to that used with the phosphoric acid method [8]. In this latter method, however, the use of hydrofluoric acid directly on a filter results in appreciable (18.7–53.2 μg/assay) silicon contamination. In the carbonate fusion method filters are first ashed. No detectable contribution was found of silicon to the assay from the filters, fluoroboric acid or the carbonate fusion system itself.

The carbonate fusion method of Dobreva [9] is less variable by a factor of 5 when compared to repetitive concurrent x-ray diffraction analyses of the same sample. One surprising finding in comparing these two analytical methods is the marked discrepancy found in analyses of complex earth samples. If the carbonate fusion determinations are correct, x-ray diffraction can underestimate quartz levels in earths by as much as 64–66%. The finding of low ($< 1\%$) quartz levels in similar clay and earth pigment samples by the carbonate fusion method suggests that this method does not overestimate quartz levels because of the presence of some interfering agent. Furthermore, analyses of various minerals found in complex earths by the carbonate fusion method [8,9], including feldspars, olivine, garnet, amphibole, mica, talc, kaolinite, tremolite, montmorillonite, perlite, and nephiline syenite, have not demonstrated any interferences.

X-ray diffraction analyses of complex earth samples can underestimate the amount of quartz present because of the presence of interfering minerals in a complex matrix. Carter et al. [7] have demonstrated such interferences in unrefined clays do to the presence of illite or feldspar, particularly in samples where an appreciable fraction of particles was greater than 5 μm in diameter. The authors demonstrated that as little as 9% iron oxide could depress the estimate of quartz by the x-ray diffraction method by 23%. They had difficulty in calibrating their method for analyses of complex, unrefined clays. Although x-ray diffraction is an excellent method for analyzing refined clays and other minerals, such interferences may explain the dichotomy in quartz determinations between this method and the carbonate fusion method when used in the analysis of complex, unrefined earths.

The American Conference of Governmental Hygienists [ACGIH] has defined respirable mass based on the characteristics of a cyclone separator [4]. Raabe [11] has reviewed various proposals for defining potentially harmful dusts and concurs in the continued usefulness of this definition of respirable dust. ACGIH has definitions for both inhalable and respirable mass. Larger particles (those with an aerodynamic equivalent diameter > 10 μm) are efficiently cleared by the upper airways even during mouth breathing while exercising: the inhalable mass is not an accurate risk parameter of particles, such as quartz, whose toxicity is limited to effects on the lung. ACGIH has recently made their definition of respirable mass more conservative by increasing the mean AED from 3.5 to 4.25 μm [12].

An interesting finding is that respirable quartz levels in complex, unrefined earths can be a small fraction of the total amount of quartz present. Because of this dichotomy clays can be refined to remove quartz. The relatively larger aerodynamic equivalent diameter of quartz particles compared to clay particles allows quartz to be selectively removed by a water slurry [8]. When complex earths are refined to remove quartz because of health concerns, an effective process, as demonstrated by the 90% reduction in the respirable quartz level in Burnt Sienna New, appears to be one that selectively removes respirable particles.

In summary, the combination of the carbonate fusion technique of Dobreva and respirable frac-

tion measurements using an Andreasen pipette allow one to measure respirable quartz levels in bulk earth samples, even when the quartz content is as low as 0.05% The sensitivity of this method allows assessment of samples collected on filters. The use of a two step process (treatment with fluoroboric acid followed by carbonate fusion) to remove non-quartz components that may interfere with the assay makes this method particularly useful for measuring quartz in complex earth samples.

REFERENCES

1 IARC Monographs on the Evaluation of Carcinogenic Risk of Chemicals to Humans, Vol. 42, Silica and Some Silicates, World Health Organization, Lyon, 1987.
2 Sixth Annual Report on Carcinogens, US Department of Health and Human Services, National Institute of Environmental Health Sciences, Research Triangle Park, NC, 1991.
3 E. Knutson and P.J. Lioy, in Air Sampling Instruments for Evaluation of Atmospheric Contaminants, American Conference of Governmental Industrial Hygienists, Cincinnati, OH, 7th edn., 1989.
4 Threshold Limit Values and Biological Exposure Indices for 1991–1992, American Conference of Governmental Industrial Hygienists, Cincinnati, OH, 1991.
5 A.H.M. Andreasen, Ber. Dtsch. Keram. Ges., 11 (1930) 675.
6 D.K. Creed, Development of a Method for Determining the Respirable Mass Fraction of a Bulk Sample, Technical Report, University of North Carolina, School of Public Health, Department of Environmental Sciences and Engineering, Chapel Hill, 1991.
7 J.R. Carter, M.T. Hatcher and L. Di Carlo, Anal. Chem., 59 (1987) 513.
8 A.K. Das and T.R. Sweet, Am. Ind. Hyg. Assoc. J., 39 (1978) 762.
9 M. Dobreva, Ann. Occup. Hyg., 18 (1975) 121.
10 D.V. Sweet, F.R. Wolowicz, and J.V. Crable, Am. Ind. Hyg. Assoc. J., 34 (1973) 500.
11 O.G. Raabe, Ann. Occup. Hyg., 26 (1982) 33.
12 Threshold Limit Values and Biological Exposure Indices for 1992–1993, American Conference of Governmental Industrial Hygienists, Cincinnati, OH, 1992.

Analytica Chimica Acta, 286 (1994) 75–80
Elsevier Science B.V., Amsterdam

Quantitative determination of quartz in calcite, dolomite, and talc by powder x-ray diffraction analysis

Gary P. Tomaino

Specialty Minerals Inc., 640 North 13th Street, Easton, PA 18042 (USA)

(Received 31st July 1992; revised manuscript received 9th February 1993)

Abstract

A detection limit of 0.05% quartz in calcitic and dolomitic carbonate and talc matrices is dependent upon significant counting time for optimal signal to noise ratio, utilization of peak area counts, absence of significant interfering phase(s), a known blank (< 0.05%) for each matrix, statistically significant replications of standards, and triplicate unknown analyses. Using the internal standard method, the quantitative determination of quartz in the range 0.05–1.0% for carbonate and talc matrices has a relative standard deviation of 25%.

Keywords: X-ray difraction; Quartz

This paper provides general guidelines for qualitative and quantitative determination of quartz, in calcitic and dolomitic carbonates and talc matrices by x-ray diffraction analysis with a maximum reportable level of 0.1%. X-ray diffraction is a specialized method for observing fundamental structural properties of crystalline materials. Upon initiating a material with a monochromatic source of x-rays, a crystalline specie generates a characteristic pattern by the atomic spacing and arrangement of the lattice planes. These fundamental properties follow the general formula of Bragg's law, $n\lambda = 2d \sin \Theta$ [1].

Significant interferences can occur at the quartz major diffraction peak of 101 and the quantity of these phases may alter the given parameters. Therefore, each analyst must scrutinize samples as to potential interferences, such as the feldspars, micas, amphiboles, barites, wollastonite, and graphite. The trace interferences can be corrected by simple deconvolution software generating acceptable peak area intensity counts for the 101 peak.

Also, the internal standard method is preferred so future analyses will rely on "type" standards and the developed matrix constant, K', rather than a new calibration curve. The matrix constant, K', is specific to instrument settings and geometry plus the level and type of internal standard. As summarized by Smith [2], the fundamental relationship of the specific analyte, quartz, to the internal standard is as follows:

$$X_i = (I_i/I_{\text{ref}})(K') \quad (1)$$

where K' is the slope of the linear equation, X_i is the quantity of quartz, I_i is the intensity of the specific hkl line used for quartz, and I_{ref} is the intensity of the specific hkl line used for the internal standard.

The base calcite sample contained < 0.03% quartz and the base dolomite sample contained 0.03–0.04% quartz as determined by several techniques. The dolomite contained trace amounts of muscovite mica at approximately 0.2%. The quartz net intensity was corrected by a pseudo-

Correspondence to: G.P. Tomaino, Specialty Minerals Inc., 640 North 13th Street, Easton, PA 18042 (USA).

SSDI 0003-2670(93)E0193-B

Voight deconvolution. The carbonates used an internal standard addition of 5% α-Al_2O_3. The talc sample contains $< 0.03\%$ quartz as determined by several techniques. An internal standard addition of 10% CaF_2 was used.

The detection limit of approximately 0.03% is determined for all three matrices. However, a conservative detection limit of 0.05% is stated because of variations in the appropriate geological quartz standard, its correct crystallinity, and particle size for each matrix.

EXPERIMENTAL

Instrumentation

A Siemens D-500 equipped with a 40-position sample changer, a fine focus copper 2200-W x-ray tube, graphite monochromator, scintillation counter coupled to a Microvax II, and vendor supplied software was used for this study. The instrumentation and software also affects the detection limit of the analyses.

Parameters

Two sets of parameters are required for this analysis. The qualitative parameters for sample scanning to identify the various phase(s) present and the specific parameters for the internal standard method of quantitation is listed in Table 1.

Sample packing

The ideal sample packing techniques are the side fill (drift) and the spray drying with side filling. These yield the least oriented materials as stated by Brindley and Brown [3].

The back-packing technique was employed for this study. This technique provides reproducible sample packs for qualitative and quantitative determinations. The possibility of orientation are typically observed with the very platy morphologies. While back-packing yields a slightly oriented preparation, it does not hinder the quantitation of quartz. Alternate instrumentation may limit the ability to prepare the sample by the back-packing technique.

TABLE 1

Instrument parameters

Matrix	Minerals scanned	Scan range (2Θ)	Step size (2Θ)	Count time (s/step)
Qualitative calcite, dolomite and talc	All	5 –85	0.03	2
Quantitative calcite and dolomite	Al_2O_3	25.2–25.8	0.02	20
	Quartz	26.0–27.12	0.02	100
Quantitative talc	CaF_2	46.24–47.56	0.02	1
	Quartz	25.12–27.12	0.02	100

Standard and sample preparation

The mineral composition of the standards should be as comparable to future samples as possible. Since variations within the ore body may develop, the analyst must scrutinize samples for similarity to the original standards. In cases of extreme changes or different interferences, a new calibration curve or set of parameters must be developed.

All standard components are scanned from 5–85° 2Θ to determine relative crystallinity and phase purity. The two internal standards of α-Al_2O_3 and CaF_2 are assayed at $> 99.5\%$ as the phase. The α-Al_2O_3 and CaF_2 are inert, stable to mixing and long term storage. The α-Al_2O_3 is a Bueller product and the CaF_2 is a Fisher product. The α-Al_2O_3 and CaF_2 samples yield comparable peak intensities to Powder Diffraction File (PDF) 10–173 and 35–816. The quartz standard is a high purity British Chemical Standards (BCS) product assayed at $> 99.5\%$ as the phase. This quartz standard must be milled to the appropriate particle size prior to standard additions into the various matrices.

The standard sample preparations should contain a particle size distribution between 1 and 10 μm. As stated by Brindley and Brown [3], the particle size of quartz generates variations in the 101 peak intensity. Improperly milled coarse quartz, > 20 μm, typically yields decreases in the intensity because of extinction effects. Excessive grinding to < 0.5 μm can yield lattice distortion and an amorphous layering of quartz generating a decreased peak intensity. The 101 peak yields its maximum intensity between 2 and 20 μm.

These variations of decreased or increased 101 peak intensity contribute to future analyzed detection limits. In bulk samples the exact degree of grinding on every particle for each phase constituent is not easily or totally measured. Therefore, an inherent deviation on the quantitative determination of quartz is present at the 101 peak intensity and the detection limits must not be overstated for each matrix.

The calibration curves presented contain an additional 5% relative standard deviation because of variations in the appropriate geological quartz standard, its crystallinity, and particle size for each matrix.

As stated by Smith [2], the theoretical peak intensities for the 101/100 peaks are 100/17. The BCS quartz was scanned and compared to the PDF 33–1161 for peak intensities of the 101/100 peaks. The relative ratio is 100/18. As mentioned by Brindley and Brown [3], this ratio may indicate extinction characteristics at the 101 peak. To achieve a particle size of 1–10 μm, the quartz standard was ground in a Spex 8510 shatterbox using a tungsten carbide (WC) 8504 puck and ring mill.

Spex literature cites that a 100-g loading of >2 mm sand dry ground at 4 min will allow 100% of the sample to pass a 44-μm sieve. In order to obtain a suitable quantity for development, the quartz standard was prepared using 20-g aliquots and ground for 6 min. These smaller aliquots prevented compacting of the sample.

This prepared quartz standard was re-analyzed and determined to contain approximately 0.2% WC. The amount of this impurity is related to the age and condition of the puck and ring mill. Therefore, a separate puck and ring mill should be maintained in the laboratory for standard preparations.

A milling study on the BCS quartz was undertaken to observe possible shifts in the 101/100 peak intensities after 0, 6, 12, and 18 min (Fig. 1). The milled samples were compared to the respirable quartz samples of NBS 1878 and Min-U-

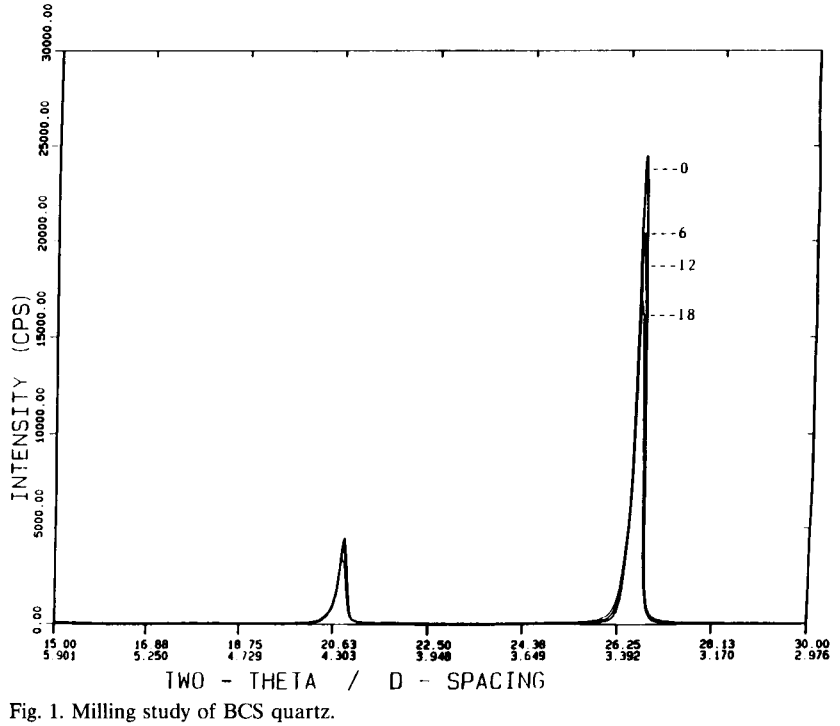

Fig. 1. Milling study of BCS quartz.

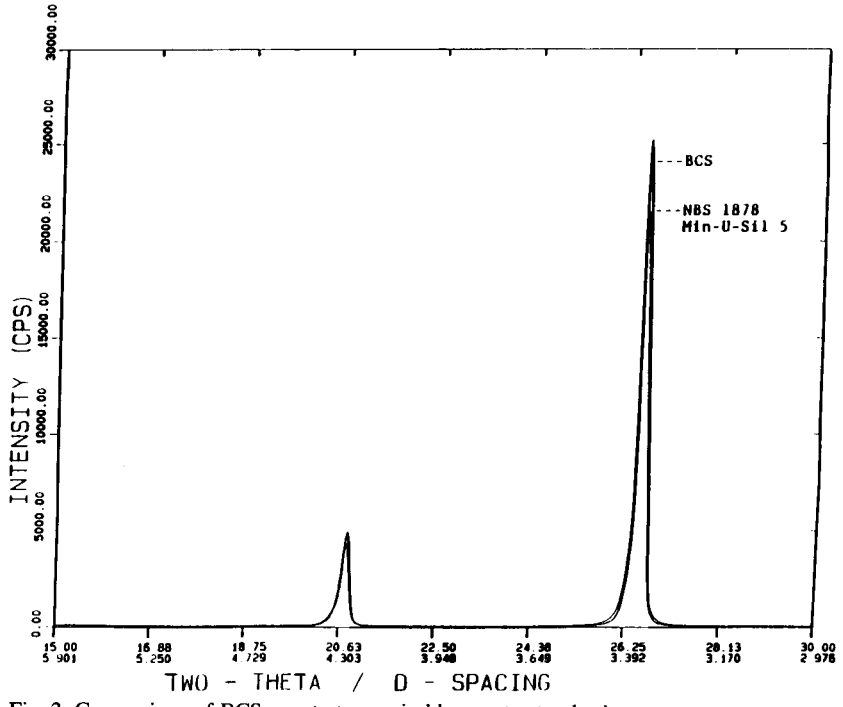

Fig. 2. Comparison of BCS quartz to respirable quartz standards.

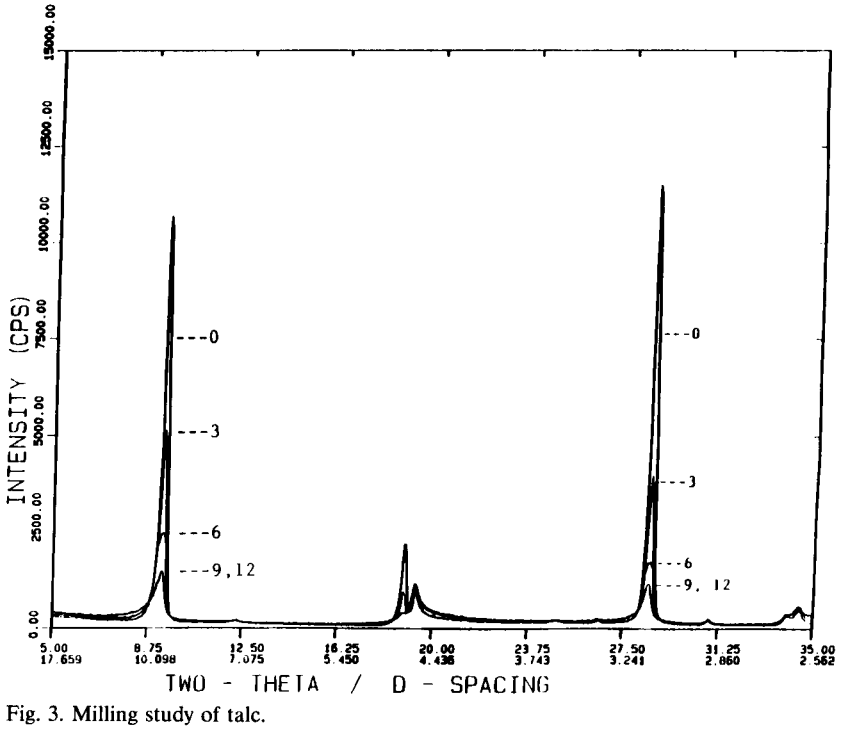

Fig. 3. Milling study of talc.

Sil 5. The 6-min milled sample is comparable to the two respirable standards with only a slight deviation in intensity (Fig. 2).

The calcite and dolomite samples were puck and ring milled for 6 min using 20-g aliquots. The talc sample milling was scrutinized to prevent delamination of the platy structure by the aggressive sheering of the puck and ring mill. This delamination generates an amorphous characteristic creating higher background counts in the area of the 101 peak. The delamination is easily observed by monitoring the talc's 001 lines. This phenomenon was verified by milling a talc sample for 0, 3, 6, 9, and 12 min (Fig. 3). A less aggressive mill, Spex 8508 WC puck mill, was used for talc. It was found from experience that milling talc for 3 min at 10-g aliquots was the proper sample preparation.

The quartz levels in the base materials were verified by several techniques. The calcite contains < 0.03% quartz, the dolomite 0.03% quartz, and the talc < 0.03% quartz. Each standard consists of 20–30 g including the internal standard and the specific level of quartz. The carbonate matrices used a 5% addition of the α-Al_2O_3 and the talc a 10% addition of the CaF_2. This mixture was mixed/milled in a Spex 8000 using a Spex 8004 WC ball and vial for a total of 6 min. Intermittent spatula re-mixing at 2 and 4 min was performed to prevent compacting of the sample.

The future samples should be treated as outlined. The analyst must always monitor samples as to artifacts/degradations generated by the puck and ring milling, puck milling, and final mixer/milling prior to the final quantitative analyses.

Calibration

The general relationship of the analyte to the internal standard is modified to

$$X_i = (I_i/I_{ref})(K')$$

where I_i is the intensity of the analyte component i's specific hkl line, I_{ref} is the intensity of the selected reference component ref's specific hkl line(s), X_i is the weight fraction of i, and K' is a restated ratio of the X_{ref} divided by K where K is the ratio constant of the standard instrument geometry and the parameters specific to the two components being analyzed within the bulk matrix. K' is the slope of the linear equation [4–6].

TABLE 2

Calibration data

Matrix	Internal standard	Quartz (%)	I_i/I_{ref}	R.S.D. (%)	n	R^2
Calcite	5% Al_2O_3	0.96	1.92	25.0	19	0.9929
		0.52	0.91	18.0	20	
		0.33	0.54	15.0	19	
		0.07	0.12	37.0	16	
Dolomite	5% Al_2O_3	1.04	1.89	16.0	20	0.9999
		0.53	1.01	16.0	20	
		0.34	0.62	17.0	20	
		0.23	0.43	27.0	19	
		0.13	0.22	30.0	19	
Talc	10% CaF_2	1.00	0.13	12.0	20	0.9963
		0.74	0.10	24.0	19	
		0.51	0.07	36.0	19	
		0.22	0.023	8.0	20	
		0.14	0.018	14.0	20	

This constant, K', contains the following: deviations of the initial sampling, sample preparation/milling aberrations, possible sample orientations effects, auto-sampler presentation of the sample to the x-ray beam, instrument (generator) fluctuations during analyses, analyst variations and variations among analysts.

The constant K' provides a factor for future sample analyses allowing specific "type" standards to be analyzed with the samples versus the entire set of calibration standards. The internal standard method is not dependent upon decreases in intensity of the tube because the pro-

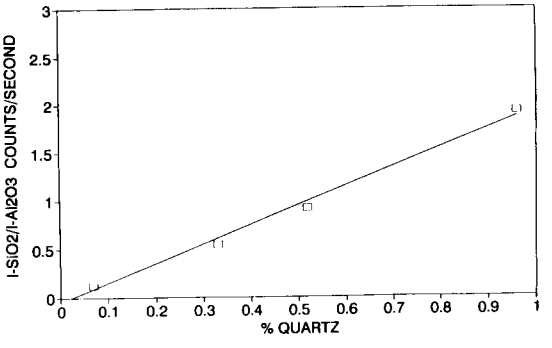

Fig. 4. Quartz in calcite matrix.

portional decrease in the intensities for both analyte and internal standard are determined. The "type" standards are the blank, one in the 0.1% range, and a standard between 0.3 and 0.5%. If for some reason the future samples contain significant differences in the phase components or interferences, a new constant must be developed for that matrix.

The development of the constant K' demands significant standard replications with each replicate represented as an individually packed sample preparation, not the same sample pack measured a specific number of times. Typically 20 replicates per standard are analyzed for each point in the calibration curve. The actual Gaussian distribution per point of the curve is generated. Since the accuracy may be greater than the precision and may not be measurable or verifiable from other independent analyses, the relative standard deviation per point and for the whole calibration range is developed by replication. Once the K' is developed for a specific calibration range and matrix, future samples are analyzed in triplicate.

For the final reported value one must correct for the internal standard dilution of the original sample:

$$\%\ \text{quartz in sample} = \frac{x(100)}{100 - y}$$

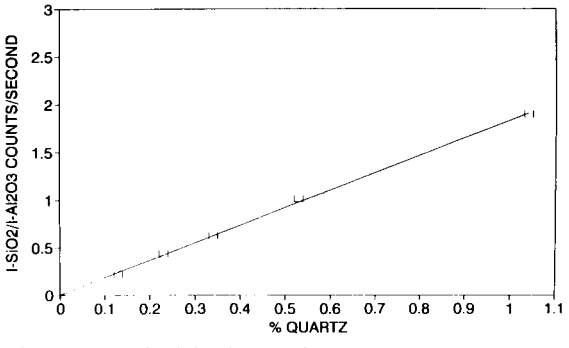

Fig. 5. Quartz in dolomite matrix.

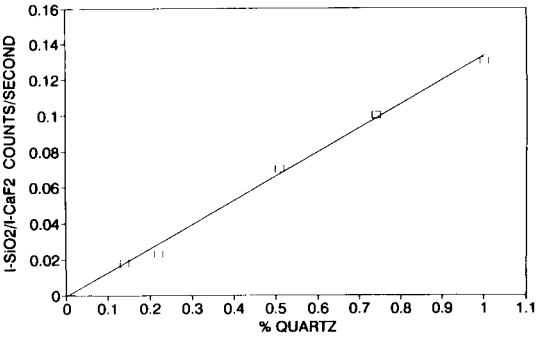

Fig. 6. Quartz in talc matrix.

where x is the % quartz in sample plus internal standard and y is the % internal standard added.

RESULTS AND DISCUSSIONS

The quantitative determinations and the calibration curves for the quartz additions in the calcite, dolomite, and talc matrices are presented in Table 2 and Figs. 4–6. From Eqn. 1 a rearranged relationship corresponding to the calibration curves is as follows:

$$(I_i/I_{\text{ref}}) = (X_i)(1/K')$$

where $1/K'$ is the slope of the line.

The author would like to thank Chad Gaul, David W. Holstein, Patricia K. Kern, R. Michael Kroc, and Lee Rogers for all their assistance in preparing this manuscript.

REFERENCES

1 H.P. Klug and L.E. Alexander, X-Ray Diffraction Procedures, Wiley, New York, 2nd edn., 1974.
2 D.K. Smith, CMA Project Report, 1992, pp. 1–77.
3 G.W. Brindley and G. Brown, Crystal Structures of Clay Minerals and their X-ray Identification, Mineralogical Society, London, 1980, Chap. 7.
4 F.H. Chung, J. Appl. Crystallogr., 7 (1974) 517.
5 F.H. Chung, J. Appl. Crystallogr., 7 (1974b) 526.
6 F.H. Chung, J. Appl. Crystallogr., 8 (1975) 17.

Analytica Chimica Acta, 286 (1994) 81–86
Elsevier Science B.V., Amsterdam

Quantitative determination of respirable quartz in bulk samples of organoclay by combined air classification/x-ray diffraction

Lawrence E. Morgan and L. DiCarlo

RHEOX, Inc., Wyckoffs Mill Road, Hightstown, NJ 08520 (USA)

(Received 20th August 1992; revised manuscript received 28th December 1992)

Abstract

There are a multitude of sampling techniques and quantitative methods for respirable silica in airborne materials but no sampling techniques exist to determine respirable silica in bulk samples. In order to determine the respirable quartz portion in an organoclay, a scheme was devised to employ air classification to separate the fines or respirable portion from the non-respirable or coarse portion. We chose $\leqslant 10$ μm material to represent the respirable portion. The total quartz content of the organoclay was determined on the "as-is" bulk sample by x-ray diffraction (XRD), using standards prepared in the laboratory and matrix matched to the organoclay being analyzed. The organoclay was then passed through an air classifier and separated into two fractions. Both the fines ($\leqslant 10$ μm organoclay) and the coarse (> 10 μm) portions were analyzed by XRD for percentage of crystalline silica. Preliminary results appear encouraging in that air classification can separate respirable material and XRD is capable of measuring quartz quantitatively to the $< 1\%$ level.

Keywords: X-Ray diffraction; Organoclay; Crystalline silica; Quartz; Respirable quartz

Numerous sampling methods have been reported for the quantitative measurement of crystalline silica in airborne materials [1]. However, no sampling techniques exist for the determination of the amount of respirable silica in bulk samples. While OSHA mandates labeling of products containing greater than 0.1% crystalline silica as a suspected carcinogen, it is the respirable portion that is truly the material of concern [2]. Therefore, it appears that it would be of greater value to know the amount of potentially respirable crystalline silica present in a bulk sample.

Most of the methods described in the literature concern themselves with the determination of quartz, cristobalite and tridymite in a specimen obtained by sampling the ambient air in the workplace [1], or the determination of the total crystalline silica present in a bulk sample [3]. This paper will propose a possible alternative to these two techniques; a method to isolate the respirable portion of the bulk sample by air classification and measure the resulting crystalline silica (quartz) content by x-ray diffraction.

From a study of the literature there appears to be some confusion as to what constitutes respirable; however, the general consensus depicts a range from $\leqslant 10$ μm [4]. However, the American Conference of Governmental Industrial Hygienists has recommended particle size-selective threshold limit values (TLVs) for respirable particulate mass as "those particles that penetrate a separator whose size collection efficiency is described by a cumulative lognormal function with a

Correspondence to: L.E. Morgan, RHEOX, Inc., Wyckoffs Mill Road, Hightstown, NJ 08520 (USA).

SSDI 0003-2670(93)E0074-H

median aerodynamic diameter of 3.5 ± 0.3 μm and with a geometric standard deviation of 1.5 ± 0.1" [5]. This describes the particle size-selective sampling criteria for airborne particulate matter. To add to the confusion, the Atomic Energy Commission (AEC) defines "respirable dust" as 2–10 μm with 10-μm material 0% respirable and 2-μm material 100% respirable [6].

To separate material in the 10-μm size range by conventional screening techniques proves to be quite difficult. The fine mesh screens required readily blind and static attraction causes the finely divided material to form agglomerates. We have attempted to resolve this problem by means of air classification.

EXPERIMENTAL

Instrumentation

The air classification is accomplished by using an Alpine A100-MZR unit. This equipment allows a small sample to be used. A 50-g amount of a commercially available organoclay was put through the air-classifier without any difficulty. This technique, which is an application of Stokes Law, relies on the sample being subjected to two forces operating simultaneously at right angles to each other. The sample is introduced into a chamber containing a revolving plate. Perpendicular to this plate is an air stream which can be supplied by either high pressure air or a vacuum. As the particles enter the chamber the coarse heavier particles are drawn to the outer edges of the revolving plate while the finer material is removed by an air stream and into a collection vessel. The coarse fraction is removed through a side port and into a second collection vessel. The cut point for the desired particle size can be changed by varying the rotation velocity of the plate and/or the air pressure gradient. The resultant fractions are then analyzed for percentage of quartz and particle size distribution is determined on each portion.

The crystalline silica (quartz) measurements were made on a SCINTAG XDS 2000 high resolution diffractometer with a standard focus copper target tube and a solid state detector. Samples were analyzed by step scanning the regions of interest at 0.01 degree per step with a counting time of 15 s per step. The resultant pattern was evaluated by profile fitting using the Pearson 7 routine (Fig. 1) and the peak area was recorded. Data handling was accomplished by means of a DEC Microvax 3100 computer with a Tektronix graphics terminal.

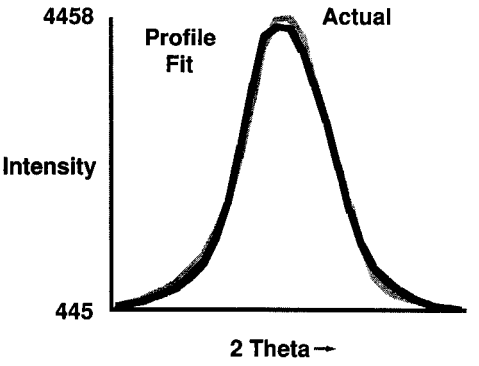

Fig. 1. Pearson 7 profile fit of quartz (101) reflection.

Particle size determination was performed using the Horiba laser diffraction particle size distribution analyzer. This instrument uses the Fraunhofer diffraction and MIE scattering theories in measuring the particle size distribution of a sample suspended in a liquid. Measurement is possible from 0.1 to 200 μm.

All samples were dispersed in isopropyl alcohol by sonicating for 45 s. A blank of the isopropyl alcohol was run and the sample was analyzed using the Horiba LA500.

Mass absorption coefficients were determined using a Spectrace Model 5000 energy dispersive x-ray spectrometer. The instrument is equipped with a rhodium target x-ray tube and solid state detector. Data reduction was accomplished via a Dell 286 computer running a program developed in this laboratory.

Standard materials

The XRD was calibrated for quartz content by using standards prepared in this laboratory. The standards were prepared by using a bentonite clay that had been triply beneficiated, then reacted with the same quaternary ammonium compound as found in the sample. A portion of the

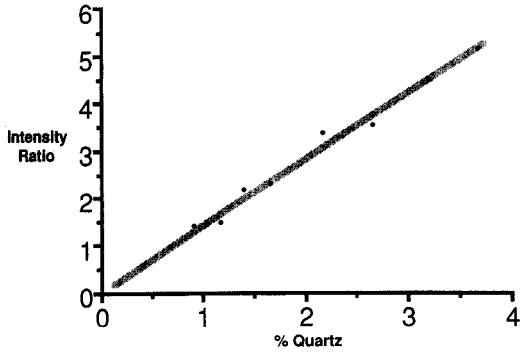

Fig. 2. Calibration quartz content (%) in organoclay versus x-ray intensity ratio for quartz (101) reflection.

purified organoclay was spiked with 5-μm MIN-U-SIL 5 and mixed for 1 h on a Spex Mixer mill, using a 75-ml vial with no pestle to insure homogeneity. Weighed portions of this master mix were diluted with the purified organoclay to produce a calibration series from 0.1 to 3.5% quartz (Fig. 2).

Of paramount concern is the problem of knowing the degree of crystallographic integrity of the quartz in the sample with respect to the standard materials used for comparison. The various effects, i.e., particle size, degree of crystallinity, interstitial impurities, lattice imperfections and the presence of amorphous silica are very difficult to determine. A suggested approach is to select standard materials that have diffraction profiles that are similar to the material being analyzed. The reader should be aware of these potential sources of error and that the estimated errors in this paper relate to the calibration standards.

Standardization of the x-ray spectrometer involved a fixed count measurement of the Compton modified rhodium radiation from materials of known mass absorption coefficient. These values were plotted versus the copper radiation mass absorption coefficient for each of the materials. The materials used covered the range of absorption coefficients from 20 to 350 $cm^2\ g^{-1}$.

An external standard for x-ray diffraction, prepared by mixing 10% by weight of 5-μm MIN-U-SIL with 90% by weight of epoxy and permanently cast in a sample holder, was used to insure reproducibility of intensity measurements. All sample readings were ratioed to this standard.

Sample preparation

A commercially available bulk sample of organoclay, a reaction product of bentonite clay and long chain fatty acid quaternary ammonium compound, was put through the air classifier, after operating conditions were optimized. A particle size of 10 μm or less was selected for the cutoff point as this would include all the respirable quartz by our definition. The resultant fine and coarse fractions became the basis for this study. The bulk organoclay sample contained 0.8% quartz; this level could be easily measured with the SCINTAG XDS. In addition, recognizing that even with matrix matched standards variations in absorption can occur, a correction using the method described by Sahores [7], whereby the mass absorption, as determined by X-ray fluorescence (XRF), was applied to all measurements.

Data collection

Standards. The series of standards are loaded in triplicate and analyzed by x-ray diffraction. Each standard is scanned between 25.9° 2Θ and 27.2° 2Θ in 0.01° steps and counted for 15 s per step, to insure inclusion of the (101) quartz reflection ($d = 3.34$ Å). The X-ray tube is operated at 45 kV and 40 mA. The external reference is measured for each set of three standards.

The mass absorption coefficient value is determined using an air path at 40 kV and 0.08 mA. A total of 400 000 counts are collected for each sample. The measurement is made at 18.9 kV using a window width of 17 channels with an energy increment of 20 eV per channel. The total time in seconds to collect this count is recorded.

Samples. The samples obtained from the air classifier, i.e., coarse and fine, as well as the feed material are loaded into sample holders and run in triplicate. The operating conditions and scan rates are the same as for the standards. Absorption measurements are run using the exact conditions described for standardization. Particle size distribution is determined on the "as-received" or feed organoclay as well as the fine and coarse portions after air classification.

Data processing

Standards. The resulting data were evaluated using the profile fitting routine described and the

peak areas ratioed to peak areas measured on an external standard, containing 10% quartz, as a means of correcting instrumental drift. The ratios obtained were multiplied by the absorption correction, and plotted versus concentration.

Samples. The peak areas obtained by profile fit were ratioed to the quartz external reference and multiplied by the absorption correction measured on portions of the same material. The resulting ratios were read from the calibration curves by means of a regression program developed in this laboratory. The resulting concentrations are then averaged and reported.

RESULTS

Air classification

Starting with 50 g of an organoclay, the material after air classification yielded a split of 33% $\leqslant$ 10-μm material, 67% + 10 μm material (Fig. 3).

Particle size distribution reveals that the air classification did not yield all 10-μm or fine material and even the coarse portion contains some 10-μm material. However, the quartz content is measured in the feed, fine and coarse portion and corrections are made to account for this.

The median particle size of the feed material before air classification is 9.6 μm and ca. 53% is 10 μm or less. The fine portion after air classification has a medium particle size of 4.7 μm and 94% is 10 μm or less while the coarse fraction

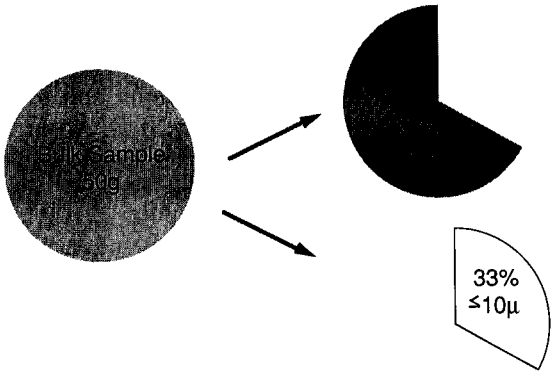

Fig. 3. Air classification of organoclay.

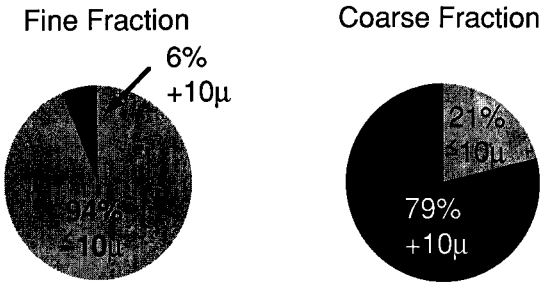

Fig. 4. Percentage of cross contamination in air classified fractions.

has a median particle size of 22.2 μm and 21% is 10 μm or less (Fig. 4).

Corrections were derived based on the simultaneous equations:

$$QF = 0.94F + 0.06C \quad (1)$$

$$QC = 0.21F + 0.79C \quad (2)$$

where F = percentage of quartz due to the ($\leqslant$) 10-μm fraction; C = percentage of quartz due to the plus (+) 10-μm fraction; QF = percentage of quartz measured in the ($\leqslant$) 10-μm fraction; and QC = percentage of quartz measured in the plus (+) 10-μm fraction.

Quartz measurement by x-ray diffraction yielded the values of 0.7% quartz in the $\leqslant$ 10-μm and 0.8% quartz in the +10 μm fractions. Solving Eqn. 1 for F gave a value of 0.69% quartz while C equals 0.83% quartz.

Thus, the quartz content in the coarse fraction is 0.83 whereas the quartz in the fine fraction is 0.69%.

Potentially respirable quartz

Starting with 50 g of organoclay, the air classification of this bulk sample resulted in 16.5 g with 94% or 15.51 g containing $\leqslant$ 10-μm material and 33.5 g (21%) containing 7.03 g of $\leqslant$ 10-μm material for a total of 22.54 g of $\leqslant$ 10-μm material. Applying the concentration of quartz in the fines of 0.69% to this yields a $\leqslant$ 10-μm quartz value of 0.155 g. Based on the original sample, the potentially respirable quartz content is 0.31% (Fig. 5).

Material balance

The starting 50 g feed contains 0.8% total quartz as measured, or 0.400 g. The quartz pre-

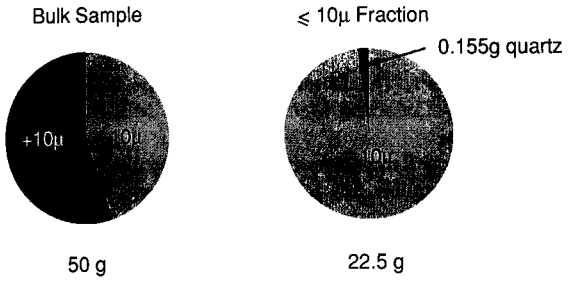

Fig. 5. Amount of potentially respirable quartz in organoclay.

sent in the fine fraction is 0.155 g. The quartz in the coarse fraction may be calculated using the particle size measurement data and the x-ray diffraction measurements. This concentration is equal to 0.228 g of quartz. The total quartz recovered from both portions is 0.383 g. This value divided by the total quartz content in the starting material yielded a recovery of 96%.

DISCUSSION

Methods have been developed [3,8] that permit the analysis of quartz in bulk sample, the NIOSH method is well known as the recommended method for the determination of quartz in samples of airborne material. The determination of respirable quartz in a bulk sample, while very desirable to know, may be difficult to determine.

This method demonstrates that it is possible to isolate a portion of a sample that could potentially become airborne. In order to do so, however, certain assumptions must be made when complete separation, i.e., 100% of $\leqslant 10$ μm and 100% > 10 μm is not accomplished. Assumptions that may or may not be true, for every material. The first such assumption is that the separated material has the same composition as the bulk sample.

Second and probably the most significant from an x-ray diffraction standpoint is the assumption that the crystallite size of the quartz in the fine and coarse fractions is equal to that present in the standards. The analyst should be aware of these potential sources of error and correct for them. In our study, the composition of the feed or "as-is" bulk organoclay, fine portion and coarse portion are similar. This was shown by thermogravimetric analysis. An additional experiment was carried out where the same organoclay is intentionally air classified under less than optimum conditions. The respirable quartz was found to be 0.31% vs. 0.31% for the "more efficient" separation. The mass balance and recovery is 96 and 98% for the more efficient and poor efficient separation, respectively. Again, this shows the samples to be homogeneous with the separate portions having a similar composition as the bulk sample.

The standards as previously mentioned were prepared with 5-μm MIN-U-SIL, the feed, fine and coarse portions all showed similar full width at half maximum, implying that the crystallite size is also similar, which eliminates or minimizes this potential source of error.

The process of air classification may not be applicable to all materials. As noted in the experimental section it was difficult to obtain fractions which were composed totally of fines or coarse material within a reasonable and practical time.

The process involves changing operating parameters to obtain the best yield of the desired particle range. This process can be time intensive and when applied to process technology may be entirely justified, however, when applied to an analytical technique that may be applied to a variety of materials, the sampling process may be more involved than the actual analysis. While the organoclay used did show some degree of separation and possibly with greater time investment, i.e., more passes, different speeds, etc., may have been possible to obtain maximum yield of $\leqslant 10$-μm material. However, we applied corrections to the measured quartz concentrations in order to calculate the amount of quartz in the respirable portion.

Conclusions

The newly developed method shows that is possible to measure the potentially respirable quartz in an organoclay. The results obtained while subject to potential errors due to particle size and composition, did produce a reasonably

good correlation as shown by the material balance and the excellent agreement between "poor" and "good" air-classification separation.

It is recognized however that this method yields results that at best produce values that are believed to be no better than $\pm 10\%$ relative error at the 1% level, and a greater error at lower levels. Therefore, in order to increase the precision at the 0.1% level, which could conceivably show larger errors than noted here, it would be necessary to run a suitably large number of replicate determinations as well as increase the counting time for each step in the diffraction scan to improve counting statistics.

While no claim is made regarding the applicability of the technique to other types of materials, there may be potential applications in other areas. These would have to be evaluated on a case by case basis.

REFERENCES

1 J.W. Thatcher, The Determination of Free Silica in Airborne Dust Collection Membrane Filters MESA, IR 1021, 1975, 16 pp.
2 Criteria for a Recommended Standard-Occupational Exposure to Crystalline Silica. HEW Publication (NIOSH) No. 75–120; U.S. Department of Health, Education and Welfare, Public Health Service, Centers for Disease Control, National Institute for Occupational Safety and Health.
3 J.R. Carter, M.T. Hatcher and L. DiCarlo, Anal. Chem., 59 (1987) 513.
4 J. Cowie, personal communication, 1992.
5 Threshold Limit Values and Biological Exposure Indices for 1989–1990, American Conference of Governmental Industrial Hygienists, 1989.
6 Air Sampling Instruments for Evaluation of Atmospheric Contaminants, 5th edn., American Conference of Governmental Industrial Hygienists, 1978.
7 J.J. Sahores, Adv. x-ray Anal. 16 (1972) 186.
8 L.E. Alexander and H.P. Klug, Powder Diffraction, 4 (1989) 66.

Analytica Chimica Acta, 286 (1994) 87–95
Elsevier Science B.V., Amsterdam

Determination of cristobalite in respirable airborne dust using x-ray diffraction

J.E. Chisholm

Occupational Medicine and Hygiene Laboratories, Health & Safety Executive, Broad Lane, Sheffield S3 7HQ (UK)

(Received 20th August 1992; revised manuscript received 17th March 1993)

Abstract

During 1993, the UK Health and Safety Executive (HSE) will publish a recommended method for the analysis of cristobalite in respirable airborne dust. Various compromises and uncertainties are inherent in such a method and place limitations on the overall accuracy of analysis. Compromises have to be made in the sampling process, in the choice of filter used for sampling, between speed and reliability in the analysis itself and in quality control. Analytical uncertainties arise mainly from variations in the intensity and profile of the cristobalite diffraction maxima, which raise doubts over the validity of the available standards; the unavoidable dependence on the primary diffraction line at low levels of cristobalite and the validity of the calibration close to the origin.

Keywords: X-Ray diffraction; Airborne dust; Cristobalite; Crystalline silica; Silica

The analysis of cristobalite in respirable airborne dusts is an essential part of the monitoring procedure required to assess and subsequently control the risk of workers developing the occupational lung disease, silicosis. Silicosis is the most widespread form of pneumoconiosis worldwide; an estimated 100 000 workers are potentially at risk in the UK alone. The disease is caused by the inhalation of dust containing crystalline silica, most commonly quartz but sometimes cristobalite or, on rare occasions, tridymite.

As a high-temperature form of silica, cristobalite is found in ceramics, refractories, furnace insulation material after use and calcined diatomaceous earth; it also occurs in bentonite clays. Cristobalite poses an occupational health hazard to workers in the ceramics and foundry industries, and in particular to workers removing insulation from furnaces. Monitoring of workplace air has to be carried out in those industries and in the UK a Maximum Exposure Limit (MEL) of 0.4 mg/m^3 has been set for respirable crystalline silica [1].

The method in use for the determination of respirable cristobalite is outlined below and the various problems and factors which limit the precision, accuracy and reliability of the analytical results are then discussed. The use of a similar x-ray diffraction method for the determination of quartz in airborne dusts is long established [2].

ANALYTICAL METHOD

Airborne dust particles vary widely in size but they are not all equally likely to penetrate into the lung and cause harm. It is the respirable particles which must be sampled and this is done using a miniature cyclone sampler [3] operated

Correspondence to: J.E. Chisholm, 004 Robens Laboratory, Health & Safety Executive, Broad Lane, Sheffield S3 7HQ (UK).

SSDI 0003-2670(93)E0259-A

under specified conditions. The worker wears the sampler in the breathing zone (within 30 cm of the nose and mouth) and air is drawn through at a measured rate for a known time so that the total volume of air sampled may be calculated. The air passes through a membrane filter (normally 25 mm in diameter), made of PVC-acrylonitrile co-polymer, which traps the respirable particles. Silver-membrane filters are also used; the background x-ray scattering from them is less and the signal-to-noise ratio better but filters of this type cannot be used for analysis by infrared spectroscopy and their use has other disadvantages discussed below.

The sample presented for analysis is normally a membrane filter having a total dust loading of a few hundred microgrammes. The mass of cristobalite in typical workplace samples rarely exceeds 100 μg and is usually below 50 μg.

HSE has recommended analysis using a direct on-filter method rather than one involving sample transfer on to a second filter for analysis [4] because its is quicker, simpler and there is less risk of losing dust during handling. The method assumes a linear relationship between the intensity of a cristobalite diffraction maximum and the mass of cristobalite on the filter, which is valid so long as the sample is thin enough for attenuation of the x-ray beam to be insignificant [2,5]. In the experience of HSE laboratories in analysing air samples from a wide range of workplaces, the thin-sample assumption has been found to hold in practice for filter loadings up to about 2000 μg cristobalite (except for samples of dust containing a high proportion of iron oxides, for which shorter sampling times and lower filter loadings have to be used).

Diffracted intensities are measured for the three strongest diffraction lines. It is essential to use the peak area for these measurements as the cristobalite maxima from some samples may be subject to broadening as a result of small particle size, stacking disorder or poor crystallinity. Instrument operating details and measurement conditions are summarised in Table 1.

Calibration is carried out using NIST standard respirable cristobalite (SRM #1879) and the same method as for analysis of respirable quartz [2,5]. A sample of the standard cristobalite is dispersed by a jet of compressed air into a dust chamber and the resulting dust cloud sampled using cyclone samplers with pre-weighed filters for different periods of time. The filters are weighed again after sampling to determine the weight of standard cristobalite collected. By trial and error with different sampling times, a set of filters covering the range of weights required for calibration (0–2000 μg) is prepared. The diffracted intensities of each of the three strongest diffraction maxima of cristobalite are measured for these prepared filters and regression analysis used to determine the calibration line. The linearity of the calibration line provides a check on the range over which the thin sample assumption is valid, at least for samples with mass absorption coefficients similar to pure cristobalite. The calibration is carried out using a large number of standard filters (about 20) and a longer counting time of 100 s at each

TABLE 1

Instrumental parameters

Philips diffractometer with a PW1050 goniometer
2.7 kW broad focus copper anode x-ray tube run at 45 kV, 45 mA
Instrument operating conditions aim to maximise diffracted intensity at the expense of resolution
Divergence slits with appropriate anti-scatter slits: To avoid changes in the divergence slit during automatic operation, 2° divergence and anti-scatter slits are used throughout although this leads to high scattered background at lower 2ϑ
Receiving slit: 0.3 mm
Graphite monochromator
Automatic sample changer
Stationary sample during data collection (no sample spinner available)
Data collection:
Step scans with steps of 0.05° 2ϑ, counting for 30 s at each step for analysis (100 s at each step for calibration)

0.05° 2ϑ interval, is used for data collection instead of 30 s, which is used for routine analysis of samples. The longer counting times were used with the aim of reducing the errors in the calibration arising from counting statistics. Subsequent analysis of the data on precision (see below) shows that the dominant error source is a combination of factors including particle statistics and variations in the distribution of particles on the filter. Accordingly, the use of many standards for calibration should be more effective than increased counting times since it should reduce the errors in the calibration arising from particle statistics as well as counting statistics.

RANDOM ERRORS, PRECISION AND DETECTION LIMIT

The random errors can be assessed by carrying out repeat measurements on filters on which a known weight of cristobalite has been deposited in the same way as the calibration samples are prepared. Estimated standard deviations for a range of filter loadings are given in Table 2 and the variation of the estimated relative standard deviation with filter loading (Fig. 1) follows the trend illustrated by the RSC Analytical Methods Committee [6]. The detection limit can be estimated by making repeat measurements on blank filters following the recommendations of the Royal Society of Chemistry [6]. The detection limits assessed in this way as $3\sigma_B$/slope of calibration line are quoted in Table 2. Such estimates are only an approximate guide to the detection limits for workplace filters which, if other material has been deposited on them as well as cristobalite, may have a different background count level from blank filters.

The relative standard deviation expected from counting statistics alone (Table 2) may be estimated as $\sigma_{cs} = 100(N_p + N_b)^{1/2}/(N_p - N_b)$ (%); where N_p is the total counts making up the peak and background, N_b the background counts contributing to the total and $(N_p - N_b)$ the counts making up the area of the peak above the back-

TABLE 2

Precision and detection limits for the three principal cristobalite reflections

[Instrument operating conditions as in Table 1. Precision based on 12 repeat measurements for each filter from which σ is calculated as the standard deviation from the mass m of cristobalite on the filter. The relative standard deviation $\sigma_{rel} = 100\ \sigma/m$ (%). The relative standard deviation derived from counting statistics alone $\sigma_{cs} = 100(N_p + N_b)^{1/2}/(N_p - N_b)$, where N_p = total counts making up the peak and background, N_b = background counts contributing to the total and $(N_p - N_b)$ = counts making up the area of the peak above background]

Weight of cristobalite on filter (μg)	Reflection								
	101 Standard Deviation			102			200/112		
	σ	σ_{rel} (%)	σ_{cs} (%)	σ	σ_{rel} (%)	σ_{cs} (%)	σ	σ_{rel} (%)	σ_{cs} (%
23	10	41	4	18	76	88	6	26	24
41	5	13	3	9	21	34	6	15	15
106	10	10	1	15	14	11	10	9	5
210	12	6	0.6	18	9	4	6	3	2
280	9	3	0.5	20	5	3	13	4	2
476	14	3	0.3	22	5	2	11	2	1

At the maximum UK exposure limit for crystalline silica (0.4 mg/m^3), a 500-l air sample will deposit 200 μg on the filter.

Detection limits [6] calculated as $3\sigma_B/s$, where σ_B is the standard deviation of the diffracted intensity from a blank filter and σ is the sensitivity in counts/s/μg cristobalite derived from the slope of the calibration curve. σ_B was determined from 12 repeat measurements made on each of three blank filters, i.e. 36 measurements in total.

Reflection	101	102	200/112
Detection limit (μg)	7	21	11

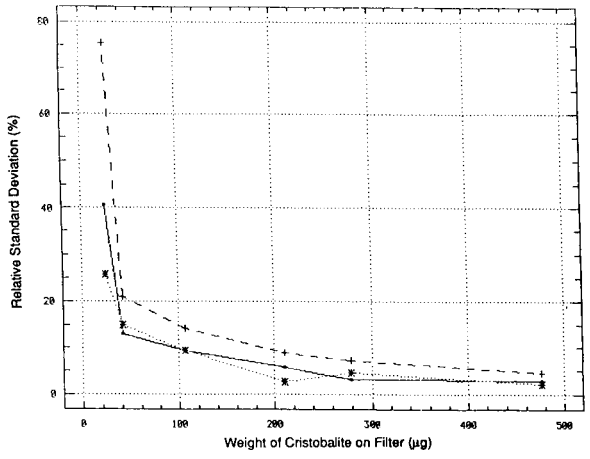

Fig. 1. Precision data for cristobalite (NIST SRN #1879) on Gelman DM800 organic membrane filters. Relative standard deviation (%), based on 12 repeat measurements for each filter, as a function of the known weight of cristobalite on the filter: 101 reflection (most intense), data points·joined by full line; combined 200 and 112 reflections (second most intense), data points * joined by dotted line; 102 reflection (third most intense), data points+joined by dashed line.

ground. It is clear from a comparison of σ_{cs} and the observed relative standard deviation σ_{rel} that counting statistics do not make a major contribution to the overall error of analyses using the strongest reflection. For the other two less intense reflections, counting statistics have a significant effect on precision and are the major contributor to the error at low filter loadings (at or below about 100 μg for 200/112, 200 μg for 102). The apparent anomalies at low filter loadings for 102 and 200/112 where σ_{cs} is greater than the observed σ_{rel} probably result from the large variations expected in estimates of σ; the 95% confidence interval for σ is wide and extends for a considerable distance on the high side of the estimated value.

Since the effect of counting statistics on the observed precision is small for the strongest reflection 101 (and for the other reflections at high filter loadings), the precision must be determined by other factors. There will be a contribution from the particle statistics, which is a function of the number of particles present and in an orientation which enables them to diffract and contribute to the reflection [7–9]. This particle statistics component must arise from a different area of the filter being examined each time (no sample spinner was available) and possibly also from slight changes in the orientation of the filter, which could easily occur with such a light material. A contribution to σ_{rel} is also to be expected from variations in the distribution of the cristobalite particles over the filter as well as the simple effect of the number of particles in the correct orientation to diffract. Both these components of σ_{rel} should decrease as the weight of cristobalite on the filter increases, giving a variation of relative standard deviation with weight on the filter of the kind observed (Fig. 1).

There should be a fixed contribution to σ_{rel} arising from instrumental and other factors inherent in the method. The variation in Fig. 1 should approach this fixed component asymptotically as the weight of cristobalite on the filter increases. Unfortunately, the range of filter loadings covered here does not extend high enough to be certain that the asymptote is reached. One can conclude from Fig. 1 only that the fixed component of σ_{rel} is not more than 3%. The corresponding residual error in the determination of quartz in bulk kaolin samples has been estimated as 1% [10].

For the strongest reflection 101, particle statistics appear to control the precision at low filter loadings (Table 2), the effect of counting statistics being small in comparison. Particle statistics have a significant effect on precision for the other reflections. Particle statistics are seldom a major contributor to the errors in the analysis of bulk samples (at analyte concentrations above about 10%) which have been adequately ground so that the diffracted intensity comes from a large number of particles [7–9]. But particle statistics is said to be the most severe limitation on the potential accuracy of quantitative x-ray diffraction [9] and this will particularly true at low concentrations. In the determination of quartz in kaolins, it was indeed found that particle statistics may be a significant source of error at low concentrations and in some samples might possibly predominate over counting statistics [10]. Particle statistics would be expected to assume even greater impor-

tance for the smaller amounts of material examined on filters used for air sampling and the results obtained in the present study suggest this is indeed the case.

The assignment of factors controlling precision has a bearing on experimental strategy. If one wishes to reduce errors in the calibration or in a particular analysis using the strongest reflection, there is little point in using longer counting times as was done in this study since counting statistics are not the major source of error. More would be achieved in the way of reducing calibration error by making repeat measurements on the calibration filters or using more filters in the calibration. For the less intense 102 and 200/112 reflections, both counting statistics and particle statistics seem to have a significant effect on precision. Repeat measurements should again be most effective in reducing the error since they reduce the contributions from both sources. However, in this case, some benefit should be obtained, particularly at low filter loadings, by using longer counting times for these reflections. But this may only be true for organic membrane filters, whose high diffuse background scattering (N_b) helps to increase σ_{cs}; silver-membrane filters have a much lower background and for them σ_{cs} should be much lower and particle statistics have a correspondingly greater influence.

The precision obtained for the strongest 101 cristobalite reflection is satisfactory for enforcement purposes and many analyses; the other two reflections are most useful as a check on interference from other crystalline phases or as confirmation of filter loadings at the high end of the range.

The precision is nevertheless poor when there is only a small amount of cristobalite on the filter. In principle, the precision could be improved in a number of ways but there may be practical difficulties.

(1) The time taken to collect the dust sample could be increased so that there is more cristobalite on the filter. However, this may not be compatible with working practice or with sampling under typical conditions (e.g. the operation in which dust is released may take a fixed time).

(2) Spinning the sample should improve the particle statistics considerably [9] and it is intended to carry out future analytical work using a more modern diffractometer fitted with a sample spinner. Wide divergence and receiving slits and a broad focus target are already in use as suggested in [9] as further ways of improving particle statistics.

(3) Repeat measurements might be made on different areas of a stationary filter by turning the filter in the sample holder. This should be more effective than simply increasing the counting time since it helps reduce the error contributions both from counting statistics and particle statistics. However, the increased time taken for each analysis may cause problems when routine monitoring of large numbers of samples is carried out. In addition, there is a law of diminishing returns – four repeat measurements are required to halve the standard deviation.

(4) The signal-to-noise ratio can be improved by using silver-membrane filters for which the background scattering is lower. This would reduce the contribution from counting statistics to the overall error. Silver-membrane filters would only be worth using when that contribution is a major one, i.e. at low filter loadings. But the higher x-ray absorption of these filters limits the precision at low filter loadings in another way: When air sampling begins, dust penetrates some way below the surface of the filter. Because of the high mass absorption of the matrix, not all of the dust in the interior of a silver-membrane filter is "seen" by the x-ray beam and in consequence the calibration line usually does not pass through the origin. Zero measured diffracted intensity corresponds to a small but significant mass and this invalidates the assumption on which the estimation of the detection limit is based. Improved precision with silver-membrane filters may therefore be achieved only at the expense of a greater but different kind of uncertainty over the ability to measure low masses of cristobalite and the accuracy at low levels. In particular, the dust which penetrates below the filter surface is pure cristobalite for the calibration filters but will be a mixture for actual workplace samples, for which the calibration at low mass will therefore not hold.

NON-RANDOM ERRORS

Serious errors can arise from the overlap of reflections from other phases which are also present and for that reason it is best to use more than one reflection for analysis; inconsistencies in the analytical results from different reflections provide a warning that interference may be occurring.

Otherwise, the greatest doubts in the analysis of cristobalite, and those which are hardest to quantify, arise from the nature of cristobalite itself and how it is defined. Analytical difficulties stem from variations in the exact position, intensity (absolute and relative) and profile of the diffraction maxima of different samples of "cristobalite".

VARIATIONS IN THE POSITION AND INTENSITY OF THE DIFFRACTION MAXIMA: α- AND β-CRISTOBALITE

The seriousness of the problem of intensity variation is described most thoroughly and completely in a survey of "cristobalites", many of which were in use as standards in various laboratories, carried out at the British Cast Iron Research Association (BCIRA) [11]. Dust from each cristobalite sample was deposited on to filters, the diffracted intensities of the three most intense maxima measured and then normalised to 1 mg filter loading for comparison. The results showed that the intensity of the primary line could vary by a factor of almost 3, that of the second strongest line also by a factor of almost 3, and that of the third strongest line by a factor of 6 or 7. Only part of this variation came from differences in the percentage of crystalline material present in different samples as was demonstrated by the variations in the relative intensity of the three principal diffraction peaks. The ratio of the second strongest to the strongest varied by at least 20% and in a few extreme examples by as much as 50%; the ratio of the third strongest to the strongest varied by up to a factor of 3. In addition, small but significant differences in the

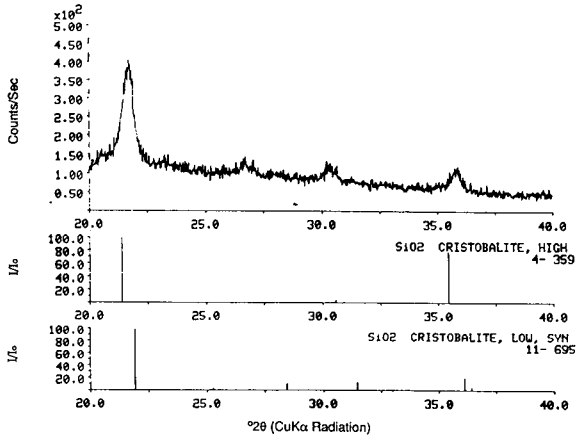

Fig. 2. Diffraction trace (Cu K_α radiation) of devitrified ceramic fibre insulation from a pottery oven compared with the reference patterns for β-cristobalite (high-) and α-cristobalite (low-) from the Powder Diffraction File. Note the differences in position and relative intensity of the diffraction maxima of the two phases. The sample appears to be closer to the β-form but could be a mixture or intermediate in character.

position of the diffraction maxima have been noted for different samples of cristobalite [12].

The existence of two different but related structural forms of cristobalite may well play a large part in these variations in diffracted intensity and d-spacing. The high-temperature β-form of pure SiO_2 has cubic symmetry and is stable above 1470°C. Transformation to quartz and tridymite, the polymorphs stable at lower temperatures, is very slow and β-cristobalite normally persists on cooling. However, below 200°C, it undergoes a rapid displacive transformation to the metastable tetragonally distorted form, α-cristobalite. The NIST standard reference material is respirable α-cristobalite and routine analyses of workplace samples have generally assumed that only α-cristobalite is present. Recent studies have shown that the β-form can be stabilised at room temperature by the presence of oxide impurities [13] and β-cristobalite has been identified in devitrified aluminosilicate ceramic insulation material after use [14,15].

Figure 2 shows a diffraction trace (Cu K_α radiation) from a bulk sample of aluminosilicate insulation blanket stripped from a pottery oven and the reference diffraction patterns for α- and

β-cristobalite. (Diffraction traces from bulk powders are used here as illustrations as they show the features under discussion more clearly. The features which give rise to uncertainty in the analysis may not always be apparent on diffraction traces from on-filter samples. The signal-to-noise ratio is worsened by the small mass present and the high background scattering from the organic membrane filter.) The positions and intensities of the two phases differ; the actual sample is close to β-cristobalite but does not match either phase exactly; it may be a mixture of the two or in some way intermediate in character between them. The diffracted intensities for α- and β-cristobalite will differ considerably and if a sample containing the β-form is analysed against an α-cristobalite standard the result is likely to be significantly in error. Unfortunately, a β-cristobalite standard suitable for quantitative x-ray diffraction analysis has not so far been available. Further, because the relative intensities of the corresponding reflections of α- and β-cristobalite differ, the analytical results will be different for the different diffraction maxima. This serves as a useful warning to the analyst that his sample of airborne dust may not match standard α-cristobalite but it does not help him to decide how much crystalline silica is present or how much of each form of cristobalite.

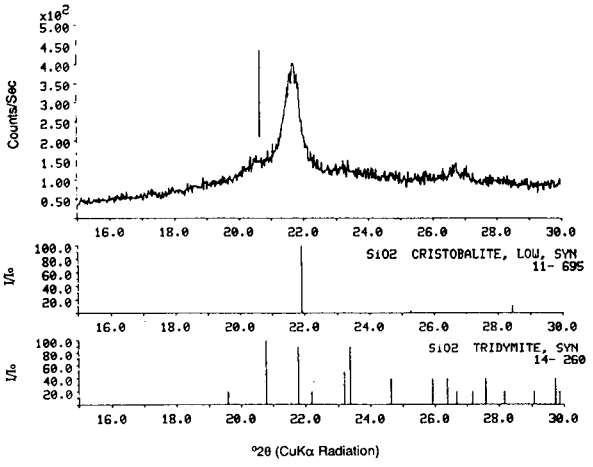

Fig. 3. The principal diffraction maximum (Cu K_α radiation) of devitrified ceramic fibre insulation from a pottery oven compared with the reference patterns for α-cristobalite (low-) and tridymite. On the low-angle side of the main maximum, there is a subsidiary maximum (marked) which is believed to result from tridymite-like regions in stacking disorder in the cristobalite. The main maximum itself may contain some intensity from the tridymite maximum which lies close to that of ordered cristobalite.

VARIATIONS IN LINE PROFILE – CRISTOBALITE OR AMORPHOUS SILICA?

The extent of variations in the profile of the principal diffraction maxima from "cristobalite" is shown in the work of Jones and Segnit [16]. Although they studied opals, the same range of variation is shown by cristobalites from other sources. Samples show a full range of behaviour from sharp peaks from highly ordered crystalline cristobalite to broad diffuse maxima from amorphous silica. At what point does the material cease to be cristobalite?

A further complication arises from the possibility of stacking disorder in cristobalite, which can also lead to broadening of the diffraction maxima. Sometimes ordered regions of the tridymite stacking sequence occur in samples which then show a subsidiary tridymite maximum near the cristobalite 101 peak [16] as shown for the bulk sample of devitirified aluminosilicate ceramic in Fig. 3. Although these ordered tridymite-like regions are not cristobalite, they may be regarded as in some sense a form of crystalline silica and may therefore still be harmful in the working environment. But the question of how to take account of the tridymite subsidiary maximum in the analysis remains problematical. In addition, if there is indeed tridymite of some kind present, another of its diffraction peaks is close enough to the principal cristobalite peak to contribute to the observed intensity and so lead to slight but unknown overestimation of the cristobalite present.

The presence of material of varying crystallinity may lead to analytical problems in some samples, particularly if devitrification has taken place. Although silica glass does not have a regular atomic arrangement, there are localised regions in which the arrangement bears some simi-

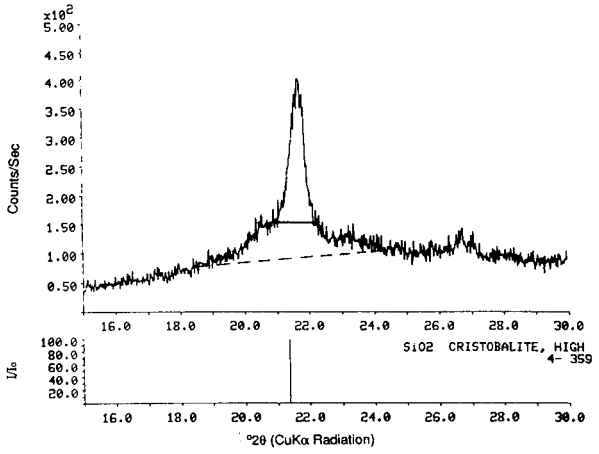

Fig. 4. The principal diffraction maximum (Cu K_α radiation) of devitrified ceramic fibre insulation from a pottery oven and the reference pattern for β-cristobalite (high-). A sharper peak from well ordered cristobalite appears to be superimposed on a diffuse maximum from poorly ordered material. Depending on how much structural order one considers cristobalite should have, the diffracted intensity may be measured above a background which includes the diffuse scattering in the intensity (dashed line) or excludes it (full line). If the measured intensity is used for quantitative analysis, the background level chosen has a marked influence on the result.

larity to the cristobalite structure. This short-range order gives rise to a diffuse maximum in approximately the same position as the strongest cristobalite maximum. Diffuse scattering from a glassy component may make it difficult to decide where to set the background level above which the diffracted intensity is measured (Fig. 4). It is possible to take only the intensity of the sharp diffraction maximum from the "crystalline" material or include some or all of the intensity from the "amorphous" component. The difficulty is in deciding where to draw the line between the contributions from the two components. Profile fitting can of course help to separate the components contributing to the observed diffracted intensity but the analyst still has to decide what model profiles to fit. As can be seen from the example in Fig. 4, the choice can result in a large difference (50% or more) to the final analytical result. For occupational hygiene purposes, it seems reasonable to take only the intensity from the sharp "crystalline" maximum since it is crystalline silica which is believed to be responsible for the most severe respiratory symptoms. But for other purposes, this may not be satisfactory.

Conclusions

Despite the efforts of many laboratories and organisations, large uncertainties still remain over the validity of results from x-ray diffraction analysis for cristobalite in airborne dusts. Among the random errors, particle statistics would appear to be more significant than counting statistics for the strongest cristobalite line and significant for the second and third strongest lines. The non-random uncertainties stem mainly from the nature of cristobalite itself.

The availability of the NIST reference respirable α-cristobalite, has made it possible to achieve a high degree of reliability in the analytical measurement itself. The method is probably standardised sufficiently to make the results comparable and this may be sufficient for some purposes, e.g. monitoring of the working environment is often concerned with detecting changes in dust levels or with comparing dust levels associated with different processes or different methods of working. The essential requirement for occupational hygiene is a measure of exposure: analysis relative to the NIST α-cristobalite standard gives a measure of the amount of well crystallised material present in the dust sample and it is this material which is implicated in occupational respiratory disease.

Nevertheless a fuller understanding of the forms of cristobalite found in airborne dust, their relationships and degree of structural regularity is the key to further improvement in analytical quality, leading perhaps to a better understanding of the factors which determine the effect of silica dust on the lung.

Thanks are due to an anonymous referee for his helpful comments on errors and in particular on the importance of particle statistics, which I believe have greatly improved the paper. I am also grateful to my colleague Dr. N.G. West for his thorough and constructive comments.

REFERENCES

1 Health and Safety Executive Publication EH40: Occupational Exposure Limits, HMSO, London, 1992.
2 Health and Safety Executive, Quartz in respirable airborne dusts, Laboratory Method using X-ray Diffraction (Direct Method) MDHS 51/2, HSE, London, 1988.
3 Health and Safety Executive, General Methods for the Gravimetric Determination of Respirable and Total Inhalable Dust MDHS 14, HMSO, London, 1989.
4 NIOSH, Silica, Crystalline, Respirable, Method 7500, NIOSH Manual of Analytical Methods (Third edition), NIOSH, Cincinnati, OH, 1984.
5 K.J. Pickard, R.F. Walker and N.G. West, Ann. Occup. Hyg., 29 (1985) 149.
6 Analytical Methods Committee, Royal Society of Chemistry, Analyst, 112 (1987) 199.
7 H.P. Klug and L.E. Alexander, X-ray Diffraction Procedures, Wiley, New York, 1974.
8 D.L. Bish and R.C. Reynolds, Jr. in D.L. Bish and J.E. Post (Eds.), Modern Powder Diffraction (Reviews in Mineralogy, Vol. 20), Mineralogical Society of America, Washington, DC, 1989, p. 73.
9 D.K. Smith, Advances in X-ray Analysis, 35A (1992) 1.
10 N.J. Elton, P.D. Salt and J.M. Adams, Anal. Chim. Acta, 286 (1994) 37.
11 P.D.E. Biggins, The Selection of a Suitable Cristobalite Standard to be used in the Analysis of Airborne Dust for Cristobalite, Report No. X.191 (Revised), British Cast Iron Research Association, Alvechurch, Birmingham, 1986.
12 M. Jeyaratnam and N.G. West, Adv. X-ray Anal., 32 (1989) 585.
13 A.J. Perrotta, D.K. Grubbs, E.S. Martin, N.R. Dando, H.A. McKinstry and C.-Y. Huang, J. Am. Ceram. Soc., 72 (1989) 441.
14 J. Young, M.S. Rea and G. Briggs, Br. Ceram. Trans. J., 88 (1989) 58.
15 R.C. Brown, E.A. Sara, J.A. Hoskins, C.R. Evans, J. Young, J.J. Laskowski, R. Acheson, S.D. Forder and A.P. Rood, Ann Occup. Hyg., 36 (1992) 115.
16 J.B. Jones and E.R. Segnit, J. Geol. Soc. Austr., 18 (1971) 57.

Analytica Chimica Acta, 286 (1994) 97–105
Elsevier Science B.V., Amsterdam

Crystalline silica analysis of Wyoming bentonite by x-ray diffraction after phosphoric acid digestion

William J. Miles

Bentonite Corporation, 1999 Broadway, Denver, CO 80202 (USA)

(Received 11th November 1992; revised manuscript received 16th February 1993)

Abstract

NIOSH Method 7601 gives incorrect high values by colorimetry for crystalline silica associated with sodium montmorillonite in Wyoming bentonite deposits because the digestion of amorphous silica and silicate minerals is incomplete in phosphoric acid at 240°C. However, the partial digestion of silicates and amorphous silicas concentrates crystalline silica for x-ray diffraction and other analytical methods to meet the 0.1% threshold for quantitative analysis required by federal and local government agencies. When the NIOSH Method 7500 x-ray procedure is applied to phosphoric acid digestion residues, use of the absorption correction factor to correct for thicker than ideal particles or films gives incorrect results and should not be used. This phosphoric acid digestion also provides a chemical method of distinguishing soluble opal ($SiO_2 \cdot xH_2O$) from inert cristobalite of high temperature origin. Based on the greater chemical reactivity in phosphoric acid of the silica phase associated with a number of Wyoming bentonites, and the x-ray diffraction patterns for these phases, the bentonite deposits are best described to contain opal-CT and not cristobalite.

Keywords: X-Ray diffraction; Bentonite; Crystalline silica

Bentonites are alteration products of volcanic ashes and tuffs that are rich in silica. Montmorillonite is the clay mineral that is formed by this alteration process and it gives bentonite its important chemical and physical properties. Opal, frequently misidentified as cristobalite, shares a genetic association with bentonite and occurs with bentonite in major commercial deposits in North America and the rest of the world.

Opal is a mineraloid with the variable chemical formula $SiO_2 \cdot xH_2O$ which is amorphous to paracrystalline. It is surprisingly common in nature, occurring primarily in sedimentary environments. Opal differs from anhydrous crystalline and amorphous silicas not only in chemical composition but also in chemical reactivity. Opal forms at low temperatures, typically below 100°C, under a number of conditions.

Opal of inorganic origin precipitates from ground waters saturated with soluble silica. Frequent sources of high concentrations of soluble silica are silica rich rocks of volcanic origin and geothermal waters. Most bentonite is formed by alteration of similar volcanic rocks.

The major geologic source of opal is soluble silica taken up by marine plants and animals or terrestrial plants with subsequent precipitation of amorphous silica hydrate (opal-A) within the organism. For example, marine and fresh water diatoms require soluble silica to form frustules or valves as a necessary part of the organism. After

Correspondence to: W.J. Miles, Bentonite Corporation, 1999 Broadway, Denver, CO 80202 (USA)

SSDI 0003-2670(93)E0199-H

death of the organism, the siliceous frustules accumulate in sediments and may undergo later diagenesis to form opal-CT.

Cristobalite is a silica mineral of high temperature origin, requiring formation conditions above 1470°C. Flynn et al. [1] have shown that sodium stabilizes its structure and allows cristobalite to form at temperatures as low as 1000°C in industrial processes. It is often associated with volcanic rocks.

Quartz is another silica mineral that occurs with bentonite and almost every other commercial mineral. Quartz comprises 12% of the earth's crust and 17% of surface rocks. It accumulates in soils and sediments due to its relative inertness and durability.

Recent federal occupational safety and state consumer protection regulations require the identification of crystalline silica polymorphs at a threshold of 0.1% and their distinction from silicates and amorphous forms of silica. It is particularly important to identify the low temperature polymorphs of opal [2], opal-A, opal-CT and opal-C, which, depending on the degree of ordering, can be mistaken for alpha cristobalite in x-ray diffraction (XRD) patterns if no other distinguishing tests are applied.

The National Institute of Occupational Safety and Health (NIOSH) published a chemical method, NIOSH Method 7601 [3], based on initial work of Talvitie [4] for analysis of respirable dusts of less than 5 μm particle size. Talvitie discovered that silicates and some amorphous silicas were soluble in refluxing phosphoric acid while crystalline silicas were much more resistant. Talvitie and Hyslop [5], Talvitie [6], and Sweet et al. [7] refined this method for concentrating quartz and cristobalite in the insoluble residue resulting from reaction of silicates and some amorphous silicas with refluxing phosphoric acid. This undissolved residue from phosphoric acid digestion is then dissolved in hydrofluoric acid, followed by formation of colored silico–molybdate complexes for spectrometric determination of total insoluble silica. NIOSH Method 7601 assumes that all residual silica is crystalline silica unless the mineralogy is known and interfering minerals are corrected for.

NIOSH Method 7601 suffers interferences from a number of partially or completely insoluble silicate minerals which create positive errors unless the mineralogy of a sample is completely identified and appropriate corrections are made. In particular, amorphous silica glasses of volcanic origin and diatomite of biogenic origin are slow to digest in refluxing phosphoric acid and lead to major positive errors if the colorimetric methods of the procedure are followed without additional corrections.

Miles and Hamilton [8] proposed that phosphoric acid digestion can be used as an effective concentration technique for subsequent x-ray diffraction analysis of the crystalline silica components. They also reported from initial results that opal appears to exhibit complete reactivity and solubility under the reflux conditions for digestion of NIOSH Method 7601. Quartz and cristobalite of high temperature origin have much lower reactivity than opal in this procedure for respirable sized particles.

This work presents evidence that the chemical reactivity in refluxing phosphoric acid of silica hydrate phases found in many Wyoming bentonite ores can be used to distinguish opal from cristobalite. Bentonite ores from several Wyoming locations are characterized in this x-ray diffraction survey for the presence of opal phases and other accessory minerals which may interfere with standard x-ray identification and quantification methods. Muscovite, gypsum, feldspars, clinoptilolite and calcite were found as secondary minerals associated with these commercial bentonite ores.

This work also presents evidence that the absorption correction factor described in the NIOSH Analytical Method 7500 [9] x-ray diffraction method gives erroneous high values when applied to phosphoric acid digestion residues. The absorption correction factor is designed to compensate for samples that are thicker than ideal thin films by measuring the reduction of the silver diffraction peaks of the support membrane. Very fine particles of phospho-silicate residue were observed by electron microscopy coating the membrane surface and penetrating the pores of the silver membrane, appearing to influence the

absorption correction factor for the silver, independent of the thickness of the sample film.

EXPERIMENTAL

The bentonite samples were initially characterized for complete mineralogy by bulk x-ray diffraction methods. National Institute for Science and Technology Standard Reference Materials (NIST SRM) for quartz and cristobalite were used for quantitative determination of these components. Table 1 lists the quantitative estimates for quartz and semi-quantitative estimates for a silica phase that is best described as opal-CT. Table 2 lists the principle reflections and spacings of the opal-CT associated with Wyoming bentonite.

NIOSH Analytical Method 7601

In 1984, NIOSH issued Analytical Method 7601 for "Silica, Crystalline". Samples are first digested in either nitric acid (MCE filters) or perchloric acid (PVC filters) to dissolve the membrane that collects the respirable dust. The sample is then added to 85% phosphoric acid (dehydrates to pyrophosphoric acid) and rapidly heated to 240°C for exactly 8 min, followed by cooling and dilution with deionized water prior to collection of the residual solids on a 0.47-μm filter membrane. After washing with hydrochloric acid, the residual solids are dissolved in 48% hydrofluoric acid. For low concentrations of dissolved silica, a silico–molybdate complex is formed and for high concentrations, a molybdenum blue complex is formed. Silica concentrations for both colored complexes are determined with a spectrophotometer. The detection limit for the colorimetric determination of silica is 0.02 mg.

TABLE 1

Bulk x-ray diffraction analysis of crystalline silica in Wyoming bentonite

Sample	%Quartz	%Opal-CT
Colony, Wyoming, ores		
Newcastle bed No. 1	4.4	
Blue Newcastle bed No. 3	4.4	
Yellow Newcastle bed No. 3	6.7	> 5
Blue commercial bed No. 1	2.1	~ 5
Yellow commercial bed No. 1	2.3	
Yellow commercial bed No. 2	1.1	
Blue commercial bed No. 3	3.3	~ 5
Lovell, Wyoming, ores		
Yellow commercial	0.6	< 5
Blue commercial	0.8	< 5
D bed	5.0	> 5
Canadian bed	1.8	
Upper bed	0.9	> 5
Rusty bed	3.1	?
Upton, Wyoming, ore		
? bed	0.6	> 5

TABLE 2

X-ray diffraction reflections of Opal-CT in Wyoming bentonite

Ore	Reflection		
	4.0 Å	2.8 Å	2.5 Å
Colony, Wyoming			
Yellow Newcastle No. 3	4.046	2.847	2.486
Blue commercial No. 1	4.046	2.847	2.486
Blue commercial No. 3	4.046	–	–
Lovell, Wyoming			
Yellow commercial	4.046	2.845	–
Blue commercial	4.037	2.837	–
D bed	4.046	2.845	2.486
Upper bed	4.046	2.846	2.489
Upton, Wyoming			
? bed	4.051	2.843	2.492

Phosphoric acid digestion conditions

For bulk samples of bentonite and crystalline silica standards, the dissolution of the respirable dust collection filter in strong acids was omitted from NIOSH 7601. Sample sizes of approximately 50 mg were used for digestion in order to provide adequate residue for subsequent x-ray diffraction analysis by NIOSH Method 7500 [8]. Method 7500 has a sensitivity of 0.01 mg for quartz and 0.03 mg for cristobalite.

Each sample was digested in duplicate to provide one residue for the colorimetric determination of Method 7601 and a second residue for x-ray diffraction analysis by NIOSH Method 7500. No problems were encountered with any of the samples during the digestion and filtration pro-

cess. The samples filtered rapidly, indicating that very little if any silica gel reprecipitation occurred after digestion of silicate or silica minerals.

NIOSH Method 7601 specifies that samples should not contain more than 2.5 mg of residual crystalline silica. This limitation was derived for the colorimetric analysis method and is not related to the amount of sample which can be digested in the volume of acid used for the digestion. In fact, the addition of up to 50 mg of magnesium silicate is recommended in Method 7601 to improve the silica recovery in samples that are predominantly amorphous silica.

Spectrometric determination of total insoluble silica

The spectrometric determination of residual silica was carried out with dissolution of the digestion residue and filter membrane in 5.0 ml of 48% HF and dilution to 10.00 ml with deionized silica free water. The colorimetric analyses were performed on 1.00 ml or greater aliquots of the fluoride solution. This ensured that adequate HF was present to digest the residual silica of large residues without exceeding the maximum concentration of 2.5 mg silica during subsequent analysis. The success of the colorimetric determination is dependent on maintaining an optimum pH for the molybdate complex formation. Failure to maintain the necessary pH can result in low total silica values for samples with large amounts of residual silica. The experimental values for residual silica from bentonite and crystalline silica standards are reported in Tables 3 and 4. In Table 4, these values are reported as total insoluble silica since there are significant contributions from residual silicates and other silica sources.

X-ray determination of insoluble crystalline silica

One of the duplicate digestion residues for each bentonite and control sample was analyzed for crystalline silica by the x-ray diffraction method described in NIOSH Method 7500. The filter membrane containing the digestion residue was placed in a platinum crucible and pre-ashed by ignition with about 5 ml of methanol. The crucible was then placed in a furnace at 600°C for 12 h to burn off the remaining organic material. This 12 h low temperature ashing prevents heating amorphous silica in the residue to temperatures where transformations to crystalline silica may occur. However, residual opal (silica hydrate) will dehydrate under these temperature conditions.

TABLE 3

Recovery of various silicas in NIOSH 7601

Silica	%Quartz	%Cristobalite	%Tridymite
SRM 1878 quartz	89.5 [a]		
SRM 1879 cristobalite		81.6 [a]	
NIOSH cristobalite		82.6 [a]	
DKS cristobalite		72.4 [a]	
NIOSH tridymite			45.2 [a]

[a] The reference standards are reported on a weight recovery basis; no x-ray diffraction analysis was carried out on their residues

TABLE 4

Concentration of crystalline silica in H_3PO_4 digestion residues of spiked bentonites

%Added		Crystalline silica detected		
Cristobalite	Tridymite	%Quartz	%Cristobalite	%Tridymite
Lovell blue commercial ore containing 0.8% quartz:				
2.0 [a]		0.62	2.34	
2.0 [a]		0.61	2.09	
20.0 [a]		1.27	20.6	
Upton Bentonite containing 0.6% quartz:				
2.0 [a]		1.82	3.57	
20.0 [a]		0.78	19.9	
3.8 [b]		0.45	3.3	
4.6 [c]		0.53	4.6	
	5.4 [d]	0.43		5.8

[a] NIST SRM 1879 cristobalite added. [b] NIOSH reference cristobalite added. [c] Gem Dugout cristobalite added. [d] NIOSH tridymite added. [e] The residual cristobalite determined by x-ray diffraction of NIOSH Method 7500 did not use the absorption correction factor because all of the crystalline silica was observed by electron microscopy to be on the surface of the silver membrane. The recovery weights for the residues of these samples are: 21.5% for Upton bentonite with 20% added cristobalite; and 21.6% for Lovell blue commercial bentonite with 20% added cristobalite, in agreement with the quartz and cristobalite values calculated without the correction factors.

TABLE 5

Crystalline silica in phosphoric acid digestion residues of wyoming bentonite

Sample	NIOSH method 7601	NIOSH 7500 XRD of phosphoric acid digestion residue					
	%Insoluble SiO_2	Quartz CF [a]	%Quartz with CF [a]	%Quartz without CF [a]	Crist. CF [a]	%Crist. with CF [a]	%Crist. without CF [a]
Colony, Wyoming, ores							
Newcastle No. 1	8.5	1.243	4.45	3.58	1.299		
Blue Newcastle No. 3	8.1	1.248	5.92	4.74	1.305		
Yellow Newcastle No. 3	11.8	1.229	4.35	3.54	1.281	?	?
Blue commercial No. 1	5.2	1.115	2.37	2.13	1.186	?	?
Yellow commercial No. 1	4.6	1.149	1.68	1.46	1.183		
Yellow commercial No. 1	2.8	1.065	0.84	0.79	1.079		
Blue commercial No. 3	5.5	1.223	2.36	1.93	1.274	0	0
Lovell, Wyoming, ores							
Yellow commercial	1.8	1.203	0.54	0.45	1.249	0	0
Blue commercial	2.4	1.076	0.42	0.39	1.092	0	0
D bed	8.0	1.231	6.00	4.87	1.283	?	?
Canadian bed	4.6	1.135	2.19	1.93	1.165	0	0
Upper bed	2.2	1.151	0.68	0.59	1.185	?	?
Rusty bed	6.9	1.274	5.96	4.68	1.338	0	0
Upton, Wyoming, ore							
? bed	2.6	1.145	0.45	0.39	1.178	?	

[a] CF is NIOSH Method 7500 correction factor for thicker than ideal sample films.

When the residual ash weighed less than 2.0 mg, the entire sample was deposited on a preweighed silver membrane. When the residue exceeded 2.0 mg, the residue was suspended in 100 ml of isopropanol and an aliquot weighing approximately 2 mg was deposited on the silver membrane. The silver membranes were weighed before and after deposition of residue to ensure that maximum thickness was not exceeded and for determination of total residue.

The amount of crystalline silica in each sample was determined using NIST Standard Reference Materials for calibration of this x-ray method. The quartz and cristobalite found in each sample are reported in Table 5.

RESULTS AND DISCUSSION

X-ray diffraction patterns of each Wyoming bentonite in this survey were determined and the accessory minerals were identified. Figure 1 illustrates the pattern for the D Bed bentonite located at Lovell, Wyoming. It has a complex mineralogy since it contains two silica minerals, quartz and opal-CT, and three silicate minerals, muscovite, potassium feldspar and clinoptilolite, in significant concentrations that may interfere with quantitative determination of the crystalline silica minerals by either chemical or x-ray diffraction methods.

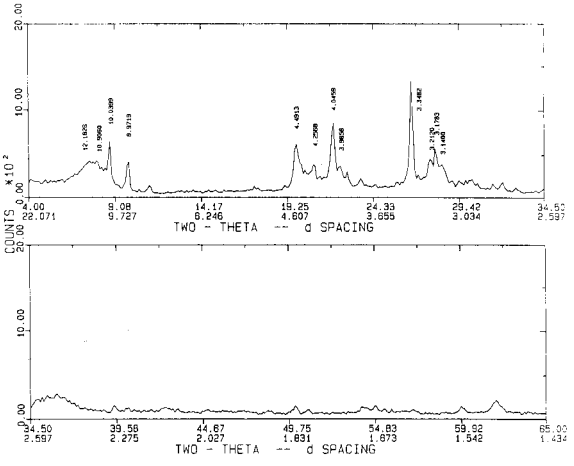

Fig. 1. D bed bentonite at Lovell, Wyoming.

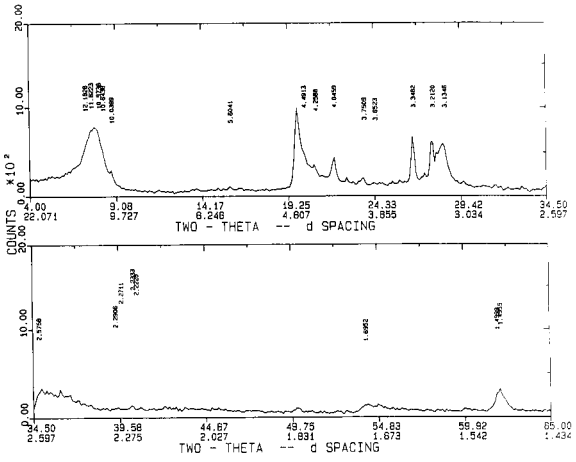

Fig. 2. No. 1 Blue commercial bed bentonite (Colony, Wyoming).

Figure 2 illustrates the x-ray diffraction pattern for No. 1 blue Commercial bentonite ore from Colony, Wyoming. It has over 90% montmorillonite content with much reduced concentrations of quartz, opal-CT, muscovite and feldspar; however, the silicate minerals also may interfere with the quantitative determination of crystalline silica minerals at these low concentrations. Several of the other bentonite ores contained gypsum and calcite in minor concentrations.

Quartz was quantitatively determined in all of the Wyoming bentonite ores by x-ray diffraction analysis of the bulk material using SRM 1878 quartz as an external calibration reference. Table 1 lists the quantitative values for quartz and semi-quantitative estimates for opal-CT. These results show a typical range for commercial bentonites from 0.6% to 6.7% quartz content and variable occurrence with opal-CT. The major quartz reflection regions were step scanned in 0.02 Å increments and counted for 5 s or more to accumulate adequate statistics for quantification.

The silica hydrates found in these bentonites are characterized by one to three reflections at 4.04 to 4.05 Å, 2.84 to 2.85 Å and approximately 2.49 Å. The reflections are somewhat sharp and easily confused with alpha cristobalite which has its three strongest reflections at 4.05, 2.84 and 2.485 Å. These reflections of opal are broader than the corresponding reflections of cristobalite. Since only three reflections are detected, the silica hydrate is best described as opal-CT and not opal-C which has an eight line x-ray diffraction pattern. Both are listed in the Powder Diffraction File as PDF-38–448 which describes opal-A, opal-CT and opal-C as silica hydrate with the chemical formula $SiO_2 \cdot xH_2O$. The literature reference given with the powder diffraction file is Jones and Segnit [2]. Table 2 lists these reflections for the bentonite ores in this survey.

A number of crystalline silica reference materials were evaluated in the phosphoric acid digestion process of NIOSH Method 7601. These were NIST SRM quartz and NIST SRM cristobalite, NIOSH cristobalite, NIOSH tridymite, and cristobalite from D.K. Smith (Gem Dugout, State College, PA). All of these reference materials are < 5 μm average particle size and have relatively large surface areas. The high surface area of these fine particles contributes to the apparent solubility of the reference standards. These crystalline silica polymorphs exhibit decreasing recovery from quartz to cristobalite to tridymite as the crystalline structure of the silica becomes less dense and apparently more subject to attack by refluxing phosphoric acid. These results are included in Table 3.

Table 4 lists crystalline silica concentrations as determined by a modification of the x-ray diffraction method described in NIOSH Method 7500 for insoluble residues of naturally occurring quartz and spiked cristobalite or tridymite that were added to two of these Wyoming bentonites. NIOSH Method 7500 was modified by omitting the correction factor designed to compensate for thicker than ideal thin films of crystalline silica or phospho-silicate residue, since calculated values using the correction factor exceeded the actual weight of the residue. Examination of residues mounted on the silver membranes revealed a very fine phospho-silicate precipitate on the surface and penetrating the silver membrane pores, attenuating the silver reflections independent of the thickness of the crystalline silica on the surface of the membrane. The composition of this residue was qualitatively determined by energy dispersive x-ray spectroscopy. In addition, the weights of the residues for additions of cristo-

balite and tridymite confirmed the values calculated without the correction factor. These results show that quartz, cristobalite and tridymite can be substantially recovered in the phosphoric acid digestion residues of Wyoming bentonite when they are added or known to be present.

Duplicate portions of each bentonite were digested in phosphoric acid by the method described in NIOSH Method 7601. This digestion did dissolve the opal-CT, muscovite, clinoptilolite, gypsum, calcite, and a portion of the feldspar accessory minerals; leaving quartz, some feldspar and occasionally a possible trace of the opal-CT.

After digestion of 50 mg samples of each bentonite in duplicate, one of the insoluble residues of each bentonite was transferred to a silver membrane and quantitatively evaluated for crystalline silica content by NIOSH Method 7500. Table 5 lists the results for quartz in these concentrated residues.

Figure 3 illustrates a partial x-ray diffraction pattern of the insoluble residue from the phosphoric acid digestion of the Upper Bed bentonite at Lovell, Wyoming. This bentonite contained the greatest initial concentration of opal of the ores in this survey. The pattern reveals the two principle reflections of quartz at 4.26 and 3.345 Å, a feldspar reflection at 3.18 Å, and a reflection at 4.05 Å which could be from either opal or feldspar or both minerals. If the latter residual silica were cristobalite, instead of opal-CT, it would be present in concentrations of 0.5%; however, the solubility of this phase is almost complete under NIOSH 7601 conditions as opposed to high temperature SRM 1979 cristobalite which has a solubility of approximately 20%. Because of this difference in solubility between opal and cristobalite, the silica phase has been reported as opal-CT. Also present in this pattern is a strong reflection from the silver membrane used in mounting the residue for analysis by NIOSH Method 7500.

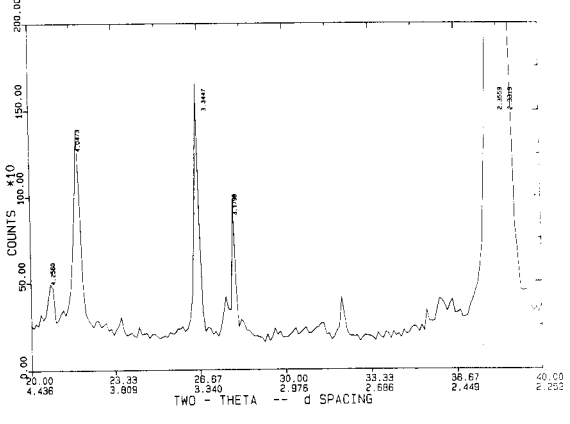

Fig. 3. Phosphoric acid insoluble residue upper bed bentonite (Lovell, Wyoming).

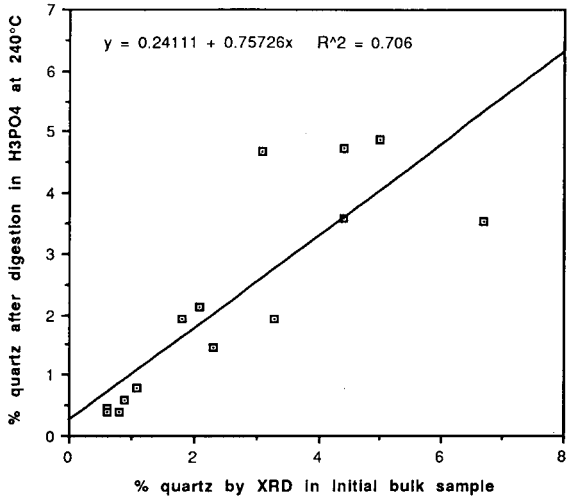

Fig. 4. Quartz concentration by XRD analysis before and after H_3PO_4 digestion.

Figure 4 shows the correlation of the quartz concentration determined in bulk samples by general x-ray diffraction methods with the %quartz found in the phosphoric acid digestion residue and evaluated by NIOSH Method 7500 without use of the correction factor. It shows some scatter, but the two sets of data are in close agreement. The best fit of data can be described by the formula $y = 0.75726x + 0.24111$ with a confidence level of $R^2 = 0.707$ where y is %quartz calculated for the original bulk sample from XRD analysis of the phosphoric acid digestion residue and x is %quartz directly determined in the bulk sample by XRD analysis.

This clearly demonstrates that quartz in bulk samples of bentonite with relatively coarse particle sizing and corresponding low surface area as found in the native ore survives the phosphoric acid digestion process with no measurable loss

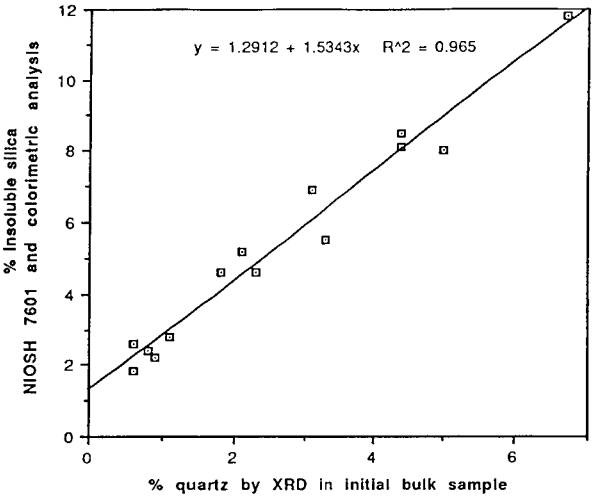

Fig. 5. Insoluble silica concentration after phosphoric acid digestion compared to %quartz in the initial bulk sample.

due to dissolution. Extrapolation of Talvitie's [5] recovery data for pure quartz suggests the first measurable losses occur with digestion times in excess of 10 min; therefore the NIOSH digestion time of 8 min is not expected to result in significant losses from coarse quartz particles of relatively low surface area.

The second digestion residue for each bentonite sample was dissolved in hydrofluoric acid, reacted with molybdate to form colored complexes, followed by spectrometric determination of total residual silica, according to NIOSH Method 7601. When compared with the results of the x-ray analyses of bulk samples and of the digestion residues (which are essentially the same), the total residual silica values for each sample are significantly higher than the expected concentration for crystalline silica. These increased values include contributions from incompletely dissolved feldspars, amorphous silica, or a trace of opal in some samples. Figure 5 gives the correlation of the total insoluble silica vs. quartz concentration by bulk x-ray diffraction analysis. The best fit of data is described by the equation $y = 1.5343x + 1.2912$ with a confidence level of $R^2 = 0.965$ where y is the %concentration of total insoluble silica by colorimetric analysis and x is %quartz in the initial bulk samples by XRD measurement. This relatively high confidence level correlation with Wyoming bentonites of various beds and locations indicates that the mineralogy of the silica and silicate accessory minerals are uniform with this type of bentonite and that they react with similar reaction rates in NIOSH Method 7601.

Figure 4 demonstrates that the total insoluble silica as determined by the colorimetric method includes other incompletely dissolved silicate or amorphous silica minerals in addition to the expected crystalline silicas. These other silica sources contribute significant positive interferences to the measured crystalline silica content if corrections are not made.

Conclusions

When applying NIOSH Method 7601 to the analysis of respirable dust and bulk samples, a detailed understanding of the mineralogy of the sample is critical for interpretation of results. There are a number of silica and silicate minerals that are incompletely dissolved in the phosphoric acid digestion process of this procedure. These minerals will contribute positive interferences to this crystalline silica analysis unless they are discovered and appropriate corrections are made. In this evaluation of Wyoming bentonite ores, NIOSH Method 7601 with its colorimetric analysis of insoluble residual silica consistently reported high values due to incompletely dissolved silicate and/or silica minerals, when compared to bulk XRD analysis prior to digestion.

NIOSH Method 7601 can be effectively used as a concentration method for subsequent crystalline silica analysis by another technique such as x-ray diffraction analysis. It dissolves and removes many silicate minerals that could contribute positive interferences to XRD analytical procedures; however, it may leave residues of these silica and silicate minerals that must be corrected for in the analytical procedure. The concentration of crystalline silica in the insoluble residue effectively increases the sensitivity of XRD and other techniques.

The phosphoric acid digestion of NIOSH Method 7601 provides a chemical method of distinguishing opal from high temperature cristo-

balite. Opal is much more reactive with refluxing phosphoric acid than cristobalite of high temperature synthesis. They are completely dissolved and removed while cristobalite shows minor solubility under NIOSH Method 7601 conditions. Therefore, the enhanced chemical reactivity of opal with refluxing phosphoric acid provides a means of distinguishing opal phases from cristobalite. This appears to be a more reliable method than a subjective judgment based on the similarities of x-ray diffraction patterns of these two minerals. Alzea et al. [10] have developed other x-ray methods to distinguish opal from cristobalite, supporting the conclusions of this work.

Based on the chemical reactivity of the silica phase present in a number of Wyoming bentonites and the XRD patterns for these phases, the silica phase should be classified as opal-CT and not cristobalite.

REFERENCES

1 P.T. Flynn, A.T. Rosol and S.D. Kinsala, Environmental Management for the 1990's, Society of Mining, Metallurgy and Engineering, Denver, CO, 1991, pp. 367–371.
2 J.B. Jones and E.R. Segnit, J. Geol. Soc., 18 (1971) 57–68.
3 P.M. Miller (Ed.), NIOSH Method 7601: Silica, Crystalline, Manual of Analytical Methods, DHHS Publication 84–100, 3rd edn., 1984.
4 N.A. Talvitie, Anal. Chem., 23 (1951) 623–626.
5 N.A. Talvitie and F. Hyslop, Am. Ind. Hyg. Assoc. J., 19 (1958) 54–58.
6 N.A. Talvitie, Am Ind. Hyg. Assoc. J., 25 (1964) 169–178.
7 D.V. Sweet, F.R. Wolowicz and J.V. Crable, Am. Ind. Hyg. Assoc. J., 34 (1973) 500–506.
8 W.J. Miles and R.D. Hamilton, Am. Ind. Hyg. Assoc. J., (1993) in press.
9 P.M. Miller (Ed.), NIOSH Method 7500: Measurement of Respirable Crystalline Silica Using X-ray Diffraction, Manual of Analytical Methods, DHHS Publication 84–100, 3rd edn., 1984.
10 J.M. Elzea, I.E. Odom and W.J. Miles, Anal. Chim. Acta, 286 (1994) 107.

Analytica Chimica Acta, 286 (1994) 107–116
Elsevier Science B.V., Amsterdam

Distinguishing well ordered opal-CT and opal-C from high temperature cristobalite by x-ray diffraction

J.M. Elzea

McCrone Associates, 850 Pasquinelli Drive, Westmont, IL 60559 (USA)

I.E. Odom

American Colloid Co., One Arlington, 1500 Shure Drive, Arlington Heights, IL 60004 (USA)

W.J. Miles

Bentonite Corp., 1999 Broadway, 43rd Floor, Denver, CO 80202 (USA)

(Received 28th July 1993)

Abstract

A critical step in quantifying the amount of crystalline silica in mineral deposits is the accurate identification of all mineral constituents. It is particularly important to correctly identify the low-temperature opaline silica polymorphs opal-C and opal-CT which, depending on degree of ordering, can be mistaken for α-cristobalite in standard x-ray diffraction patterns. Misidentification occurs because there is limited x-ray diffraction data available from the literature and because these minerals have diffraction maxima that coincide with those of high temperature cristobalite. X-ray diffraction patterns of opal have been collected in 20 bentonite, fuller's earth, and diatomaceous earth deposits to illustrate the range in ordering that naturally occurs in these polymorphs. Two opaline silica polymorphs are commonly observed. Opal-C is characterized by sharp, intense (101) reflections centered near 4.0 Å with peak widths ranging from 0.222 to 0.453 Å and opal-CT is characterized by broader, less intense (101) reflections centered near 4.07 to 4.10 Å with peak widths ranging from 0.506 to 0.883 Å. Opal-A was observed in one sample. Opal-A is easily distinguished from the other opaline silica polymorphs and from α-cristobalite using x-ray diffraction. Opal-C and opal-CT, however, are not as readily distinguished from α-cristobalite. The position and width of the (101) peak can be used to distinguish these polymorphs from one another or a simple heating test can be used. Because opaline silica is hydrated, the position of the (101) reflection shifts and sharpens as a result of heating. When α-cristobalite is heated no change in peak position is observed. It has also been found that opaline silica, when reacted with phosphoric acid, potassium pyrosulfate, and sodium sulfide solutions, is considerably more chemically reactive than the crystalline silica minerals. Based on results of the heating test and the position and width of the 4 Å peak of the unheated sample, none of the 20 bentonite, fuller's earths, or diatomaceous earth deposits analyzed contain high temperature α-cristobalite.

Keywords: X-ray diffraction; Cristobalite; Crystalline silica; Opal-CT; Opal-C

In 1987, the International Agency for Research on Cancer (IARC) declared crystalline silica a probable human carcinogen. This classification triggered OSHA's Hazard Communication Standard which requires that any material containing $> 0.1\%$ crystalline silica be appropriately labelled. Minerals that are specifically regulated include quartz, cristobalite, and tridymite. In addition to these polymorphs, there are other forms

Correspondence to: J.M. Elzea: Thiele Kaolin Co., P.O. Box 1056, Sandersville, GA 31082-1056 (USA).

SSDI 0003-2670(93)E0471-I

TABLE 1
Hydrous and non-hydrous forms of SiO_2

Polymorph	Crystallinity
α-Quartz (low T°)	SiO_2
β-Quartz (high T°)	SiO_2
α-Cristobalite (low T°)	SiO_2
β-Cristobalite(high T°)	SiO_2
α-Tridymite (low T°)	SiO_2
β-Tridymite (high T°)	SiO_2
Coesite	SiO_2
Stishovite	SiO_2
Melanophlogite	SiO_2
Keatite	SiO_2
Silica glass	$SiO_2 \cdot H_2O$
Opal-A	$SiO_2 \cdot H_2O$
Opal-CT	$SiO_2 \cdot H_2O$
Opal-C	$SiO_2 \cdot H_2O$

of silicon dioxide including several hydrated forms (Table 1).

The most common naturally occurring hydrated silica polymorphs are the opaline silicas, which have a composition given by the formula $SiO_2 \cdot nH_2O$. These minerals are found in economically important deposits such as bentonite, fuller's earth, flint kaolin and diatomaceous earth. Deposits containing these secondary silica minerals are found in the United States, Japan, Canada, Indonesia, Italy, Spain, Greece, Yugoslavia, Czechoslovakia, Australia and Turkey [1]. In the United States opaline silica-bearing bentonites are located in Alaska [2], Texas [3], Georgia [1], Alabama [4], Idaho, Utah, Nevada and Wyoming [5]. These minerals, which are considered noncrystalline from a regulatory point of view, have been and are confused with high temperature cristobalite.

The confusion between opaline silicas and α-cristobalite is based on several factors. One is that the term "cristobalite" is often interchangeably used with "opal-CT", "opal-cristobalite", "opaline silica" and various other names. This ambiguous terminology is commonly found in older publications [e.g., 2,6–8] and less often in more recent literature [e.g., 9–11]. The other factor that has contributed to this confusion is the similarity between the x-ray diffraction patterns of well-ordered low temperature opal-CT and opal-C and high temperature α-cristobalite (Fig. 1).

Cristobalite is generally considered a high temperature phase and is often associated with volcanic rocks. The opal minerals, with perhaps the exception of opal-C, form at low temperatures, usually below 100°C. These minerals may form under a number of different geologic conditions. For example opal-A may be precipitated by marine organisms as skeletal material or it may precipitate from silica saturated solutions formed as a result of water interacting with silica-rich rocks such as volcanic ash or tuff. This genetic association explains why opal-CT and opal-C commonly occur in bentonite deposits which form by the alteration of volcanic ash. Opal-A converts to opal-CT during diagenesis.

The common association of secondary opal-CT and opal-C with bentonite has led to the interpretation that these minerals form simultaneously with smectite during ash alteration [12]. However, Henderson et al. [6] demonstrated that authigenic opal-cristobalite (opal-CT) in the Helms bentonite did not precipitate with smectite, but formed much later and in contact with meteoric water. Other investigators have proposed that, in some cases, cristobalite was a component of the original ash and is therefore a high temperature phase that has no genetic relationship to the smectite [13]. Mount St. Helens ash, for instance, contained up to 2 weight percent α-cristobalite [14].

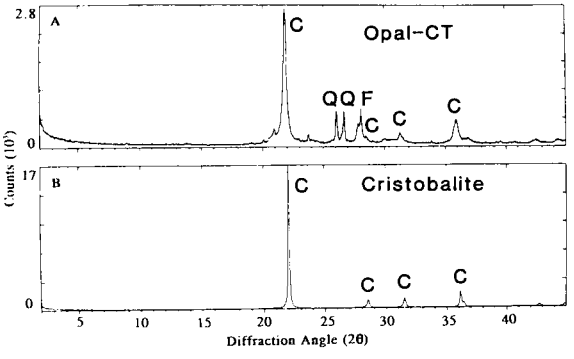

Fig. 1. X-ray diffraction patterns of opal-CT (top) and α-cristobalite (bottom). Peaks marked with the letter "C" are cristobalite peaks. Those marked with "Q" are quartz peaks (α and β) and those marked with "F" are feldspar peaks.

This paper attempts to eliminate the confusion surrounding these minerals by characterizing the low temperature hydrated silica polymorphs commonly found in commercial grade clay deposits and describing a simple test for distinguishing well-ordered opaline silica from α-cristobalite.

CLASSIFICATION OF LOW-TEMPERATURE SILICA POLYMORPHS

A large number of experimental, theoretical and descriptive studies of low-temperature silica phases are described in the literature. A review of this literature indicates that the classification of hydrous silica proposed by Jones and Segnit [15] is currently widely accepted by the geologic community. They propose a three-fold classification based on atomic structure. X-ray diffraction, infrared spectroscopy and differential thermal analyses data all support this classification scheme. According to this classification, the naturally occurring hydrous silica polymorphs are grouped as opal-A, opal-CT, and opal-C.

Opal-A is a highly disordered near amorphous polymorph and includes precious opal, all biogenically precipitated opal and geyserities. When analyzed by x-ray diffraction it produces a single diffuse band centered at approximately 4.1 Å (Fig. 2). Biogenic opal-A may occur as radiolarian tests, diatom frustules, or sponge spicules. Inorganically precipitated opal-A forms when a solution becomes saturated with respect to silica causing silicic acid polymers to precipitate. These polymers then grow by Ostwald ripening to form colloidal sols and gels [16,17].

Opal-CT is interpreted as disordered microcrystallites of α-cristobalite in a matrix of amorphous silica. These crystallites exhibit varying degrees of stacking disorder, which may lead to the appearance of x-ray maxima that coincide with those of α-tridymite [18]. Opal-CT has an XRD pattern characterized by two broad reflections in the 4.05 to 4.10 Å and 2.50 Å regions and a single small reflection at 4.25 to 4.35 Å (Fig. 2). Opal-CT typically occurs as lepispheres composed of bladed crystals. Fibrous crystals of opal-CT have also been observed [19]. Opal-CT exhibits a range of

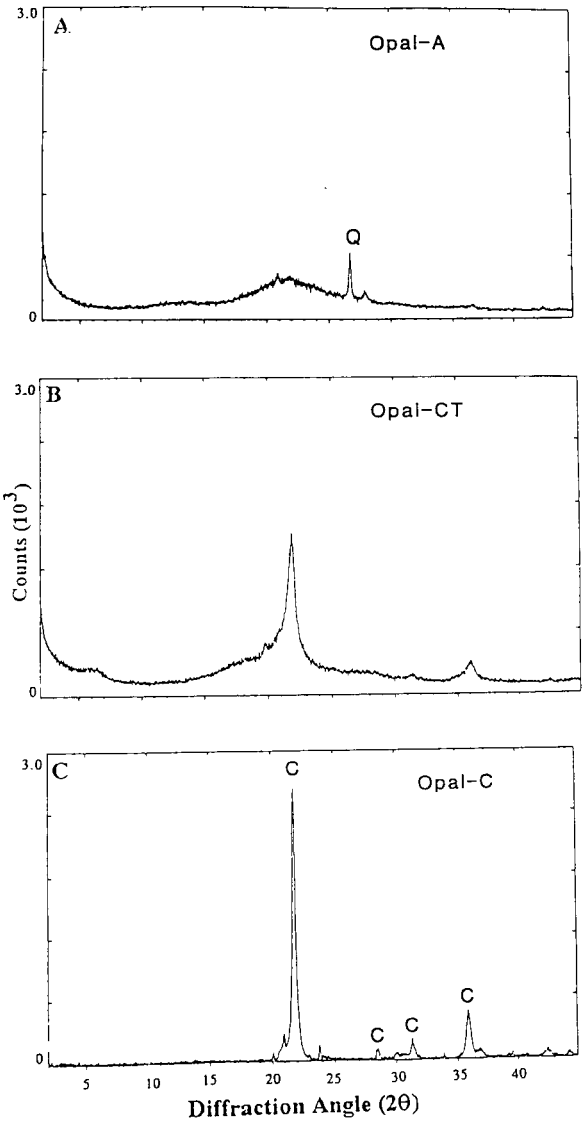

Fig. 2. X-ray diffraction patterns of opal-A, opal-CT and opal-C.

ordering that is most clearly documented in sediments, such as the Monterey Formation, that have undergone burial diagenesis. It has been observed in these and other sediments that opal-CT becomes better ordered during diagenesis [20]. This increased ordering manifests itself as sharper more intense x-ray diffraction maxima

that are often slightly shifted in position relative to the unaltered silica.

It has been suggested that opal-CT may be reinterpreted as disordered α-tridymite [21]; however, this reinterpretation does not appear to have been widely accepted. Only one report of disordered low tridymite, identified in diatomaceous sediments from Japan where it was precipitated as lepispheres from percolating groundwater, was found in the literature [22].

Recently, de Jong et al. [23] have challenged the idea that opal-CT is a mixture of cristobalite–tridymite microcrystallites in an amorphous silica matrix. In their study the structures of both opal-CT and opal-A were re-examined using XRD and ^{29}Si MAS NMR. Conclusions drawn from these data suggest that opal-CT is not comprised of cristobalite-tridymite microcrystallites but instead exhibits long-range ordering of oxygen atoms followed by short-range ordering of silicon atoms. Opal-CT has a ^{29}Si MAS NMR spectrum much more like that of amorphous silica than that of cristobalite or tridymite.

Opal-C closely resembles cristobalite and is recognized by major reflections occurring as sharp, symmetrical peaks centered at 4.04, 3.13, 2.84, and 2.47 Å (Fig. 2). Opals associated with lava flows and other high temperature environments commonly occur as opal-C. However, reports of authigenic well-ordered opal-C [22,24], suggest that high temperatures may not be required for the formation of this phase. Although, this mineral is structurally similar to α-cristobalite it is not true α-cristobalite. This conclusion is based on the fact that the x-ray diffraction pattern of opal-C may show minor tridymite peaks, and when heated does not convert to β-cristobalite [25].

Alpha-cristobalite is metastable under 268°C and persists at lower temperature due to strong Si–O bonds [15]. Structurally, cristobalite is built of layers consisting of 6-membered rings of silicon and oxygen tetrahedra that are vertically stacked. These layers are linked by the vertices of tetrahedra that alternately point up and down. This ring structure is a low energy structure and, therefore, promotes the metastable precipitation of cristobalite over other crystalline silica polymorphs [26].

CHARACTERIZATION OF LOW-TEMPERATURE HYDROUS SILICA POLYMORPHS

Sample materials and methods

Twenty samples of commercially mined minerals that commonly contain opaline silica were examined by a number of analytical techniques including optical microscopy, scanning electron microscopy (SEM), transmission electron microscopy (TEM) and x-ray diffraction.

Results

From these data two opaline silica polymorphs were recognized based on chemistry, particle size, particle shape and structure (Table 2). These polymorphs are distinguished from one another primarily on the basis of x-ray diffraction data including peak position, intensity and width (Table 3 and Fig. 3) and correspond to opal-C and opal-CT as described by Jones and Segnit [15]. Only one sample contained opal-A.

In these samples the (101) peak of opal-C occurs at lower d-spacings and tends to have narrower peaks than opal-CT (Fig. 4). Opal-C is characterized by a relatively sharp intense 4 Å peak with a d-spacing close to 4.04 Å. Opal-CT exhibits a range of x-ray diffraction peak intensities and positions (Fig. 4) and appears to be less ordered. In general, the position of the most intense peak of this phase varies from 4.07 to 4.09 Å. It is interesting to note that the degree of ordering in these polymorphs, as measured by dividing the peak width at half height by peak position (FWHM/d (101) Å), appears to increase with age of the deposit (Fig. 5).

TABLE 2

Distinguishing characteristics of two opaline silica polymorphs

Polymorph 1	Polymorph 2
Sharp, intense (101) reflection ≈ 4.04 Å	Broad, less intense (101) reflection ≈ 4.07 to 4.10 Å
Large crystallites along edges of clay grains	Smaller crystallites, large agglomerates and lepispheres
Si + trace amounts of Al and Fe	Si only
Opal-C	Opal-CT

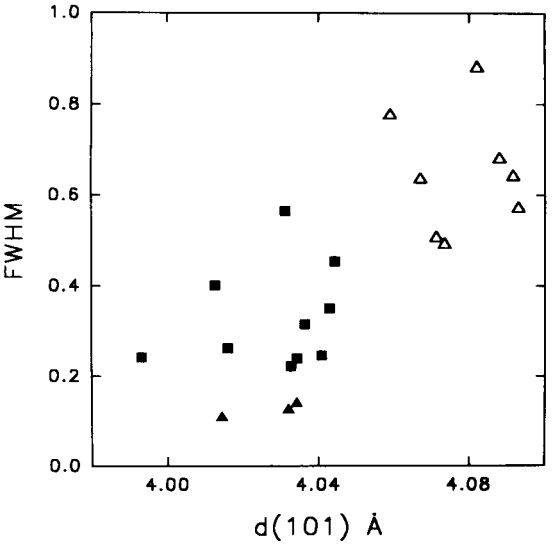

Fig. 3. Plot of peak width at half height (FWHM) vs position of the 4 Å peak (d(101)) for the two opaline silica polymorphs.

Scanning and electron microscopy reveals some other differences between these polymorphs. Opal-C tends to form large crystallites that aggre-

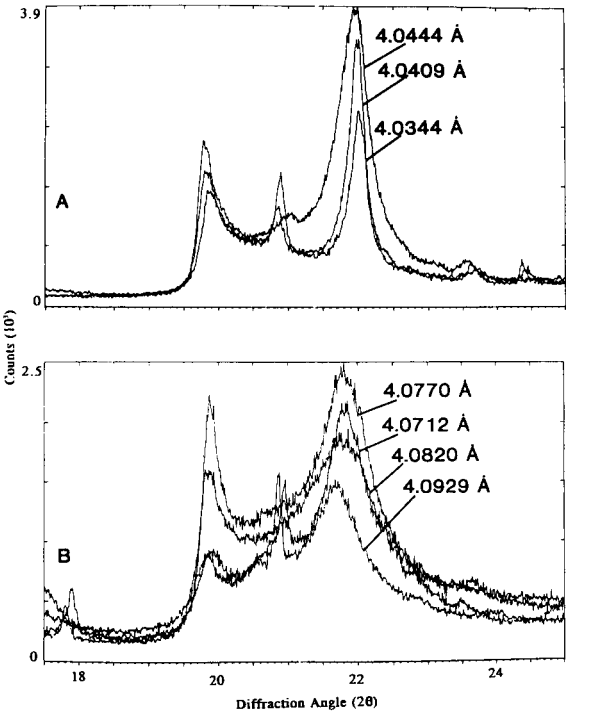

Fig. 4. X-ray diffraction patterns of opal-C (A) and opal-CT (B).

TABLE 3

Summary of x-ray diffraction data for opaline silica polymorphs

Name/location	Rock type	d(101)Å	FWHM	Heated d(101)Å	Heated FWHM	Polymorph
Australia	Bentonite	4.0344	0.239	4.0781	0.248	opal-C
Nevada	Bentonite	4.0444	0.453	4.0921	0.244	opal-C
Commercial Bed, WY	Bentonite	4.0409	0.246	4.0761	0.193	opal-C
Lower Mowry, WY	Bentonite	4.0127	0.401	–	–	opal-C
Yellow CB, WY	Bentonite	4.0328	0.222	4.0766	0.202	opal-C
Blue CB, WY	Bentonite	4.0161	0.262	4.0818	0.283	opal-C
Yellow New Castle, WY	Bentonite	4.0365	0.315	4.0628	0.352	opal-C
Upper Bed, Lovell, WY	Bentonite	4.0430	0.350	4.0713	0.362	opal-C
D-Bed, Lovell, WY	Bentonite	3.9932	0.242	4.0834	0.242	opal-C
Utah	Fuller's Earth	4.0313	0.564	4.0737	0.3135	opal-C
Flux Calcined Diatomite	DE	4.0734	0.491	4.05286	0.305	opal-CT
Texas	Bentonite	4.0770	0.681	4.0837	0.349	opal-CT
Chalk Hills Fm, ID	Bentonite	4.0590	0.776	4.0927	0.222	opal-CT
Turkey	Bentonite	4.0820	0.883	4.0497	0.215	opal-CT
Mozambique	Bentonite	4.0670	0.636	4.0904	0.447	opal-CT
Porters Creek	Fuller's Earth	4.0929	0.571	4.1007	0.402	opal-CT
Mississippi	Fuller's Earth	4.0712	0.506	4.0761	0.343	opal-CT
Monterey	DE	4.0915	0.642	4.0769	0.390	opal-CT

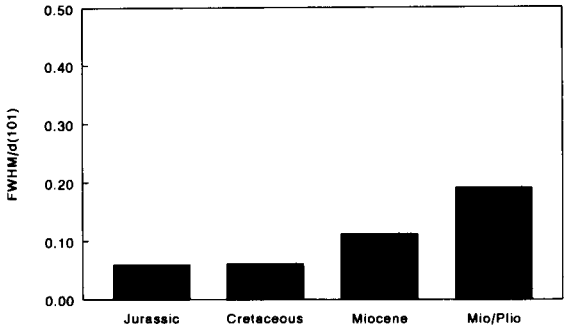

Fig. 5. Bar graph showing the relationship between peak width and age. Younger deposits contain less ordered opaline silica compared to older deposits.

gate along the edges of clay flakes (Fig. 6). Opal-CT is characterized by small crystallites that commonly form lepispheres and agglomerates (Fig. 7).

DISTINGUISHING WELL-ORDERED OPALINE SILICA FROM α-CRISTOBALITE

X-Ray diffraction

Although the x-ray diffraction pattern of cristobalite is distinct from that of opal-A and poorly ordered opal-CT, it can be confused with that of well-ordered opal-CT and opal-C particularly if only the 4 Å peak is examined. This is because these minerals have diffraction maxima that are almost identical to those of α-cristobalite. Despite these shortcomings, x-ray diffraction is the best method for routinely distinguishing between these minerals.

Because peak position cannot be used as a diagnostic tool to distinguish α-cristobalite from the opal minerals, peak shape must be considered as an alternative means for identification. Typi-

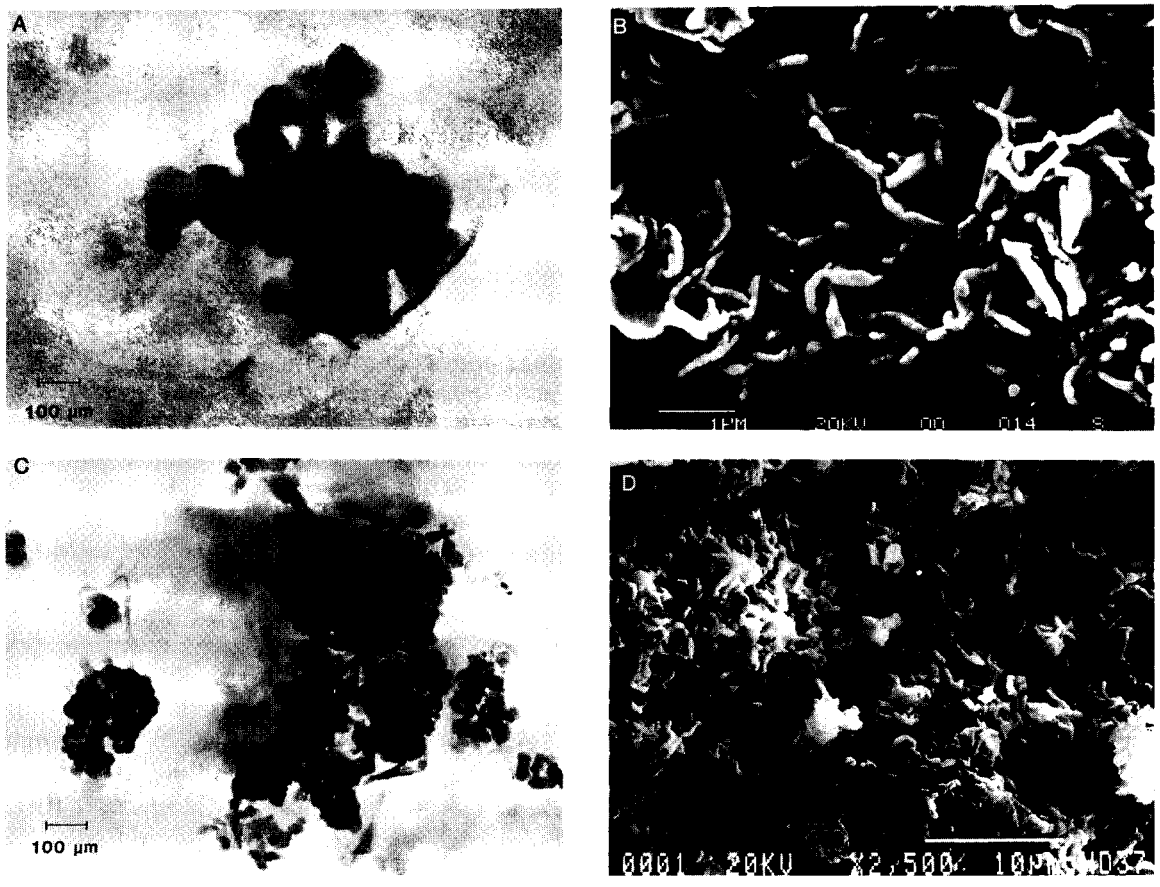

Fig. 6. TEM (a and c) and SEM (b and d) images of opal-C.

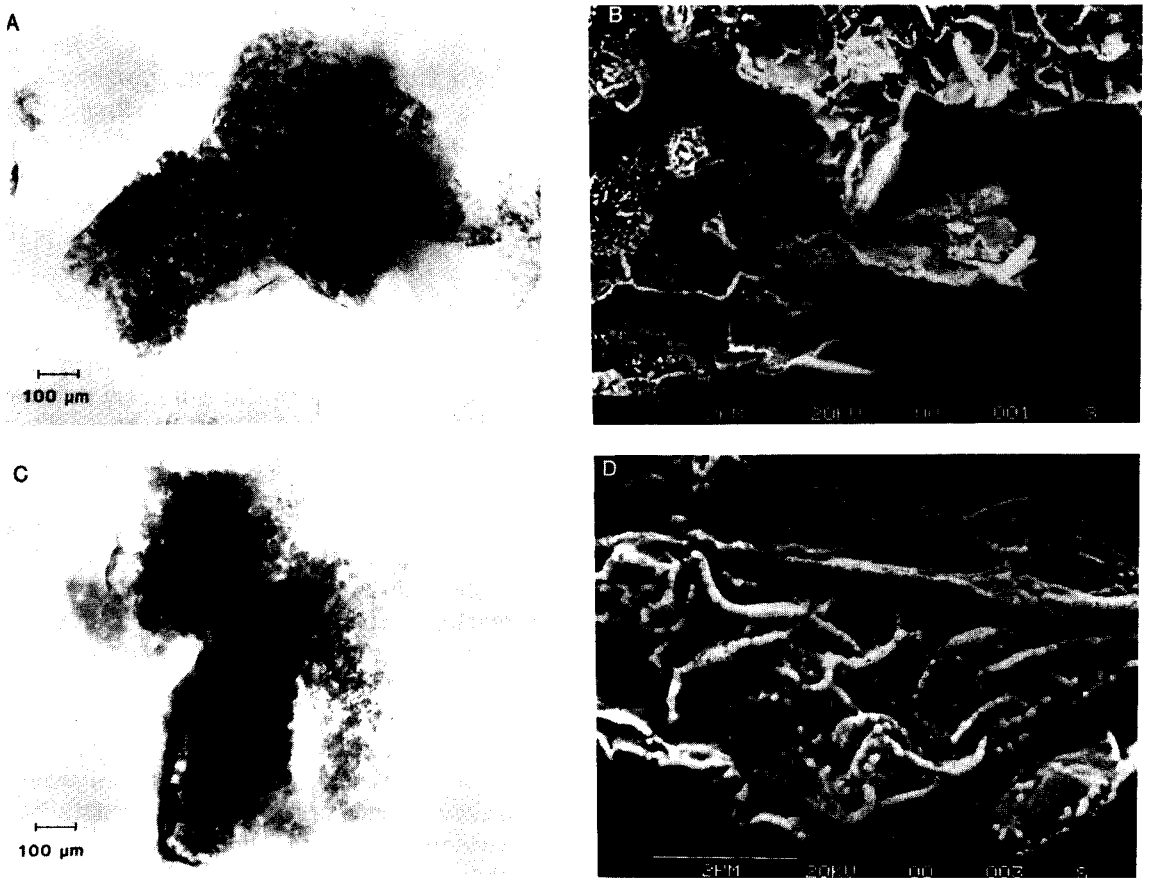

Fig. 7. TEM (a and c) and SEM (b and d) images of opal-CT.

cally opal minerals exhibit line broadening due to their very small crystallite size. An examination of three cristobalite standards indicates that cristobalite does not exhibit line broadening (Table 4). Therefore, a quick check of the peak width at half height (FWHM) has the potential for indicating whether opal or cristobalite is present.

TABLE 4

Peak width at half height (FWHM) for opal-A, opal-CT, opal-C, and cristobalite

FWHM	Opal-A	Opal-CT	Opal-C	Cristobalite
Minimum	3.492	0.506	0.222	0.109
Maximum	3.492	0.883	0.453	0.140
Mean	3.492	0.671	0.306	0.125
n	1	8	10	3

Another way to distinguish the opaline silica minerals from cristobalite is to x-ray the sample before and after heating. Approximately 2 g of powdered clay were heated for 24 h at 1050°C in a platinum crucible. The sample was then x-rayed from 17.5 to 25.0° 2θ and the results were compared to those obtained for the unheated sample. For both opal-CT and opal-C an increase in

TABLE 5

X-Ray diffraction data for α-cristobalite

Standard	d(101) Å	FWHM	Heated d(101) Å	Heated FWHM
NIOSH CB-25	4.0321	0.126	4.0320	0.126
NBS SRM 1879	4.0145	0.109	4.0279	0.109
D. Smith	4.0343	0.140	4.0341	0.140

intensity of approximately 10 000 counts per second and as much as a 0.09 Å shift in the position of the (101) peak (Fig. 8) were observed. This shift may be attributed to dehydration and/or an increase in ordering. The change in peak shape and intensity is probably due to recrystallization accompanied by an increase in crystallite size. By contrast, the diffraction pattern of high temperature α-cristobalite does not change with heating (Table 4, Fig. 9). This test, therefore, provides a relatively simple way to differentiate the hydrated opaline silica minerals from the crystalline silica minerals.

Chemical reactivity

Opaline silica differs from the anhydrous crystalline silicas not only in chemical composition but also in chemical reactivity. Amorphous and opal silica are much more reactive than crystalline silica with refluxing phosphoric acid, potassium pyrosulfate fluxes, and refluxing sodium sulfide solutions. The crystalline forms of silica, quartz, cristobalite, and tridymite, are relatively inert to these chemical reagents.

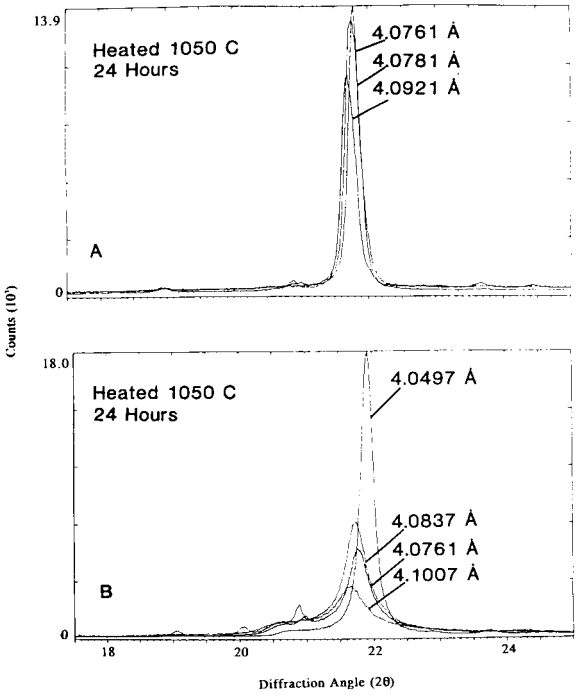

Fig. 8. Patterns obtained after heating opal-C (A) for 24 h and opal-CT (B) for 24 h.

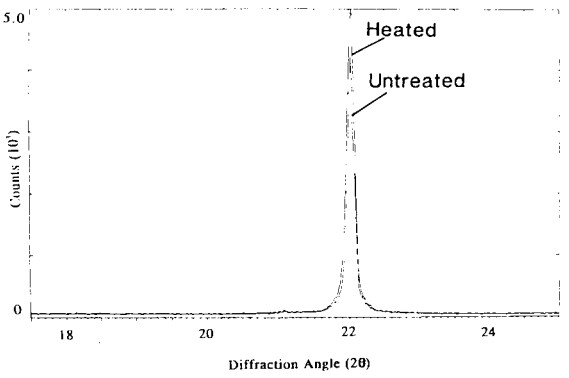

Fig. 9. X-ray diffraction pattern of heated and untreated α-cristobalite.

The phosphoric acid digestion of silicates was first developed to remove reactive silicates and amorphous silicas and to concentrate the residual crystalline silica for further analysis [e.g., 27]. Talvite dissolved the residue from phosphoric acid in hydrofluoric acid. A molybdate–silica complex formed as a result of this treatment for calorimetric determination. This procedure was later developed and published as NIOSH Method 7601 "Silica, Crystalline [28]."

The NIOSH method suffers in that there are a number of partially or completely insoluble silicate minerals that create positive interferences and errors unless the mineralogy is completely identified and appropriate corrections are made. Amorphous silica of volcanic origin or inorganic origin, such as perlite and obsidian, are particularly slow to react with the refluxing phosphoric acid. Miles and Hamilton [30] have shown that phosphoric acid digestion can be used as a concentration technique for crystalline silica, followed by subsequent x-ray diffraction analysis for the quantitative determination of crystalline silicas. The opal silicas, including opal-C and opal-CT, exhibit almost complete reactivity and solubility in refluxing phosphoric acid under the conditions specified in NIOSH analytical Method 7601, while quartz and cristobalite of high temperature origin exhibit slight solubilities of approximately 10% for respirable sized particles.

In other unpublished work, Miles has concentrated opal-CT from a Mozambique bentonite and removed clay components from opal-CT in the Monterey formation of California. He has confirmed that the silica is hydrated opal by determining loss on ignition and index of refraction. Both silica concentrates give x-ray patterns that are consistent with opal-CT.

Other methods

Other methods that can be used to differentiate these minerals include differential thermal analysis [15], infrared spectroscopy [29] and under some circumstances, light microscopy. In general, light microscopy is not possible to use because these minerals often have particle sizes of less than 0.5 Å. If individual particles are large enough for optical examination then refractive index measurements can be used to identify cristobalite, which has a higher refractive index than opal.

Conclusions

Twenty samples of bentonite, fuller's earth and diatomaceous earth were examined by x-ray diffraction, TEM and SEM to characterize the opaline silica phase(s) in these deposits. One purpose of this characterization was to determine whether or not α-cristobalite occurs in these deposits. Numerous references to the presence of cristobalite in bentonite, for instance, can be found in a number of publications. A careful examination of the mineral that has often been referred to as "cristobalite" indicates that it is actually opaline silica. Part of the reason that this mineral has been misidentified as cristobalite is because of the similarity between the diffraction patterns of some opals and cristobalite. Because x-ray diffraction is the most commonly used method for quantifying crystalline silica, it is critical that anyone analyzing a bentonite, or any other deposit of low temperature origin, for crystalline silica be aware of the fact that opaline silica, which forms and is stable at low temperatures, is more likely to occur in these deposits than is α-cristobalite which is a high temperature phase.

In many cases opaline silica is relatively easy to distinguish from α-cristobalite, especially if it is poorly ordered. There are, however, many examples of deposits containing well-ordered opaline silica that can be mistaken for α-cristobalite based on x-ray diffraction patterns. The simple heating test described in this paper will quickly reveal whether the mineral in question is opaline silica or cristobalite. It is recommended that this heating test be performed on all bentonite, fuller's earth and diatomaceous earth samples whenever there is a question concerning the identification of the silica minerals.

Thus far, no true α-cristobalite has been identified in any of the bentonite and fuller's earth deposits examined for this study. Samples used in this investigation were collected from deposits from around the world. These deposits range in age from Jurassic to Miocene, represent a range of compositions, and were formed under a variety of geologic environments.

REFERENCES

1 R.E. Grim and N. Güven, Bentonites, Geology, Mineralogy, Properties and Uses, Developments in Sedimentology 24, Elsevier, Amsterdam, 1978, p. 256.
2 R.C. Reynolds Jr. and D.M. Anderson, J. Sed. Pet., 37 (1967) 966.
3 P.-Y. Chen, Geology and Mineralogy of the White Bentonite Beds of Gonzales County, Texas, Ph.D. Thesis, University of Texas, Austin (1968).
4 W.R. Reynolds, Formation of Cristobalite, Zeolite and Clay Minerals in the Paleoecene and Lower Eocene of Alabama, Ph.D. Thesis, Florida State University, Tallahassee (1966).
5 M. Slaughter and J.W. Earley, Wyoming. Geol. Soc. Amer. Special Paper Number 83 (1965).
6 J.H. Henderson, M.L. Jackson, J.K. Syers, R.N. Clayton and R.W. Rex, Clays Clay Miner., 19 (1971) 229.
7 K.G. Papke, Clays Clay Miner., 16 (1969) 221.
8 G.W. Brindley, Clay Min. Bull., 3 (1957) 167.
9 G.K. Moncure, R.C. Surdan, H. McKague and H. Lawrence, Clays Clay Miner., 29 (1981) 385.
10 J.R. Carter, M.T. Hatcher and L. DiCarlo, Anal. Chem., 59 (1987) 513.
11 B. Velde and A. Iijima, Clays Clay Miner., 36 (1988) 4.
12 R.E Grim, Clay Mineralogy, McGraw-Hill, New York, 1953.
13 J.W. Gruner, Am. Mineralogist, 25 (1940) 587.
14 B.L. Davis, R.L. Johnson, D.T. Griffen, W.R. Phillips, R.K. Stevens and D.Maugham, J. Appl. Meteorol., 20 (1981) 8.

15 J.B. Jones and E.R. Segnit, J. Geol. Soc. Aust., 18 (1971) 57.
16 R.K. Iler, The Colloid Chemistry of Silica and Silicates, Cornell University Press, Ithaca, New York, 1955, p. 324.
17 D.A. Crerar, E.V. Axtemann and R.C. Axtemann, Geochim. Cosmochim. Acta, 45 (1981) 1259.
18 O.W. Flörke, Neues Jahr B. Mineral. Montash., (1955) 217.
19 L.S. Land, J. Sed. Pet., 49 (1979) 223.
20 L.A. Williams and D.A. Crerar, J. Sed. Pet., 55 (1985) 3.
21 M.J Wilson, J.D Russel and J.M. Tait, Contrib. Mineral. Petrol., 47 (1974) 1.
22 A. Iijima and R. Tada, Sedimentology, 28 (1981) 185.
23 B.H.W.S. de Jong, J.Van Huek, W.S.Veeman and D.V. Manson, Am. Mineral., 72 (1987) 1195.
24 A. Iijima, R. Matsumoto and R. Tada, Initial Reports of the Deep-Sea Drilling Project, Vol. LVI, LVII, Part 2, 1980, pp. 1143–1158.
25 E.C. Dapples, in G. Larsen and G.V. Chillingar (Eds.), Diagensis in Sediments and Sedimentary Rocks, Elsevier, Amsterdam, 1979, pp. 99–142.
26 T. Zoltai and M.J. Buerger, Z. Kristallogr., 114 (1960) 1.
27 N.A. Talvite, Anal. Chem., 23 (1951) 623.
28 P.M. Miller (Ed.), NIOSH Method 7601, Silica, Crystalline, Manual of Analytical Methods, 3rd edn., DHHS Publication 84-100, 1984.
29 K. Langer and O.W. Flörke, Fortschr. Mineral., 52 (1974) 17.
30 W.J. Miles and R.D. Hamilton, Anal. Chim. Acta, 286 (1994) 3.

Analytica Chimica Acta, 286 (1994) 117–123
Elsevier Science B.V., Amsterdam

Determining a viable x-ray diffraction technique for routine quantification of the quartz content of powdered carbonates

A. M. Blount

Department of Geological Sciences, Rutgers University, Newark, NJ 07102 (USA)

F. Patrick Carr

OMYA, Inc., 61 Main Street, Proctor, VT 05765 (USA)

(Received 5th August 1992; revised manuscript received 6th October 1992)

Abstract

Powdered carbonate samples are digested in hydrochloric acid, and the resulting residue is analyzed using an internal standard method. Because the acid-insoluble residues of carbonates are mixtures of many different minerals, severe overlap problems occur with most commonly used standards. Spinel (synthetic) having a simple cubic pattern with 2Θ (Cu) peaks at 19.04°, 31.30° and 36.88° is generally free of overlap problems. Not only are the primary and secondary quartz peaks between the first two spinel peaks, but the spinel peaks can be used to determine and correct for inadequate thickness of the x-ray diffraction samples when necessary. The peak intensity of the quartz and of the standard are applied to an experimentally determined intensity ratio vs. percent quartz curve in the usual way. In addition, however, the intensities of the three spinel peaks are measured for each sample. Apparent increases in intensity of the low 2Θ peaks compared with the peak at 36.88° ($I = 100$) indicate a sample of insufficient thickness. The sample can be re-prepared or a correction made. Changes of intensity ratio of the spinel peaks as $\mu^* g$ varies vs. intensity correction (in percent) to the 20.88° and 26.66° quartz peaks had been graphed. Knowing the spinel intensity ratios, a correction can be read directly from the graph without determining g or μ^* and is generally no greater than 1–2% for the 20.88° peak intensity. The technique of acid digestion followed by percentage determination with an internal standard permits, in most cases, measurement to levels such that the upper confidence limit is well below 0.1%.

Keywords: Digestion techniques; X-ray diffraction; Carbonate rocks; Internal standard; Quartz; Silica; Spinel

Since IARC's Monograph 42 was published in 1987 [1], producers of mineral products have been faced with the daunting task of analyzing crystalline silica at levels below 0.1%. Due to the wide variety of substances to be analyzed, each with unique problems, most investigators would probably agree that no one method will work for all. In this paper we report on an x-ray diffraction technique designed to be used for analyses of carbonate samples containing low levels of quartz. It has often been pointed out that if enough time and money can be expended on a problem, then a solution can be devised. However, a key consideration in this study was to determine a method which could be routinely used rather than one so involved or complex as to be impractical.

Several problems are presented by ground car-

Correspondence to: A.M. Blount, Department of Geological Sciences, Rutgers University, Newark, NJ 07102 (USA).

SSDI 0003-2670(93)00386-F

bonate samples of high purity. First, the amounts of acid-insoluble components are very low. Whereas the carbonate samples can be acid treated to obtain the acid-insoluble residue, it is difficult to obtain sufficient residue to prepare a sample which may be considered "infinitely thick". Second, the acid-insoluble components are highly variable in mineralogical make-up from sample to sample. Iron-bearing minerals are often present; therefore, the mass absorption is different for each sample. Third, the acid-insoluble residues generally contain six to twelve crystalline components, several of which have severe overlap problems with commonly used standards. Two examples are α-Al_2O_3, which can be present in the sample having been acquired during mineral processing, and CaF, which has a reference peak at 28.3° (2Θ) too near the 28.6° peak of talc and amphiboles. In addition, high mass absorption and high density made several possible standards, such as Cr_2O_3, ZnO and TiO_2, undesirable.

Several solutions described in the literature have been considered to address this difficulty with carbonate samples. Emig and Smith [2] obtained quantitative results for quartz in dolostone by measuring the intensity of x-ray diffraction (XRD) peaks of quartz in bulk samples. This technique utilized the feature that mass absorption of the sample was equal to that of the carbonate minerals because the insoluble minerals occurred in such low amounts that the mass absorption was not appreciably affected. Johnson and Davis [3] have used the "transmission method" whereby the mass absorption is determined for each sample by measurement in the transmission mode and then applied to the diffraction results. Carter et al. [4] likewise determine the mass absorption but by means of Compton scattering. In general, however, measuring the mass absorption is not recommended because the measurement is extremely error prone [5]. The method of known additions, or spiking, has also been tried. This method is useful for an occasional check of results but generally is too lengthy for routine analyses. Thus, after considering the options, the use of an internal standard appeared to offer the best solution.

EXPERIMENTAL

Selecting a standard

The intensity of a diffraction peak is affected by the mass absorption of the sample as follows [6]:

$$I_{kl} = K_{kl} x_l / \rho_l \mu_T^* \quad (1)$$

where I_{kl} is the intensity of kth line of component l, K_{kl} a constant which depends upon characteristics of the apparatus, the x-ray wavelength and structure of component l, ρ_l the density of component l, x_l the weight fraction of l in the mixture and μ_T^* the mass absorption of the mixture. However, when relative intensities are measured the mass absorption of the mixture is canceled out.

$$I_{ij}/I_{kl} = K_{ij} x_j \rho_l / K_{kl} x_l \rho_j \quad (2)$$

where i is the internal standard and j the phase being referred to standard. For analyzing acid-insoluble residues which show great variation in mineralogy, it is desirable to use an internal standard so that relative intensities are compared as shown in Eq. 2. Because of problems with standards generally used, we sought a new material to use as a standard.

A number of properties are desirable for a standard. A material with a simple pattern and with peaks of high intensity is desirable so that overlap problems are minimized. Peaks from the standard should be in the region of, but not overlapping those of the minerals likely to be found in the samples. The mass absorption should be low, preferably near those of quartz and the silicates. A material with equidimensional grains and little or no cleavage is desirable so that the grains will not tend toward preferred orientation and will promote random orientation in the sample to be analyzed. Finally, the material should be easily available.

Synthetic spinel ($MgAl_2O_4$) was found to best meet these criteria. Spinel is cubic, thus it has a simple and strong pattern (Table 1). Peaks at 19.04° and 31.30° are near the primary (26.66°) and secondary (20.88°) quartz peaks. In addition, spinel has a low mass absorption ($\mu^* = 30$) and

TABLE 1

d-Spacing and 2Θ (λ = 1.5418) values for spinel

d(Å)	*I*	2Θ (°)
4.66	35	19.04
2.858	40	31.30
2.437	100	36.88
2.335	4	38.56
2.020	65	44.87
1.650	10	55.71
1.5554	45	59.42

has no cleavage [7] so that the grains are approximately equidimensional (Fig. 1).

Sample preparation

As indicated previously, we chose to determine the quartz content of the carbonate samples from analysis of the acid-insoluble residue. Each carbonate sample was ground to less than 325 mesh if it was not already that fine. To eliminate any moisture, the material was dried for one hour at 105°C and cooled in a desiccator. A 5–10 g sample depending on the expected acid-insoluble level was weighed and rinsed with deionized water into a 600-ml beaker. The volume was brought up to 200–300 ml with deionized water. The beaker was covered with a watch glass, and slowly 25 ml of 6M hydrochloric acid were added keeping the watch glass in place to prevent loss of sample during the effervescence. When the reaction had subsided, the beaker covered with the watch glass was placed on a hot plate and brought to boiling for 10 min. The sample was then removed from the hot plate and allowed to cool to at least 75°C.

The cooled solution was then vacuum filtered through a 0.8-micron membrane filter (Millipore AAWP 04700) assuring that all the sample was washed from the beaker and filtered. The filter was washed several times with deionized water. The membrane filter was placed on a watch glass, dried at 105°C for 30 min and cooled in a desiccator. The sample was weighed, and the amount of acid-insolubles (AI) determined; if there was not enough for x-ray analysis additional sample was prepared as described.

Each sample was scrapped from the filter and weighed. The spinel standard was added and the sample weighed a second time. The prepared mixture was ground with 5–7 ml of water in a McCrone micronizing mill for 5 min, after which the ground slurry was transferred to a glass slide with a pipette. The slurry was dried quickly by means of a petrographic-slide heater.

Whereas we recognize that it is possible that this procedure may permit segregation of particles according to size and density [8], testing by various other techniques suggests that the effect was negligible for the quartz/spinel ratio. The method of Moore and Reynolds [9] was tried; this method consisted of depositing a slurried sample on a membrane filter by suction. A glass slide was

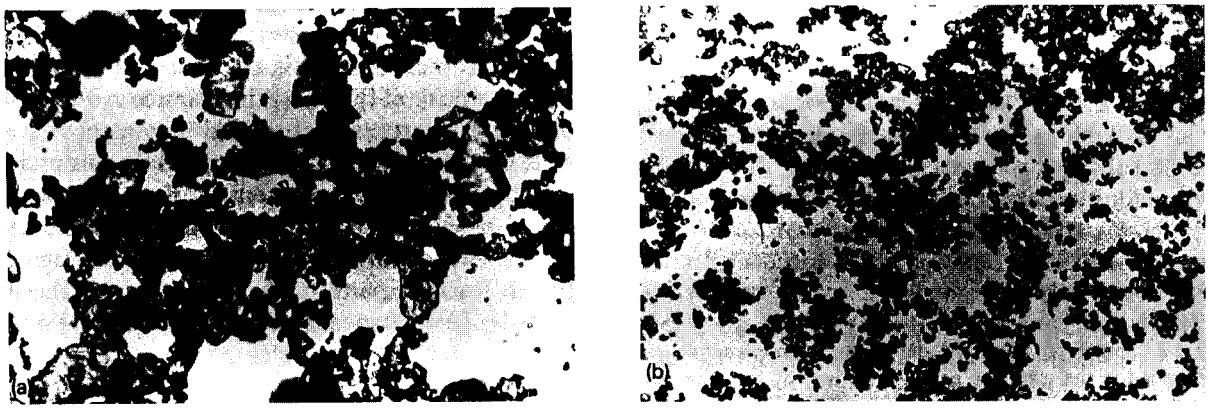

Fig. 1. (top) Spinel particles photographed in air. Spinel has a parting but no cleavage. This photograph shows that the parting is not sufficiently prominent to cause preferred orientation. (bottom) Spinel particles in air after having been ground for 15 min. Individual particles are approximately 1–2 μm in length.

placed over the side of the filter containing the mineral deposit and when partly dried the filter was carefully stripped off. This procedure avoided any density settling of mineral particles. Similarly, the mixture was placed on a glass slide as a paste so that particles were unable to segregate. This method, however, requires drying of the sample obtained from the micronizer and adding a few drops of water to make a paste. It was more complex than the pipette method, and it was also difficult to produce an absolutely flat surface on a paste. Because these two methods were less convenient, the results reported herein were obtained from dried slurries.

Standard curve for quartz

Acid-insoluble residues of carbonate rocks contain a variety of minerals, several of which overlap with the 26.66° peak of quartz. For this reason, quantitative analysis generally must be based on the secondary quartz peak at 20.88° (2Θ). A standard curve for the 20.88° quartz peak intensity relative to the 19.04° spinel peak intensity was prepared using Arkansas quartz, calcined kaolinite and synthetic spinel (Fig. 2). The quartz and kaolinite were mixed in various proportions and the spinel (internal standard) was added to each sample as a constant fraction of the total. All spinel to be used as an internal standard was ground 15 min and dried prior to mixing with other components or unknowns.

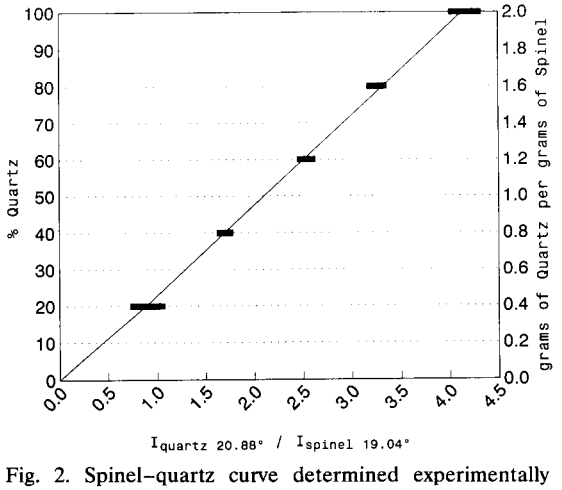

Fig. 2. Spinel–quartz curve determined experimentally as described in the text. The equation derived by linear regression is $y = 24.602x - 1.771$, where y is percent quartz and x is the intensity of the 20.88° quartz peak relative to the 19.04° spinel peak. y must be multiplied by 2 (weight spinel:weight unknown) when spinel:unknown is other than 1:2.

Before using the quartz, a test was done to determine the appropriate particle size (i.e., grinding time) to use. A quartz sample was ground 5, 10, 15, 20 and 25 min in the micronizing mill. After each 5-min grind an x-ray diffraction scan was done on the material. It was determined that after 15 min the XRD pattern did not show further change with additional grinding. Thus, the material used in the experiments was ground 15 min before drying and weighing together with the kaolinite and spinel. In additional, after the mixtures had been weighed, they were ground for an additional 5 min in water to facilitate thorough mixing. Three XRD samples were prepared, as described above, of each mixture representing a given percentage of quartz.

Correction for inadequate sample thickness

The selection of a good standard and a carefully prepared quartz–internal standard curve are not the only requirements for an accurate analysis. The relationship between intensity and concentration is linear only if the sample is infinitely thick, and with acid-insoluble residue this can commonly be a problem. When the sample is less thick, beam intensity is lost through the back of the sample. The amount so lost is greater at high 2Θ angles than at low 2Θ angles. Since the peak of the internal standard is at a different 2Θ angle than the peak of quartz, a thin sample mount will affect the quartz/spinel ratio.

It is, however, possible to correct for this problem by measuring the intensity of two or more spinel peaks and correcting according to the effects observed in the standard. Examination of the diffraction pattern of a thin sample shows that the low 2Θ peaks of the spinel standard at 19.04° and 31.30° show greater intensity than expected relative to the 36.88° peak (where I of this peak is considered to be 100). Those peaks at higher 2Θ appear to show lower intensities than expected. The variation in intensity between an

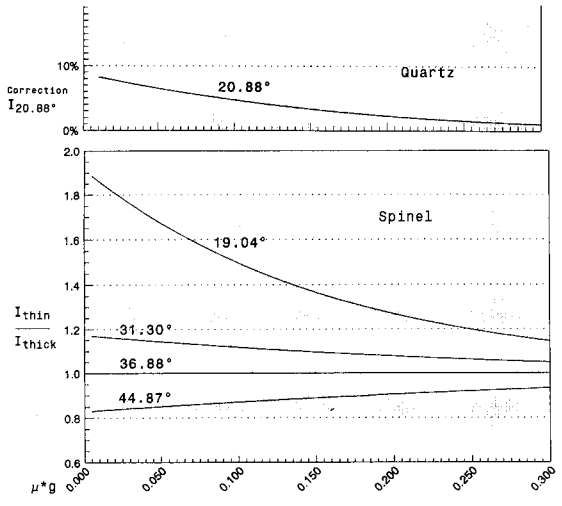

Fig. 3. Intensity of 19.04°, 31.30° and 44.87° peaks relative to 36.88° peak (assuming $I = 100$ for this peak) for thin vs. infinitely thick samples at varying $\mu^* g$ is shown on the lower portion of the graph. Using observed intensity of diffraction peaks of spinel, the correction to be applied to the 20.88° quartz relative to 19.04° spinel peak can be determined from the top graph.

infinitely thick sample and a thin sample can be expressed (derived from Eq. 10 [10]):

$$I_{thin}/I_{thick} = 1 - \exp(-2\mu^* g/\sin\Theta) \qquad (3)$$

where I_{thin} is the intensity of peak in thin sample, I_{thick} the intensity of same peak in infinitely thick sample, μ^* the mass absorption of sample and g the mass of sample in grams per cm^2. This equation permits one to correct for loss of intensity in the 20.88° quartz peak relative to the 19.04° spinel peak by reading from a graph (Fig. 3). This graph was constructed by arbitrarily permitting $\mu^* g$ to vary and plotting the results for each 2Θ peak. To use the graph, let us suppose that the 19.04° spinel peak is 1.5 times the expected intensity and the 31.30° peak 1.1 times. These values are located on the bottom curves and indicate that $\mu^* g$ is 0.1. This value when followed upward to the top graph shows that the correction to the intensity of the 20.88° quartz peak is approximately 4.5%.

This correction procedure was tested using the 60% quartz mixture which had been prepared for determining the quartz–spinel curve and preparing some thin sample mounts (0.0004, 0.0008 and 0.0016 g/cm^2). The results using corrected intensities were 57.8, 58.2 and 58.5% or within about 2% of the true value. The corrections of 10–7% applied to the quartz intensity were derived from the graph. In actual practice, the intensity of the 20.88° peak of quartz rarely needs correcting by more than 1 or 2% for intensity lost due to thinness of the mount. It should be noted, however, that this correction factor becomes quite large when one attempts to use the spinel 36.88° peak relative to the secondary or primary quartz peak. There may be some temptation to do so when the sample contains appreciable chlorite which overlaps the two lower spinel peaks.

RESULTS AND DISCUSSION

Routine analyses

Values within ±4% (relative) of the true value can be obtained with careful measurement of triplicate samples [11]; however, routine scans of samples are generally done more rapidly and with less attention to detail. Since large numbers of samples have been analyzed blindly (i.e., identity of product not known and samples intermixed), it is instructive to examine some of the results.

Both the percent quartz and a rough quantification of all minerals present in the acid-insoluble residue are important. For this reason a 20-min scan was done on each sample. The instrument used at this point was a GE XRD-5 and, being an old instrument, required manual determination of the intensity. The intensity was considered to be the peak height times the half width (i.e., width measured across the peak at half the peak height). Due to the uncertainty inherent in this measurement, we did not make any correction for sample thinness when the correction was only a few percent. When more than a few percent, the sample was prepared over again as a thicker mount. A rough quantification of all minerals present was carried out using the method of Chung [12]. Obviously, better results were obtained for those samples low in layer silicates. Quartz was determined using the intensity ratio

TABLE 2

Comparison of quartz content of ground carbonates determined using hydrochloric and acetic acid for dissolution (AI indicates acid-insoluble residue)

Number	HCl treated		Acetic acid treated		Quartz/bulk Δ (%)
	AI (%)	Quartz/bulk (%)	AI (%)	Quartz/bulk (%)	
1705	2.14	0.53	2.55	0.59	+0.06
1706	2.18	0.83	2.45	0.76	−0.07
1707	1.02	0.36	1.24	0.32	−0.04
1708	1.54	0.32	2.14	0.29	−0.03
1709	4.02	1.56	4.65	1.65	+0.09

between the spinel 19.04° peak and the quartz 20.88° peak and the equation in the caption in Fig. 2.

Routine analyses showed values for quartz within 12% (relative) of one another where the samples were prepared in two different ways (Table 2). The carbonate samples were divided and portions dissolved in HCl or acetic acid. As expected a distinct difference in percent acid-insoluble residue was seen. The percent quartz in bulk, however, was similar for both treatments. The variations shown here are consistent with other samples which were prepared and run several times.

An important consideration in analyses of products made from naturally occurring materials is whether we may expect the composition to remain uniform for some length of time. To test this, a group of samples were collected once a week over ten weeks. The results of two such sets are shown in Table 3. Both the percent acid-insoluble residue and the percent quartz vary but within a restricted range. The variations appear to be real in that they are greater than expected from simple analytical uncertainty. One can clearly make valid conclusions about the amount and variation of quartz content of each product. Note that product A shows a low quartz value on 5/20. A second analysis of a new sample preparation showed a similar value, thus this low value is believed to truly reflect the quartz content.

Conclusions

Whereas we recognize some problems with the method presently being used, it does compare favorably with NIOSH Method 7500 recommended by OSHA. The coefficient of variation (CV) of Method 7500 is 0.106 for quartz. This means that the measured values should be within plus or minus 21% of the true value. Our values are well within that range.

TABLE 3

Results from routine x-ray diffraction analyses of samples representative of production on different dates (AI indicates acid-insoluble residue)

Date	Quartz in AI (%)	AI (%)	Quartz in bulk (%)
Product A			
5/06	30.9	0.06	0.0185
5/13	21.9	0.05	0.0110
5/20	6.9 [a]	0.05	0.0035
5/27	20.3	0.04	0.0081
6/03	20.8	0.04	0.0083
6/10	13.3	0.04	0.0051
6/17	27.1	0.03	0.0081
6/24	26.8	0.03	0.0080
7/01	24.3	0.04	0.0097
7/08	28.4	0.03	0.0085
$\bar{x}$	22.1	0.041	0.0089
S.D. (R.S.D.)	7.3(33%)	0.01(24%)	0.0040(45%)
Product B			
5/06	25.5	0.88	0.224
5/13	26.2	0.89	0.233
5/20	24.7	1.06	0.263
5/27	20.9	0.76	0.159
6/03	23.9	1.14	0.272
6/10	34.1	0.61	0.208
6/17	22.5	0.79	0.178
6/24	24.3	0.66	0.160
7/01	18.9	0.68	0.129
7/08	23.6	0.55	0.130
$\bar{x}$	24.5	0.802	0.196
S.D. (R.S.D.)	4.0(16%)	0.192(24%)	0.052(27%)

[a] A second mount prepared and run gave 7.3% quartz.

Despite results on routine analyses which compare well with OSHA's favored method, there are a number of things that we are doing to improve these analyses. First, the filter-invert-peel method of Moore and Reynolds [9], described previously, will be used to insure that segregation of particles by settling from water is not occurring. Second, the instrumentation is being updated so that intensity measurements can be determined using slower step scans and computer curve fitting. This will eliminate some of the uncertainty in measuring intensity which has existed. A particular problem with manual intensity determination is that placement of the baseline can have a great effect on measured intensity for weak reflections.

Spinel has proven to be a useful internal standard for analysis of quartz. Its peak at 19.04° is near the 20.88° secondary quartz peak. In general, there are few overlap problems. The main exception is chlorite which when present in high quantities can overlap the 19.04° and 31.30° peaks of spinel. As indicated previously, it is not wise to use the 36.88° spinel peak for intensity reference unless one is certain that the preparation is infinitely thick. The chlorite overlap problem is eliminated by heating the preparation for several hours at 650°C. Heat treatment causes an increase of intensity of the 14-Å peak of chlorite and a decrease in all other basal peaks. This treatment can be done on the sample to which spinel has been added. Spinel is not altered until 2135°C, at which point it melts [7]. After the chlorite peaks are reduced in intensity the 19.04° or 31.30° spinel peak can be measured as usual.

Finally, the mean and standard deviation of quartz content of product samples over a given time period can be determined using the spinel internal standard method. To demonstrate compliance the mean plus two standard deviations, i.e., the upper confidence limit (UCL), should be less than 0.1%. In most cases the products can be demonstrated to be clearly below or above these limits. It should be noted that the calculations shown here are based on a normal distribution curve. A number of investigators, however, have shown that trace elements in geological situations and pollutants in the environment are better described by a log-normal distribution [13,14,15]. At the present there is insufficient data to determine which distribution more properly describes the quartz content at low or trace levels. This aspect will be examined as more analytical results become available.

REFERENCES

1 IARC Monographs on the Evaluation of the Carcinogenic Risk of Chemicals to Humans: Silica and Some Silicates, IARC Monograph 42, World Health Organization, Lyon, 1987.
2 J.A. Emig and D.K. Smith, Powder Diffr., 4 (1989) 209.
3 L.R. Johnson and B.L. Davis, Norelco Reporter, 29 (1982) 28.
4 J.R. Carter, M.T. Hatcher and L. Di Carlo, Anal. Chem., 59 (1987) 513.
5 R.L. Snyder and D.L. Bish, in D.L. Bish and J.E. Post (Editors), Modern Powder Diffraction, Reviews in Mineralogy, Vol. 20, Mineralogical Society of America, Washington, DC, 1989, p. 217.
6 R.H. Bragg, in E.F. Kaelbler (Ed.), Handbook of x-rays, McGraw Hill, New York, 1967, p. 12-1.
7 W.A. Deere, R.A. Howie and J. Zussman, Rock-Forming Minerals, Vol. 5, Non Silicates, Longman, London, 1972.
8 R.J. Gibbs, Am. Mineral., 50 (1965) 741.
9 D.M. Moore and C. Reynolds, Jr., X-ray Diffraction and the Identification and Analysis of Clay Minerals, Oxford University Press, New York, 1989.
10 R.C. Reynolds, in D.R. Pevear and F.A. Mumpton (Eds.), Quantitative Mineral Analysis of Clays, Vol. 1, Clay Minerals Society, Evergreen, CO, 1989, p. 4.
11 A.M. Blount and F.P. Carr, in D.J. Lootens, W.M. Greenslade and J. M. Barker (Eds.), Environmental Management for the 1990's, SEM, Littleton, CO, 1991, p. 373.
12 F.H. Chung, J. Appl. Crystallogr., 7 (1974) 519.
13 N.A. Leidel, K.A. Busch and J.R. Lynch, Occupational Exposure Sampling Strategy Manual, NIOSH, Cincinnati, OH, 1977.
14 C. Lepeltier, Econ. Geol., 64 (1969) 538.
15 A.W. Rose, H.E. Hawkes and J.S. Webb, Geochemistry in Mineral Exploration, Academic Press, New York, 1979, p. 32.

Analytica Chimica Acta, 286 (1994) 125–128
Elsevier Science B.V., Amsterdam

Quantitative measurement of crystalline silica by thermal analysis

Gary S. Sheffield

Orton Ceramic Foundation, Westerville, OH 43081 (USA)

(Received 20th August 1992; revised manuscript received 22nd March 1993)

Abstract

A thermal analysis method for quantitative measurement of crystalline silica with potential for detection below 0.1% has been demonstrated. Thermal analysis techniques are specifically tuned for this application. The energy associated with phase changes is measured during heating/cooling of the samples containing quartz and cristobalite. Feasibility of the method has been tested on crystalline silica. Operational and calibration procedures are described and precision of the method presented.

Keywords: Crystalline silica; Thermal analysis

Silica is the most abundant constituent in the earth's crust and is widely used throughout industry. Crystalline silica has long been identified as the cause for silicosis and more recently, in 1987, crystalline silica was classified by the International Agency for Research on Cancer (IARC) as Group 2A (Probably Carcinogenic to Humans). Therefore methods for detection and accurate quantitative determination of crystalline silica in its various forms are extremely important. One method, thermal analysis, appears promising because it can be made ultra sensitive to crystalline silica phases, such as quartz and cristobalite. Thermal analysis is also relatively free from interference effects and seemingly unfavorable operational parameters can generally be overcome by careful system design.

Enthalpy changes of crystalline silica

The quantitative measurement of quartz and cristobalite in various substances by thermal analysis is based on enthalpy changes associated with the alpha–beta transition in quartz at about 573°C and the alpha–beta transition in cristobalite over the temperature range 100–270°C. Tridymite, a third form of crystalline silica is rarely found at room temperature. The crystalline changes (reconstructive and displacive) in silica are shown in Fig. 1.

Quartz is the thermodynamically stable form of crystalline silica at ambient temperature. It has been reported [1] that the transition temperature in about 95% of quartz samples from numerous natural sources was 573 ± 2.5°C. Cristobalite is a metastable form which can exist at ambient tem-

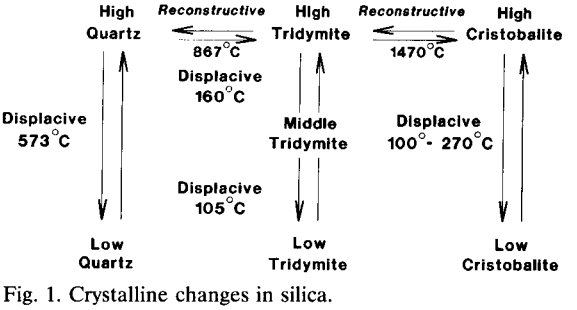

Fig. 1. Crystalline changes in silica.

Correspondence to: G.S. Sheffield, Orton Ceramic Foundation, Westerville, OH 43081 (USA).

SSDI 0003-2670(93)E0291-E

TABLE 1

Enthalpy change at the alpha–beta quartz transition

Source	Year	ΔH_t (cal/g)
Sosman [4]	1927	2.5
Moser [5]	1936	1.2
USBM [6]	1952	2.49
Sabatier [7]	1957	1.5
Majumdar et al. [8]	1964	1.4 ± 0.3
MacKenzie and Ritchie [9]	1972	3.20
Gray [3]	1974	1.57 ± 0.05

peratures, depending upon the thermal history of the sample. The inversion temperature of cristobalite depends on origin and previous thermal history of the sample. For well-crystallized cristobalite, Hill and Roy [2] assigned inversion points at 267°C (heating) and 242°C (cooling).

The results of the change in enthalpy at the alpha–beta quartz transition as reported by various investigators are assembled in Table 1. The more recent values are in the range 1.4–1.57 cal/g. Gray [3] used NBS-ICTA SRM 760 as his quartz source and found that the peak area obtained by differential scanning calorimetry (DSC) to be very reproducible. He set a 3% uncertainty on the value obtained due largely to baseline interpretation.

Reported values for the alpha–beta cristobalite transition heat are listed in Table 2. These data show that this transition is about twice as energetic as the alpha–beta quartz transition.

Thermal analysis methods for determination of crystalline silica

The applicability of thermal analysis techniques to the quantitative determination of crystalline quartz, and in limited instances, cristobalite, has been demonstrated in a number of experimental investigations. In early work, Grimshaw et al. [11] and Grimshaw [12] using differential thermal analysis (DTA) demonstrated a linear relationship between peak height and percent quartz for quartz samples from various localities. They were less successful with cristobalite as different forms were recognized and appeared to give different inversion heats.

More recently el Kolali and Gad [13] used DTA for accurate quantitative determination of quartz in Egyptian feldspars and clays, the results of which agreed favorably with analysis by chemical methods. By adding up to 10% quartz, Rowse and Jepson [14] have determined quartz in clay minerals with a standard error of 0.2–0.3% using DTA. Schelz [15] found that the DTA method was sensitive, specific, and relatively rapid but required standardized preparation and experimental parameters for the technique to be definitive. The minimum level of quartz detectable in talc was 0.5%. All of the work previously described used DTA equipment in which thermocouples are contained within the sample, a condition under which the results are certain to be influenced to some degree by sample parameters, depending on rigidity of standardized operation conditions.

TABLE 2

Enthalpy change at the alpha–beta cristobalite inversion

Source	Year	ΔH_t (cal/g)
Lakoday et al. [10]	1956	3.2
Sabatier [7]	1957	4.4
Majumdar et al. [8]	1964	3.3

EXPERIMENTAL

The determination of crystalline quartz has been approached using two different thermal analysis instruments specifically tuned for detection and measurement of crystalline quartz. Some preliminary work has also been done in measuring the heats of transition of cristobalite.

The standard resolution unit uses a 3-junction Type K thermopile with 10^{-3}°C resolution and 0.3 ml alumina sample cups. The thermopile is located outside the sample cup and depending upon the sample powder characteristics, the sample size is typically 200–500 mg. The effective range of the instrument is about 0.5 to 100% crystalline silica and all relevant data are collected in the vicinity of the quartz transition on cooling at rates between 5.5 and 8°C/min, depending on operating conditions.

A second, high resolution unit has recently been constructed for detecting and determining crystalline silica at low concentration levels, typically those below 0.5%. This unit uses a 21 junction Type K thermopile with temperature resolution approaching 10^{-4}°C and a larger sample holder capable of accommodating samples in excess of 2 g. Data is collected in the vicinity of the quartz transition at cooling rates of about 7°C/min. All samples (for both instruments) were generally heated to about 700°C before cooling was initiated.

Samples were made from artificial mixtures of quartz and alumina in known amounts weighed to ±0.1 mg and sized so that after mechanical mixing, all of the sample could be quantitatively transferred from the weighing paper to the sample holder. For the alumina–silica artificial mixtures between 1 and 100%, Norton 100NF (99.8%) alumina was used. The silica source was NBS-ICTA Standard Reference Material 760. In cases where high purity alumina was required, Linde C (99.98%) was used.

RESULTS AND DISCUSSION

The applicability of the standard thermal analysis unit to the measurement of crystalline quartz is demonstrated by the calibration curve shown in Fig. 2, where artificial mixtures of various compositions of NBS-ICTA SRM 760 silica in Linde C are shown. The actual percent quartz shown in the Fig. 2 are 2.05%, 20.0%, 51.35%, 74.38% and 100% quartz.

An indication of the repeatability of the standard unit is reflected by the following results obtained on repeated measurements on quartz in alumina: 17.31%, 17.50%, 17.19%, 17.16% and 17.33%. The mean of these results is 17.30%, with a standard deviation of 0.13% quartz, which indicates the precision by which crystalline quartz can be determined at this level. These data were taken with Orton's standard resolution unit. This unit has demonstrated a capability of quantitatively measuring crystalline quartz below 1%.

The high resolution unit is anticipated to be capable of measuring crystalline silica at the 0.1% level or below. The estimated accuracy is expected to be ±10% of the measurement value; however, insufficient experimental data exists to substantiate the accuracy and repeatability of this instrument.

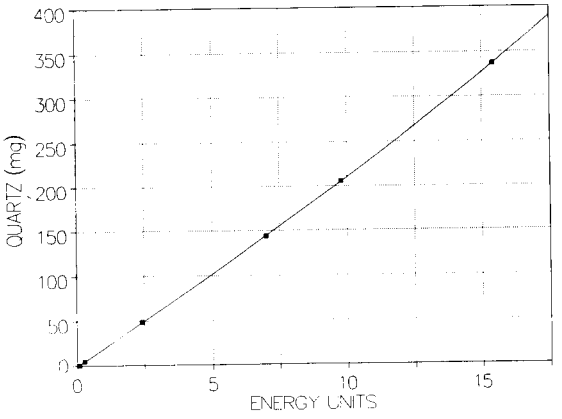

Fig. 2. Calibration curve relating magnitude of quartz and arbitrary energy units.

Future testing of this method will be on-going to further define optimum design and operating conditions. We believe that this thermal analysis method offers the potential for measurements between 0.05% and 0.1%.

Review of the literature and limited experimental results at Orton indicate that variation in enthalpy exists between different sources of crystalline silica, less so with quartz and much more with cristobalite, which is a metastable form of crystalline silica at room temperature. Reduction in particle size by grinding can produce amorphous layers on quartz surfaces which diminishes crystallinity. Hence, the apparent heat of transition will be reduced. This phenomenon needs extended study.

REFERENCES

1 M.L. Keith and O.F. Tuttle, Am. J. Sci., Bowen Vol., Part 1 (1952) 203.
2 V.G. Hill and R. Roy, Trans. Br. Ceram. Soc., 57 (1958) 496.
3 A.P. Gray, Proceedings of the Fourth ICTA, 3 (1974) 991.
4 R.B. Sosman, The Properties of Silica, Monograph Am. Chem. Soc., 37 (1927) 312.

5 H. Moser, Phys. Z., 37 (1936) 737.
6 Selected Values of Chemical Thermodynamic Properties, U.S. National Bureau of Standards, Washington, DC, Circular 500, 1952.
7 G. Sabatier, Bull Soc. Fr. Miner. Crystallogr., 80 (1957) 444.
8 A.J. Majumdar, H.A. McKinstrey and R. Roy, J. Phys. Chem. Solids, 25 (1964) 1487.
9 R.C. MacKenzie and P.F.S. Ritchie, Thermal Analysis (ICTA), 1 (1972) 441.
10 P. Lakoday, C. Eyraud and M. Prettre, C.R. Hebd. Seances Acad. Sci., Paris, 242 (1956) 3071.
11 R.W. Grimshaw, A. Westerman and A.L. Roberts, Trans. Br. Ceram. Soc., 47 (1948) 269.
12 R.W. Grimshaw, Clay Miner. Bull., 2 (1953) 2.
13 Abd el-Ghany A el Kolali and G. Gad, J. Appl. Chem. Biotechnol., 21 (1971) 343.
14 J.B. Rowse and W.B. Jepson, J. Thermal Analysis, 4 (1972) 169.
15 John P. Schelz, Thermochim. Acta, 15 (1976) 17.

Analytica Chimica Acta, 286 (1994) 129–133
Elsevier Science B.V., Amsterdam

New x-ray diffraction method of additions for crystalline silica

Jacques Renault, Chris McKee and James Barker

New Mexico Bureau of Mines and Mineral Resources Division, New Mexico Institute of Mining and Technology, Campus Station, Socorro, NM 87801 (USA)

(Received 20th August 1992; revised manuscript received 17th November 1992)

Abstract

A new method of additions is described for x-ray diffraction determination of trace crystalline silica. The method is derived from Klug and Alexander, *X-ray Diffraction Procedures* (Wiley, 1974, p. 536, Eqn. 7–14) and is expressed as $x = sR_x(1 - R_s)/(R_s - R_x)$ where x and s are the concentrations of analyte and spike, and R_x and R_s are the relative intensities of analyte and spike. The method is particularly attractive because the mass absorption coefficient of the matrix can be very different from silica, and large spikes can be used which minimize homogenization errors. In addition, non-zero intercepts are avoided. Trace determination of quartz at the < 0.1 wt.% level can be routinely accomplished by using the new method with rotating pressed-powder briquettes and a peak deconvolution strategy due to Wiedemann et al. [*Powder Diffraction*, 2 (1987a, b) 130, 137.].

Keywords: X-ray diffraction; Additions method; Crystalline silica

Quartz has been of interest in occupational health for years, because it can cause silicosis if exposure is prolonged. Occupational Safety and Health Administration (OSHA) regulations require that industrial materials containing more than 0.1 wt.% free silica be labeled. This regulation is based on the classification of free silica as a probable carcinogen in humans by the International Agency for Research on Cancer [1]. Although there are three common polymorphs of crystalline silica, quartz is by far the most abundant form, so initial research has concentrated on its trace determination [2,3].

Practical methods for the determination of quartz have included potassium pyrosulfate digestion [4–6], optical microscopy, heavy liquid separation [2,3], and x-ray diffraction (XRD). The first three methods are time consuming and lack the required precision to meet OSHA regulations. Traditional XRD determination of quartz in industrial dusts uses well established procedures [7] that are insensitive below the 1 wt.% level of quartz. In order to meet the new regulations, Manville Sales Co. (Denver, CO) [2,3] initiated the development of an XRD method to determine quartz in perlite at the 0.1 wt.% level. Work at the New Mexico Bureau of Mines and Mineral Resources confirmed their work [8]. Subsequently McKee et al. [9] showed how trace determination of quartz could be accomplished with artificial standards by mixing quartz with window glass. Renault et al. [10,11] described the use of chemical mass-balance calculations and a new spiking method to effect trace quartz determination and summarized their calibration experience.

The present report derives a new equation for determination of an analyte by the method of standard additions. Although described for trace XRD determination of quartz, it is quite general, subject to constraints of sample preparation.

Correspondence to: J. Renault, New Mexico Bureau of Mines and Minerals Resources Div., New Mexico Institute of Mining & Technology, Campus Station, Socorro, NM 87801 (USA).

SSDI 0003-2670(93)00472-T

DERIVATION

The method of additions is commonly used in chemical analysis of solutions when a solution can be spiked with a very small concentration of the analyte. The instrumental response to the unknown analyte plus spike is directly proportional to that of the unknown alone provided that the solutions remain dilute.

When powders are analyzed, however, it is difficult to homogeneously blend a small spike of low concentration with the unknown sample. On the other hand, if the original unknown is homogeneous, good blending can be routinely achieved with large spike concentrations (say, 25 wt.%), and weighing error is reduced.

Unfortunately, large spikes can cause substantial changes in the mass absorption coefficient of the spiked sample, and this makes the assumption of linearity of instrumental response untenable. If large spikes are to be used, the non-linearity of instrument response must be accommodated in the data reduction.

Snyder and Bish [12] describe the method of standard additions due to Lennox [13]. This method accounts for mass absorption and permits large spikes, but requires measurement of an additional phase without overlapping lines. The method described below makes that unnecessary.

Klug and Alexander [1] show that for a single analyte, the analyte and matrix can be treated as a two-component system.

$$R_x = \frac{x\mu_x}{x(\mu_x - \mu_m) + \mu_m} \tag{1}$$

where R_x is the ratio of the intensity of the analyte in the unknown to the pure analyte, x is the concentration of the analyte in the unknown mixture, and μ_x and μ_m are the mass absorption coefficients of the pure analyte and the matrix respectively. Rearranging Eqn. 1,

$$\frac{\mu_m}{\mu_x} = \frac{x\left[\frac{1}{R_x} - 1\right]}{1 - x} \tag{2}$$

introducing s, a spike per mass-unit of the unknown,

$$\frac{\mu_m}{\mu_x} = \frac{(x+s)\left[\frac{1}{R_s} - 1\right]}{1 - x} \tag{3}$$

and setting Eqn. 2 equal to Eqn. 3, the mass absorption term cancels and we solve for the analyte:

$$x = \frac{sR_x(1 - R_s)}{R_s - R_x} \tag{4}$$

Equation 4 is in a convenient form for determining an unknown concentration, x, given the spike, s, per g of sample and the relative intensities of the natural unknown and the spiked unknown. Note that the denominator of Eqn. 4 is a difference. The solution of the equation is thus sensitive to small differences in R_x and R_s, so it is best to use large spikes, say, 0.25 g per g of sample with small values of x.

A mass-absorption coefficient of the matrix is easily computed from Eqn. 2 given x. However, our experience and the experience of Leroux and Mahmud [14] show that the intensity vs. composition curve of packed samples has a different curvature than that predicted by Eqn. 1. Leroux and Mahmud [14] attribute this to the geometry specific to particular diffractometers. Under constant instrumental conditions, the curves are stable, but only an apparent mass absorption coefficient ($\langle\mu\rangle$) can be computed.

TREATMENT OF ERRORS

It is apparent from the denominator of Eqn. 4 that as R_x approaches R_s, their differences become small and contribute substantially to the accumulated error. Other contributions are not intuitively so apparent, but the maximum derived error in x can be easily computed from the sum of the partial derivatives of x with respect to each of the variables s, R_x, and R_s and their error coefficients.

To illustrate the variation in derived error as a function of μ and x, we assume a relative weigh-

TABLE 1

Variation of error with μ and analyte wt.%

Analyte constant at 5 wt.%		μ constant at 33.6	
μ	Relative error	wt. %	Relative error
7.1	0.037	1.0	0.105
20.7	0.082	2.5	0.112
33.6	0.125	5.0	0.125
55.3	0.196	10.0	0.153
85.6	0.298	25.0	0.256
164	0.556	50.0	0.558

ing error in s of 0.01, and counting errors in R_x of 0.10, and in R_s of 0.01. These are conservative measurement errors, but there is an unknown mixing error which we have not included. The maximum derived error for various conditions is given below in Table 1.

The table shows that at constant quartz concentration in the unspiked sample, the error increases linearly with mass absorption coefficient, μ. At constant μ, however, the derived error increases more rapidly than the increase in quartz concentration.

These data show that this method of spiking should be confined to low quartz concentrations, and will have the lowest error in matrices of low mass absorption coefficient. Fortunately, many industrial materials, e.g., perlite, kaolinite, muscovite, and bauxite have μ values with low to middle values. Others such as lime and rutile have high mass absorption coefficients, and the determination of them for trace analytes will be inherently less accurate.

EXPERIMENTAL

Sample preparation procedures are described in McKee et al. [9] and Renault et al. [11]. Samples were analyzed with a Rigaku D/MAX diffractometer controlled by a DEC PDP 11/23 computer using Rigaku software. The diffractometer was equipped with a long, fine focus, Cu x-ray tube operating at 40 kV and 25 mA with a graphite monochromator and a scintillation counter.

The diffractometer was set up to step scan over the 101 quartz peak at 26.66° 2θ using 1° divergence and scatter slits and 0.3 mm receiving slits. To obtain the best deconvolution, a step width of 0.01° and a count time of 40 s per step were used. A scan range of 26.20° to 27.00° 2θ was dictated by software limitations.

The raw data were reduced by the deconvolution program of Wiedemann et al. [15]. This program precisely establishes background and enhances peak resolution without changing the integrated intensity. After deconvolution, the peaks were examined and extraneous signals removed. The profile of a pure quartz sample served as an instrumental standard and was used to normalize integrated intensities.

Figures 1 and 2 show the results of experiments in which mixtures of LiF–quartz and KCl–quartz were prepared by successively diluting 1:1 mixtures with the halides in 1:1 steps. The LiF–quartz mixtures were accomplished by repeated cone and quartering, and the KCl–quartz mixtures by grinding in a Spex mixer-mill. The mixtures were spiked by adding 0.250 g quartz per g of mixture and then remixed as before.

When we began to process the intensity data, it became apparent that the mixtures were not as planned. Some of this is probably due to inhomogeneity. When the quartz concentrations are computed from Eqn. 4, the four low concentration samples in the LiF mixtures have an average $\langle\mu\rangle$ of 10.0 as opposed to the accepted μ of 12.0 for the LiF matrix. The five lower concentration

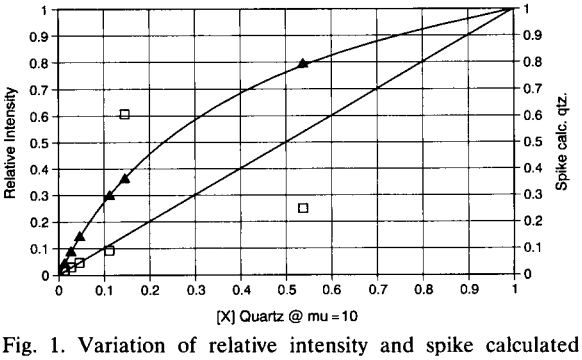

Fig. 1. Variation of relative intensity and spike calculated quartz concentration versus quartz weight fraction in a LiF matrix of apparent mass absorption coefficient equal to 10.0. Filled triangles are intensities of unspiked mixtures, and open squares are spike calculated quartz concentrations.

samples in the KCl series have an average $\langle \mu \rangle$ of 94.4 as opposed to the accepted value of 120 for KCl. These are to be expected as noted earlier.

In Figs. 1 and 2, the abscissa values are the Eqn. 4 concentrations using the average $\langle \mu \rangle$ values above. The filled triangles show how the integrated quartz intensity relative to pure quartz varies with quartz concentration in matrices with widely different $\langle \mu \rangle$.

Good mixing was not attained at the high concentrations as can be seen from the divergence of spike results from the 1:1 line. The 1:3 sample in the LiF series should have had an intensity of 0.55 for a concentration of 0.25 as mixed. When the spike was added, a serious error resulted in the calculation of quartz concentration. The 1:1 sample shows that at high concentrations a small error in homogeneity results in a large error after spiking. This is mainly due to the difference term in the denominator of Eqn. 4. The mixing error in the KCl series is not as severe. Apparently mixing by grinding together is more effective than cone and quartering.

In both series, the lower four points lie close to the 1:1 diagonal line showing the close correspondence of the spike results to the expected quartz concentrations. This illustrates the declining error as concentration diminishes, and shows that this spiking method is good for low concentrations as described for perlites below.

Manville Sales Co. provided us with six of their in-house natural perlite standards. They determined the quartz concentration in the standards by optical microscopy and their results are given in Table 2. The table summarizes our quartz spike data on their perlite standards. The mean coefficients of variation of the intensity data are 0.298 and 0.251 for R_x and R_s respectively, and the estimated standard deviations are 0.15 and 0.16, respectively. These errors include mixing error as well as counting error. Note that they are almost three times higher than were assumed in the derived error computations which included counting time only.

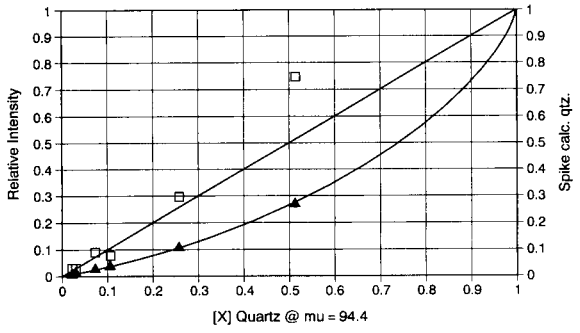

Fig. 2. Variation of relative intensity and spike calculated quartz concentration versus quartz weight fraction in a KCl matrix of apparent mass absorption coefficient equal to 120. Filled triangles are intensities of unspiked mixtures, and open squares are spike calculated quartz concentrations.

TABLE 2
Summary of perlite analyses for quartz

	Relative intensity	Reported	Spike	Eqn. 1	$\langle \mu \rangle$
1	0.00083	n.d.	0.0007	0.0008	28.3
2	0.00156	0.004	0.0009	0.0014	19.2
3	0.00157	0.001	0.0011	0.0014	23.8
4	0.00162	0.002	0.0026	0.0015	53.2
5	0.00167	0.002	0.0016	0.0015	32.0
6	0.00230	0.002	0.0018	0.0021	25.8

The $\langle \mu \rangle$ values computed from Eqn. 2 vary by a factor of almost 3. We attribute this to lower homogeneity of the perlite standards, they being natural rock samples. Notice that sample 4 has an exceptionally high $\langle \mu \rangle$. We don't know if this is due to a homogeneity error or if the sample really has a higher mass absorption coefficient. The mean $\langle \mu \rangle$ is 30.4 and was used to compute the concentration of quartz in the perlite standards using Eqn. 1.

Figure 3 shows how the intensity and the reported and spike calculated quartz vary with quartz concentration from Eqn. 1. The intensities lie systematically above the 1:1 line because the $\langle \mu \rangle$ is less than that of quartz. The reported values have greater scatter than the spike results because the sampling is necessarily sparse in the optical microscopy method. The spike values are reasonably close to the 1:1 line showing that the effect of mass absorption has been accounted for correctly.

Conclusions

In certain samples, the mass absorption coefficient of an analyte may differ substantially from

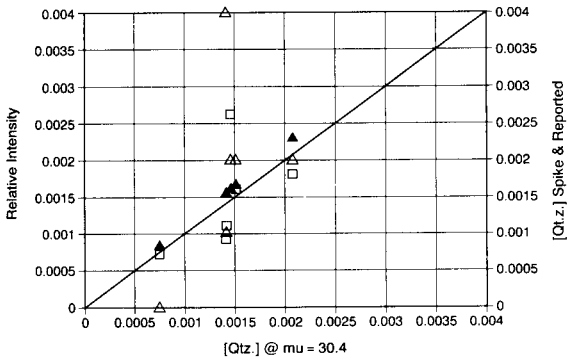

Fig. 3. Variation of relative intensity, reported quartz concentration, and spike calculated quartz concentration versus quartz weight fraction in Manville perlite standards with matrix of apparent mass absorption coefficient equal to 30.4. Filled triangles are relative intensity of unspiked samples, open triangles are reported quartz concentrations, and open squares are spike calculated quartz concentrations.

that of the matrix. In those cases, the XRD calibration curve is not linear. We derived a simple equation from Klug and Alexander's Eqn. 7–14 [7] that removes the mass absorption effect. The calculation is especially applicable to the determination of raw materials with variable mass absorption coefficients. Furthermore, for trace quartz determination, a 20 wt.% spike presents a less onerous mixing task than spiking with the very small amount of quartz required by other methods. Unlike other spiking and calibration methods, zero intensity always corresponds to zero wt.% analyte.

We showed that the derived error in an XRD spiking experiment depends on the concentration of the analyte and the mass absorption coefficient of the matrix. With a constant spike of 0.25 g spike per g of sample, the error of the calculation decreases with matrix mass absorption and with analyte concentration in the unknown. Of course, the counting error will ordinarily increase as the concentration of the analyte diminishes, but to some degree, that can be controlled by the analytical design.

The method presented here requires no calibration curve. Once a pure analyte standard has been measured, say, at the beginning of each day, only one determination is required on each unspiked and spiked sample. If the $\langle \mu \rangle$ values are found to be stable, then spiking need only be intermittently performed. Our principle concern is that the spiked sample be properly blended. We recommend grinding the unknown, then grinding a representative split of it with the spike.

We wish to thank the Manville Sales Co. for providing us with their in-house perlite standards. Publication of this paper is authorized by the Director of the New Mexico Bureau of Mines and Mineral Resources, Charles E. Chapin.

REFERENCES

1 IARC Monographs on the Carcinogenic Risks of Chemicals to Humans, Vol. 42, 1987, pp. 1–144; and supplement 7, pp. 29–74 and 341–343.
2 R.D. Hamilton and N.G Peletis, The Determination of Quartz in Perlite by X-ray Diffraction, Unpublished Report, Corporate Research and Engineering Center, Manville Sales Co., Denver, CO, 1988, 11 pp.
3 R.D. Hamilton and N.G. Peletis, in C.S. Barrett, J.V. Gilfrich, T.C., Huang, R. Jenkins, and P.K. Predecki (Eds.), Advances in X-ray Analysis, Vol. 33, Plenum Press, New York, 1989, p. 493.
4 L.J. Trostel and D.J. Wynne, J. Am. Ceram. Soc., 23 (1940) 18.
5 M. Gysin and D. Reelfs, Soc. Phys. Hist. Nat. Genève, 4 (1951) 245.
6 M. Gysin and D. Reelfs, Soc. Phys. Hist. Nat. Genève, 5 (1952) 181.
7 H.P. Klug and L.E. Alexander, X-ray Diffraction Procedures, Wiley, New York, 2nd ed., 1974, p. 536.
8 J.M. Barker and C. McKee, SME Preprint 89–184, Annual Meeting, Littleton, CO, 1989, 31 pp.
9 C. McKee, J. Renault and J. Barker, New Mexico Bureau of Mines and Mineral Resources Open-File Report 364, 1990, 16 pp.
10 J. Renault, C. McKee and J. Barker, in D.J. Lootens, W.M. Greenslade, J.M. Barker (Eds.), Environmental Management for the 1990s; Proceedings of the Symposium, Society for Mining, Metallurgy, and Exploration, Littleton, CO, 1991, Chap. 46, pp. 361–362.
11 J. Renault, C. McKee and J. Barker, Calibrating for X-ray Diffraction Analysis of Trace Quartz. Advances in X-ray Analysis, Vol. 35, Plenum Press, New York, 1992, p. 363.
12 R.L. Snyder and D.L. Bish, in D.L. Bish and J.E. Post (Eds.), Modern Powder Diffraction, Vol. 20, Reviews in Mineralogy, Mineralogical Society of America, Washington, DC, 1989, Chap. 5, pp. 125–126.
13 D.H. Lennox, Anal. Chem., 29 (1957) 767.
14 J. Leroux and M. Mahmud, Advances in X-ray Analysis, Vol. 3, Plenum Press, New York, 1960, p. 337.
15 K.E. Wiedemann, J. Unnam and R.K. Clark, Powder Diffraction, 2 (1987a,b) 130, 137.

Announcement from the Publisher

Elsevier encourages submission of articles on floppy disk.

All manuscripts may now be submitted on computer disk, with the eventual aim of reducing production times still further.

The preferred storage medium is a 5¼ or 3½ inch disk in MS-DOS format, although other systems are welcome, e.g. Macintosh.

After **final acceptance**, your disk plus one final, printed and exactly matching version (as a printout) should be submitted together to the editor. **It is important that the file on disk and the printout are identical.** Both will then be forwarded by the editor to Elsevier.

Illustrations should be provided in the usual manner.

Please follow the general instructions on style/arrangement and, in particular, the reference style of this journal as given in 'Instructions to Authors'.

Please label the disk with your name, the software & hardware used and the name of the file to be processed.

For further information on the preparation of compuscripts please contact:

Elsevier Science B.V.
Analytica Chimica Acta
P.O. Box 330
1000 AH Amsterdam, The Netherlands
Phone: (+31-20) 5862 758 Fax: (+31-20) 5862 459

ELSEVIER SCIENCE B.V.

ANABIOTEC 94

5th International Symposium on Analytical Techniques, Systems & Strategies in Biotechnology

---

31 October – 2 November 1994

Minneapolis Hilton & Towers, USA

Learn of the new instruments and techniques for analytical chemistry
Improve monitoring of industrial scale processes
Update your strategies for clinical diagnosis
Meet international colleagues and contacts

The analytical chemistry of complex matrices involving species of a biological origin is a rapidly developing research frontier.

ANABIOTEC 94 – consisting of plenary sessions, selected original papers, posters and an exhibition – will address the wide array of research issues involved in this field. This symposium is the ideal forum for information exchange between the fields of analytical chemistry, biochemistry, clinical chemistry and biotechnology: you need to be there!

For further information send a copy of this advert, complete with your address details to:

Anabiotec 94 Conference Secretariat, Elsevier Science Ltd,
PO Box 150, Kidlington, Oxford OX5 1AS, UK.
Tel: +44 (0) 865 512242
Fax: +44 (0) 865 310981

anabiota 3d (21.12.93

PUBLICATION SCHEDULE FOR 1994

	S'93	O'93	N'93	D'93	J	F	M	A	M			
Analytica Chimica Acta	281/1 281/2 281/3	282/1 282/2 282/3	283/1 283/2	283/3 284/1 284/2	284/3 285/1-2 285/3	286/1 286/2 286/3	287/1-2 287/3 288/1	288/2 288/3 289/1	289/2-3 290/1 290/2			
Vibrational Spectroscopy		6/1			6/2		6/3		7/1			

INFORMATION FOR AUTHORS

Detailed "Instructions to Authors" for *Analytica Chimica Acta* was published in Volume 256, No. 2, pp. 373–376. Free reprints of the "Instructions to Authors" of *Analytica Chimica Acta* and *Vibrational Spectroscopy* are available from the Editors or from: Elsevier Science B.V., P.O. Box 330, 1000 AH Amsterdam, The Netherlands. Telefax: (+31-20) 5862459.

Manuscripts. The language of the journal is English. English linguistic improvement is provided as part of the normal editorial processing. Authors should submit three copies of the manuscript in clear double-spaced typing on one side of the paper only. *Vibrational Spectroscopy* also accepts papers in English only.

Rapid publication letters. *Letters* are short papers that describe innovative research. Criteria for letters are novelty, quality, significance, urgency and brevity. Submission data: max. of 2 printed pages (incl. Figs., Tables, Abstr., Refs.); short abstract (e.g., 3 lines); *no* proofs will be sent to the authors; submission on floppy disc; *no* revision will be possible.

Abstract. All papers and reviews begin with an Abstract (50–250 words) which should comprise a factual account of the contents of the paper, with emphasis on new information.

Figures. Figures should be prepared in black waterproof drawing ink on drawing or tracing paper of the same size as that on which the manuscript is typed. One original (or sharp glossy print) and two photostat (or other) copies are required. Attention should be given to line thickness, lettering (which should be kept to a minimum) and spacing on axes of graphs, to ensure suitability for reduction in size on printing. Axes of a graph should be clearly labelled, along the axes, outside the graph itself. All figures should be numbered with Arabic numerals, and require descriptive legends which should be typed on a separate sheet of paper. Simple straight-line graphs are not acceptable, because they can readily be described in the text by means of an equation or a sentence. Claims of linearity should be supported by regression data that include slope, intercept, standard deviations of the slope and intercept, standard error and the number of data points; correlation coefficients are optional.

Photographs should be glossy prints and be as rich in contrast as possible; colour photographs cannot be accepted. Line diagrams are generally preferred to photographs of equipment. Computer outputs for reproduction as figures must be good quality on blank paper, and should preferably be submitted as glossy prints.

Nomenclature, abbreviations and symbols. In general, the recommendations of IUPAC should be followed, and attention should be given to the recommendations of the Analytical Chemistry Division in the journal *Pure and Applied Chemistry* (see also *IUPAC Compendium of Analytical Nomenclature, Definitive Rules*, 1987).

References. The references should be collected at the end of the paper, numbered in the order of their appearance in the text (*not* alphabetically) and typed on a separate sheet.

Reprints. Fifty reprints will be supplied free of charge. Additional reprints (minimum 100) can be ordered. An order form containing price quotations will be sent to the authors together with the proofs of their article.

Papers dealing with vibrational spectroscopy should be sent to: Dr J.G. Grasselli, 150 Greentree Road, Chagrin Falls, OH 44022, U.S.A. Telefax: (+1-216) 2473360 (Americas, Canada, Australia and New Zealand) or Dr J.H. van der Maas, Department of Analytical Molecular Spectrometry, Faculty of Chemistry, University of Utrecht, P.O. Box 80083, 3508 TB Utrecht, The Netherlands. Telefax: (+31-30) 518219 (all other countries).

0003-2670/94/$07.00

This issue is printed on acid-free paper.

PRINTED IN THE NETHERLANDS

Environmental Analysis

Techniques, Applications and Quality Assurance

Edited by **D. Barceló**

Techniques and Instrumentation in Analytical Chemistry Volume 13

Three aspects of environmental analysis are treated in this book:

- the use of various analytical techniques
- their applications to trace analysis of pollutants, mainly organic compounds
- quality assurance aspects, including the use of certified reference materials for quality control of the entire analytical process.

The book will serve as a general reference for post-graduate students as well as a practical reference for environmental chemists who need to use the analytical techniques for environmental studies. Analytical chemists needing information on the complexity of environmental sample matrices and interferences will also find this an invaluable reference.

Contents: Part 1. Field Sampling Techniques and Sample Preparation. 1. Sampling techniques for air pollutants (R. Niessner). 2. Sample handling strategies for the analysis of organic contaminants from environmental samples (M.-C. Hennion, P. Scribe). 3. Extraction, clean-up and recoveries of persistent trace organic contaminants from sediment and biota samples (D.E. Wells). **Part 2. Application Areas.** 4. Current developments in the analysis of polychlorinated biphenyls (PCBs) including planar and other toxic metabolites in environmental matrices (D.E. Wells). 5. Official methods of analysis of priority pesticides in water using gas chromatographic techniques (D. Barceló). 6. Coupled-column reversed phase liquid chromatography as a versatile technique for the determination of polar pesticides (E.A. Hogendoorn, P. van Zoonen). 7. Liquid chromatographic determination of phenols and substituted derivatives in water samples (G. Marko-Varga). 8. HPLC methods for the determination of mycotoxins and phycotoxins (J.F. Lawrence, P.M. Scott). 9. Determination of radionuclides in environmental samples (V. Valkovic). **Part 3. Quality Assurance and Reference Materials.** 10. Quality assurance in environmental analysis (W.P. Cofino). 11. Certified reference materials for the quality control of measurements in environmental monitoring (E.A. Maier). 12. Standard reference materials for the determination of trace organic constituents in environmental samples (S.A. Wise). **Part 4. Emerging Techniques.** 13. Application of fluorescence spectroscopic techniques in the determination of PAHs and PAH metabolites (F. Ariese, C. Gooijer, N.H. Velthorst). 14. Characterization of surfactants in water by desorption ionization methods (F. Ventura). 15. Utilization of various LC-MS interfacing systems in environmental analysis; application to polar pesticides (M.H. Lamoree, R.T. Ghijsen, U.A.Th. Brinkman). 16. Hyphenated techniques applied to the speciation of organometallic compounds in the environment (O.F.X. Donard, R. Ritsema). 17. The potential of capillary electrophoresis in environmental analysis (M.W.F. Nielen). Subject index.

© 1993 660 pages Hardbound
Price: Dfl. 465.00 (US $ 265.75)
ISBN 0-444-89648-1

ELSEVIER
SCIENCE

ORDER INFORMATION

For USA and Canada
ELSEVIER SCIENCE

P.O. Box 945
Madison Square Station
New York, NY 10160-0757
Fax: (212) 633 3880

In all other countries
ELSEVIER SCIENCE

P.O. Box 330
1000 AH Amsterdam
The Netherlands
Fax: (+31-20) 5862 845

US$ prices are valid only for the USA & Canada and are subject to exchange rate fluctuations; in all other countries the Dutch guilder price (Dfl.) is definitive. Customers in the European Community should add the appropriate VAT rate applicable in their country to the price(s). Books are sent postfree if prepaid.

414/143/0382

0003-2670(19940210)286:1;1-F